BULLETIN

OF THE KARAGANDA UNIVERSITY

CHEMISTRY Series

№ 3(99)/2020

July–August–September
September 30th, 2020

Founded in 1996

Published 4 times a year

Karaganda, 2020

CONTENTS

ORGANIC CHEMISTRY

ORGANIC CHEMISTRY

M.Zh. Burkeev, A.Zh. Sarsenbekova, A.N. Bolatbay[*], E.M. Tazhbaev, S.Zh. Davrenbekov, E. Nasikhatuly, E.Zh. Zhakupbekova, A.A. Muratbekova

Karagandy University of the name of academician E.A. Buketov, Kazakhstan
(Corresponding author´s e-mail: abylai_bolatbai@mail.ru)

The use of differential calculation methods for the destruction of copolymers of polyethylene glycol fumarate with the acrylic acid

In this work, the thermal decomposition of copolymers based on polyethylene glycol fumarate with the acrylic acid using various ratios of initial monomers has been studied for the first time. The samples were studied in air and nitrogen. According to the thermograms analysis, it was found that the copolymer sample decomposition begins at higher temperatures for a copolymer with high content of polyester resin. The copolymer is vigorously oxidized by the oxygen when heated in air, and one can observe almost complete sample decomposition, whereas it decomposes with a residue of ~15 % in an inert medium. The activation energies for copolymers with different compositions were estimated using the differential methods of Freeman-Carroll, Achar and Sharpe-Wentworth. The activation energy values found by the three methods demonstrated a good convergence. It was shown that, the activation energy values are higher (~200 kJ/mol in the inert medium, and ~95 kJ/mol in the oxygen atmosphere) for a copolymer with a lower composition of polyester resin, and the activation energy is ~180 and ~85 kJ/mol for a copolymer with a greater composition of p-EGF-AA. The copolymer is more thermostable in the nitrogen atmosphere according to the kinetic parameters. Additionally, there were determined the thermodynamic characteristics, such as the Gibbs energy (ΔG) and the entropy (ΔS). They also confirm the destruction process dependence on the components ratio in the synthesized copolymer.

Keywords: dynamic thermogravimetry, decomposition, thermal destruction, copolymer, thermodynamic characteristics.

Introduction

Currently the volumes of produced unsaturated polyesters and materials based on them are annually increasing in the most industrialized countries. This is due to both the presence of a wide raw material base and the simplicity of processing polyesters into products, and the possibility of obtaining on their basis a large number of different materials with various practically valuable properties [1].

One of the most promising comonomers for getting new «smart» materials based on the unsaturated polyesters are unsaturated carboxylic acids, where the presence of carboxyl groups in the main chain determines their physicochemical behavior [2]. In this case, the interaction of unsaturated polyesters with above monomers of vinyl series was referred to the copolymerization reactions by V.G. Benig [3], whose monograph contains extensive data on the interaction of the above polyesters with styrene, vinyl acetate, methyl methacrylate and a number of other compounds. And there has been no information on the unsaturated polyesters copolymerization with the ionic monomers prior to the work carried out by the authors [4], that opens up prospects for the «smart» materials synthesis and significantly expand the scope of their application.

---

[*] *Corresponding author*

Previously, the authors of [5] by the radical copolymerization of unsaturated polyester resins with a number of unsaturated carboxylic acids have synthesized copolymers with carboxyl groups in the side chains and showing sensitivity to various environmental changes.

Continuing the work, it seemed interesting to evaluate the thermal stability of the previously synthesized copolymers of polyethylene glycol fumarate with the acrylic acid under the dynamic conditions in the inert atmosphere and in the air.

Experimental

Previously synthesized copolymers of polyethylene glycol fumarate (p-EGF) with the acrylic acid (AA) (7.95:92.05 and 89.05:10.95 molar ratio) have been used as the objects of study [6–7]. The study of the copolymers thermal properties was performed using a synchronous TGA/DSC thermal analyzer LabSYS evo DTA/DSC (Setaram, France) in the dynamic mode within the 30–1000 ºC temperature range. The heated rate was 10 ºC·min^{-1} in nitrogen and air atmosphere, and the flow rate was 30 ml·min^{-1} in a crucible of Al_2O_3. The sample weight was 10–12 mg. Experimental data processing was performed using Microsoft Excel and Processing programs.

Results and Discussion

As previously shown, the unsaturated polyester resins' copolymers with unsaturated carboxylic acids have a number of practically valuable properties, thus it was interesting to evaluate their thermal stability.

The copolymers thermal stability in various temperature ranges allows us to predict the possibility of their use in certain areas. The study objects used are the 7.95:92.05 and 89.05:10.95 molar ratio copolymers of polyethylene glycol fumarate with acrylic acid with the «smart-systems» and sealants properties, respectively.

The composition and properties of polyethylene glycol fumarate with the acrylic acid copolymers obtained by the radical copolymerization in solution are shown in the Table 1.

T a b l e 1

Composition and properties of the copolymers of p-EGF (M1) with AA (M2)

Composition of initial mixture, mol. %		Composition of copolymer, mol. %		α, %	Yield, %
M_1	M_2	m_1	m_2		
p-EGF:AA					
10.09	89.91	7.95	92.05	1412	88.23
90.08	9.92	89.05	10.95	512	63.02

The Table 1 data comparison represents that the swelling ratio (α) decreases, and the content of maleate groups increases under reducing of the acrylic acid fraction in the copolymer content; it appears to be related to a decrease in side chains and an increase in the polyethylene glycol fumarate fraction.

In this work, we have evaluated the thermal degradation of p-EGF:AA copolymers using the dynamic thermogravimetric analysis. The Figures 1, 2 show thermograms for the 7.95:92.05 and 89.05:10.95 molar ratio copolymers of polyethylene glycol fumarate with the acrylic acid with the 10 ºC·min^{-1} constant heating rate at the temperature range of 30–1000 ºC in the nitrogen and air atmosphere.

As can be seen in Figure 1 on the thermogravimetric curves, both substances do not undergo any transformations leading to a mass change in the 30 ºC to 150 ºC temperature range. There is observed a slight decomposition with the release of volatile products and a weight loss of up to ~12 % for a 7.95:92.05 mol.% copolymer in the 200–330 ºC temperature range. Then, an intensive decrease in the sample mass occurs with the process total completion at a ~600 ºC temperature. Total weight loss is ~80 %. The release process of volatile substances begins at higher temperatures and reaches its maximum at 320 ºC for the copolymer with a high content of polyester resin. There is composition of the copolymer's basic mass with the total residue of ~15 % in the 340–500 ºC temperature range.

There is observed a slight change in the rate in the range from 0 to 0.11 mg·min^{-1} for both copolymers on the curves of the mass loss rate (Fig. 1, b) in the 30–260 ºC temperature range. A sharp increase in the rate is observed for the copolymer with a high content of acrylic acid at the above 300 ºC temperature range. There is observed a shift to high temperatures, achieving its 1.7 mg·min^{-1} numerical value maximum at

400 ℃. A peak is observed for a 89.05:10.95 mol.% copolymer at 350 ℃, and then a gradual decrease in rate occurs with stabilization in the region of ~500 ℃ for both copolymers.
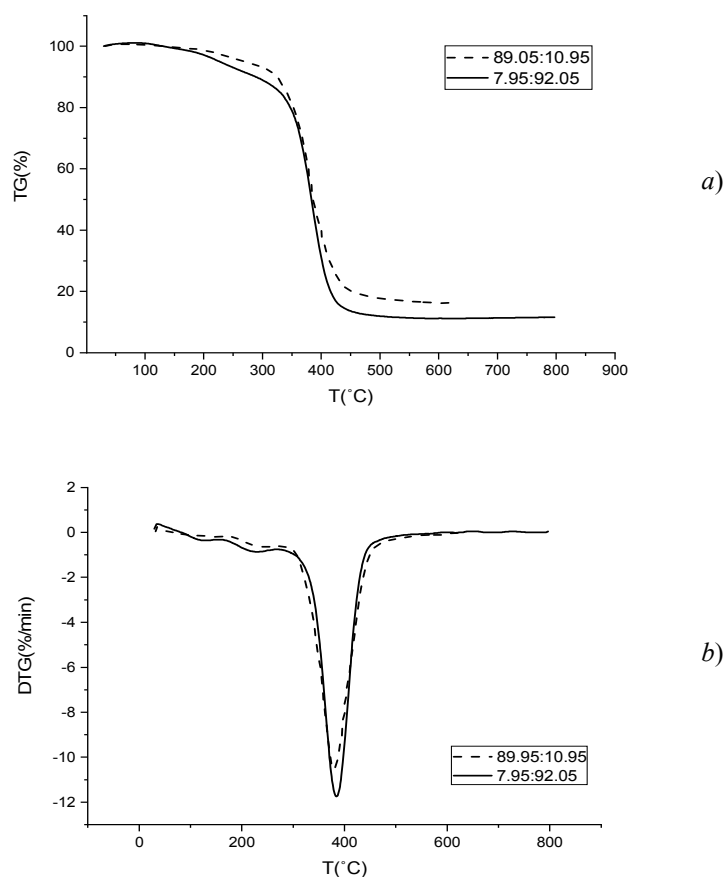
Figure 1. Temperature dependences of mass change (TG curve) (*a*), mass change rate (DTG curve) (*b*)
for p-EGF:AA copolymers with 7.95:92.05 mol.% and 89.05:10.95 mol.% initial ratios M1:M2
(in nitrogen atmosphere)

Continuing the work, the thermogravimetric studies of the p-EGF copolymers with AA in air were carried out. From the data obtained by comparison (Fig. 2, a), it can be seen that the 7.95:92.05 mol.% copolymer of polyethylene glycol fumarate with acrylic acid begins to decompose at a temperature of 200 ℃ when heated in air. An intensive decrease in the sample mass occurs followed by a gradual decomposition in the 300–420 ℃ temperature range. The afterburning phase accompanied by almost a complete decomposition of the copolymer can observed on the thermogravimetric curves. A copolymer with a high content of polyester resin begins to decompose at the lower temperatures, a shift to high temperatures is also observed. The substance does not undergo transformation leading to a change in its mass in the temperature range from 30 ℃ to 100 ℃. Further, there is a slight decomposition with the release of volatile products. An intensive decrease in the sample mass occurs in the 300–430 ℃ temperature range, after which there is a gradual decomposition of the copolymer with the total process completion at the 750 ℃.

There is observed a slight change in the rate from 0 to 0.24 mg·min^{-1} in the 30–300 ℃ temperature range on the curves of the mass loss rate (Fig. 2, b). The curve shows a peak at 392 ℃ for the copolymer with a lower acrylic acid content, and for the p-EGF:AA copolymer 7.95:92.05 the peak is observed at 375 ℃ with a numerical value of ~1.9 mg·min^{-1}.
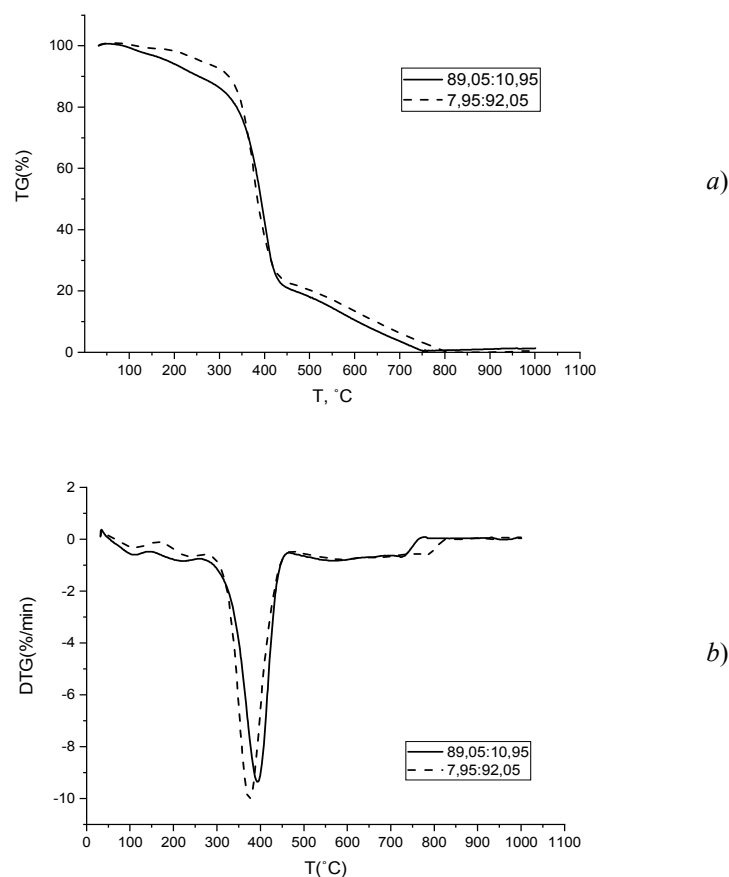
Figure 2. Temperature dependences of mass change (TG curve) (*a*), mass change rate (DTG curve) (*b*)
for p-EGF:AA copolymers with 7.95:92.05 mol.% and 89.05:10.95 mol.% initial ratios M1:M2 (in air)

Based on the copolymers thermal analysis result obtained, the activation energy and the reaction order were calculated using the methods of Achar [8], Sharp-Wentworth [9] and Freeman-Carroll [10] (Fig. 3). By comparing the graphs obtained using different methods, it can be conclude that the points have a larger scatter for the Freeman-Carroll method (Fig. 3, c), that leads to an error in estimating the activation energy. So, the line intersects the ordinate axis at the point +33.17 and has a slope corresponding to activation energy equal to 196.13 kJ/mol. Principally, the Achar and Sharp-Wentworth methods give the same results. The correlation coefficient of these three methods has a good convergence and tends to unity.

Such thermodynamic characteristics as change in Gibbs energy (ΔG) and entropy (ΔS) have been calculated using the obtained values of the activation energy (Table 2).

T a b l e 2

Kinetic parameters of thermal degradation of the p-EGF:AA copolymer in air and nitrogen atmosphere

$M_1:M_2$ copolymer composition, mol.%	Methods					
	Achar	S-W	F-C			
	E, kJ/mol	E, kJ/mol	E, kJ/mol	n	ΔS, J/(mol·K)	ΔG, kJ/mol
Nitrogen						
7.95:92.05	196.13	196.18	211.09	0.37	-177.68	85.47
89.05:10.95	165.11	165.45	190.12	0.61	-94.65	101.65
Air						
7.95:92.05	95.06	95.08	94.09	0.36	-192.32	143.37
89.05:10.95	81.06	81.08	93.09	0.71	-84.60	108.63

a)

b)

c)
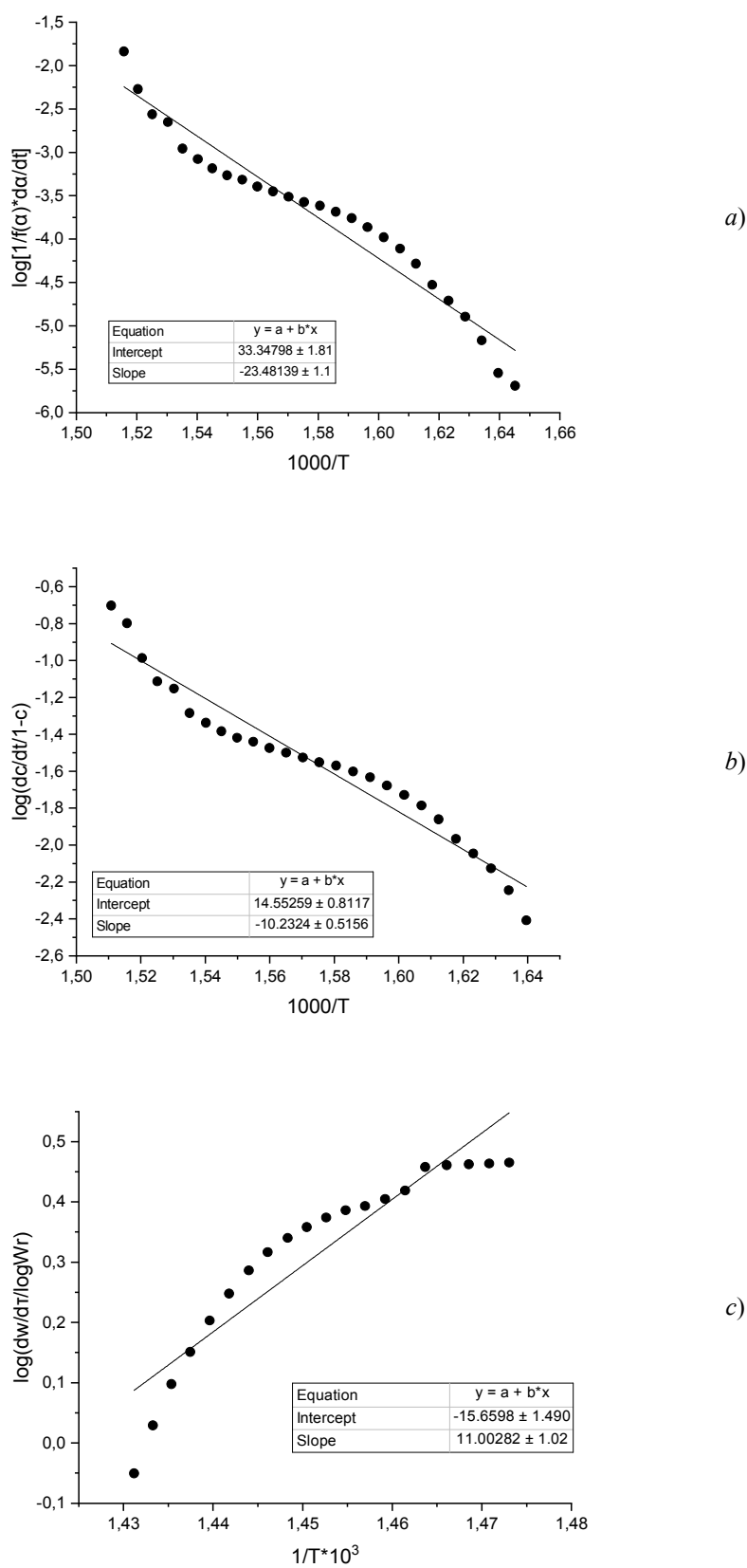
Figure 3. Linearization of thermogravimetric data of the studied 7.95:92.05 mol.% p-EGF: AA copolymer, using (*a*) Achar, (*b*) Sharp-Wentworth, (*c*) Freeman-Carroll method (10 °C·min^{-1} heating rate, nitrogen atmosphere)

The Table 2 shows the values of the activation energies of destruction obtained from the TGA data. As follows from the table, the dependence of the activation energy from the copolymers composition is extreme. The copolymers of the composition 7.95: 92.05 mol.% have a higher value of activation energy. The activation energy value decreases with an increase in the composition of polyethylene glycol fumarate. It is in the range of 81–90 kJ/mol for the copolymer with the composition of 7.95: 92.05 mol.% in the nitrogen atmosphere. It can be note, that calculated using the Freeman-Carroll method parameters have higher values, while the Achar and Sharpe-Wentworth methods give the same results. The positive value of the Gibbs energy ΔG and its growth with an increase in the copolymer composition of the unsaturated polyester p-EGF indicates the impossibility of spontaneous implementation of the destruction process.

Thermal destruction in the air atmosphere leads to a decrease in the thermal stability of copolymers. Due to that its effective activation energy is relatively small. This indicates that the polymer temperature resistance in air is lower than in inert medium.

Conclusions

Thus, the kinetic characteristics and thermodynamic parameters of copolymers of polyethylene glycol fumarate with the acrylic acid were determined for the first time. The activation energy values, calculated by the methods of Freeman-Carroll, Sharp-Wentworth and Achar, confirm the destruction process dependence on the components ratio in the synthesized copolymer. It was found that, the activation energy values have higher values with an increase in the content of the unsaturated polyester copolymer p-EGF. The copolymer is less thermostable when heated in the air. If the material is heated in absence of air, i.e. in the nitrogen atmosphere, the copolymer is split into low molecular weight products.

References

1   Benny C. Epoxidized Phenolic Novolac: A Novel Modifier for Unsaturated Polyester Resin. / C. Benny, T.T. Eby // Journal of Applied Polymer Science. — 2006. — Vol. 1. — P. 457.

2   Kandelbauer A. In Handbook of Thermoset Plastics / A. Kandelbauer, G. Tondi, O.C. Zaske, S.H. Goodman. — Amsterdam: Elsevier Inc. Chapters, 2014. — P. 6–111.

3   Boenig H.V. Unsaturated Polyesters. Structure and Properties / H.V. Boenig. — Amsterdam: Elsevier Publishing Company, 1964.

4   Wu Y. Acrylatedepoxidized soybean oil as a styrene replacement in a dicyclopentadiene-modified unsaturated polyester resin / Y. Wu, K. Li // Journal of Applied Polymer Science. — 2018. — Vol. 135, № 19. — P. 46212.

5   Burkeev M.Zh. Thermal destruction of copolymers of polypropylene glycol maleate with acrylic acid / M.Zh. Burkeev, A.Zh. Sarsenbekova, E.M. Tazhbaev // Russian Journal of Physical Chemistry A. — 2015. — Vol. 89, № 12. — P. 2183–2189.

6   Burkeev M.Zh. New polyampholyte polymers based on polypropylene glycol fumarate with acrylic acid and dimethylaminoethyl methacrylate / M.Zh. Burkeev, G.K. Kudaibergen, G.K. Burkeeva et al. // Russian Journal of Applied Chemistry. — 2018. — Vol. 91, № 7. — P. 1145–1152.

7   Burkeev M.Zh. Comparative analysis of the thermal decomposition kinetics of polyethylene glycol fumarate–acrylic acid copolymers / M.Zh. Burkeev, G.K. Kudaibergen et al. // Russian Journal of Physical Chemistry A. — 2019. — Vol. 93, № 7. — P. 1252–1257.

8   Achar B.N. Kinetics and mechanism of dehydroxylation processes, III, applications and limitations of dynamic methods / B.N. Achar, G.W. Brindley, J.H. Sharp // Proc. Int. Clay. Conf. — 1966. — P. 67–73.

9   Sharp J.H. Kinetic analysis of thermogravimetric data / J.H. Sharp, S.A. Wentworth // Anal. Chem. — 1969. — Vol. 41, № 14. — P. 2060.

10 Freeman E.S. The application of thermoanalytical techniques to reaction kinetics: The thermogravimetric evaluation of the kinetics of the decomposition of calcium oxalate monohydrate / E.S. Freeman, B. Carroll // J. Phys. Chem. 1958. — Vol. 62, № 4. — P. 394–397.

М.Ж. Буркеев, А.Ж. Сарсенбекова, А.Н. Болатбай, Е.М. Тажбаев, С.Ж. Давренбеков,
Е. Насихатұлы, Э.Ж. Жакупбекова, А.А. Муратбекова

Полиэтиленгликольфумарат пен акрил қышқылы негізіндегі сополимерлердің термиялық ыдырауына дифференциалды есептеу әдістерін қолдану

Жұмыста бастапқы мономерлердің әртүрлі қатынастарында полиэтиленгликольфумарат пен акрил қышқылы негізіндегі сополимерлердің термиялық ыдырауы алғаш рет зерттелді. Үлгілерді зерттеу ауа мен азот ортасында жүргізілді. Термогравиметриялық қисықтарды талдау нәтижелері бойынша полиэфирлі шайыры көп құрамды сополимер үлгісінің ыдырауы жоғары температураларда

басталатыны анықталды. Ауа атмосферасында қыздыру кезінде сополимер оттегінің әсерінен қатты тотығады және қисықтардан үлгінің толық ыдырауын байқауға болады, ал инертті ортада сополимер шамамен ~15 % қалдығымен ыдырайды. Фримен-Кэррол, Ахар және Шарп-Уэнтворттың дифференциалдық әдістері негізінде әртүрлі құрамды сополимерлердің активтендіру энергиясы анықталды. Үш әдіс арқылы анықталған активтендіру энергиясының мәндері жақсы бір-бірімен үйлесімдік көрсетеді. Полиэфирлі шайырдың аз құрамы бар сополимер үшін активтендіру энергиясының мәні жоғары (~200 кДж/моль инертті ортада және оттегі атмосферасында ~95 кДж/моль), ал п-ЭГФ-АҚ үлкен құрамы бар сополимер үшін активтендіру энергиясы ~180 және ~85 кДж/моль құрайды. Кинетикалық параметрлер бойынша азот атмосферасында сополимер термостенді. Сонымен қатар, Гиббс энергиясы (ΔG) және энтропия (ΔS) сияқты кейбір термодинамикалық сипаттамалар анықталды, олар да деструкция үрдісінің синтезделген сополимердегі компоненттердің құрамына тәуелділігін растайды.

Кілт сөздер: динамикалық термогравиметрия, ыдырау, термиялық деструкция, сополимер, термодинамикалық сипаттамалар.

М.Ж. Буркеев, А.Ж. Сарсенбекова, А.Н. Болатбай, Е.М. Тажбаев, С.Ж. Давренбеков, Е. Насихатулы, Э.Ж. Жакупбекова, А.А. Муратбекова

Использование дифференциальных методов расчета при деструкции сополимеров полиэтиленгликольфумарата с акриловой кислотой

В статье впервые изучено термическое разложение сополимеров на основе полиэтиленгликольфумарата с акриловой кислотой с различными соотношениями начальных мономеров. Исследование образцов проводилось в среде воздуха и азота. По результатам анализа термогравиметрических кривых установлено, что для сополимера с большим содержанием полиэфирной смолы разложение образца сополимера начинается при более высоких температурах. При нагревании в атмосфере воздуха сополимер энергично окисляется под воздействием кислорода и на кривых можно наблюдать почти полное разложение образца, тогда как в инертной среде сополимер разлагается с остатком ~15 %. Дифференциальными методами Фримена-Кэррола, Ахара и Шарпа-Уэнтворта оценены энергии активации для сополимеров с различным составом. Найденные тремя методами значения энергии активации показывают хорошую сходимость. Установлено, что для сополимера с меньшим содержанием полиэфирной смолы значения энергии активации имеют более высокие показатели (~200 кДж/моль в инертной среде и ~95 кДж/моль в атмосфере кислорода), а для сополимера с большим содержанием п-ЭГФ-АК энергия активации составляет ~180 и ~85 кДж/моль. По кинетическим параметрам видно, что в атмосфере азота сополимер более термостабилен. Кроме того, были определены некоторые термодинамические характеристики, такие как энергия Гиббса (ΔG) и энтропия (ΔS), которые также подтверждают зависимость процесса деструкции от соотношения компонентов в синтезированном сополимере.

Ключевые слова: динамическая термогравиметрия, разложение, термическая деструкция, сополимер, термодинамические характеристики.

References

1   Benny, C., & Eby, T.T. (2006). Epoxidized Phenolic Novolac: A Novel Modifier for Unsaturated Polyester Resin. *Journal of Applied Polymer Science, 1*, 457.

2   Boenig, H.V. (1964). *Unsaturated Polyesters. Structure and Properties*. Amsterdam: Elsevier Publishing Company.

3   Kandelbauer, A. (2014). In *Handbook of Thermoset Plastics*. Amsterdam: Elsevier Inc. Chapters. 6, 111.

4   Wu, Y., & Li, K. (2018). Acrylated epoxidized soybean oil as a styrene replacement in a dicyclopentadiene-modified unsaturated polyester resin. *Journal of Applied Polymer Science, 135(19)*, 46212.

5   Burkeev, M.Zh., Sarsenbekova, A.Zh., & Tazhbaev, E.M. (2015). Thermal destruction of copolymers of polypropylene glycol maleate with acrylic acid. *Russian Journal of Physical Chemistry A, 89(12)*, 2183–2189.

6   Burkeev, M.Zh., Kudaibergen, G.K., & Burkeeva, G.K., et al. (2018). New polyampholyte polymers based on polypropylene glycol fumarate with acrylic acid and dimethylaminoethyl methacrylate. *Russian Journal of Applied Chemistry, 91(7)*, 1145–1152.

7   Burkeev, M.Zh., Sarsenbekova, A.Zh., & Kudaibergen, G.K., et al. (2019). Comparative analysis of the thermal decomposition kinetics of polyethylene glycol fumarate–acrylic acid copolymers. *Russian Journal of Physical Chemistry A, 93(7)*, 1252–1257.

8   Achar, B.N., Brindley, G.W., & Sharp, J.H. (1966). Kinetics and mechanism of dehydroxylation processes, III, applications and limitations of dynamic methods. *Proc. Int. Clay. Conf.*, 67–73.

9   Sharp, J.H., & Wentworth, S.A. (1969). Kinetic analysis of thermogravimetric data. *Anal. Chem., 41(14)*, 2060.

10 Freeman, E.S., Carroll, B. (1958). The Application of Thermoanalytical Techniques to Reaction Kinetics: The Thermogravimetric Evaluation of the Kinetics of the Decomposition of Calcium Oxalate Monohydrate. *Journal of Physical Chemistry, 62(4)*, 394–397.

S.D. Fazylov[1*], O.A. Nurkenov[1, 2], Z.M. Muldakhmetov[1], A.M. Gazaliev[1],
A.E. Arinova[1, 3], M.K. Ibraev[2], L.M. Vlasova[4], A.S. Fazylov[2]

[1]Institute of Organic Synthesis and Coal Chemistry of the Republic of Kazakhstan, Karaganda, Kazakhstan;
[2]Karaganda State Technical University, Kazakhstan;
[3]Karagandy University of the name of academician E.A. Buketov, Kazakhstan;
[4]Karaganda Medical University, Kazakhstan
(Corresponding author′s e-mail: iosu8990@mail.ru)

Biologically active derivatives of fullerene C60.
Current state and development prospects

The article presents literature review on the physicochemical and biological properties of fullerene C60, as well as the authors' own experimental data on the synthesis of fullerene derivatives of amines and natural alkaloids. It is shown that the presence of a fullerene fragment in the structure of the compound provides a significant improvement or the appearance of qualitatively new mechanical, chemical, physical, biological and other properties associated with the manifestation of nanoscale factors. The issues of the relationship of the structure, water solubility and biological activity of fullerene C60 derivatives are considered. Many biologically active effects of various modified derivatives of fullerene C60 are described, which have membrane-active, antibacterial, antiviral, immunomodulating, HIV inhibitory enzymes and other properties. It was noted that preparations containing a fullerene fragment are effective against hepatitis C virus, and are also able to efficiently trap free radicals. Derivatives of fullerenes can also be used as antioxidant, neuroprotective and other agents. Particular attention is paid to the authors' own results on the synthesis of amino derivatives of fullerenes.

Key words: fullerene C60, fulleropyrrolidines, nanoscale factors, amino fullerenes, Prato reaction.

Introduction

At present, in organic chemistry, fullerene bioorganic chemistry has acquired particular promise and is developing, turning abroad into an independent branch of organic chemistry. The presence of a fullerene fragment in the structure of the compound provides a significant improvement or the appearance of qualitatively new mechanical, chemical, physical, biological and other properties associated with the manifestation of nanoscale factors [1–3]. From a chemical point of view, the behavior of fullerenes defines the presence in the molecules of conjugated, and also strained, bonds. The spherical fullerene molecule is highly stressed, since usually flat six-membered aromatic (benzene) rings must be bent to build a sphere (voltage energy $dH_f = 10.16$ kcal/mol per carbon atom), which causes less thermodynamic stability of fullerene compared to graphite ($dH_f = 0$ kcal/mol) [2–4]. Therefore, the driving force of the reactions of addition to fullerene C60 is the reduction of voltage in the fullerene framework. Consequently, the reactions leading to the formation of saturated sp^3-hybridized carbon atoms relieve such stress.

The range of possible applications of fullerene compounds includes: a) new classes of superconductors, semiconductors, magnets, ferroelectrics, nonlinear optical materials [4]; b) new technologies for the synthesis of diamonds and diamond-like compounds of ultrahard hardness [5]; c) new classes of polymers with specified mechanical, optical, electrical, magnetic properties for recording and storing information [6]; d) new types of catalysts and sensors for determining the composition of liquid and gaseous media [6]; e) new classes of antifriction coatings and lubricants, including those based on fluorine-containing fullerene compounds [7].

Main part

One of the most interesting areas of research is the study of the biological activity of fullerene derivatives. The literature describes many biologically active effects of various modified derivatives of fullerene C60, which have antibacterial [7], antiviral [1], immunomodulating and HIV inhibitory enzymes [6, 7]. Drags containing a fullerene fragment have been shown to be effective against hepatitis C virus [8], and are

---

* *Corresponding author*

also able to efficiently trap free radicals and can be used as neuroprotective [9] and other agents [10]. Currently, the volume of work on the biological activity of fullerenes has reached thousands of articles per year. At this time available scientific data demonstrate the significant potential of fullerene C60 in biomedicine and the pharmacodynamics of various biological environments.

The biological effects of fullerene C60 are based on its complementary interaction with the protein, which was first expressed in [1, 3, 10]. The fullerene molecule has been shown to purely sterically block the lipophilic channel of the HIV-1 virus protease. The size and shape of the carbon skeleton in the C60 molecule exactly matches the size and shape of the active center of a number of enzymes. Therefore, some fullerene compounds allosterically inhibit HIV enzymes (HIV protease and reverse transcriptase), which makes them promising for the development of AIDS drugs [3–11]. The high electron deficiency of these molecules explains the ability of fullerenes to attach free radicals that form in living systems. For this property, fullerene was given the name «radical sponge» [7].

The biological activity of fullerenes is based on three properties of these molecules: lipophilicity, which determines membranotropic properties, electron deficiency, which leads to the ability to interact with free radicals, and the ability of their excited state to transfer energy to an ordinary oxygen molecule and turn it into singlet oxygen [7]. A significant limitation for the practical use of fullerenes and many of its derivatives in biological media is their low solubility in aqueous solutions, since the C60 molecule is hydrophobic and its solubility in water is only $1.3 \cdot 10^{-11}$ [12]. Therefore, the preparation of water-soluble fullerenes is important for pharmacology. The study of the reactions of fullerenes in water is also of independent interest for chemical science. Researchers consider two approaches to obtaining water-soluble forms of fullerene C60:

1) non-covalent interaction with water-soluble carriers, for example, polyvinylpyrrolidone, cyclodextrins [3], proteins or liposomes [4];

2) covalent chemical modification by addition of polar groups, for example hydroxyl [4–14], carboxyl or amino groups [3, 4, 15].

Non-covalent interaction with water-soluble carriers allows the introduction of fullerenes into a living organism without changing their conjugation system, and hence the physicochemical properties. Surfactant solutions can also conduct water-insoluble organic compounds into a colloidal state or solubilize. However, due to hydrophobicity, the problem arises of their elimination from the body: fullerenes can accumulate in the liver [16], lungs [17], bones [18].

The second approach allows one to obtain water-soluble fullerene derivatives by covalent modification of the fullerene sphere with various functional groups (addends) — dienes and nucleophilic agents having various hydrophilic components. Thus, various pharmacophore groups can be grafted onto fullerene C60 and additional physiological activity can also be obtained. The result of this modification is molecules that can conditionally be divided into two groups:

1) compounds in which addends uniformly cover the entire surface of the fullerene carcass, as a result of which numerous addends attached over the entire surface change the electronic structure of the carbon carcass and make it inaccessible for interaction with biological targets;

2) compounds having one or more addends grouped on a small part of the frame.

The latter option is most often used in the synthesis of potentially bioactive water-soluble fullerene cycloadducts. Several examples of such water-soluble fullerene derivatives can be given. For example, compound (**1**) allows reaching a maximum concentration of 1.5×10^{-5} mol/l in a mixture of H$_2$O-DMSO, 9:1 [4, 19]. Good solubility was achieved for the dendromer shown in the diagram (**2**): its solubility in water was 34 mg/ml at pH 7.4 and 254 mg/ml at pH 10 [4, 11]. As can be seen from the structure of compounds (**1**) and (**2**), they contain a sufficient amount of solubilizing additions (NH, OH, COOH, C=O-groups).

1

2
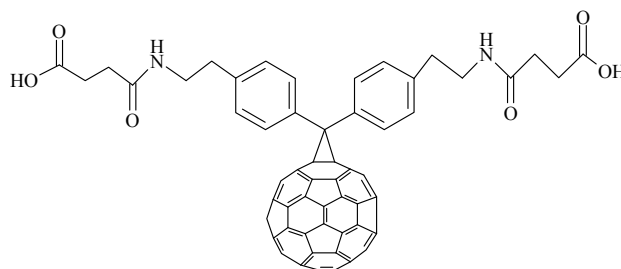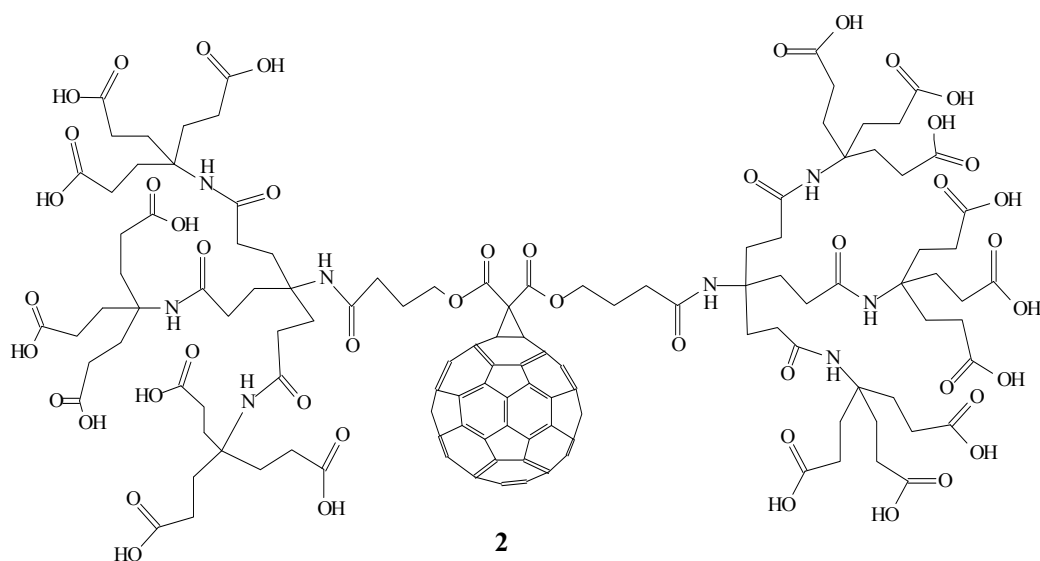
O.A. Troshina et al. [11] reported on the development of a universal method for the conversion of any low-polar derivatives of C60 into water-soluble compounds. The solubility of all the compounds obtained in water exceeds 100 mg/ml at pH = 7.0, which is a record for water-soluble derivatives of fullerenes. Thus, the introduction of hydrophilic substituents into the C60 sphere allows for sufficient solubility in water.

The most promising results in this direction were obtained using chemically modified fullerene C60, mainly containing ionic groups — amine, carboxyl and hydroxyl [7, 11].

Amino derivatives of fullerene. The reactions of addition of primary and secondary amines to C60 were one of the first to be discovered in the chemistry of fullerene. Due to their high nucleophilicity, primary and secondary aliphatic amines are attached to electron-deficient C60-fullerene.

When fullerene C60 is treated with a 40-fold excess of morpholine over a week, it is possible to isolate dimorpholin-1,4-dihydro [C60] fullerene from the reaction medium (**3**). In contrast to the reaction with morpholine, the reaction with an excess of secondary diamine (e.g., N,N'-dimethylethylenediamine) leads to a stable six-membered adduct (**4**) due to the addition of a 6–6 double bond, which eliminates the formation of undesired 5–6 double bonds in the molecule, violating the aromaticity of six-membered rings [11].

3   **4**
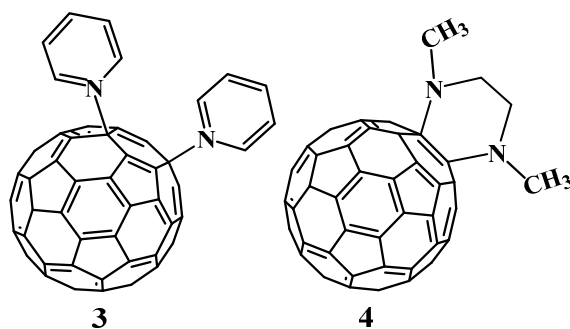
For several years, we have been working at the Institute of Organic Synthesis and Coal Chemistry of the Republic of Kazakhstan on the functionalization of the C60 molecule with the participation of molecules of various amines, including natural compounds (alkaloids) and their derivatives. This is an interesting direction that can lead to important results in terms of creating new therapeutic drugs.

We carried out the amination of fullerene C60 with 2-(aminomethyl)pyridine in middle chlorobenzene with heating (80–100 ºC) and stirring for 18–24 hours. The yield of obtained aminofullerene (**5**) was 19 % [12–14]. UV spectrum of compound (**5**) contains a maximum at λ = 875 nm, characteristic of 1,4-di[2-(aminomethyl)pyridine]fullerene C60.

Similar syntheses were carried out with alkaloid cytisine and salsolin. The reactions were carried out in toluene at 100 ºC for 28–30 hours. However, the isolation of C60 amination products with alkaloids was unsuccessful.

5
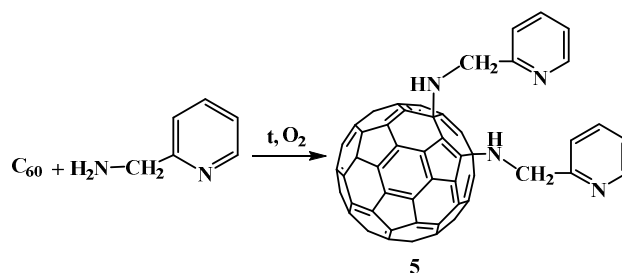
Among the most convenient methodologies for the functionalization of C60 by the amines described in recent years, the 1,3-dipolar azomethynilide cycloaddition is widely used, leading to the formation of fulleropyrrolidines. This method is based on the generation of azomethinilides during decarboxylation of the ammonium salts obtained by condensation of α-amino acids with aldehydes. This method is called in the literature the Prato reaction [4, 8]. Following this technique, the synthesis of new fullerenepyrrolidines (6–12) was carried out, by the interaction of C60 fullerene with sarcosine and substituted aromatic aldehydes (4-fluorobenzaldehyde, 2-chlorobenzaldehyde, 2-hydroxy-5-bromobenzaldehyde, 4-morpholino-benzaldehyde, 4-piperidinediethylaminobenzaldehyde, 4-diethylamino-2-hydroxybenzaldehyde) in boiling toluene in argon atmosphere according to the following scheme [15–17]:

R= F, R$_1$=H (6); R=Cl, R$_1$=H (7);

R= Br, R$_1$=OH (8).

R= —N◯O , R$_1$=H (9);   R= —N◯ , R$_1$=H (10);

R= -N(C$_2$H$_5$)$_2$, R$_1$=H (11); R= -N(C$_2$H$_5$)$_2$, R$_1$=OH (12);
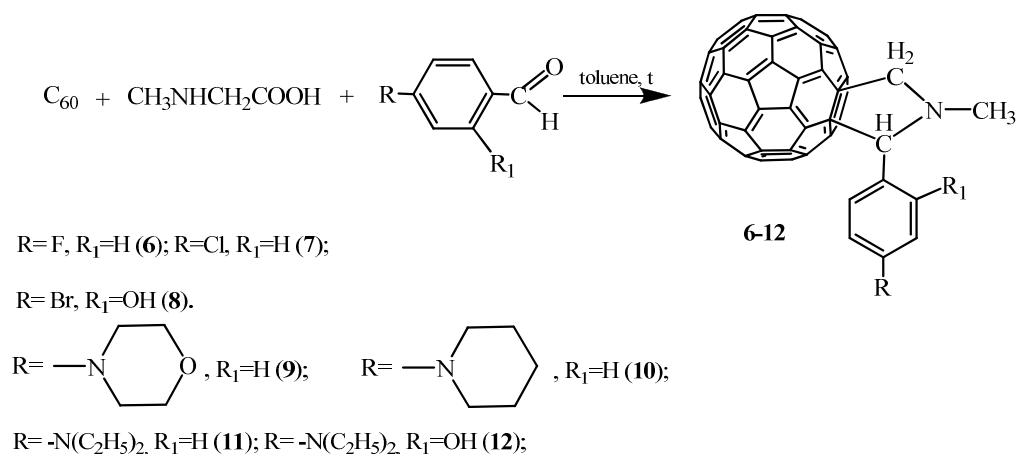
Unreacted starting materials and reaction products (6–12) after the reaction were separated by column chromatography on SiO$_2$, eluting with toluene and then with pyridine. At the same time, at the beginning, the initial unreacted fullerene C60 is released, and then the target fulleropyrrolidines (4–10). The structure of the obtained compounds (6–12) was established by the data of IR, NMR[1]H, and H-^{1}H NOESY spectroscopy and mass spectrometry.

The Prato method considered above was used by us in the synthesis of new derivatives of fullerene C60 with alkaloids. To involve the alkaloid molecule in the reaction, we obtained 4-cytisinobenzaldehyde, which was then used in the Prato reaction in boiling toluene according to the following scheme [15, 16]:

13
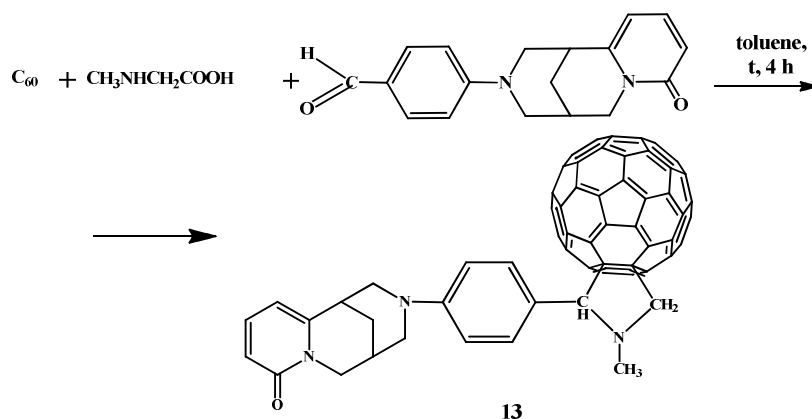
In order to expand the arsenal of new fulleropyrrolidines, we carried out a three-component condensation of fullerene C60, N-methylglycine (sarcosine) and new substituted benzaldehydes: [4-(oxiran-2-ylmethoxy)benzaldehyde, 4-(2-hydroxy-3-morpholinopropoxy)benzaldehyde and 4-(2-hydroxy-3-cytisino-propoxy)benzaldehyde] under the conditions of the Prato reaction in toluene [15–17].
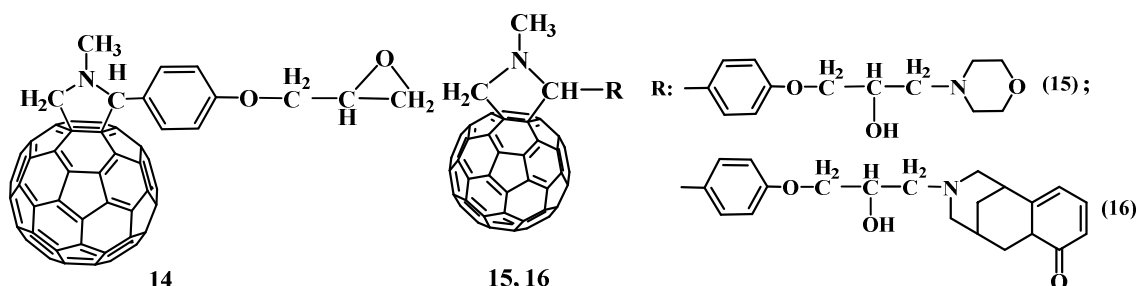
The synthesized fulleropyrrolidines (14–16) are of interest as acceptor materials for organic solar cells. A signal (2.67–2.80 ppm) of the methyl group is observed in the ^{1}H NMR spectrum of compounds (14–16) in the high-field region. Signals at 2.59 and 3.77 ppm correspond to the protons of the methylene and methine groups of the nitrogenous heterocycle. The protons of the ethylene oxide (oxirane) link in (14) resonate at 2.87 and 3.5 ppm. In the high frequency region (6.95–7.85 ppm), the symmetric protons of the aromatic system resonate. In addition to the indicated resonance lines, the signals of impurity substances are also observed in the ^{1}H NMR spectra.

To obtain water-soluble forms of the fullerene-containing pyrrolidines synthesized above, N-methyl-1-[(4-diethylaminophenyl]-fullerene-C60-[1,9c]-pyrrolidine (11) and N-methyl-1-[(4-diethylamino-2-hydroxy-phenyl]-fullerene-C60-[1.9c]-pyrrolidine (12) carried out reactions with tartaric acid to form the corresponding pyrrolidinium tartrates (17, 18). The resulting fulleropyrrolidinium tartrates (17, 18) are soluble in water-dimethyl sulfoxide (3:1) in contrast to the starting fulleropyrrolidines [15–17].
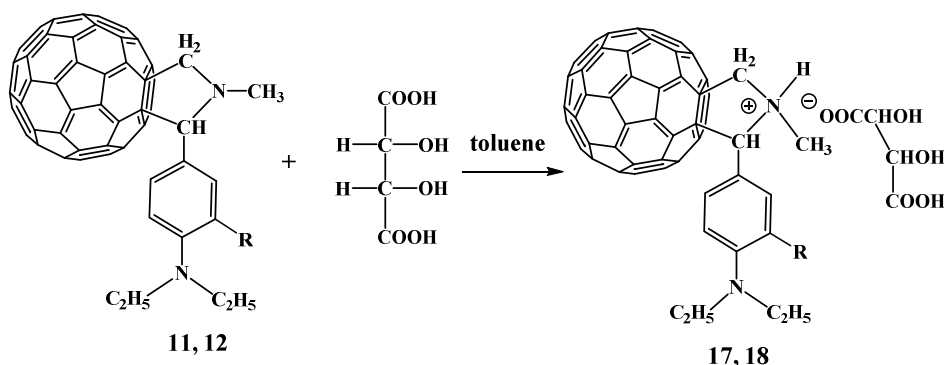
R = H (11, 17); R = H (12, 18)

An interesting reaction for the preparation of a water-soluble cyclodextrin derivative of triazolino fullerene is described in [18, 19]. The formation of supramolecular complexes based on fullerenes (19) with therapeutic agents can improve the bioavailability and pharmacokinetics of the latter, which opens the way to the creation of targeted drug delivery systems.
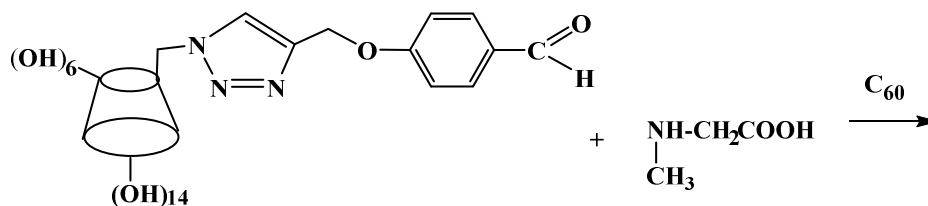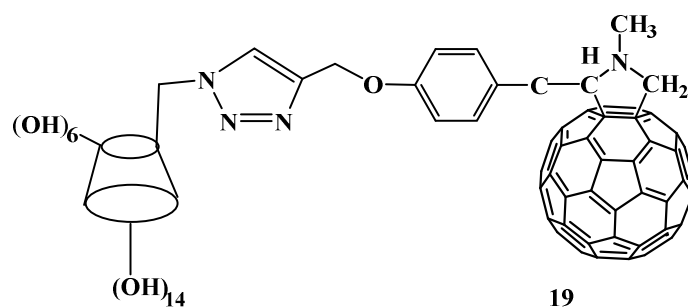
Fullerenols. An important group of water-soluble derivatives of fullerene C60 are fullerenols. By this term «fullerenol» («fullerol») is meant derivatives of fullerene C60 of composition $C60(OH)_x$. Hydroxylatedfullerenols are also of great interest in the search for possible applications in medicine. There are several methods for the synthesis of fullerenols with a different number of hydroxyl groups [7].

For example, hydrolysis of the ether functional groups of polyorganocarboxylated fullerene derivatives yielded water-soluble fullerenols $C60(OH)_n$ with 18–20 hydroxyl groups [13].
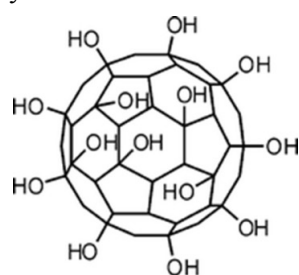
They have antioxidant properties, anticancer and antiviral activity, are able to prevent ischemia, which is caused by a sharp increase in ROS with energy depletion of organs and tissues [14]. Fullerenol $C60(OH)_{24}$ has antiproliferative properties (prevents cell division) and, due to its ability to attach free radicals, prevents the cytotoxic effects of the use of doxorubicin used in cancer chemotherapy [18–20].

Fullerenols $C60(OH)_{44}$ possess antibacterial and antifungal activity [19]. The antifungal activity of fullerenols is quite high. It seems that fullerenols are capable of interacting with carbohydrate components of fungal cell walls, such as β-glucan and chitin, to a greater extent than with peptidoglycans of bacterial cell membranes. Among fullerenols, substances with anti-allergic properties have also been found [20].

Carboxylated derivatives of fullerenes. Another important group of fullerenes with important biological properties is its carboxylated derivatives. For example, they can suppress neuronal apoptosis caused by glutamate receptor agonists NMDA and AMPA, and neutralize the action of the amyloid peptide responsible for the occurrence of Alzheimer's disease [7, 21–23].

They delay the development of functional impairment and death of the rats having the mutant human SOD gene. Also, these compounds are able to bind superoxide anion and H_2O_2, are effective inhibitors of lipid peroxidation. It was found that when introduced into the lateral ventricles of the brain, carboxyfullerene can eliminate the effects of oxidative damage caused by reperfusion ischemia [7, 18].

Aminacid derivatives of fullerenes. The synthesis of water-soluble derivatives of C60 fullerene with sodium salts of aminobutyric and ε-aminocaproic acids, as well as hybrid structures based on the fullerene derivative with proline and carnosine (β-alanyl-L-histidine) are described [19–23, 24]. The considered derivatives possessed antioxidant activity. For the first time, the authors found a relationship between the suppression of the development of cytomegalovirus infection (CMVI) and the activation of peroxidation of lipid. Moreover, an effective inhibitor of CMVI from the class of amino acid derivatives of fullerene was obtained [23, 25–28]. Antiviral activity was also found in fullerene — (*tris*-aminocaproic acid) hydrate in non-toxic concentrations (up to 100 μg/ml) with respect to the respiratory syncytial virus. The antiviral agent is offered as a 1 % ointment of fullerene hydropolyaminocaproic acid as an active substance.

Conclusions

Thus, an analysis of the literature on the study of C60 fullerene derivatives allows us to draw the following conclusions about the current state of research in this area:

a) The uniqueness of fullerenes as a class of chemical compounds is determined by the peculiarities of their structure. They attract the attention of researchers for their practical applications in science, biology and medicine, in semiconductor technology and nanoelectronics.

b) Fullerenes have an unusually large number of equivalent reaction centers (in terms of the number of double bonds), which leads to the possibility of the formation of a large number of reaction products during

the functionalization of their structure. Thus, most chemical reactions with fullerenes are not selective, which complicates the synthesis of individual compounds.

c) Most of the syntheses of derivatives of fullerenes described in the literature relate to the modification of fullerene C60. The data on the biological activity of fullerene derivatives presented in the literature are incomplete and fragmentary. In many works, the molecular mechanism of its manifestation has not been reliably established.

d) The most important properties of the structure of C60, affecting the spectrum of its biological action, are lipophilicity, membranotropicity and water solubility of its derivatives. The size, shape and high lipophilicity of fullerene allow its molecule to quite easily penetrate into cells of a living organism.

e) The formation of supramolecular complexes and therapeutic agents can improve the bioavailability and pharmacokinetics of the latter, which opens the way to the creation of targeted drug delivery systems.

References

1   Dumpis M.A. Biological activity of fullerenes — reality and prospects / M.A. Dumpis, D.N. Nikolaev, E.V. Litasova, V.V. Iljin, M.A. Brusina , L.B. Piotrovsky // Reviews on Clinical Pharmacology and Drug Therapy. — 2018. — Vol. 16. — P. 4–20. DOI: 10.17816/RCF1614–20.

2   Petrone L. Recombinant HPV16 E7 assembled into particles induces an immune response and specific tumour protection administered without adjuvant in an animal model / L. Petrone, M.G. Ammendolia, A. Cesolini, S. Caimi, F. Superti, C. Giorgi, P. Di Bonito // J. Transl. Med. — 2011. — No. 9. — P. 2–9.

3   Penkova A.V. Fullerene derivatives as nano-additives in polymer composites / A.V. Penkova, S.F. Acquah, L.B. Piotrovskiy, D.A. Markelov, A.S. Semisalova, H.W. Kroto // Russ. Chem. Rev. — 2017. — Vol. 86, No. 6. — P. 530–566. DOI: 10.1070/RCR4712.

4   Piotrovsky L.B. Fullerenes and Viruses / L.B. Piotrovsky, O.I. Kiselev // Fullerenes, Nanotubes and Carbon Nanostructures. — 2005. — Vol. 12, No. 1–2. — P. 397–403. DOI: 10.1081/fst-120027198.

5   Bosi S. Fullerene derivatives: an attractive tool for biological applications / S. Bosi, T. Da Ros, G. Spalluto, M. Prato // Eur. J. Med. Chem. — 2003. — Vol. 38, No. 11–12. — P. 913–923. DOI: 10.1016/j.ejmech.2003.09.005.

6   Ikeda A. Cyclodextrin complexed [60] fullerene derivatives with high levels of photodynamic activity by long wavelength excitation / A. Ikeda, T. Iizuka, N. Maekubo // ACS medicinal chemistry letters. — 2013. — Vol. 4, No. 8. — P. 752–756. DOI:10.1007/s10847–013–0319–9.

7   Mizuno K. Antimicrobial Photodynamic Therapy with Functionalized Fullerenes: Quantitative Structure-activity Relationships / K. Mizuno, T. Zhiyentayev, L. Huang, S. Khalil, F. Nasim, G.P. Tegos, H. Gali, A. Jahnke, T. Wharton, M.R. Hamblin // J. Nanomed. Nanotechnol. — 2011. — Vol. 2, No. 2. — P. 100109–100117. DOI: 10.4172/2157–7439.1000109.

8   Komatsu T. Structural and mutagenic approach to create human serum albumin-based oxygen carrier and photosensitizer / T. Komatsu, A. Nakagawa, X. Qu. // Drug metabolism and pharmacokinetics. — 2009. — Vol. 24, No. 4. — P. 287–299.

9   Bogdanovic V. Fullerenol $C_{60}(OH)_{24}$ effects on antioxidative enzymes activity in irradiated human erythroleukemia cell line / V. Bogdanovic, K. Stankov, I. Icevic, D. Zikic, A. Nikolic // Journal of radiation research. — 2008. — Vol. 49, No. 3. — P. 321–327.

10   Трошина О.А. Водорастворимые производные фуллеренов — потенциальные медицинские препараты / О.А. Трошина, Р.А. Трошин, А.С. Перегудов, Р.К. Любовская // Журн. инновации. — 2007. — № 5. — С. 105. ISSN: 2071–3010.

11   Bhoi V.I. The self-assembly and aqueous solubilization of [60] fullerene with disaccharides / V.I. Bhoi, S. Kumar, C.N. Murthy // Carbohydr. Res. — 2012. — Vol. 359. — P. 120–127. DOI: 10.1016/j.carres.2012.07.010.

12   Bosi S. Synthesis and water solubility of novel fullerene bisadduct derivatives / S. Bosi, L. Feruglio, D. Milic, M. Prato // Eur. J. Org. Chem. — 2003. — P. 4741–4747. DOI:10.1002/ejoc. 200300494.

13   Fazylov S.D. Synthesis and structure of N-methyl-1-phenylfullereno-C-60[1,9]pyrrolidines based on aminoaldehydes / S.D. Fazylov, O.A. Nurkenov, A.E. Arinova, A.P. Tyktarov, A.A. Khuzin, K.M. Turdybekov // Journal of General Chemistry. — 2014. — Vol. 84, No. 10. — P. 2058–2059. DOI: 10.1134/S1070363214100375.

14   Fazylov S.D. Synthesis and Structure of N-methyl-1-[(4-bromo-3,5-dime-thyl-1H-pyrazol-1-yl)phenyl]fullerene-C60-[1,9-c]pyrrolidine / S.D. Fazylov, O.A. Nurkenov, A.E. Arinova, T.M. Seilkhanov, A.R. Tuktarov, A.A. Khuzin, R.E. Bakirova, L.E. Muravleva // Russian Journal of General Chemistry. — 2015. — Vol. 85, No. 5. — P. 1049–1051. DOI: 10.1134/S1070363215050072.

15   Roy P. Exploring the inhibitory and antioxidant effects of fullerene and fullerenol on ribonuclease A. / P. Roy, S. Bag, D. Chakraborty, S. Dasgupta // ACS Omega. — 2018. — Vol. 3, No. 9. — P. 12270–12283. DOI: 10.1021/acsomega.8b01584.

16   Hu Z. Photodynamic anticancer activities of water-soluble C60 derivatives and their biological consequences in a HeLa cell line / Z. Hu, C. Zhang, Y. Huang // Chemico-biological interactions. — 2012. — Vol. 195, No. 1. — P. 86–94.

17   Xu J.-Y. Protective effects of fullerenol on carbon tetrachloride-induced acute hepatotoxicity and nephrotoxicity in rats / J.-Y. Xu, Y.-Y. Su, J.-S. Cheng // Carbon. — 2010. — Vol. 48, No. 5. — P. 1388–1396.

18   Jiao F. Studies on anti-tumor and antimetastatic activities of fullerenol in a mouse breast cancer model / F. Jiao, Y. Liu, Y. Qu // Carbon. — 2010. — V. 48, No. 8. — P. 2231–2243.

19   Djordjevic A. Antioxidant properties and hypothetical radical mechanism of fullerol $C_{60}(OH)_{24}$ / A. Djordjevic, J. Canadanovic-Brunet, M. Vojinovic Miloradov // OxidCommun. — 2005. — Vol. 27, No. 4. — P. 806–812.

20 Injac R. Acute doxorubicin pulmotoxicity in rats with malignant neoplasm is effectively treated with fullerenol $C_{60}(OH)_{24}$ through inhibition of oxidative stress / R. Injac, N. Radic, B. Govedarica // Pharmacological Reports. — 2009. — Vol. 61, No. 2. — P. 335–342.

21 Jiang G. Synthesis and properties of novel water-soluble fullerene-glycine derivatives as new materials for cancer therapy / G. Jiang, F. Yin, J. Duan, G. Li // J. Mater. Sci: Mater. Med. — 2015. — Vol. 26. — P. 1–7. DOI: 10.1007/s10856–014–5348–4.

22 Hu Z. Photodynamic anticancer activities of water-soluble C60 derivatives and their biological consequences in a HeLa cell line / Z. Hu, C. Zhang, Y. Huang // Chemico-biological interactions. — 2012. — Vol. 195, No. 1. — P. 86–94. DOI: 10.1016/j.carbon.2007.10.041.

23 Kotelnikova R.A. Antioxidant properties of water-soluble amino acid derivatives of fullerenes and their role in the inhibition of herpes virus infection / R.A. Kotelnikova, A.V. Smolina, V.V. Grigoryev, I.I. Faingold, D.V. Mishchenko, D.A. Poletaeva // Rus. Chem. Bull. — 2011. — Vol. 6. — P. 1172–1176. DOI: 10.1039/ C4MD00194J.

24 Fazylov S.D. Synthesis of New Chromene-Containing Fulleropyrrolidines / S.D. Fazylov, O.A. Nurkenov, A.E. Arinova, T.M. Seilkhanov, M.K. Ibraev, E.M. Tazhbaev // Journal of General Chemistry. — 2020. — Vol. 90, No. 7. — P. 1143–1145.

25 Teradal N.L. Carbon Nanomaterials in Biological Studies and Biomedicine / N.L. Teradal, R. Jelinek // Adv Healthc Mater. — 2017. — Vol. 6(17). — P. 1700574. DOI: 10.1002/adhm.201700574.

26 Ilyin V.V. The study of the stability of fullerene C60 films / V.V. Ilyin, L.B. Piotrovskii // Reviews on Clinical Pharmacology and Drug Therapy. — 2017. — Vol. 15, No. 2. — P. 42–45.

27 Misra C. Glycinated fullerenes for tamoxifen intracellular delivery with improved anticancer activity and pharmacokinetics / C. Misra, M. Kumar, G. Sharma // Nanomedicine (Lond). — 2017. — Vol. 12, No. 9. — P. 1011–1023. DOI: 10.2217/nnm-0432.

28 Ikeda A. Improved photodynamic activities of liposome-incorporated [60]fullerene derivatives bearing a polar group / A. Ikeda, T. Mae, M. Ueda // Chem Commun (Camb). — 2017. — Vol. 53, No. 20. — P. 2966–2969. DOI: 10.1039/c7cc00302a.

С.Д. Фазылов, О.А. Нүркенов, З.М. Молдахметов, А.М. Ғазалиев,
А.Е. Аринова, М.К. Ибраев, Л.М. Власова, А.С. Фазылов

Фуллерен С60 биологиялық белсенді туындылары. Қазіргі заманғы жағдайы мен даму болашағы

Мақалада С60 фуллереннің ғылыми әдебиеттердегі физикалық-химиялық және биологиялық қасиеттері туралы, сонымен бірге мақала авторларының аминдер мен табиғи алкалоидтарының фуллеренді туындыларын синтездеу реакцияларын зерттеу нәтижелері келтірілген. Заттардың құрылысында фуллеренді фрагменттің болуы оларға жаңа сапалы механикалық, физикалық, химиялық, биологиялық және басқа да қасиеттер әкелетіні наномасштабтық факторлардың пайда болуымен көрсетілген. С60 фуллеренді туындылардың биологиялық қасиеттерінің, құрылысының және суда ерігіштігінің арасындағы байланыс сұрақтары қарастырылған. Фуллерен С60 көптеген мембранотропты, бактериялық, вирустарға қарсы, иммунды түрлендірушілік, АҚТҚ тежеушілік және тағы да басқа қасиеттері бар көптеген түрлендірілген туындыларының биологиялық белсенділік әсерлері зерттелген. Құрамында фуллерені бар препараттардың гепатит С вирусына қарсы, сонымен бірге олардың бос радикалдарды ұстап алу қасиеттері өте жоғары. Фуллерендердің туындыларының сондай-ақ нейротроптылық пен антиоксиданттылық және басқа да тиімді әсерлері бар екені көрсетілген. Мақала авторларының фуллереннің аминотуындыларын синтездеу жұмыстары нәтижелеріне де аса көп көңіл бөлінген.

Кілт сөздер: фуллерен С60, фуллеропирролидиндер, наномасштабты факторлар, аминді фуллерендер, Прато реакциясы.

С.Д. Фазылов, О.А. Нуркенов, З.М. Мулдахметов, А.М. Газалиев,
А.Е. Аринова, М.К. Ибраев, Л.М. Власова, А.С. Фазылов

Биологически активные производные фуллерена С60. Современное состояние и перспективы развития

В статье представлен обзор литературы о физико-химических и биологических свойствах фуллерена С60, а также даны собственные экспериментальные данные авторов по синтезу фуллереновых производных аминов и природных алкалоидов. Показано, что наличие фрагмента фуллерена в структуре соединения обеспечивает значительное улучшение или появление качественно новых механических, химических, физических, биологических и других свойств, связанных с проявлением наноразмерных факторов. Рассмотрены вопросы взаимосвязи структуры, растворимости в воде и биологической активности производных фуллерена С60. Описано множество биологически активных эффектов различных модифицированных производных фуллерена С60, которые обладают мембранотропными, антибактериальными, противовирусными, иммуномодулирующими, ингибирующими ВИЧ ферментными

и другими свойствами. Было отмечено, что препараты, содержащие фрагмент фуллерена, эффективны против вируса гепатита С, а также способны улавливать свободные радикалы. Производные фуллеренов также могут использоваться в качестве антиоксидантных, нейропротекторных и других средств. Особое внимание уделено собственным результатам авторов по синтезу аминопроизводных фуллеренов.

Ключевые слова: фуллерен С60, фуллеропирролидины, наноразмерные факторы, аминопроизводные фуллеренов, реакция Прато.

References

1   Dumpis, M.A., Nikolaev, D.N., Litasova, E.V., Iljin, V.V., Brusina, M.A., & Piotrovsky, L.B. (2018). Biological activity of fullerenes — reality and prospects. *Reviews on Clinical Pharmacology and Drug Therapy, 16*, 4–20.

2   Petrone, L. Ammendolia, M.G., Cesolini, A., Caimi, S., Superti, F., Giorgi, C., & Bonito, P. Di. (2011). Recombinant HPV16 E7 assembled into particles induces an immune response and specific tumour protection administered without adjuvant in an animal model. *J. Transl. Med., 9*, 2–9.

3   Penkova, A.V., Acquah, S.F., Piotrovskiy, L.B., Markelov, D.A., Semisalova, A.S., & Kroto, H.W. (2017). Fullerene derivatives as nano-additives in polymer composites. *Russ. Chem. Rev.*, *86*(6), 530–566.

4   Piotrovsky, L.B., & Kiselev, O.I. (2005). Fullerenes and Viruses. *Fullerenes, Nanotubes and Carbon Nanostructures, 12*(1–2), 397–403.

5   Bosi, S., Da Ros, T., Spalluto, G., Prato, M. (2003). Fullerene derivatives: an attractive tool for biological applications. *Eur. J. Med. Chem., 38(11–12)*, 913–923.

6   Ikeda, A., Iizuka, T., Maekubo, N. (2013). Cyclodextrin complexed [60] fullerene derivatives with high levels of photodynamic activity by long wavelength excitation. *ACS medicinal chemistry letters, 4(8)*, 752–756.

7   Mizuno, K., Zhiyentayev, T., Huang, L., Khalil, S., Nasim, F., & Tegos, G.P., et al. (2011). Antimicrobial Photodynamic Therapy with Functionalized Fullerenes: Quantitative Structure-activity Relationships. *J. Nanomed. Nanotechnol.*, *(2)2,* 100109–100117.

8   Komatsu, T., Nakagawa, A., & Qu., X. (2009). Structural and mutagenic approach to create human serum albumin-based oxygen carrier and photosensitizer. *Drug metabolism and pharmacokinetics, 24(4)*, 287–299.

9   Bogdanovic, V., Stankov, K., Icevic, I., Zikic, D., & Nikolic, A. (2008). Fullerenol $C_{60}(OH)_{24}$ effects on antioxidative enzymes activity in irradiated human erythroleukemia cell line. *Journal of radiation research, 49(3)*, 321–327.

10   Troshina, O.A., Troshin, R.A., Peregudov, A.S., & Liubovskaia, R.K. (2007). Vodorastvorimye proizvodnye fullerenov — potentsialnye meditsinskie preparaty [Water Soluble Derivatives of Fullerenes — Potential Medicines]. *Zhurnal innovatsii — Innovation Magazine, 5,* 105 [in Russian].

11   Bhoi, V.I., Kumar, S., & Murthy, C.N. (2012). The self-assembly and aqueous solubilization of [60]fullerene with disaccharides. *Carbohydr, 359*, 120–127.

12   Bosi, S., Feruglio, L., Milic, D., & Prato, M. (2003). Synthesis and water solubility of novel fullerene bisadduct derivatives. *Eur. J. Org. Chem.*, *23,* 4741–4747.

13   Fazylov, S.D., Nurkenov, O.A., Arinova, A.E., Tyktarov, A.P., Khuzin, A.A., & Turdybekov, K.M. (2014). Synthesis and structure of N-methyl-1-phenylfullereno-C-60[1,9]pyrrolidines based on aminoaldehydes. *Journal of General Chemistry, 84(10)*, 2058–2059.

14   Fazylov, S.D., Nurkenov, O.A., Arinova, A.E., Seilkhanov, T.M., Tuktarov, A.R., & Khuzin, A.A., et al. (2015). Synthesis and structure of N-methyl-1-[(4-bromo-3,5-dime-thyl-1H-pyrazol-1-yl)phenyl] fullerene-C60-[1,9-c]pyrrolidine. *Russian Journal of General Chemistry, 85(5)*, 1049–1051.

15   Roy, P., Bag, S., Chakraborty, D., & Dasgupta, S. (2018). Exploring the inhibitory and antioxidant effects of fullerene and fullerenol on ribonuclease A. *ACS Omega, 3(9)*, 12270–12283.

16   Hu, Z., Zhang, C., & Huang, Y. (2012). Photodynamic anticancer activities of water-soluble C60 derivatives and their biological consequences in a HeLa cell line. *Chemico-biological interactions, 195(1)*, 86–94.

17   Xu, J.-Y., Su, Y.-Y., & Cheng, J.-S. (2010). Protective effects of fullerenol on carbon tetrachloride-induced acute hepatotoxicity and nephrotoxicity in rats. *Carbon, 48(5)*, 1388–1396.

18   Jiao, F., Liu, Y., & Qu, Y. (2010). Studies on anti-tumor and antimetastatic activities of fullerenol in a mouse breast cancer model. *Carbon*, *48(8)*, 2231–2243.

19   Djordjevic, A., Canadanovic-Brunet, J., & Vojinovic Miloradov, M. (2005). Antioxidant properties and hypothetical radical mechanism of fullerol $C_{60}(OH)_{24}$. *OxidCommun.*, *27(4)*, 806–812.

20   Injac, R., Radic, N., & Govedarica, B. (2009) Acute doxorubicin pulmotoxicity in rats with malignant neoplasm is effectively treated with fullerenol $C_{60}(OH)_{24}$ through inhibition of oxidative stress. *Pharmacological Reports, 61(2)*, 335–342.

21   Jiang, G., Yin, F., Duan, J., & Li, G. (2015). Synthesis and properties of novel water-soluble fullerene-glycine derivatives as new materials for cancer therapy. *J. Mater. Sci: Mater. Med., 26*, 1–7.

22   Hu, Z., Zhang, C., & Huang, Y. (2012). Photodynamic anticancer activities of water-soluble C60 derivatives and their biological consequences in a HeLa cell line. *Chemico-biological interactions, 195(1)*, 86–94.

23   Kotelnikova, R.A., Smolina, A.V., Grigoryev, V.V., Faingold, I.I., Mishchenko, D.V., & Poletaeva, D.A. (2011) Antioxidant properties of water-soluble amino acid derivatives of fullerenes and their role in the inhibition of herpes virus infection. *Rus. Chem. Bull., 6,* 1172–1176.

24 Fazylov, S.D., Nurkenov, O.A., Arinova, A.E., Seilkhanov, T.M., Ibraev, M.K., & Tazhbaev, E.M. (2020) Synthesis of New Chromene-Containing Fulleropyrrolidines. *Journal of General Chemistry*, *90(7)*, 1143–1145.

25 Teradal, N.L., & Jelinek, R. (2017). Carbon Nanomaterials in Biological Studies and Biomedicine. *Adv Healthc Mater.*, *6(17)*, 1700574.

26 Ilyin, V.V., & Piotrovskii, L.B. (2017). The study of the stability of fullerene C60 films. *Reviews on Clinical Pharmacology and Drug Therapy, 15(2)*, 42–45.

27 Misra, C., Kumar, M., Sharma, G. (2017). Glycinated fullerenes for tamoxifen intracellular delivery with improved anti-cancer activity and pharmacokinetics. *Nanomedicine (Lond), 12(9)*, 1011–1023.

28 Ikeda, A., Mae, T., & Ueda, M. (2017). Improved photodynamic activities of liposome-incorporated [60]fullerene derivatives bearing a polar group. *Chem Commun (Camb).*, *53(20)*, 2966–2969.

S.Yu. Panshina[1, 2*], O.V. Ponomarenko[3], A.A. Bakibaev[1],
V.S. Malkov[1], O.A. Kotelnikov[1], A.K. Tashenov[3]

[1]National Research Tomsk State University, Russia;
[2]National Research Tomsk Polytechnic University, Russia;
[3]L.N. Gumilyov Eurasian National University, Nur-Sultan, Kazakhstan
(Corresponding author′s e-mail: janim_svetatusik@mail.ru)

Study of glycoluril and its derivatives by ^{1}H and ^{13}C NMR spectroscopy

Bicyclic bisureas, especially 2,4,6,8-tetraazabicyclo[3.3.0.]octan-3,7-dione (glycoluril), have a special place in chemistry of heterocyclic compounds. The carbamide fragment in glycoluril structure determines the properties of the molecule, which are due to the presence of two reaction centers (NH-groups and C=O-groups) in the molecule. In this work, we analyzed the proton and carbon chemical shifts of glycoluril and its derivatives (86 compounds) in the NMR spectra to reveal the effect of the donor-acceptor substituents on the changes in the electron density in the bicyclic framework from the position of symmetry and asymmetry. A general analysis of the 1H and 13C NMR spectra of glycolurils makes it possible to accurately determine the spatial configurations of molecular symmetry, in the presence of which (σ1 and / or σ2) the enantiotopic hydrogen and carbon atoms of the bicyclic framework are manifested by equivalent signals. Also, according to the 1H and 13C chemical shifts in the NMR spectra, glycolurils with electron-acceptor substituents can be clearly distinguished by the shielding of carbon atoms of C=O-groups, and with electron-donating substituents by the deshielding of CH-CH-carbons, due to the rearrangement of electron density and the occurrence of local paramagnetic contributions owing to anisotropy

Keywords: glycoluril, NMR, chemical shifts, symmetry, enantiotopic atoms, shielding, deshielding, X-ray diffraction.

Introduction

In the chemistry of heterocyclic compounds, bicyclic ureas have a special place, among which the greatest interest are 2,4,6,8-tetraazabicyclo[3.3.0.]octan-3,7-dione **1** (glycoluril) (Fig. 1) and its derivatives. The history of glycoluril chemistry dates back to the second half of the 19th century, when a number of researchers succeeded in synthesizing the progenitor 1 of this class of compounds. Since then, the chemistry of glycolurils, first of all, due to polyfunctionality of their structure, has developed rapidly. It was reflected in the creation of valuable substances in various fields of human activity such as disinfectants [1, 2], medicines [3; 86, 4], polymer stabilizers [5], independent explosives or their components [6–8] and other important substances and materials based on these compounds.
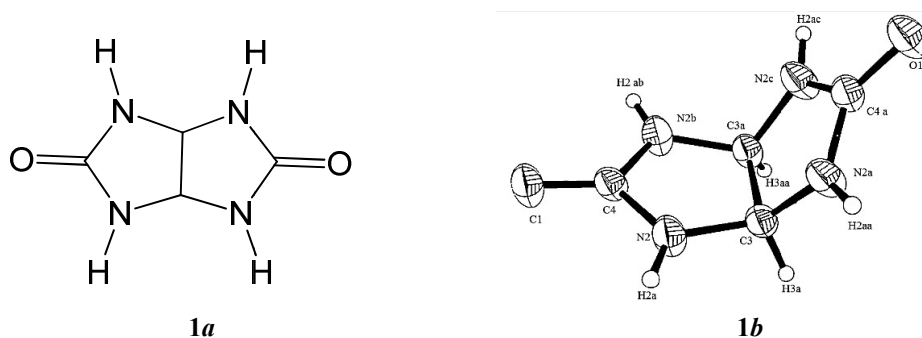
Figure 1. The structural formula of glycoluril 1 (**1a**) and its spatial configuration in the crystal (**1b**)

Glycoluril **1** is a polyfunctional compound in which the carbamide fragment (Fig. 2) essentially determines the properties of the molecule **1** being resulted from the presence of two reaction centers (4 donor groups (–NH) and 2 acceptor groups (C=O)) in the molecule. Glycoluril **1** has the properties of a highly ac-

---

* *Corresponding author*

tive N-nucleophile and a significantly deactivated p-nucleophile. Despite its weak basicity, glycoluril 1 is rather difficult to protonate, but it is capable of N-alkylation, N-acylation, N-halogenation, N-nitration, N-nitrosation, N-hydroxyalkylation reactions, etc. [9; 126–129].
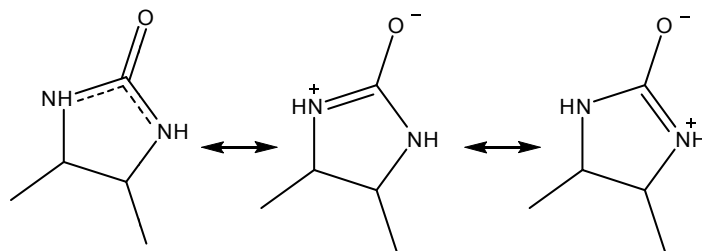
Figure 2. Resonance structures of the carbamide fragment of the glycoluril molecule 1

The synthesis and study of the chemical properties of bicyclic bisureas allows creating of new classes of nitrogen-containing heterocyclic compounds with other practically useful properties. For example, polycyclic condensed systems such as cucurbit[n]urils [10–12] and bambus[n]urils [13, 14], the building blocks of which is glycoluril 1.

Due to the complex structure of glycoluril derivatives, the problem arises of the precise identification of the studied compounds, where the most convenient method for solving structural problems is the method of nuclear magnetic resonance spectroscopy (NMR).

The molecule of glycoluril 1 contains nitrogen, oxygen, carbon and hydrogen atoms, for the analysis of the bonds of which it is convenient to record the spectra on ^{1}H, ^{13}C, ^{15}N, ^{17}O nuclei. NMR spectroscopy on these nuclei can provide enough information to determine the structure of a molecule, its electronic and conformational features. Due to the low content of natural isotopes ^{15}N and ^{17}O, there is no information in the literature on the use of NMR on ^{17}O nuclei for a number of glycolurils. To obtain information of the position of the ^{15}N chemical shifts of glycoluril 1 and its derivatives 2D heterocorrelation of the ^{1}H–^{15}N spectra [15] and the establishment of the direct coupling constant ^{15}N–^{1}H [16] are most often used. Therefore, in this work, we analyzed the chemical shifts (further in the text, CS) of the NMR of glycoluril 1 and its derivatives 2-13, recorded on ^{1}H and ^{13}C nuclei (Table 1-10).

Taking into account the specific and limited solubility of glycoluril 1 and its derivatives 2-13, which depends on the presence of substituents, in practice, the universal solvents DMSO-d$_6$ and D$_2$O are most often used for analysis. N-acylderivatives of glycoluril 12 is convenient to analyze in a CDCl$_3$ solvent to avoid overlapping signals of atoms.

When recording the NMR spectra of glycoluril 1, it was found that in the proton magnetic resonance spectrum there are 2 CS in the regions of 5.24 ppm and 7.16 ppm, which correspond to signals of the CHCH and NH groups, and in the ^{13}C spectrum, the carbons of the CH-CH and C=O groups resonate at 64.60 ppm, 160.30 ppm respectively. These data certainly indicate the spatial symmetry of glycoluril 1. Indeed, in the molecule 1, there are two planes of symmetry σ^1 and σ^2 (Fig. 3), where the plane σ^1 passes along the methine CH–CH bridge, and the plane σ^2 intersects two carbonyl oxygen atoms (Fig. 3) [17].
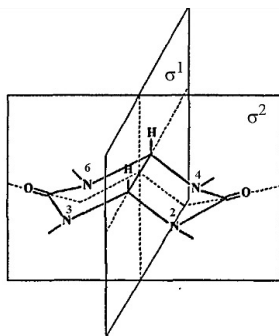
Figure 3. Symmetry planes σ^1 and σ^2 in the molecule of glycoluril 1

However, when studying the crystal structure of glycoluril 1 by X-ray diffraction (Fig. 1b), it was first established [18] that, in addition to symmetry, the conformation of bicyclic framework 1 due to the rigidity

of the cis-joint of annelated imidazolidinone rings has a folded structure in the form of a «half-opened book». The dihedral angle between the imidazolidinone rings in molecule **1** is 124.1°. In addition, it was found that the nitrogen atoms in molecule **1** are located equidistant from each other. The hydrogen atoms of the CH-CH group are cis-oriented, and the imidazolidinone rings are characterized by an almost flat structure with a slight deviation of the C=O groups from the plane.

Thus, the goal of this work was to study CS of glycoluril **1** and its derivatives **2-13** to identify the effect of substituents on changes in electron density in the bicyclic framework, taking into account the symmetry and asymmetry of the 86 molecules considered.

Experimental

The substances **2e–g**, **3c**, **d**, **4b–c**, **5d**, **e**, **g**, **6c–f** were synthesized in accordance with the methods of [9; 113]. NMR spectra for substances **2e–g**, **3c**, **d**, **4b–c**, **5d**, **e**, **g**, **6c–f** were recorded on a Bruker AVANCE III HD spectrometer (Bruker Corporation, Germany) with an operating frequency of 400 and 100 MHz for ^{1}H and ^{13}C nuclei respectively, in a solution of DMSO-d_6 with a concentration of 0.001 mol of the substance in 0.5 ml of solvent. The internal standard is tetramethylsilane (TMS).

Results and Discussion

N-Monosubstituted glycolurils. First of all, it should be noted that with N-monosubstitution in the glycoluril framework, the symmetry of the molecule is violated (glycolurils **2a–g**). In the analyzed molecules **2a–g**, there are no symmetry planes σ^1 and σ^2, which, as we have found, is reflected in the change of CS in the ^{1}H and ^{13}C NMR spectra (Table 1).

T a b l e 1

Chemical shifts of N-monosubstituted glycolurils 2a–g

№	Substituent R_1	^{1}H NMR, ppm, (J/Hz) CH–CH	^{1}H NMR, ppm, (J/Hz) NH	^{13}C NMR, ppm CH–CH	^{13}C NMR, ppm C=O
1[19]	H	5.24 (s. 2H)	7.16 (s. 4H)	64.60	160.30
2a[19]	CH$_3$	5.14 (d. 1H, J = 8.0) 5.19 (d. 1H, J = 8.0)	7.20 (s. 1H) 7.30 (s. 2H)	62.54 69.89	159.75 161.79
2b[20]	CH$_2$CONHCH(CH$_3$)C$_2$H$_5$	5.22 (d. 1H, J = 7.9) 5.29 (d. 1H, J = 7.9)	7.29 (s. 2H) 7.44 (s. 1H)	62.39 68.55	159.40 161.14
2c[21]	CH$_2$CH$_2$N(CH$_3$)$_2$	5.21 (d. 1H, J = 8.2) 5.32 (d. 1H, J = 8.2)	7.29 (s. 1H) 7.40 (s. 2H)	62.24 67.75	159.13 161.00
2d[21]	CH$_2$CH$_2$NHCOCH$_3$	5.18 (d. 1H, J = 8.1) 5.31 (d. 1H, J = 8.1)	7.25, 7.30, 7.39 (3s. 3H)	62.33, 67.74	159.36 161.15
2e	CH$_2$OH	5.45 (d. 1H, J = 8.0) 5.65 (d. 1H, J = 8.0)	7.17, 7.29, 7.22 (3s. 3H)	64.10 67.70	158.30 160.08
2f	COCH$_3$	5.68 (d. 1H, J = 8.0) 5.23 (d. 1H, J = 8.0)	8.55, 7.57, 7.49 (3s. 3H)	61.55 63.24	151.40, 154.80
2g	NO	5.34 (d. 1H, J = 7.6) 5.66 (d. 1H, J = 7.6)	7.94, 7.97, 9.38 (3s. 3H)	62.11 63.48	152.30 160.68
Chemical shift range (Δ)		5.14–5.68	7.17–9.38	61.55–69.89	151.40–161.79

An analysis of the NMR data for compounds **2a–g** shows that in the absence of planes of symmetry σ^1 and σ^2, the protons and carbons of methine (CH–CH) groups appear to be non-equivalent peaks. In the PMR spectra, CH-protons resonate in pairs in the form of doublet signals in the region from 5.1 ppm to 5.7 ppm, and in the ^{13}C NMR spectra, shielding of signals of one CH up to 2 ppm (**2f**) and CH carbon deshielding from the substitution side up to 4.4 ppm (**2a**) relative to the CS of similar glycoluril atoms **1** are observed. The deshielding of CH atoms in substances **2a–e** is probably due to the positive inductive effect of electron-donating substituents on nitrogen atoms [22; 712], which makes its unshared electron pair more available for sharing with a five-membered ring. Such an effect of electron-donating groups makes C–C carbons on the substitution side partially sp^2-hybridized atoms due to an increase in electron density, which shifts the CS of carbon CH to the fields of «molecular currents» or π-conjugated systems.

The CS of NH groups in compounds **2a–g** become unequal and resonate in the form of two or three singlets in the regions from 7.2 ppm to 9.4 ppm. In compounds **2a–e** with electron-donating substituents at nitrogen atoms, a shift in the CS of NH groups in the range of ±0.5 ppm relatively to **1** is observed. These
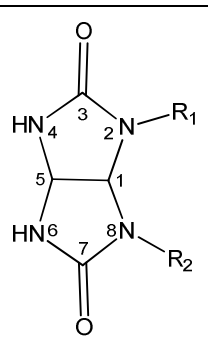
changes indicate a weak effect of the substituents on the inhibition of amide conjugation in the urea fragment of the molecules **2a–g** (Fig. 2). While in the case of substances **2f, g** with acceptor substituents, the CS of the NH group shifts to the low-field region by 2.2 ppm relatively to glycoluril **1**, due to the inductive effect of the substituent on the unshared pair of electrons of the neighboring unsubstituted amino group, which is isolated and not shared with the imidazolidine ring.

The CS of carbons of C=O groups are shielded in substituted imidazolinone rings in average up to 2.0 ppm (**2a–e**), and for compounds **2f, g** with electron-acceptor substituents (–NO, –COCH$_3$) the carbonyl signals shift to the high-field region by 8.9 ppm. The observed effect of strong shielding of the C=O group in compounds **2f, g** is explained by the circulation of electron-acceptor substituents' electrons due to the presence of π-bonds, which leads to the appearance of a field additionally strengthening the external [23; 183] or «anisotropy cone» [24]. This effect is similar for 2,6-N-disubstituted compounds **5e–h** and is shown in Figure 4.

2,8-N-disubstituted glycolurils. The absence of plane of symmetry σ^2 in 2,8-N-disubstituted glycoluril **3a-d** molecules can also be detected in the ^{1}H and ^{13}C NMR spectra (Table 2).

T a b l e 2

Chemical shifts of 2, 8-N-disubstituted glycoluril 3a-d

	№	Substituent	^{1}H NMR, ppm, (J/Hz)		^{13}C NMR, ppm	
		R$_1$	CH–CH	NH	CH–CH	C=O
	1[19]	H	5.24 (s. 2H)	7.16 (s. 4H)	64.60	160.30
	3a[19]	CH$_3$	5.15 (d. 1H, J = 8.4) 5.18 (d. 1H, J = 8.4)	7.39 (s. 2H)	60.63 75.63	160.19
	3b[25]	CH$_2$Ph	4.98 (d. 1H, J = 8.5) 5.39 (d. 1H, J = 8.5)	7.64 (s. 2H)	60.40 70.70	159.70
	3c	CH$_2$OH	5.41 (d. 1H, J = 8.0) 5.58 (d. 1H, J = 8.0)	7.39 (s. 2H)	64.10 67.70	160.90
	3d	COCH$_3$	5.25 (d. 1H, J = 7.2) 6.44 (d. 1H, J = 7.2)	8.74 (s. 2H)	59.50 63.31	154.73
Chemical shift range (Δ)			4.98–6.44	7.39–8.69	59.50–75.63	154.73–160.19

The CS of 2,8-N-disubstituted glycolurils **3a–d** indicates the equivalence of the C=O signals in the ^{13}C spectra and the NH groups in the ^{1}H NMR spectra due to the presence of the plane of symmetry σ^1 of the molecules that passes through the C–C bond. The lack of symmetry along the σ^2 plane is demonstrated by the nonequivalence of carbons and protons of methine groups (CH–CH) in such a way that the carbons resonate with pair signals in the regions of 59.5–75.6 ppm, and the protons appear doublets in the range of 4.9–6.4 ppm.
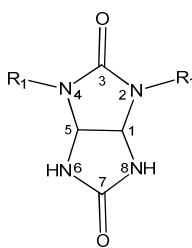
The CS of the NH groups in the compounds **3a–d** appear as singlet peaks, and, in the case of glycolurils **3a–c**, with a shift to a low-field of up to 0.5 ppm, and for 2,8-N-diacetylglycoluril **3d** to 1.6 ppm relatively to **1**. The shielding of carbonyl carbon atoms for compounds **3a–c** is on average 1 ppm. For compound **3d** a shift of CS of the C=O groups to the high-field by 5.6 ppm relatively to the parent **1** is observed. The general character of the shift of the C=O groups signal for **3a–d** is similar to substances **2a–h**, but **2a–h** have in their structure only one substituted imidazolinone ring, and compounds **3a–d** combine the properties of two similarly substituted rings. In the structures of glycolurils **3a–d**, there is a synergistic effect of pairs of substituents on the electronic density of glycoluril framework, distribution of which is reflected in NMR spectra by stronger shielding and deshielding of the corresponding atoms relatively glycoluril **1**. So in ^{13}C NMR spectra of glycolurils **3a–d** there is the shielding of signals of one CH in **3d** (up to 5.1 ppm) and a significantly higher deshielding of CH carbon in **3a–c** from the substitution side (up to 11 ppm) relatively to CS of similar glycoluril atoms **1**. In the latter case, the found effect is due to the positive inductive effect of electron-donating groups to nitrogen atoms [22; 712], which determines the «pushing out» of unshared pairs of nitrogen electrons to C–C carbons from the substitution side, making them partially sp^2-hybridized. This interpretation can explain the shift of CS of CH-carbons to fields of «molecular currents» or π-conjugated systems.

2,4-N-Disubstituted glycolurils. In the molecules of 2,4-N-disubstituted glycolurils **4a–e**, in the case of equivalent substituents, there is a symmetry corresponding to the σ^2 plane. This fact is confirmed by the CS in the NMR spectra (Table 3), where the signals of protons of equivalent NH groups give singlet peaks in the region of 7.5–8.9 ppm, the CS of carbons (62.6–76.7 ppm) and protons (5.1–5.7 ppm) of the CH–CH groups appear in the form of single signals. The absence of symmetry along the σ^1 plane is indicated by nonequivalent CS of C=O-groups.

T a b l e 3

Chemical shifts of 2, 4-N-disubstituted glycolurils 4a–e

	№	Substituent		^{1}H NMR, ppm, (J/Hz)		^{13}C NMR, ppm	
		R_1	R_2	CH–CH	NH	CH–CH	C=O
	1[19]	H	H	5.24	7.16 (s. 4H)	64.60	160.30
	4a[19]	CH$_3$	CH$_3$	5.12 (s. 2H)	7.54 (s. 2H)	76.67	158.22 160.20
	4b	CH$_2$OH	CH$_2$OH	5.55 (s. 2H)	7.47 (s. 2H)	66.86	158.01 161.47
	4c	COCH$_3$	COCH$_3$	5.65 (s. 2H)	8.87 (s. 1H)	62.62	154.68 161.10
	4d[21]	CH$_3$	CH$_2$CH$_2$NHCOCH$_3$	5.10 (d. 1H, J = 8.1) 5.27 (d. 1H, J = 8.1)	7.49 (s. 1H) 7.56 (s. 1H)	66.16 67.93	158.36 161.61
	4e[21]	Ph	CH$_2$CH$_2$NHCOCH$_3$	5.41 (d. 1H, J = 8.3) 5.82 (d. 1H, J = 8.3)	7.71 (s. 1H) 7.87 (s. 1H)	65.11 66.24	155.17 161.11
Chemical shift range (Δ)				5.10–5.82	7.47–8.87	62.62– 76.67	154.68– 161.61

The structures of compounds **4a–e** combine the properties of unsubstituted and disubstituted by nitrogen atoms imidazolinone rings, where the CS of C=O groups for **4a, b, d** in the substituted fragment are shielded by an average of 2.0 ppm, and in the case of compounds **4c, e** with substituents of acceptor type — up to 5.5 ppm relatively to glycoluril **1**. In the unsubstituted cycle of compounds **4a–e**, on the contrary, carbonyl carbon atoms are deshielded up to 1.3 ppm compared to **1**.

For compounds **4a** and **4c**, the symbatic effect of two substituents is observed. Acetyl substituents (**4c**) lower the electron density of the adjacent annelated ring, this is reflected in the shift of the CS of NH groups by 1.7 ppm in a low-field relatively to **1**. Methyl substituents in **4a** increase the electron density in the disubstituted cycle, which affects the deshielding of signals of CH–CH groups by 12 ppm relatively to **1**.
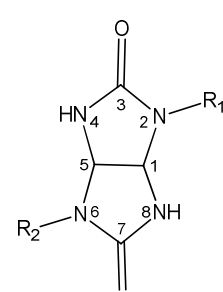
In compounds **4a, b, d**, aminogroups are deshielded by an average of 0.5 ppm, which corresponds to the range of compounds **2, 3** considered above with electron-donating substituents at nitrogen atoms.

The presence of various functional groups at 2,4-N-positions in compounds **4d** and **4e** leads to asymmetry of the molecule and, accordingly, to a change in the number of signals in the NMR spectra for NH, C=O, and CH-CH groups. For the substance **4e**, the CS of unsubstituted NH groups also reflect a moderate acceptor effect of the phenyl substituent, which deshields NH by 0.7 ppm relatively to **1**.
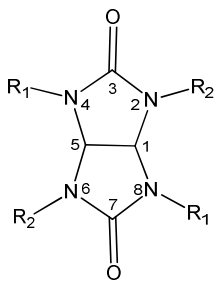
2,6-N-disubstituted glycolurils; and 2,4,6,8-N-tetrasubstituted glycolurils. Similarly to the glycoluril molecule **1**, 2,6-N-di- **5a–h** (Table 4) and 2,4,6,8-N-tetra-substituted compounds **6a–i** (Table 5) have two planes of symmetry (σ^1 and σ^2). In ^{1}H NMR spectra of substances **5a–h** and **6a–i**, we observe the equivalent singlets of protons of CH–CH groups of a bicyclic framework and in ^{13}C NMR spectra the equivalent CS of CH–CH and C=O groups, as well as singlet peaks of two unsubstituted NH-groups in **5a–h**.

T a b l e 4

Chemical shifts of symmetric 2, 6-N-disubstituted glycoluril 5a–h

	№	Substituent	^{1}H NMR, ppm, (J/Hz)		^{13}C NMR, ppm	
		R_1	CH-CH	NH	CH-CH	C=O
	1[19]	H	5.24 (s. 2H)	7.16 (s. 4H)	64.60	160.30
	5a[19]	CH$_3$	5.10 (s. 2H)	7.57 (s. 2H)	67.39	159.66
	5b[26]	CH$_2$C$_6$H$_5$	5.04 (s. 2H)	7.81 (s. 2H)	64.88	158.86
	5c[27]	CH$_2$CH$_2$NHCOCH$_3$	5.25 (s. 2H)	7.49 (s. 2H)	65.40	159.20
	5d	CH$_2$OH	5.53 (s, 2H)	7.61 (s. 2H)	66.34	160.56
	5e	COCH$_3$	5.66 (s. 2H)	8.85 (s. 2H)	61.80	154.34
	5f[28]	COCH$_2$Cl	5.34 (s. 2H)	8.83 (s. 2H)	63.32	154.03
	5g	NO	5.64 (s. 2H)	9.96 (s. 2H)	60.19	152.00
	5h[29]	NO$_2$	6.03 (s. 2H)	9.83 (s. 2H)	63.80.	149.00
Chemical shift range (Δ)			5.10–6.03	7.49–9.96	60.19–67.39	149.00–160.56

T a b l e 5

Chemical shifts of symmetric 2, 4, 6, 8-N-tetrasubstituted glycolurils 6a–i

№	Substituent		^{1}H NMR, ppm, (J/Hz)	^{13}C NMR, ppm	
	R_1	R_2	CHCH	CHCH	C=O
1[19]	H	H	5.24 (s. 2H)	64.60	160.30
6a[19]	CH_3	CH_3	5.06 (s. 2H)	71.92	159.05
6b[26]	$CH_2C_6H_5$	$CH_2C_6H_5$	4.84 (s. 2H)	67.71	159.54
6c	CH_2OH	CH_2OH	5.59 (s. 2H)	70.65	158.62
6d	CH_2OCH_3	CH_2OCH_3	5.52 (s. 2H)	74.86	158.45
6e	Cl	Cl	5.48 (s. 2H)	72.72	160.51
6f	$COCH_3$	$COCH_3$	6.33 (s. 2H)	62.69	151.58
6g[31]	NO_2	NO_2	7.77 (s. 2H)	65.90	142.40
6h[20]	CH_3	CH_2NHSO_2Ph	4.70 (s. 2H)	66.75	156.80
6i[20]	C_2H_5	CH_2NHSO_2Ts	4.65 (s. 2H)	65.38	156.85
Chemical shift range (Δ)			4.65–7.77	62.69–74.86	142.40–163.81

Structures **5a–h** are two annelated monosubstituted imidazolinone rings with *anti*-arrangement of substituents relatively to each other.

The type of the action of the substituents on the shift of the signals of NH groups to a low-field for substances **5a–h** is similar to compounds **2, 3** considered above. In the substances **5a–d**, electron-donating substituents of nitrogen atoms deshield the nuclei of NH groups by 0.6 ppm, and acceptor substituents (**5e–h**) deshield the CS of NH groups at 2.8 ppm relatively to **1**.

The CS of C=O-group carbons undergo shielding on average up to 1.5 ppm (**5a–d**), and for compounds **5e–h** with electron-acceptor substituents on nitrogen atoms, a synergy of electronic effects with shielding of carbonyl signals by 11 ppm is observed, which is due to the formation of π-electron shielding regions (Fig. 4, **5e**).
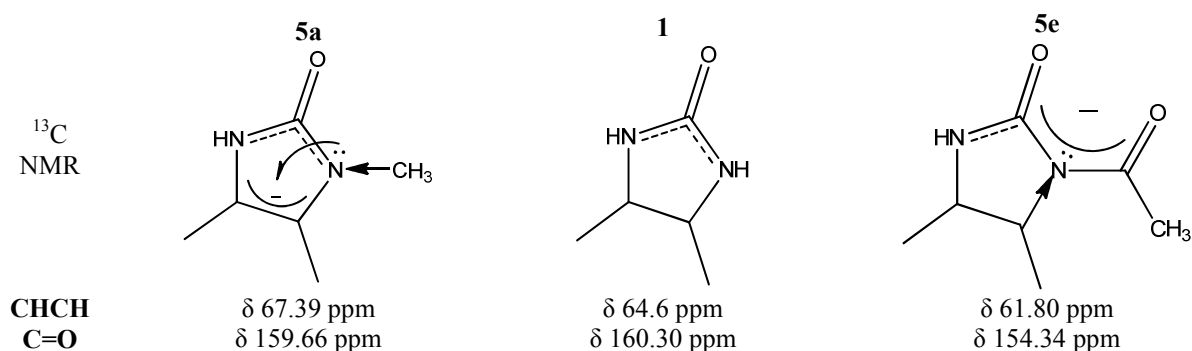
Figure 4. Diagram of the distribution of electron density in the imidazolinone fragment of glycolurils **1, 5a, 5e**

It was found, that the CS of CH–CH protons in compound **5h** is most deshielded compared to **5a–g** and is shifted to the low-field region by 0.8 ppm relatively to **1**. This effect can be explained by the spatial intramolecular interaction of nitrogroups with methine protons, which was discovered by studying the substance **5h** by X-ray diffraction analysis (Fig. 5, **5h**) [30], where it is reported that one of the oxygen atoms of the two nitrogroups is maximally reversed towards the *cis*-protons of the methine bridge.

The structures of compounds **6a–i** combine the properties of two N-disubstituted imidazolidinone rings, where for substances **6f, g,** the symbatic effect of 4 acceptor substituents is reflected in the spectral data. In this case, shielding of C=O groups to 17.9 ppm relative to **1** is observed. Electron-donating substituents in glycolurils **6a–e**, **h**, **i** increase the electron density in disubstituted imidazolinone rings, which is shown in ^{13}C NMR spectra by deshielding of CH-CH carbons to 10.2 ppm relatively to **1**.

In the PMR spectra of compounds **6f, g**, the singlets of protons CH-CH are most deshielded compared to the CS of the corresponding atoms of compounds **6a–e**, **h**, **i** and are shifted to a low-field by more than 1.1 ppm (**6f**) and 2.5 ppm (**6g**) relative to **1**. Intramolecular interactions between substituents (-$COCH_3$, -NO_2) and *cis*-protons of the CH–CH groups may be present in these compounds. In the case of tetraacetylsubstituted glycoluril **6f**, these interactions were recorded by X-ray diffraction [32] (Fig. 5, **6f**),

where it was shown that the oxygen atoms of the two most twisted acetylgroups are maximally turned toward the protons of the methine bridge.

5h

6f
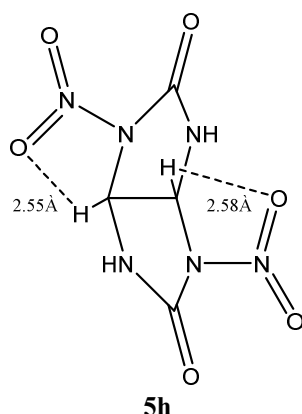
Figure 5. Intermolecular interactions between the oxygen atoms of the substituents and the protons of the methine bridge in 2,6-N-dinitroglycoluril **5h** according to X-ray diffraction data
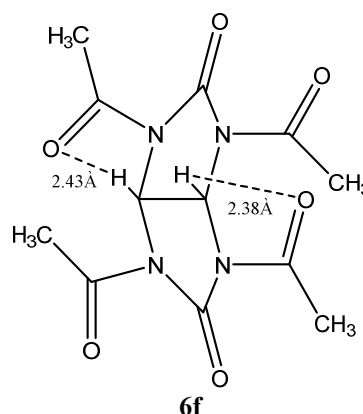
Figure 6. Intermolecular interactions between the oxygen atoms of the substituents and the protons of the methine bridge in 2, 4, 6, 8-N-tetraacetyl glycoluril **6f** according to X-ray diffraction data

2,4-N-Dimethylderivatives of glycoluril. Comparing CS of **1** and substances **2a**, **3a**, **4a**, **5a**, **6a**, it should be noted that the presence of CH_3 groups at nitrogen atoms causes deshielding of CH-carbon signals by an average of 10 ppm. Based on these data, CS in the series of asymmetric 2,4-N-dimethylderivatives of glycolurils **7a–f** are further considered (Table 6).

Table 6

Chemical shifts of asymmetric 2,4-N-dimethylderivatives of glycolurils 7a–f

	№	Substituting group	^{1}H NMR, ppm, (J/Hz)		^{13}C NMR, ppm	
		R_1	CH–CH	NH	CH–CH	C=O
	1[19]	-	5.24 (s. 2H)	7.16 (s. 4H)	64.60	160.30
	4a[19]	H	5.12 (s. 2H)	7.54 (s. 2H)	76.67	158.22
	7a[19]	CH_3	5.08 (d. 1H, J = 8.3) 5.22 (d. 1H, J = 8.3)	7.62 (s. 2H)	65.30 72.92	158.07 159.54
	7b[20]	CH_2COOH	5.15 (d. 1H, J = 8.3) 5.22 (d. 1H, J = 8.3)	7.90 (s. 1H)	65.93 71.85	158.08 160.05
	7c[21]	C(CH_3)_2COOH	5.18 (d. 1H, J = 8.1) 5.41 (d. 1H, J = 8.1)	7.77 (s. 1H)	66.51 70.54	158.45 160.09
	7d[21]	CH_2CH_2NH(CH_3)_2Cl	5.16 (d. 1H, J = 9.5) 5.34 (d. 1H, J = 9.5)	7.91 (s. 1H)	65.81 70.92	158.43 159.45
	7e[21]	CH_2CH_2NHCOCH_3	5.06 (d. 1H, J = 8.3) 5.22 (d. 1H, J = 8.3)	7.65 (s. 1H)	65.65 71.31	158.25 159.51
	7f[27]	N=CHPh	5.33 (d. 1H, J = 8.4) 5.62 (d. 1H, J = 8.4)	8.43 (s. 1H)	63.10 72.10	156.70 157.60
Chemical shift range (Δ)			5.06–5.61	7.54–8.42	63.10– 76.67	156.00– 160.09

When analyzing the CS of 2,4-N-dimethylglycolurils **7a–f**, the asymmetry of the structures is clearly distinguished. The carbon atoms of the carbonyl groups of compounds **7a–e** shift toward a high-field in the range from 0.2 ppm up to 2.2 ppm relative to the CS C=O of glycoluril **1**. For compound **7f** shielding of the carbonyl group to 4.3 ppm, and the shift of the CS of NH groups to a low-field by 1.3 ppm relative to **1** are observed, which is probably due to the positive mesomeric and negative inductive effect of the N=CHPh substituent.

In the spectra of compounds **7a–f**, the highest deshielding of CH-carbons up to 8.3 m from the N-2,8-disubstitution of the molecule was recorded, and the CS of the neighboring CH carbons are manifested in NMR spectra with a shift of ±1.5 ppm relative to **1**.

Tricycles and tetracycles. It was interesting to trace the influence of the hard formation of substituents in polycyclic structures **8a–c** and **9a–c** on the CS of the reference atoms of NH, CH–CH, C=O groups of the glycoluril framework (Table 7).

Table 7

**Chemical shifts of asymmetric tricyclic 8a–c
and symmetric tetracyclic structures 9a–c, derivatives of glycoluril 1**

№	Substituting group		^{1}H NMR, ppm, (J/Hz)		^{13}C NMR, ppm	
	R$_1$	R$_2$	CH-CH	NH	CH-CH	C=O
1[19]			5.24 (s. 2H)	7.16 (s. 4H)	64.60	160.30
8a[20, 33]	t-Bu	C$_2$H$_5$	5.25 (d. 1H, J = 8.0) 5.52 (d. 1H, J = 8.0)	8.03 (s. 1H)	63.40 64.20	157.20 159.40
8b[20, 33]	t-Bu	Pr	5.20 (d. 1H, J = 8.0) 5.52 (d. 1H, J = 8.0)	8.00 (s. 1H)	63.40 64.30	157.30 159.50
8c[20, 33]	t-Bu	s-Bu	5.25 (d. 1H, J = 8.0) 5.51 (d. 1H, J = 8.0)	7.92 (s. 1H)	63.39 64.35	157.02 159.28
9a[20]	c-C$_6$H$_{11}$	c-C$_6$H$_{11}$	5.50 (s. 2H)	–	64.27	159.27
9b[20]	(CH$_2$)$_2$COOH	(CH$_2$)$_2$COOH	5.56 (s. 2H)	–	64.42	159.37
9c[20]	CON(CH$_3$)$_2$	CON(CH$_3$)$_2$	5.59 (s. 2H)	–	53.18	160.02
Chemical shift range (Δ)			5.20–5.59	7.92–8.03	53.18–64.42	157.02–160.02

Analysis of the CS of tricyclic pentaazabicyclo[5.3.1.0]undecane-1,5-diones **8a–c** and tetracyclic hexahydrohexaazacyclopeite[*def*]fluoren-4,8-diones **9a–c** made it possible to establish that these substances do not have significant differences in NMR signals for glycoluril scaffolds indicating the presence of polycyclicity and a rigid frame. It was found that the CS of CH-CH carbons in the **9c** polycycle are shielded by 11 ppm, relative to **1**, which is probably due to the additional shielding field, created by the π-group of NCON(CH$_3$)$_2$.

The obtained values of CS make it possible to conclude that there is no symmetry in **8a–c** molecules and its presence in **9a–c** substances.

1,5-C-Substituted glycolurils. In comparison with N-substituted tetracycles **9a–c,** in the NMR spectra of 1,5-C-substituted glycolurils **10a–h** and their diester polycyclic derivatives **11a–d**, the influence of ether fragments on the CS of atoms of the glycoluril framework is noticeable (Table 8).

From the obtained data of ^{13}C NMR spectra of substances **10a–h**, **11a–d**, it is seen that the diester fragments shield the signals of the carbon of C–C and C=O groups by an average of 2 ppm.

In compounds **10a–d**, **11a**, **b**, **d**, the CS of C$_1$–C$_5$ carbons, due to their «Quaternary», are shifted to the low-field up to 10 ppm on average and in the case of phenyl substituents at C$_1$-C$_5$ atoms in substances **10e–g**, **11c** up to 15 ppm.

The drift of the CS of NH-groups of substances **10a–h** directly depends on the nature of the substituent at the C–C bond. Thus, electron-donating substituents in substances **10a–d** cause a displacement of the CS on average ± 0.5 ppm relative to **1**, and the inductive effect of electron-withdrawing substituents in substances **10e–h** deshields the nuclei of NH group protons by 0.6–1.6 ppm relative to **1**.

It is noteworthy, that acceptors at the 1, 5-C-substitution (**10e–h**) do not affect the shielding of C=O in ^{13}C NMR spectra as compared to the N-substitution (**2f**, **g**, **3d**, **4c**, **e**, **5e–h**, **6f**, **g**, **7f**), which probably indicates the absence in this case of the formation of π-electronic «anisatropy cones» with an additional shielding field.

T a b l e 8

Chemical shifts of symmetric 1,5-C-substituted glycolurils 10a–h and their diester polycyclic derivatives 11a–d

№	Substituting group		^{1}H NMR, ppm, (J/Hz)		^{13}C NMR, ppm	
	R_1	R_2	CH-CH	NH	CH-CH	C=O
1[19]			5.24	7.16 (s. 4H)	64.60	160.30
10a[34, 35]	CH_3	CH_3		7.10 (s. 4H)	75.20	159.30
10b[34]	H	CH_3	4.8 (s. 1H)	7.10 (s. 2H) 7.20 (s. 2H)	69.80 73.10	160.30
10c[34]	CH_3	C_2H_5		7.10 (s. 2H) 7.20 (s. 2H)	77.80	159.70
10d[34]	-CH$_2$CH$_2$CH$_2$CH$_2$-			7.00 (s. 4H)	73.60	160.30
10e[34, 35]	C_6H_5	C_6H_5		7.80 (s. 4H)	81.70	160.60
10f[35]	3-ClC$_6$H$_4$	3-ClC$_6$H$_4$		7.98 (s. 4H)	81.30	160.40
10g[35]	4-ClC$_6$H$_4$	4-ClC$_6$H$_4$		7.88 (s. 4H)	81.20	160.30
10h[36]	CF_3	CF_3		8.83 (s. 4H)	77.11	158.27
11a[34, 37]	CH_3	CH_3		–	73.40	157.40
11b[34]	CH_3	C_2H_5		–	73.40 75.60	157.60
11c[34, 37]	C_6H_5	C_6H_5		–	79.00	158.00
11d[38]	–CH$_2$CH$_2$CH$_2$CH$_2$–			–	72.20	158.00
Chemical shift range (Δ)				7.00–8.83	69.80–81.70	157.40–160.60

C,N-Substituted glycolurils. In considering particular cases — compounds **12a–k** (Table 9) and **13a–r** (Table 10) with a mixed type of N- and C-substitution the ^{13}C NMR spectra are the most informative for the analysis of electronic properties and conformational changes in the glycoluril framework. In the presence of an unsubstituted NH group, its signals in the PMR spectra are observed in the region of 5.91–6.19 ppm for **12a–k** and 7.95–8.66 for **13a–r**.

T a b l e 9

Chemical shifts of 1,5-C-dimethyl-2,6-N-dimethylglycolurils 12a-k

	№	Substituting group		^{1}H NMR, ppm, (J/Hz)	^{13}C NMR, ppm	
		R_1	R_2	NH	CH-CH	C=O
1	2	3	4	5	6	7
	1[19]	-	-	7.16 (s. 4H)	64.60	160.30
	12a[39]	H	H	5.91 (s. 1H)	74.70 83.10	161.00
	12b[39]	CH_3CO	H	6.00 (s. 1H)	76.40 78.50	153.00 157.20
	13c[40]	$CH_3(CH_2)_8COCH_2CO$	H	6.05 (s. 1H)	76.60 76.71	152.73 157.14
	12d[39]	$CH_3CH=CHCO$	H	6.13 (s. 1H)	76.20 78.20	152.60 157.10
	12e[39]	CH_3COCH_2CO	H	5.95 (s. 1H)	76.60 78.70	152.80 157.10
	12f[39]	$(CH_3)CCOCH_2CO$	H	6.04 (s. 1H)	78.60 86.60	152.60 157.20
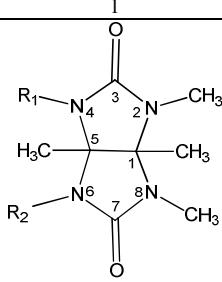
1	2	3	4	5	6	7
	12g[39]	CH₃C(OH)CH₂CO	H	6.19 (s. 1H)	76.70 78.70	152.09 157.10
	12h[39]	CH₃COCH(CH₃)CO	H	5.94 (s. 1H)	76.90 78.90	153.00 157.20
	12i[39]	CH₃CO	CH₃CO	-	77.30 80.40	153.10
	12j[39]	(CH₃)₃CCO	CH₃CO	-	78.40 80.50	152.80 153.60
	12k[39]	CH₂=CHCO	CH₃CO	-	77.90 80.50	153.00
Chemical shift range (Δ)				5.91–6.19	74.70–86.60	152.09–161.00

Structure label: Solvent CDCl₃ (R₁–N4–3–N2–CH₃; H₃C–5–CH₃; R₂–N6–7–8N–CH₃)

Table 10

Chemical shifts of 1, 5-C-diphenylglycoluril 13a–r

	№	Substituting group			¹H NMR, ppm, (J/Hz)	¹³C NMR, ppm	
		R₁	R₂	R₃	NH	CH-CH	C=O
	13a [41]	CH₃	CH₃	H	8.31 (s. 2H)	83.70	159.00 160.10
	13b[21, 42]	CH₃	CH₃	(CH₂)₂OH	8.54 (s. 1H)	82.64 87.74	158.62 159.86
	13c[21, 42]	CH₃	CH₃	CH₂COOH	8.61 (s. 1H)	82.85 87.05	158.58 159.46
	13d[21, 43]	CH₃	CH₃	CH₂COOCH₃	8.66 (s. 1H)	83.00 87.98	158.64 158.94
	13e[21]	CH₃	CH₃	(CH₂)₂NH(CO)CH₃	7.95 (s. 1H)	82.48 87.64	158.42 159.52
	13f[27]	CH₃	CH₃	(CH₂)₂N(CH₃)₂	8.49 (s. 1H)	83.00 87.90	158.40 161.00
	13g[21]	H	CH₂COOCH₃	CH₂COOCH₃	8.28 (s. 2H)	83.70	158.69
	13h[21]	CH₂COOCH₃	H	CH₂COOCH₃	8.29 (s. 2H)	79.95 88.28	159.00
	13i[21]	(CH₂)₂OH	H	(CH₂)₂OH	8.16 (s. 2H)	79.44 89.79	160.28
	13j[21]	(CH₂)₂OH	H	CH₃	8.11 (s. 2H))	79.11 89.05	159.59 160.09
	13k[21]	(CH₂)₂OH	H	CH₂COOPr-i	8.12 (s. 1H) 8.26 (s. 1H)	79.85 89.02	159.12 159.92
	13l[21]	CH₃	H	n-Bu	7.98 (c. 1H) 8.11 (s. 1H)	79.02 89.04	159.65
	13m[21]	CH₃	H	COOPr-i	8.10 (s. 1H)	79.37 88.44	159.10 159.36
	13n[21]	CH₃	H	(CH₂)₂NH⁺(CH₃)₂Cl	8.23 (s. 1H) 8.40 (s. 1H)	79.33 89.17	159.52 159.84
	13o[21]	CH₃	H	(CH₂)₃COOPr-i	8.04 (s. 1H) 8.14 (s. 1H)	79.03 89.07	159.63
	13p[21]	CH₃	H	(CH₂)₃CHCOOHNH₂	8.08 (s. 1H) 8.12 (s. 1H)	79.00 89.19	158.78 159.68
	13q[21]	CH₃	H	COOPr-i	8.26 (s. 1H)	79.37 88.44	159.10 159.36
	13r[27]	(CH₂)₃COOCH₃	H	(CH₂)₃COOCH₃	8.21 (s. 1H)	83.90	159.00
	Chemical shift range (Δ)				7.95–8.66	79.00–89.79	158.40–161.00

Structure label (left of Table 10): R₁–N4–3–N2–R₂; Ph–5–1–Ph; R₃–N6–7–8NH; with O atoms.

It should be noted that in the analysis of the CS of 1,2,5,6-tetramethylglycolurils **12a–k**, the solvent plays an important role, because the spectra of these compounds were recorded in the $CDCl_3$ solvent and the proton signals of unsubstituted NH-groups are shifted to the region of high-field (5.9–6.2 ppm) relative to **1**, due to the absence of interactions with the solvent. In this case, the effect of the solvent on the CS of carbon atoms is negligible.

In 1,2,5,6-tetramethylglycolurils **12a–k**, the CH-carbon signals are deshielded due to their «Quaternary», on average, by 10 ppm, and in N-alkylglycoluril **12a** from the N-dimethyl substitution side, up to 22 ppm, relative to the CS of glycoluril **1**. In this case, the positive mesomeric effect of methyl groups [22; 712] «pushes out» an unshared pair of electrons from nitrogen atoms to generalize with the ring, partially hybridizing neighboring C–C atoms to the sp^2 state.

The CS of the C=O groups of compounds **12b–k** (field interval from 152.1 ppm to 157.2 ppm) demonstrate the presence of acceptor acylsubstituents as π-electron groups that create «anisatropy cones» (Fig. 4), due to which shielding occurs of carbonyl carbon relative to **1** and **12a**.

After analyzing the NMR data for compounds **13a–r** (Table 10), it is possible to clearly determine the presence of symmetry in the molecules and its type (σ^1 or σ^2).

The CS of NH-protons of 1,5-C-diphenylglycolurils **13a–r** appear singlet peaks and are shifted to a low-field by 0.8–1.5 ppm relative to **1**, which may be due to the electron-withdrawing effect of phenyl substituents. The effect of the latter is also clearly observed in unsubstituted at nitrogen atoms diphenylglycoluril **10e** (Table 8, (7.80 ppm)).

Carbons of the methine group in substances **13a–r** are deshielded at 14.4–24.6 ppm relative to 1, where the largest shift of the CS of C5-carbon to the low-field region is observed from the 4, 6-N-substitution side.

Conclusions

The analysis of CS in the NMR spectra of glycoluril **1** and its derivatives **2–13** (86 compounds in total) makes it possible to accurately identify the spatial symmetry configurations of glycolurils, in the presence of which (σ^1 and/or σ^2) one half of the molecule is a mirror image of the other, where the enantiotopic hydrogen and carbon atoms of the bicyclic framework are manifested by equivalent signals.

In the NMR spectra of asymmetric derivatives of glycolurils, in particular N-monosubstituted **2**, N-trisubstituted **7**, tricyclic derivatives **8** and glycolurils with a mixed type of N-,C,C-substitution **12**, **13**, it is seen that the molecules lose the symmetry planes σ^1 or σ^2 and the equivalent CS of protons and carbons of glycoluril bicycles manifest as nonequivalent peaks

Molecules **3** having one plane of symmetry σ^1 give equivalent signals of carbonyl carbons and singlet signals of two unsubstituted NH-groups, but protons and carbons of the CH–CH fragment in such symmetric molecules resonate in pairs. Glycolurils with the symmetry plane σ^2 (**4**), on the contrary, are identified only by nonequivalent CS of C=O-groups.

The CS of ^{1}H and ^{13}C of the glycoluril framework of the symmetric molecules N-anti-**5**, N-tetra-**6**, and C-substituted compounds **10**, **11** are present in the NMR spectra in the form of equivalent singlet signals, which indicates the presence of symmetry planes σ^1 and σ^2 in the molecules.

In the presence of alkylsubstituents at the nitrogen atoms in the structures of the studied glycolurils **2–13**, the shielding of C=O by 1-3 ppm relative to the signal C=O glycoluril **1** is observed, which can be determined by the effects of steric inhibition of conjugation in the amide fragment with a corresponding decrease in the order of the amide bond [44]. However, in the study of N-alkylglycolurils by the X-ray diffraction method [45], it was determined that nitrogen atoms with their unshared electron pairs participate in conjugation with C=O groups and have a flattened geometry; therefore, N-C(Alk) bonds are almost coplanar to the rings. In the presence of a decrease in the order of the amide bond, the coplanarity of this fragment should probably be violated, as in the case of glycolurils with acceptor substituents [30, 46].

It was shown that for mono- (**2**) and disubstituted glycolurils (**3, 4, 5**) at nitrogen atoms, the positions of the signals of unsubstituted NH groups in the NMR spectra are in the range from 7.0 ppm up to 9.9 ppm.

In the presence of electron-donating substituents in the structures of substances **2a–e**, **3a–c**, **4a**, **b**, **d**, **5e–h**, **7a–e**, the shift of the CS of the NH-groups occurs in the range of ± 0.6 ppm. relative to **1**, which indicates a weak effect of substituents for inhibition of amide conjugation. And in the presence of acceptor substituents in substances **2f**, **g**, **3d**, **4c**, **5e–h**, **7f**, the CS of the NH-group shifts in the low-field region. Moreover, the stronger the inductive effect of the acceptor, the farther the position of the signal in the PMR spectrum (up to 9.9 ppm, (**5g, h**), glycoluril **1** (7.14 ppm)). This fact is explained by a violation of the electron density of the amide fragment (Fig. 2), where the substituents reduce the bond multiplicity and the unshared

pair of electrons of the neighboring unsubstituted NH group is isolated from the plane of the imidazolinone ring. Such regularities are also observed for 1, 5-C-substituted glycolurils **10**, **12**, **13**, where electron-donating substituents in substances **10a–d** cause a shift of the CS of NH-groups on average ±0.5 ppm, relative to **1**. The negative inductive effect of electron-withdrawing substituents in substances **10e–h**, **13a–r** redistributes the electron density from imidazolinone rings, thereby the nuclei of NH-groups are deshielded by 0.6–1.6 ppm, relative to **1.**

In the ^{13}C NMR spectra of compounds **2f**, **g**, **3d**, **4c**, **5e–h**, **7f**, **12b–k**, in which substituents with an electron-withdrawing property are present, shielding of the C=O signal to 18 ppm is observed, moreover, the stronger its acceptor character, the signal C=O shifts more to the region of a high-field. There are a number of factors [47; 163] that can affect the shielding constant of the carbonyl fragment in glycolurils **2–13** of which the most significant are the hybridization and resonance effects of substituents with magnetic anisotropy of neighboring groups. In the presence of an electron-withdrawing substituent at nitrogen atoms in the glycoluril framework, more efficient hybridization of carbonyl carbon atoms to the sp^2 state and in the C–N fragment to the sp^3 state occurs [48]. An additional effect is exerted by the circulation of electrons of electron-withdrawing substituents with the presence of π-bonds [23; 183], which leads to the appearance of additional fields or «anisotropy cones» (Fig. 4). This circumstance mainly depends on the geometry of the molecule [24].

It should be added that the shielding of carbonyl carbon in the ^{13}C NMR spectra correlates with the C=O bond length established by X-ray diffraction studies [18, 30, 32]. In compounds **5h** and **6f**, the nuclei of carbonyl carbon atoms show the CS at 149.00 ppm and 151.58 ppm respectively, and the length of C=O bond is on average 1.19 Å, whereas the CS of the carbonyl carbon atoms of glycoluril **1** is 160.30 ppm, and the length of the C=O bond is 1.21 Å. Thus, the results of NMR and X-ray diffraction studies of compounds **5h** and **6f** are consistent with each other and complement each other.

In compounds with electron-donating substituents at nitrogen atoms (in substances **2f**, **g**, **3d**, **4c**, **5e–h**, **7f**, **12b–k**), deshielding of C–C-carbon signals on average by 10–22 ppm is observed, which also can be explained by the general redistribution of electron density in imidazolinone cycles. Thus, the enhanced electron supply by electron-donating groups to nitrogen atoms [22; 712] affects the possibility of pairing its unshared pair of electrons with a five-membered cycle. Therefore, C-C-carbons can partially acquire the properties of sp^2-hybridized atoms due to an increase in the electron density, which shifts the CS carbon in the field of «molecular currents» or π-conjugated systems. In this case, a local paramagnetic contribution arises due to the anisotropy of the electron density distribution on C–C carbons for which the CS is measured.

Around the C–C nuclei, an electron circulation occurs, which creates either a secondary magnetic field in the same direction as the superimposed field, or a diamagnetic field that is weaker due to circulation restrictions, which makes a significant contribution to the CS of the CH–CH groups. A similar effect in the case of other nuclei (N, F, O) is observed, in which the ground and excited states are closer in energy [50].

However, anisotropic electron circulation for CH-CH proton atoms in **2f**, **g**, **3d**, **4c**, **5e–h**, **7f**, **12b–k**, substances is not observed, because the excitation energies of empty orbitals of a hydrogen atom with higher energies are very high. The excited state is far removed from the ground one, and this effect can only make an insignificant contribution to most the CS of protons [49; 163].

In a general analysis of the ^{1}H and ^{13}C NMR spectra of glycolurils **1–13**, it is clearly seen that for any type of N-,C-substitution, shielding of the carbonyl atom C=O in the imidazolidinone ring is observed.

Thus, in this work, an analysis of the nuclear magnetic resonance for glycoluril derivatives was carried out, where the NMR signals were characterized from the position of molecular symmetry and the nature of the substituents.

The generalization performed makes it possible to distinguish between symmetric and asymmetric molecules, to distinguish impurity signals, which can often accompany the synthesis of bicyclic bisureas. According to NMR spectra, glycolurils with electron-withdrawing N-substituents by shielding the signals of the carbon atom of C=O groups and electron-donating N-substituents by deshielding of CH–CH-carbons can be clearly distinguished.

References

1   Patent 102004059041 Germany. Verwendung von Formaldehyd und Formaldehyd freisetzenden Verbindungen in einer Zusammensetzung zur Bekämpfung von Mykobakterien / Beilfuss W., Gradtke R., Krull I., Steinhauer, K. Publication date 08.06.2006.

2 Patent 2354771 Great Britain. Bactericide combinations in detergents / Denk A., Emter A., Moddick C. Publication date 04.04.2001.

3 Машковский М.Д. Лекарственные средства: пос. для врачей: справоч. — 15-е изд. / М.Д. Машковский. — М.: Новая волна, 2005. — 1164 с.

4 Прокопов А.А. Экспериментальная фармакокинетика альбикара / А.А. Прокопов, Н.В. Костебелов, А.А. Берлянд // Хим.-фарм. журн. — 2002. — № 3. — С. 13–16.

5 Bakibaev A.A. Methods of synthesis of nitrogen-containing heterocycles using ureas and related compounds / A.A. Bakibaev, A.Yu. Yagovkin, S.N. Vostretsov // Russ. Chem. Rev. — 1988. — Vol. 67, No. 4. — P. 295–314. — URL: https://doi.org/10.1070/RC1998v067n04ABEH000295

6 Cui K. Synthesis and characterization of a thermally and hydrolytically stable energetic material based on N-nitrourea / K. Cui, G. Xu, Z. Xu, P. Wang, M. Xue, Z. Meng et al. // Propellants, Explos., Pyrotech. — 2014. — Vol. 39, No. 5. — P. 662–669. — URL: https://doi.org/10.1002/prep.201300100

7 Zharkov M.N. Nitraton of glycoluril derivatives in liquid carbon dioxide / M.N. Zharkov, I.V. Kuchurov, I.V. Fomenkov, S.G. Zlotin, V.A. Tartakovsky // Mendeleev Commun. — 2015. — Vol. 25, No. 5. — P. 15–16. DOI: 10.1016/j.mencom.2015.01.004

8 Fang Y. / Y. Fang, F. Li // Hanneng cailiao. — 1996. — Vol. 4, No. 2. — P. 62–67.

9 Бакибаев А.А. Препаративные методы синтеза азотсодержащих соединений на основе мочевин: сб. / А.А. Бакибаев, Е.А. Мамаев, В.А. Яновский, А.Ю. Яговкин, Е.Л. Быстрицкий. — Томск: Аграф-Пресс, 2007. — 164 с.

10 Assaf K.I. Cucurbiturils: from synthesis to high–affinity binding and catalysis / K.I. Assaf, W.M. Nau // Chem. Soc. Rev. — 2015. — Vol. 44. — P. 394–418. DOI: 10.1039/C4CS00273C

11 Barrow S.J. Cucurbituril-Based Molecular Recognition/ S.J. Barrow, S. Kasera, M.J. Rowland, J. del Barrio, O.A. Scherman // Chem. Rev. — 2015. — Vol. 115, No. 22. — P. 12320–12406. DOI: 10.1021/acs.chemrev.5b00341

12 Khan R. Cucurbituril-based Functional Materials / R. Khan, D. Tuncel. — London: The Royal Society of Chemistry — Vols. 1–12. — Vol. 7. — 289 p. — URL: https://doi.org/10.1039/9781788015950

13 Havel V. Modulation of Bambusuril Anion Affinity in Water / V. Havel, M. Babiak, V. Sindelar // Chem. Eur. J. — 2017. — Vol. 23, No. 37. — P. 8963–8968. — Режим доступа: https://doi.org/10.1002/chem.201701316

14 Svec J. Bambus[6]uril / J. Svec, M. Necas, V. Sindelar // Angew. Chem., Int. Ed. — 2010. — Vol. 122. — P. 2428–2431. — URL: https://doi.org/10.1002/anie.201000420

15 Mason J. Nitrogen NMR Spectroscopy of Metal Nitrosyls and Related Compounds / J. Mason, L.F. Larkworthy, E.A. Moore // Chem. Rev. — 2002. — Vol. 102, No. 4. — P. 913–934. DOI:10.1021/cr0000751

16 Chegaev K.Yu. New Functional Glycoluril Derivatives / K.Yu. Chegaev, A.N. Kravchenko, O.V. Lebedev, Yu.A. Strelenko // Mendeleev Commun. — 2001. — Vol. 11, No. 1. — P. 32–33. DOI: 10.1070/MC2001v011n01ABEH001357

17 Kravchenko A.N. Synthesis of 2-monofunctionalized 2,4,6,8-tetraazabicyclo[3.3.0]octane-3,7-diones / A.N. Kravchenko, E.Yu. Maksareva, P.A. Belyakov, A.S. Sigachev, K.Yu. Chegaev, K.A. Lyssenko et al. // Russ. Chem. Bull. — 2003. — Vol. 52. — P. 192–197. — Режим доступа: https://doi.org/10.1023/A:1022473004714

18 Xu S. Glycoluril / S. Xu, K.P. Gantzel, L.B. Clark // Acta Crystallogr. — 1994. — Vol. 50, No. 12. — P. 1988–1989. — Режим доступа: https://doi.org/10.1107/S0108270194006955

19 Kurgachev D.A. Isolation, Identification, and Chromatographic Separation of N-Methyl Derivatives of Glycoluril / D.A. Kurgachev, O.A. Kotelnikov, D.V. Novikov, V.R. Kusherbaeva, S.I. Gorbin, E.V. Tomilova et al. // Chromatographia. — 2018. — Vol. 81. — P. 1431–1437. — Режим доступа: https://doi.org/10.1007/s10337–018–3599–9

20 Кравченко А.Н. Бициклические бисмочевины, их предшественники и аналоги: синтез, стереохимические особенности и свойства: дис. ... д-ра хим. наук: 02.00.03 — «Органическая химия» / Ангелина Николаевна Кравченко. — М., 2007. — 313 с.

21 Баранов В.В. Синтез новых биологически активных гликолурилов и тиогликолурилов: дис. ... канд. хим. наук: 02.00.03 — «Органическая химия» / Владимир Владимирович Баранов. — М., 2011. — 187 с.

22 Моррисон Р. Органическая химия: учеб. пос. / Р. Моррисон, Р. Бойд. — М.: Мир, 1974. — 1133 с.

23 Пиккеринг У.Ф. Современная аналитическая химия: учеб. пос. / У.Ф. Пиккеринг. — М.: Химия, 1977. — 559 с.

24 Baranac-Stojanovi M. New insight into the anisotropic effects in solution-state NMR spectroscopy / M. Baranac-Stojanovi // RSC Advances. — 2014. — Vol. 4. — P. 308–321. — URL: https://doi.org/10.1039/C3RA45512B

25 Stancl M. 1,6-Dibenzylglycoluril for synthesis of deprotected glycoluril dimer / M. Stancl, M.S.A. Khan, V. Sindelar // Tetrahedron — 2011. — Vol. 67. — P. 8937–8941. — URL: https://doi.org/10.1016/j.tet.2011.08.097

26 Sinitsyna A.A. A search for synthetic routes to tetrabenzylglycoluril / A.A. Sinitsyna, S.G. Il'yasov, M.V. Chikina, I.V. Eltsov, A.A. Nefedov // Chem. Pap. — 2019. — Vol. 74, No. 3. — P. 1019–1025. — URL: https://doi.org/10.1007/s11696–019–00941–4

27 Газиева Г.А. Синтез биологически ориентированных би- и полигетероциклических систем на основе 4,5-дигидрокси-имидазолидин-2-онов (тионов): дис. ... д-ра хим. наук: 02.00.03 — «Органическая химия» / Галина Анатольевна Газиева. — М., 2018. — 449 с.

28 Паньшина С.Ю. Синтез и изучение некоторых бисгалогенацильных производных гликолурила / С.Ю. Паньшина, Е.К. Тайшибекова, Л.К. Салькеева, А.А. Бакибаев, Е.А. Мамаева // Современные проблемы органической химии: тез. докл. Всерос. науч. конф. с междунар. участием, посвящ. 110-летию со дня рожд. акад. Николая Николаевича Ворожцова (5–9 июня 2017 г.). — Новосибирск: Изд-во НИОХ, 2017. — С. 106.

29 Zharkov M.N. Nitration of glycoluril derivatives in liquid carbon dioxide / M.N. Zharkov, I.V. Kuchurov, I.V. Fomenkov, S.G. Zlotin, V.A. Tartakovsky // Mendeleev Commun. — 2015. — Vol. 25. — P. 15–16. — URL: https://doi.org/10.1016/j.mencom.2015.01.004

30 Boilea J. Structure of 1,4-dinitroglycoluril / J. Boileau, E. Wimmer, R. Gilardi, M.M. Stinecipher, R. Gallo, M. Pierrot // Acta Crystallogr. — 1988. — Vol. 44. — P. 696–699. — URL: https://doi.org/10.1107/S0108270187012204

31 Born M. Investigation on the sodium and potassium tetrasalts of 1,1,2,2-tetranitraminoethane / M. Born, M.A.C. Härtel, T.M. Klapötke, M. Mallmann, J. Stierstorfer // Zeitschrift für anorganische Chemie — 2016. — Vol. 624, No. 24. — P. 1412–1418. DOI: 10.1002/zaac.201600339

32 Stancl M. 1,6-Dibenzylglycoluril for synthesis of deprotected glycoluril dimer / M. Stancl, M.S.A. Khan, V. Sindelar // Tetrahedron — 2011. — Vol. 67, No. 46. — P. 8937–8941. — URL: https://doi.org/10.1016/j.tet.2011.08.097

33 Сигачев А.С. Новые аспекты реакций уредоалкилирования мочевин и их аналогов: дис. ... канд. хим. наук: 02.00.03 — «Органическая химия» / Андрей Сергеевич Сигачев. — М., 2006. — 167 с.

34 Jansen K. Glycoluril derivatives as precursors in the preparation of substituted cucurbit[n]urils / K. Jansen, A. Wego, H.-J. Buschmann, E. Schollmeyer, D. Döpp // Des. Monomers Polym. — 2003. — Vol. 6, No. 1. — P. 43–55. — URL: https://doi.org/10.1163/156855503321127529

35 Shiri A. Preparation of Several Active N-Chloro Compounds from Trichloroisocyanuric Acid / A. Shiri, A. Khoramabadi-zad // Synth. — 2009. — Vol. 16. — P. 2797–2801. DOI: 10.1055/s-0029–1216889

36 Saloutina L.V. Reactions of Internal Perfluoroolefin Oxides with Urea / L.V. Saloutina, A.Ya. Zapevalov, V.I. Saloutin, M.I. Kodess, P.A. Slepukhin // Russ. J. Org. Chem. — 2009. — Vol. 45, No. 6. — P. 865–871. DOI: 10.1134/S1070428009060116

37 Niele F.G.M. Palladium (II) cage compounds based on diphenylglycoluril / F.G.M. Niele, R.J.M. Nolte // J. Am. Chem. Soc. — 1988. — Vol. 110, No. 1. — P. 172–177.

38 Wu F. Day locating the cyclopentano cousins of the cucurbit[n]uril family / F. Wu, L.-H. Wu, X. Xiao, Y.-Q. Zhang, S.-F. Xue, Zh. Tao et al. // J. Org. Chem. — 2012. — Vol. 77, No. 1. — P. 606–611. — URL: https://doi.org/10.1021/jo2021778

39 Sun S. Glycoluril as an efficient molecular template for intramolecular Claisen-type condensations/ S. Sun, L. Edwards, P. Harrison // J. Chem. Soc., Perkin Trans. 1. — 1998. — Vol. 1. — P. 437–448. — URL: https://doi.org/10.1039/A706855G

40 Cow C. Synthesis of the fatty acid of pramanicin / C. Cow, D. Valentini, P. Harrison // Can. J. Chem. — 2011. — Vol. 75, No. 6. — P. 884–889. DOI: 10.1139/v97–106

41 Kravchenko A.N. HNO$_2$-Assisted Triazine Cycle Contraction in 3-oxo-, 3-thioxo- and 3-imino-5,7-dimethyl-4a,7a-diphenyl-perhydroimidazo[4,5-e][1,2,4]triazin-6-ones / A.N. Kravchenko, G.A. Gazieva, S.V. Vasilevskii, P.A. Belyakova, Y.V. Nelyubinab // Mendeleev Commun. — 2012. — Vol. 22, No. 6. — P. 299–301. — URL: https://doi.org/10.1016/j.mencom.2012.11.006

42 Gazieva G.A. 4,5-Dihydroxyimidazolidin-2-ones in α-ureidoalkylation of N-carboxyalkyl-, N-hydroxyalkyl-, and N-aminoalkylureas 5. Synthesis of N-hydroxyalkyl-1,5-diphenylglycolurils / G.A. Gazieva, V.V. Baranov, A.N. Kravchenko // Russ. Chem. Bull. — 2010. — Vol. 59. — P. 1296–1299. — URL: https://doi.org/10.1007/s11172–010–0236–7

43 Baranov V.V. 4,5-Dihydroxyimidazolidin-2-ones in the reaction of α-ureidoalkylation of N-(carboxyalkyl)-, N-(hydroxy-alkyl)-, and N-(aminoalkyl)ureas / V.V. Baranov, Yu.V. Nelyubina, A.N. Kravchenko, N.N. Makhova // Russ. Chem. Bull. — 2010. — Vol. 59, No. 7. — P. 1427–1432. DOI: 10.1007/s11172–010–0258–1

44 Reynolds D.I. Calculation of some ^{15}N and ^{13}C nuclear shielding parameters for some ureas and thioureas / D.I. Reynolds, G.A. Webb, M.L. Martin // J. Mol. Struct. — 1982. — Vol. 90, No. 3–4. — P. 379–382. DOI: 10.1016/0166–1280(82)80076–6

45 Shamuratov E.B. Three-dimensional structures and spectra of 2,6- and 2,8-diethyl-2,4,6,8-tetraazabicyclo[3.3.0]octane-3,7-diones / E.B. Shamuratov, A.S. Batsanov, Yu.T. Struchkov, A.Yu. Tsivadze, M.G. Tsintsadze, L.I. Khmelnitskii et al. // Chem. Heterocycl. Compd. — 1991. — Vol. 27. — P. 745–749. — URL: https://doi.org/10.1007/BF00476206

46 Stancl M. 1,6-Dibenzylglycoluril for synthesis of deprotected glycoluril dimer / M. Stancl, M.S.A. Khan, V. Sindelar // Tetrahedron. — 2011. — Vol. 67. — P. 8937–8941. DOI: 10.1016/j.tet.2011.08.097

47 Silverstein R.M. Spectrometric Identification of Organic Compounds / R.M. Silverstein, G.C. Bassler, T.C. Morrill. — New York: John Wiley, 2005. — 550 p.

48 Popov E.M. Relationships between the lengths, orders, hybridization of the atoms, and force constants of carbon–nitrogen and carbon–oxygen bonds / E.M. Popov, G.A. Kogan, V.N. Zheltova // Theor. Exp. Chem. — 1972. — Vol. 6. — P. 11–19.

49 Драго Р. Физические методы в неорганической химии / Р. Драго; пер. с англ. А.А. Соловьянова. — М.: Мир, 1981. — 424 с.

С.Ю. Паньшина, О.В. Пономаренко, А.А. Бакибаев,
В.С. Мальков, О.А. Котельников, А.К. Ташенов

Гликолурил және оның өнімдерін ^{1}H және ^{13}C ЯМР спектроскопия әдісімен зерттеу

Гетероциклдық қосылыстар химиясында бициклды зәр қышқылдары, әсіресе 2,4,6,8–тетра-азабицикло[3.3.0]октан-3,7-дион 1 (гликолурил) ерекше орынға ие. Гликолурил — молекула құрамында екі реакциялық орталықтың (4 донорлық топ (–NH) және 2 акцепторлы (C=O)) болуымен байланысты құрамындағы карбамидті фрагменті молеканың қасиетін анықтайтын жартылай функционалды қосылыс. Жұмыста гликолурил және оның өнімдерінің (86 қосылыс) ^{1}H және ^{13}C ЯМР спектріндегі химиялық қозғалысқа талдау жасалды. Зерттеу барысында орнын алмастырушылардың донорлық-акцепторлық қасиетінің симметрия және ассиметрия позициясынан бициклды каркастағы электрондық тығыздыққа әсері анықталды. Гликолурилдің ^{1}H және ^{13}C ЯМР спектрінің жалпы талдамасы бициклды каркастың сутегі мен көмірқышқылдың энантиотопты атомдары баламалы сигналдармен белгіленетін молекула симметриясының кеңістіктегі конфигурациясын нақты анықтауға мүмкіндік береді. Сонымен қатар N-алмастырылған гликолурилды каркастың ЯМР спектріндегі ^{1}H және ^{13}C химиялық қозғалыс бойынша C=O-топтың көміртек атомдарын экрандау

бойынша электронды акцепторлы орын басушылары бар гликолурилдерді және CH-CH-көміртектерді экрандамайтын электронды донорлы орын басушылары бар гликолурилдерді айыруға болады. Бұл анизотропия салдарынан электронды тығыздық қайта бөлініп, локальді парамагнитті салымдардың пайда болуына байланысты. Гликолурилдердің ^{1}H және ^{13}C ЯМР спектрінің жалпы талдамасында N-, C-алмастырудың қай түрінде болмасын C=O карбонильді атомның имидазолидинді сақинада экрандалатыны айқын көрінеді.

Кілт сөздер: гликолурил, ЯМР, химиялық қозғалыстар, симметрия, энантиотопты атомдар, экрандау, экрандалған, SAR талдау.

С.Ю. Паньшина, О.В. Пономаренко, А.А. Бакибаев,
В.С. Мальков, О.А. Котельников, А.К. Ташенов

Исследование гликолурила и его производных методами ^{1}H и ^{13}C ЯМР спектроскопии

В химии гетероциклических соединений особое место занимают бициклические мочевины, а именно 2,4,6,8–тетраазабицикло[3.3.0.]октан-3,7-дион (гликолурил). Гликолурил — полифункциональное соединение, в котором карбамидный фрагмент определяет свойства молекулы, обусловленные наличием двух реакционных центров в составе молекулы (4 донорные группы (–NH) и 2 акцепторные (С=О)). В данной работе проведен анализ химических сдвигов в спектрах ^{1}H и ^{13}C ЯМР гликолурила и его производных (86 соединений), для выявления влияния донорно-акцепторного характера заместителей на изменения электронной плотности в бициклическом каркасе с позиции симметрии и ассиметрии. Общий анализ спектров ^{1}H и ^{13}C ЯМР гликолурилов позволяет точно выявить пространственные конфигурации симметрии молекул, при наличии которой (σ^1 и/или σ^2), энантиотопные атомы водорода и углерода бициклического каркаса проявляются эквивалентными сигналами. Также по химическим сдвигам ^{1}H и ^{13}C в спектрах ЯМР N-замещенного гликолурильного каркаса можно четко различать гликолурилы с электроноакцепторными заместителями по экранированию атомов углерода C=O-групп и электронодонорными заместителями по дезэкранированию CH-CH-углеродов, что обусловлено перераспределением электронной плотности и возникновением локальных парамагнитных вкладов вследствие анизотропии. При общем анализе спектров ЯМР ^{1}H и ^{13}C гликолурилов отчетливо видно, что при любом типе N-, C-замещения наблюдается экранирование карбонильного атома C=O в имидазолидиноновом кольце.

Ключевые слова: гликолурил, ЯМР, химические сдвиги, симметрия, энантиотопные атомы, экранирование, дезэкранирование, РСА анализ.

References

1   Beilfuss, W., Gradtke R., Krull I., & Steinhauer, K. (2006). *Patent DE No. 102004059041(A1)*. Munich, Germany: DE Deutsches Patent- und Markenamt.

2   Denk, A., Emter, A., & Moddick, C. (2001). *UK Patent No. GB2354771(A)*. London, Great Britain: The Patent Office.

3   Mashkovskij, M.D. (2005). *Lekarstvennye sredstva: posobie dlia vrachei [Medicines: a manual for doctors]*. (15th ed.). Moscow: Novaia volna [in Russian].

4   Prokopov, A.A., Kostebelov, A.A., & Berland, N.V. (2002). Eksperimentalnaia farmakokinetika albikara [Experimental pharmacokinetics of albicar]. *Khimiko-farmatsevticheskii zhurnal — Pharmaceutical Chemistry Journal, 3*, 13–16 [in Russian].

5   Bakibaev, A.A., Yagovkin, A.Yu., & Vostretsov, S.N. (1998). Methods of synthesis of nitrogen-containing heterocycles using ureas and related compounds. *Russian Chemical Reviews, 67(4)*, 295–314.

6   Cui, K., Xu, G., Xu, Z., Wang, P., Xue, M., Meng, Z., et al. (2014). Synthesis and characterization of a thermally and hydrolytically stable energetic material based on N-nitrourea. *Propellants, Explosives, Pyrotechnics, 39(5)*, 662–669.

7   Zharkov, M.N., Kuchurov, I.V., Fomenkov, I.V., Zlotin, S.G., & Tartakovsky, V.A. (2015). Nitraton of glycoluril derivatives in liquid carbon dioxide. *Mendeleev Communications, 25*, 15–16. DOI: 10.1016/j.mencom.2015.01.004

8   Fang, Y., & Li, F. (1996). Hanneng cailiao. *Chinese Journal of Energetic Materials, 4(2)*, 62–67.

9   Bakibaev, A.A., Mamaeva, E.A., Yanovskij, V.A., Yagovkin, A.Yu., & Bystrickij. E.L. (2007). *Preparativnye metody sinteza azotsoderzhashchikh soedinenii na osnove mochevin [Preparative methods for the synthesis of nitrogen-containing compounds based on urea]*. Tomsk: Ahraf-Press [in Russian].

10   Assaf, K.I., & Nau, W.M. (2015). Cucurbiturils: from synthesis to high–affinity binding and catalysis. *Chemical Society Reviews, 44*, 394–418. DOI: 10.1039/C4CS00273C

11   Barrow, S.J., Kasera, S., Rowland, M.J., del Barrio, J., & Scherman, O.A. (2015). Cucurbituril-Based Molecular Recognition. *Chemical Reviews, 115(22)*, 12320–12406. DOI: 10.1021/acs.chemrev.5b00341

12   Khan, R., & Tuncel, D. (2019). *Cucurbituril-based Functional Materials*. (Vols. 1–12; Vol. 7). London, Great Britain: The Royal Society of Chemistry.

13 Havel, V., Babiak, M., & Sindelar, V. (2017). Modulation of Bambusuril Anion Affinity in Water. *Chemistry-A European Journal*, *23(37)*, 8963–8968.

14 Svec, J., Necas, M., & Sindelar, V. (2010). Bambus[6]uril. *Angewandte Chemie International Edition*, *122*, 2428–2431.

15 Mason, J., Larkworthy, L.F., & Moore, E.A. (2002). Nitrogen NMR Spectroscopy of Metal Nitrosyls and Related Compounds. *Chemical Reviews*, *102(4)*, 913–934. DOI:10.1021/cr000075l

16 Chegaev, K.Yu., Kravchenko, A.N., Lebedev, O.V., & Strelenko, Yu.A. (2001). New Functional Glycoluril Derivatives. *Mendeleev Communications, 11(1)*, 32–33. DOI: 10.1070/MC2001v011n01ABEH001357

17 Kravchenko, A.N., Maksareva, E.Yu., Belyakov, P.A., Sigachev, A.S., Chegaev, K.Yu., & Lyssenko, K.A., et al. (2003). Synthesis of 2-monofunctionalized 2,4,6,8-tetraazabicyclo[3.3.0]octane-3,7-diones. *Russian Chemical Bulletin, 52*, 192–197.

18 Xu, S., Gantzel, K. P., & Clark, L.B. (1994). Glycoluril. *Acta Crystallographica*, *C50(12)*, 1988–1989.

19 Kurgachev, D.A., Kotelnikov, O.A., Novikov, D.V., Kusherbaeva, V.R., Gorbin, S.I., & Tomilova, E.V., et al. (2018). Isolation, identification, and chromatographic separation of N-methyl derivatives of glycoluril. *Chromatographia*, *81*, 1431–1437.

20 Kravchenko, A.N. (2007). Bitsiklicheskie bismocheviny, ikh predshestvenniki i analohi: sintez, stereokhimicheskie osobennosti i svoistva [Bicyclic bisureas, their precursors and analogues: synthesis, stereochemical features and properties]. *Doctor's thesis*. Moscow [in Russian].

21 Baranov, V.V. (2011). Sintez novykh biolohicheski aktivnykh hlikolurilov i tiohlikolurilov [Synthesis of new biologically active hlycolurilyls and thiohlycololuryls]. *Candidate's thesis*. Moscow [in Russian].

22 Morrison, R., & Bojd, R. (1974). *Orhanicheskaia khimiia [Organic chemistry]*. Moscow: Mir [in Russian].

23 Pikkering, U.F. (1977). *Sovremennaia analiticheskaia khimiia [The modern analytical chemistry]*. Moscow: Khimiia [in Russian].

24 Baranac-Stojanovi, M. (2014). New insight into the anisotropic effects in solution-state NMR spectroscopy. *RSC Advances*, *4*, 308–321.

25 Stancl, M., Khan, M.S.A., & Sindelar, V. (2011). 1,6-Dibenzylglycoluril for synthesis of deprotected glycoluril dimer. *Tetrahedron*, *67*, 8937–8941.

26 Sinitsyna, A.A., Ilyasov, S.G., Chikina, M.V., Eltsov, I.V., Nefedov, A.A. (2019). A search for synthetic routes to tetrabenzylglycoluril. *Chemical Papers*, *74(3)*, 1019–1025.

27 Gazieva, G.A. (2018). Sintez biolohicheski orientirovannykh bi- i poliheterotsiklicheskikh sistem na osnove 4,5-dihidroksi-imidazolidin-2-onov (tionov) [Synthesis of biologically oriented bi- and polyheterocyclic systems based on 4,5-dihydroxy-imidazolidin-2-ones (thions)]. *Doctor's thesis*. Moscow [in Russian].

28 Panshina, S.Yu., Taishibekova, E.K., Salkeeva, L.K., Bakibaev, A.A., & Mamaeva E.A. (2017). Sintez i izuchenie nekotorykh bishalohenatsilnykh proizvodnykh hlikolurila [Synthesis and study of some bishaloacylderivatives of glycoluril]. Proceedings from The Modern problems of organic chemistry. *Vserossiiskaia nauchnaia konferentsiia s mezhdunarodnym uchastiem, posviashchennaia 110-letiiu so dnia rozhdeniia akademika Nikolaia Nikolaevicha Vorozhtsova (5–9 iunia 2017 hoda) — All-Russian Scientific Conference with international participation dedicated to the 110th birthday of Academician Nikolai Nikolaevich Vorozhtsov*. (p. 106). Novosibirsk: NIOKh [in Russian].

29 Zharkov, M.N., Kuchurov, I.V., Fomenkov, I.V., Zlotin, S.G., & Tartakovsky, V.A. (2015). Nitration of glycoluril derivatives in liquid carbon dioxide. *Mendeleev Communications*, *25*, 15–16.

30 Boileau, J., Wimmer, E., Gilardi, R., Stinecipher, M.M., Gallo, R., & Pierrot., M. (1988). Structure of 1,4-dinitroglycoluril. *Acta Crystallographica, 44*, 696–699.

31 Born, M., Härtel, M.A.C., Klapötke, T.M., Mallmann, M., & Stierstorfer, J. (2016) Investigation on the sodium and potassium tetrasalts of 1,1,2,2-tetranitraminoethane. *Zeitschrift für anorganische Chemie*, *624(24)*, 1412–1418. DOI: 10.1002/zaac.201600339

32 Stancl, M., Khan, M.S.A., & Sindelar. V. (2011). 1,6-Dibenzylglycoluril for synthesis of deprotected glycoluril dimer. *Tetrahedron*, *67(46)*, 8937–8941.

33 Sigachev, A.S. (2006). Novye aspekty reaktsii uredoalkilirovaniia mochevii i ikh analohov [New aspects of ureidoalkylation reactions of ureas and their analogues]. *Candidate's thesis*. Moscow [in Russian].

34 Jansen, K., Wego, A., Buschmann, H.-J., Schollmeyer, E., & Döpp, D. (2003). Glycoluril derivatives as precursors in the preparation of substituted cucurbit[n]urils. *Designed Monomers and Polymers*, *6(1)*, 43–55.

35 Shiri, A., & Khoramabadi-zad, A. (2009). Preparation of several active N-chloro compounds from trichloroisocyanuric acid. *Synthesis*, *16*, 2797–2801. DOI: 10.1055/s-0029–1216889

36 Saloutina, L.V., Zapevalov, A.Ya., Saloutin, V.I., Kodess, M.I., & Slepukhin, P.A. (2009). Reactions of internal perfluoroolefin oxides with urea. *Russian Journal of Organic Chemistry*, *45(6)*, 865–871. DOI: 10.1134/S1070428009060116

37 Niele, F.G.M., & Nolte, R.J.M. (1988). Palladium (II) Cage Compounds Based on Diphenylglycoluril. *Journal of the American Chemical Society*, *110(1)*, 172–177.

38 Wu, F., Wu, L.-H., Xiao, X., Zhang, Y.-Q., Xue, S.-F., & Tao, Zh., et al. (2012). Day Locating the cyclopentano cousins of the cucurbit[n]uril family. *The Journal of Organic Chemistry*, *77(1)*, 606–611.

39 Sun, S., Edwards, L., & Harrison, P. (1998). Glycoluril as an efficient molecular template for intramolecular Claisen-type condensations. *Journal of the Chemical Society, Perkin Transactions, 1*, 437–448.

40 Cow, C., Valentini, D., & Harrison, P. (2011). Synthesis of the fatty acid of pramanicin. *Canadian Journal of Chemistry, 75(6)*, 884–889. DOI: 10.1139/v97–106

41 Kravchenko, A.N., Gazieva, G.A., Vasilevskii, S.V., Belyakova, P.A., & Nelyubinab, Y.V. (2012). HNO$_2$-assisted triazine cycle contraction in 3-oxo-, 3-thioxo- and 3-imino-5,7-dimethyl-4a,7a-diphenyl-perhydroimidazo[4,5-e][1,2,4]triazin-6-ones. *Mendeleev Communications*, *22(6)*, 299–301.

42 Gazieva, G.A., Baranov, V.V., & Kravchenko, A.N. (2010). 4,5-Dihydroxyimidazolidin-2-ones in α-ureidoalkylation of N-carboxyalkyl-, N-hydroxyalkyl-, and N-aminoalkylureas 5. Synthesis of N-hydroxyalkyl-1,5-diphenylglycolurils. *Russian Chemical Bulletin, International Edition*, *59*, 1296–1299.

43 Baranov, V.V., Nelyubina, Yu.V., Kravchenko, A.N. & Makhova, N.N. (2010). 4,5-Dihydroxyimidazolidin-2-ones in the reaction of α-ureidoalkylation of N-(carboxyalkyl)-, N-(hydroxyalkyl)-, and N-(aminoalkyl)ureas. *Russian Chemical Bulletin, International Edition*, *59(7)*, 1427—1432. DOI: 10.1007/s11172–010–0258–1

44 Reynolds, D.I., Webb, G.A., & Martin, M.L. (1982). Calculation of some ^{15}N and ^{13}C nuclear shielding parameters for some ureas and thioureas. *Journal of Molecular Structure*, *90(3–4)*, 379-382. DOI: 10.1016/0166–1280(82)80076–6

45 Shamuratov, E.B., Batsanov, A.S., Struchkov, Yu.T., Tsivadze, A.Yu., Tsintsadze, M.G., & Khmel'nitskii, L.I., et al. (1991). Three-dimensional structures and spectra of 2,6- and 2,8-diethyl-2,4,6,8-tetraazabicyclo[3.3.0]octane-3,7-diones. *Chemistry of Heterocyclic Compounds*, *27*, 745–749.

46 Stancl, M., Khan, M.S.A., & Sindelar, V. (2011). 1,6-Dibenzylglycoluril for synthesis of deprotected glycoluril dimer. *Tetrahedron*, *67*, 8937–8941. DOI: 10.1016/j.tet.2011.08.097

47 Silverstein, R.M., Bassler, G.C., Morrill, T.C. (2005). *Spectrometric identification of organic compounds*. New York: John Wiley.

48 Popov, E.M., Kogan, G.A., & Zheltova, V.N. (1972). Relationships between the lengths, orders, hybridization of the atoms, and force constants of carbon–nitrogen and carbon–oxygen bonds. *Theoretical and Experimental Chemistry, 6, 11–19.*

49 Drago, R. (1981). *Fizicheskie metody v neorhanicheskoi khimii [Physical methods in inorganic chemistry]*. Moscow: Mir [in Russian].

K.K. Pirniyazov[*], S.Sh. Rashidova

Institute of Polymer Chemistry and Physics, Academy of Sciences of the Republic of Uzbekistan, Tashkent, Uzbekistan
(Corresponding author′s e-mail: qudrat.pirniyazov@mail.ru)

Study of the kinetics of *Bombyx mori* chitosan ascorbate formation

In this work, for the first time, a water-soluble natural biopolymer of chitosan ascorbate based on *Bombyx mori* chitosan and ascorbic acid was obtained and kinetic features of the process were determined. Samples of chitosan ascorbate were synthesized, the interaction of chitosan with ascorbic acid was studied by analytical titration. The synthesis was carried out in order to determine the activation energy of formation of the reaction of chitosan ascorbate, in the ratio of chitosan and ascorbic acid (4:1) components for 15 minutes with a reaction temperature ranging from 25 °C to 65 °C. The results of the kinetic studies show that in the interaction under the study the reaction order on ascorbic acid concentration exceeds the reaction order on chitosan concentration, while the reaction activation energy was determined, which equals to 13.38 kJ/mol. This result allows us to conclude that during the formation of chitosan ascorbate at 55 °C the highest equilibrium constant is established, and a further increase in temperature leads to a decrease in the yield and equilibrium constant. The results obtained indicate that with an increase in the concentration of ascorbic acid compared to the one of chitosan, the reaction rate increased almost twice. It was found that with an increase in the reaction time, the average rate of synthesis gradually decreases. This is due to the fact that with an increase in the duration of the reaction in the solution the concentration of unbound (free) ascorbic acid decreases, and as a result, the reaction rate decreases as well.

Keywords: chitosan ascorbate, ascorbic acid, donor-acceptor bond, reaction rate, degree of binding.

Introduction

Ascorbic acid plays an important role in metabolism, acting as both an acceptor and a proton donor in enzymatic systems, due to the mobility of hydrogen atoms in enol hydroxyls at C-3 (pK_a = 4.2) and C-2 (pK_a = 11.6). Chitosan is biodegradable, nontoxic biopolymer and has properties to stimulate plant growth and inhibit phytopathogenic fungi [1, 2]. Water-soluble, environmentally safe derivatives of chitosan, in particular, chitosan ascorbate are of great interest in the world. A wide possibility of chitosan (CS) modification allows to obtain its water-soluble derivatives, which exhibits pronounced bioactivity in the growth and development of plants [2, 3].

In the literature, there are different views about the mechanisms of interaction of chitosan with ascorbic acid, therefore, the study of the structural and kinetic characteristics of chitosan ascorbate remains relevant. The formation of chitosan ascorbate could be explained based on the interaction of the third (C3-OH) enol hydroxyl group of ascorbic acid and the chitosan amino group with the formation of a donor-acceptor bond [2].

As the authors' [2–6] work shows, donor-acceptor bonds are formed due to the more reactive third (C2-OH, C3-OH) enol hydroxyl group of ascorbic acid with the amino group of chitosan. In the reaction of a lone electron pair, the amino groups possess donor properties and confirmed the structure of ascorbate chitosan by using NMR and IR spectroscopy. For obtaining chitosan ascorbate, a potential source of raw materials is chitosan obtained from chitin of *Bombyx mori* silkworm pupae and widely available ascorbic acid. Scientific research in this aspect is in the initial stage in spite of the fact that there is a great demand for chitosan ascorbate in agriculture. It is known from the scientific literature that the optimal conditions and kinetic features of the reaction of chitosan ascorbate formation are not well understood, therefore, it's synthesizing and the study of the physicochemical and kinetic aspects of the formation of chitosan ascorbate is an urgent task, with special attention being paid to the rational use of natural resources. Chitosan ascorbate was synthesized, kinetic characteristics and energy activation of the process were established on this purpose.

---

* Corresponding author

Experimental

For the purpose of determining E_a, we used the rheology method in the temperature range 20–50 ºC according to the Arrhenius equation [7]. We have carried out a synthesis, for the first time determined the order of reaction and the activation energy of the reaction of chitosan ascorbate formation. We carried out the reaction of the formation of chitosan ascorbate under the constant conditions with varying concentrations of the initial chitosan to determine the reaction order of the formation of ascorbate chitosan from the concentration of chitosan. The reaction took 30 minutes and the molar concentration differed in the interval of 0.0125–0.1 M of ascorbic acid. The degree of binding of chitosan (CS) to ascorbic acid (AA) was evaluated by the ratio of (M_{AA}) exp./(M_{AA}) calc. The reaction rate (v) was calculated by the formula,

$$v = \frac{\Delta C}{t \times v},$$

where ΔC is the change in AA concentration during the complexation reaction; v is the volume of the reaction mixture.

Ethyl alcohol in a 1:3 ratio to the reaction system was used as a precipitate. The excess amount of ascorbic acid was determined by the alkaline titration method with phenolphthalein indicator or iodometric titration on the basis of the following equation [2]:

$$C_5H_7O_5{-}COH + NaOH \rightleftharpoons [C_5H_7O_5{-}CO{-}]Na^+ + HOH$$
$$2C_5H_7O_5{-}COH + J_2 \rightleftharpoons 2[C_5H_7O_5{-}C{=}O] + 2HJ$$
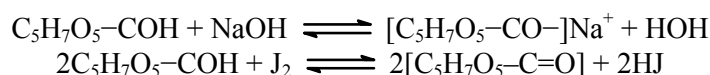
The influence of synthesis time and ratio of the initial components on the formation chitosan ascorbate were studied by potentiometric titration.

Results and Discussion

The results of potentiometric studies were shown that changing molecular weight of initial chitosan slightly effects on formation of chitosan ascorbate. There was detected an increase in the pH of the medium to 6.3 over 30 minutes during the formation of the reaction of the chitosan ascorbate. Then, the pH remains constant [8], which could be explained by the maximum interaction of ascorbic acid with chitosan. Therefore, the experiments were carried out during 15–30 minutes. The results are presented in Table 1.

Table 1

Dependence of binding degree of chitosan with ascorbic acid and chitosan ascorbate formation reaction rates from molar concentration of chitosan

Concentration of CS, mol/l	AA[*] concentration, ΔC mol/l	Degree of binding, %	Reaction rate 10^{-5} mol/l s
0.2	0.0531	53.1	1.20
0.3	0.0604	60.4	1.47
0.4	0.0670	67.0	1.70
0.5	0.0710	71.0	1.90

[*]AA concentration change

It was clear from the results that there is an increased degree of binding of ascorbic acid and the average reaction rate of ascorbate chitosan formation by increasing molar ratio of initial chitosan compared to ascorbic acid. To estimate the order of the reaction, the dependence of the logarithm of the reaction rate of ascorbate chitosan formation on the concentration of initial chitosan were compiled and the necessary value was determined from the angle.

Figure 1 shows that with an increase in the amount of chitosan, an increase in rate occurs, and the tangent of the angle of inclination is 0.8, which corresponds to the order of chitosan.

In order to determine the reaction order of the formation of chitosan ascorbate by the amount of ascorbic acid, we synthesized chitosan ascorbate under constant conditions with varying initial acid concentrations. The reaction time is 30 minutes and the molar concentration of chitosan is 0.1 M. The results are presented in Table 2.

The results of experiments showed that with an increase in the molar ratio of the starting ascorbic acid compared to chitosan, its percentage in the composition of the obtained chitosan ascorbate increases, while with an increase in the ratio of ascorbic acid, the degree of binding decreases.
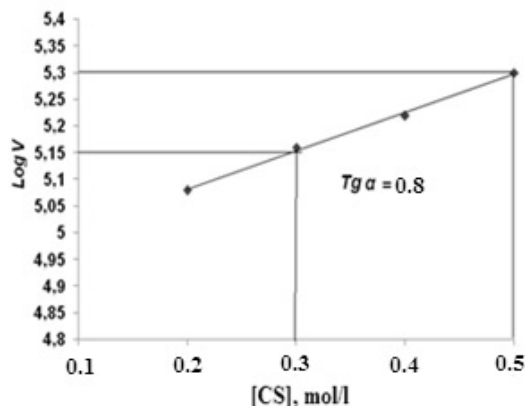
Figure 1. Dependence of the logarithm of the reaction rate of chitosan ascorbate formation
on the concentration of the initial chitosan

T a b l e 2

Dependence of the degree of ascorbic acid binding and the rate of chitosan ascorbate formation reaction on the molar concentration of chitosan (t = 25 °C, τ = 30 minutes). The molar concentration of chitosan is 0.1 mol/l

Molar concentration AA, mol/l	Concentration of AA, ΔC mol/l	Degree of binding, %	Reaction rate·10^{-5} mol/l s
0.0125	0.00875	70.0	0.49
0.025	0.01835	73.4	1.10
0.0375	0.03075	82.0	1.70
0.0500	0.0315	63.0	1.75

To estimate the order of the reaction, the dependence of the logarithm of reaction rate of ascorbate chitosan formation on the concentration of initial ascorbic acid was compiled and the order of the reaction of ascorbate chitosan formation was determined from the slope.
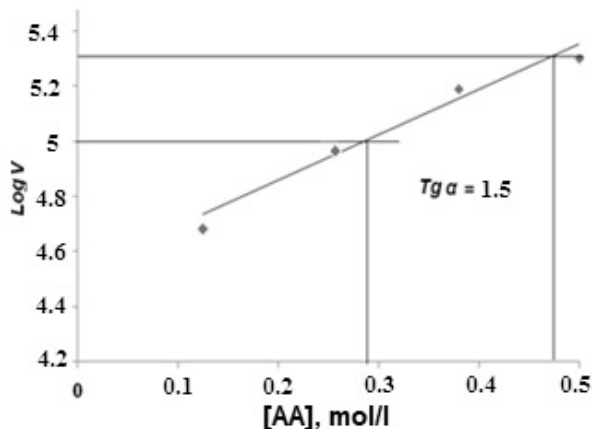
Figure 2. Dependence of the logarithm of the reaction rate of chitosan ascorbate formation on the concentration of the initial ascorbic acid

Figure 2 shows that with an increase in the amount of ascorbic acid, an increase in rate is observed, and the slope is 1.5, which corresponds to the order of reaction of ascorbic acid. Thus, the reaction rate of the formation of chitosan ascorbate is noticeably higher with an increase in ascorbic acid compared to chitosan. In order to determine the energy, we activated the reaction of ascorbate chitosan formation in the ratio of the

components CS: AA 4:1 for 15 minutes with the reaction temperature varying from 25 ºC to 65 ºC. The concentration of ascorbic acid is 0.033 M. The data obtained are presented in Table 3.

T a b l e   3

Dependence of the degree of ascorbic acid binding and the rate of chitosan ascorbate formation reaction on the reaction temperature. The ratio of the components of CS:AA = 0.132:0.033 mol/l, τ = 15 minutes

T, ºC	N, %	Estimated concentration AA, $C\%$	Experimental concentration AA, $C\%$	Degree of binding, %	K_e	Reaction rate 10^{-5} mol/l s
25	3.95	20.0	11.2	55.0	1.04	2.01
35	3.77	20.0	14.0	70.0	3.20	2.56
45	3.74	20.0	15.1	75.5	5.08	2.77
55	3.71	20.0	15.4	77.0	5.80	2.83
65	3.75	20.0	14.6	73.3	4.20	2.72

The results show that with increasing temperature there is an increase in the content (in the range from 11.2 % to 15.4 %) and in the degree of binding of ascorbic acid. In this case, an increase in the reaction rate from $2.01 \cdot 10^{-5}$ to $2.83 \cdot 10^{-5}$ was found. With an increase of the content of ascorbic acid, a decrease of the fraction of elemental nitrogen was found which confirms the dependence on temperature.

However, after the temperature rises above 55 ºC, there is no increase in the content of ascorbic acid, which could be explained by the establishment of a high equilibrium constant under the influence of high temperatures. To calculate the activation energy of the reaction to form a chitosan ascorbate, a graph of the inverse temperature dependence of the reaction rate logarithm was constructed (Fig. 3), and the activation energy is determined from the angle of inclination tangent by the following formula:

$$\ln\frac{V_1}{V_2} = \frac{E}{R\left[\dfrac{1}{T_1} - \dfrac{1}{T_2}\right]} \; ; \; E_a = \frac{2.3R\log(V_2 - V_1)T_1 \times T_2}{\Delta T} ,$$

where V_1, V_2 are the reaction rate values; R is the universal gas constant; $T_1 - T_2$ is the temperature change.

$$\frac{\log(V_2 - V_1)T_1 \times T_2}{\Delta T} = \mathrm{tg}\,\alpha ,$$

where tg α is equal to the sum of equations.
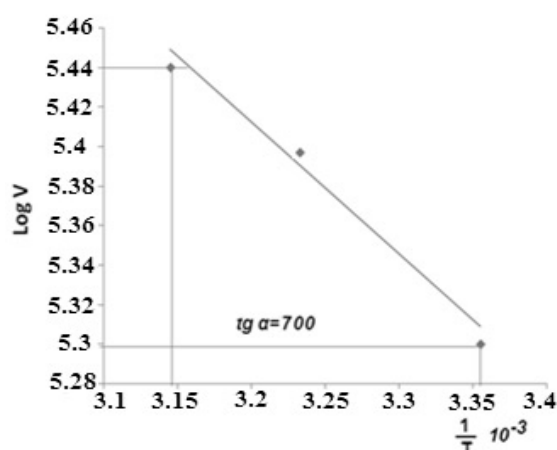
Figure 3. Dependence of the logarithm of the reaction rate of chitosan ascorbate formation
on the versus inverse temperature

From the obtained calculations it is clear that the activation energy of the reaction of ascorbate chitosan formation is 13.38 kJ/mol. This suggests that with increasing temperature, the reaction rate increases gradually and affects the value of activation energy. This result allows us to conclude that during the formation of chitosan ascorbate at 55 ºC, the highest equilibrium constant is established and a further increase in temperature leads to a decrease in the yield and reaction formation constant.

Conclusions

The reaction orders for the formation of chitosan ascorbate by chitosan and ascorbic acid were determined and were equal to 0.8 — 1.5, respectively, which indicates that with an increase in the concentration of ascorbic acid compared to chitosan, the reaction rate almost doubled. The effect of temperature on the chitosan ascorbate formation reaction were determined and the results confirmed that temperature 55 ºC was the optimal condition. Decreases in equilibrium constant and ascorbic acid binding degree were found at temperatures above 55 ºC. The activation energy value of the reaction confirmed the interaction of chitosan with ascorbic acid to form a donor-acceptor bond.

References

1   Ваел Ш.М. Наночастицы хитозана как носители биологически активных веществ: автореф. дис. … канд. хим. наук: спец. 02.00.06 — «Высокомолекулярные соединения» / Ш.М. Ваел. — М., 2012. — 23 с. — URL: http://www.dissercat.com.

2   Pirniyazov K.K. Synthesis and structural characteristics of the ascorbate chitosan *Bombyx mori* / K.K. Pirniyazov, S.Sh. Rashidova // American journal of research. — 2019. — № 7–8. — P. 114–119. DOI: http://dx.doi.org/10.26739/2573–5616–2019-8-10.

3   Hafsa J.B. Synthesis, characterization, antioxidant and antibacterial proprieties of chitosan ascorbate / J.B. Hafsa, M.A. Charfeddine, K.L. Smach, et al. // International journal of pharmaceutical, chemical and biological sciences. — 2014. — № 4 (4). — P. 1072–1081. — URL: www.ijpcbs.com.

4   Tian X.L. Synthesis and evaluation of chitosan-vitamin C complex / X.L. Tian, D.F. Tian, et al. // Indian J. Pharm Sci. — 2009. — Vol. 71(4). — P. 371–376. DOI: 10.4103/0250–474X.57284.

5   Карапетян Г.Э. Использование аскорбата хитозана в мембранном дренировании гнойных ран: автореф. дис. … канд. мед. наук: спец. 14.00.27 — «Хирургия» / Г.Э. Карапетян. — Красноярск, 2005. — 27 с. — URL: http://www.dissercat.com.

6   Малинкина О.Н. Оценка химического взаимодействия гидрохлорида хитозана с аскорбиновой кислотой методами ИК- и ЯМР-спектроскопии / О.Н. Малинкина, А.А. Провозина, А.Б. Шиповская // Изв. Саратов. ун-та. Сер. Химия. Биология. Экология. — 2014. —Т. 14, № 3. — С. 20–24.

7   Ying-Chien Ch. Preparation and characterization of water-soluble chitosan produced by by Maillard reaction / Ch.Ying-Chien, F.T. Cheng, F.L. Chin // Fisheries Science. — 2006. — Vol. 72. — P. 1096–1103. DOI: 101111/J.1444–2906.2006.01261.x.

8   Пирниязов К.К. Потенциометрические исследования аскорбата хитозана *Bombyx mori* / К.К. Пирниязов, С.Ш. Рашидова // VII Всерос. Каргинская конф.: сб. тез. — М., 2017. — С. 332. — URL: http://www.kargin.msu.ru.

К.К. Пирниязов, С.Ш. Рашидова

Bombyx mori аскорбат хитозанының пайда болу кинетикасын зерттеу

Мақала алғаш рет *Bombyx mori* хитозаны (ХЗ) және аскорбин қышқылының (АҚ) негізінде суда еритін табиғи биополимер аскорбат хитозаны (АХЗ) алынған және кинетикалық ерекшеліктері анықталған. Хитозан аскорбатының үлгілері синтезделді, хитозанның аскорбин қышқылымен аналитикалық титрлеу арқылы әрекеттесуі зерттелді. Хитозан аскорбатының түзілу реакциясының активтендіру энергиясын анықтау үшін біз компоненттердің арақатынасы ХЗ:АК 4:1 болғанда, 15 минут аралығымен реакция температурасы 25 ºС-тен 65 ºС-ке дейін бақыланды. Кинетикалық зерттеулердің нәтижелері зерттелген өзара әрекеттесуде аскорбин қышқылының концентрациясы бойынша реакция тәртібі хитозанның концентрациясындағы реакция тәртібінен асып кететінін, реакцияның активтену энергиясы бір уақытта анықталатындығын және 13,38 кДж/мольге тең болатындығын көрсетті. Нәтижелер тепе-теңдіктің ең жоғары тұрақты мәні 55 ºС-те аскорбатты хитозан түзілгенде, температураның артуымен реакция тұрақты және төмендеуіне әкелетіндігін растады. Реакцияның орташа жылдамдығы реакция ұзақтығының артуымен төмендегені анықталды. Бұл реакция ұзақтығының ұлғаюына байланысты ерітіндідегі бос аскорбин қышқылының концентрациясының төмендеуіне байланысты реакция жылдамдығының төмендеуін сипаттайды.

Кілт сөздер: хитозан аскорбаты, аскорбин қышқылы, донор-акцепторлық байланыс, реакция жылдамдығы, байланысу дәрежесі.

К.К. Пирниязов, С.Ш. Рашидова

Изучение кинетики образования аскорбата хитозана *Bombyx mori*

В статье впервые был получен водорастворимый природный биополимер — аскорбат хитозана (АХЗ) на основе хитозана (ХЗ) *Bombyx mori* и аскорбиновой кислоты (АК) и определены кинетические осо-

бенности. Синтезированы образцы аскорбата хитозана, изучено взаимодействие хитозана с аскорбиновой кислотой аналитическим титрованием. С целью определения энергии активации реакции образования аскорбата хитозана проводили синтез в соотношении компонентов ХЗ:АК 4:1 в течение 15 мин с варьированием температуры реакции от 25 до 65 ºС. Результаты проведенных кинетических исследований показывают, что в изучаемом взаимодействии порядок реакции по концентрации аскорбиновой кислоты превышает порядок реакции по концентрации хитозана, одновременно определена энергия активация реакции, которая равняется 13,38 кДж/моль. Данный результат позволяет сделать вывод о том, что в процессе образования аскорбата хитозана при 55 ºС устанавливается самая высокая константа равновесия, а дальнейшее увеличение температуры приводит к уменьшению выхода и константы равновесия. Полученные результаты свидетельствуют о том, что с увеличением концентрации аскорбиновой кислоты по сравнению с хитозаном скорость реакции повысилась практически в два раза. Установлено, что с увеличением времени реакции постепенно уменьшается средняя скорость синтеза. Это связано с тем, что с повышением продолжительности реакции в растворе уменьшается концентрация несвязанной (свободной) аскорбиновой кислоты, вследствие этого происходит снижение скорости реакции.

Ключевые слова: аскорбат хитозана, аскорбиновая кислота, донорно-акцепторная связь, скорость реакции, степень связывания.

References

1 Waiel, Sh.M. (2012). Nanochastitsy khitozana kak nositeli biolohicheski aktivnykh veshchestv [Chitosan nanoparticles as carriers of biologically active substances]. *Extended abstract of candidate's thesis.* Moscow. Retrieved from http://www.dissercat.com [in Russian].

2 Pirniyazov, K.K., & Rashidova, S.Sh. (2019). Synthesis and structural characteristics of the ascorbate chitosan *Bombyx mori. American journal of research, 7–8,* 114–119. DOI: http://dx.doi.org/10.26739/2573–5616–2019–8-10.

3 Hafsa, J.B., Charfeddine, M.A., & Smach, K.L. et al. (2014). Synthesis, characterization, antioxidant and antibacterial proprieties of chitosan ascorbate. *International journal of pharmaceutical, chemical and biological sciences, 4(4),* 1072–1081. Retrieved from www.ijpcbs.com.

4 Tian, X.L., & Tian, D.F., et al. (2009). Synthesis and evaluation of chitosan-vitamin C complex. *Indian J. Pharm Sci., 71, 4,* 371–376. Retrieved from DOI: 10.4103/0250–474X.57284.

5 Karapetian, H.E. (2005). Ispolzovanie askorbata khitozana v membrannom drenirovanii hnoinykh ran [Use of chitosan ascorbate in membrane drainage of purulent wounds]. *Extended abstract of candidate's thesis.* Krasnoyarsk. Retrieved from http://www.dissercat.com [in Russian].

6 Malinkina, O.N., Provozina, A.A., & Shipovskaia, A.B. (2014). Otsenka khimicheskoho vzaimodeistviia hidrokhlorida khitozana s askorbinovoi kislotoi metodami IK- i YaMR-spektroskopii [Assessment of the chemical interaction of chitosan hydrochloride with ascorbic acid by IR and NMR spectroscopy]. *Izvestiia Saratovskoho universiteta. Seriia Khimiia. Biolohiia. Ekolohiia — News of the Saratov University. Ser. Chemistry. Biology. Ecology, 14, 3,* 20–24 [in Russian].

7 Ying-Chien, Ch., Cheng, F.T., & Chin, F.L. (2006). Preparation and characterization of water-soluble chitosan produced by by Maillard reaction. *Fisheries Science, 72,* 1096–1103. DOI: 101111/J.1444–2906.2006.01261.x.

8 Pirniiazov, K.K., Rashidova, S.Sh. (2017). Potentsiometricheskie issledovaniia askorbata khitozana *Bombyx mori* [Potentiometric study of chitosan ascorbate *Bombyx mori*]. *VII Vserossiiskaia Karhinskaia konferentsiia — VII All-Russian Karginsky Conference of Polymers.* (p. 332). Retrieved from http://www.kargin.msu.ru [in Russian].

A.Sh. Zhanzhaxina[1], Ye.M. Suleimen[2,3*], M.Yu. Ishmuratova[4],
Zh.B. Iskakova[1], T.M. Seilkhanov[2], D.A. Birimzhanova[1], R.N. Suleimen[1]

[1]L.N. Gumilyov Eurasian National University, Nur-Sultan, Kazakhstan;
[2]Sh. Ualikhanov Kokshetau State University, Kazakhstan;
[3]Republican collection of microorganisms, Nur-Sultan, Kazakhstan;
[4]Karagandy University of the name of academician E.A. Buketov, Kazakhstan

(Corresponding author′s e-mail: syerlan75@yandex.kz)

Essential oil of *Pulicaria vulgaris* (*prostrata*) and its biological activity

The investigation of the chemical composition, antioxidant and cytotoxic activities of the essential oil of *Pulicaria vulgaris* wild growing in Akmola region, Kazakhstan was the aim of the study. The essential oil was obtained by hydrodistillation and analyzed by gas chromatography-mass spectrometry (GC/MS). A total of 49 compounds were identified representing 86.4 % and the major components were patchoulane (37.4%), buddledin C (13.9 %), T-cadinol (4.7 %), trans-sesquisabinene hydrate (4.1 %), dyhydro-β-agarofuran (2.7 %), (Z)-α-atlantone (1.8 %) and corymbolone (1.2 %). Six components were identified as unknown (2.6 %). The antioxidant activity was evaluated by using 2,2-diphenyl-1-picrylhydrazyl (DPPH) free radical scavenging and the essential oil demonstrated an average scavenging effect at 0.75 and 1 mg/ml concentrations compared with butylhydroxyanisole (BHA). The antiradical activity results of the *P. vulgaris* essential oil is published for the first time. Cytotoxic activity assay was studied against *Artemia salina* larvae and it can be concluded that the essential oil has a good lethal toxicity in all tested concentrations (10–1 mg/ml). The authors attribute this result to the presence of the patchoulane as a major component, which is known for its activity against ovarian cancer cells.

Keywords: *Pulicaria vulgaris (prostrata)*, essential oil, water distillation, GC/MS, patchoulane, antioxidant, cytotoxic activities.

Introduction

Pulicaria Gaertn. is a plant genus in the family of *Asteraceae* (*Compositae*) with approximately 80 species which are widely distributed in Europe, North Africa and Asia [1]. A review of the literature showed that the genus *Pulicaria* has been associated with various biological activities, such as *P. inuloides* known as «sekba», is used in Yemen to treat wounds, *P. jaubertii* is distributed in the southern Arabian Peninsula, and is used traditionally as a diuretic and antipyretic, *P. stephanocarpa*, known as «derbeb» in Soqotra, has been traditionally used in a variety of health conditions including headache, abscesses, boils and sores, *P. undulata*, known as «kho'ah», is used in the central Sahara to treat chills, diabetes, cardiac disorders, skin diseases, and abscesses, and in Egypt to treat inflammation, as an insect repellent, and an herbal tea [2]. The essential oil of *P. inuloides* has showed antimicrobial and antioxidant (DPPH) activities and the main components were carvotanacetone (47.3 %) and palmitic acid (12.8 %) [3], the major component of *P. jaubertii* was carvotanacetone (64.0 %) and the oil was active against MCF-7 and Hep-G2 cells (IC$_{50}$= 3.8 and 5.1 µg ml^{-1}, respectively) [4], *P. stephanocarpa* contained α-cadinol (42.5 %), β-caryophyllen (10.8 %), spathulenol (6.8 %) and it had high antimicrobial and antioxidant (DPPH, IC$_{50}$= 330 µg ml^{-1}) [5] properties, *P. odora* L. contained thymol (47.8 %) and thymol isobutyrate (30.0 %) and it was active in antibacterial assay [6].

The essential oil of *P. undulata* was studied by different scientist from different countries and the results were signicantly different from each other. For instance, the oil from Algeria contained mainly carvotanacetone (14.8 %), δ-cadinene (8.2 %), α-cadinol (4.7 %) and thujanol (4.7 %) [7]. The oil from Yemen contained carvotanacetone (91.4 %), 2,5-dimethoxy-*p*-cymene (2.6 %) and it has demonstrated good antimicrobial and moderate cytotoxic activities against MCF-7 cells (IC50= 64.6 ±13.7 µg ml^{-1}) [8]. The oil from Egypt contained carvacrol (46.5 %), xanthoxylin (18.1 %), carvotanacetone (8.7 %) and it had a powerful antioxidant, a good antiacetylcholinesterase (IC50 = 139.2 µg ml^{-1}), moderate cytotoxic against three cell lines (A375, T98G, HCT116) activities [9]. The oil from Iran contained 4-terpineole (20.1 %), 1S-*cis*-calamenene (13.4 %), junipene (8.7 %), *cis*-sabinene hydrate (8.3 %) and γ-terpinene (7.0 %) [10].

---

* *Corresponding author*

Pulicaria vulgaris (prostrata) Gaertn (*Asteraceae*) is an herbaceous annual plant, erect, more than 30 cm high, much branched. The leaves are linear-oblong, subobtuse orsubacute, mucronate, sessile, cordate semiamplexicaul, entire or denticulate. It grows on the wet banks of rivers and lakes, meadow depressions of bumpy sands. It is found in all areas of Kazakhstan, excepting mountains area. It is used as a remedy for dysentery in folk medicine [11]. Italian scientists studied before the essential oil of *P. vulgaris* and its antimicrobial activity, and the main components were hexadecanoic acid (21.7 %), β-caryophyllene (14.3 %) and geranyl propionate (8.2 %). The oil showed a quite good antimicrobial activity against gram positive bacterial strains [12]. According to the study of Iranian scientists, the main components of this essential oil were thymol (50.2 %), carvotanacetone (20.2 %), thymolisobutyrate (16.9 %), menthan-2-one (4.3 %), 1-methyl-1,2-propanedione (4.1 %), 2,5-dimethoxy-*p*-cymene (4.0 %), myrtenol (1.2 %) and it has showed antimicrobial and antifungal activities. Also in this study, the cytotoxic activity of essential oil was tested against MCF-7 and Hep-G2 cell lines (IC_{50}= 5.36 and 7.16 µg ml^{-1} respectively) [13]. The results of other study have shown that essential oil of *P. vulgaris* may serve as an alternative or complementary treatment for leishmaniasis [14].

The purpose of this study is to determine the component composition of essential oil of *P. vulgaris* from Kazakhstan, which has great prospects, to test its cytotoxic and antiradical activity and compare with previous studies.

Experimental

The plant material of *P. vulgaris (Asteraceae)* was collected during the flowering period on September 1, 2017, near Eski Koluton village, in Astrakhan District, Akmola region, Kazakhstan. A voucher specimen (No. 1996.07.27.02.04.) was deposited in the Herbarium of the Biology and Geography Faculty, E.A. Buketov Karaganda State University.

The essential oil was distilled from the dried aerial parts using a Clevenger-type water distillation apparatus for two hours. Hexane was used as a trap for essential oil. Determination of chemical composition of the essential oil was carried out on the Clarus-SQ 8 (Perkin Elmer) Gas Chromatograph equipped with Mass-spectrometer (GC/MS apparatus).

Preparation of sample: 25 mg of the essential oil were placed into a 25 ml volumetric flask, dissolved in 15 ml of hexane, adjusted to volume and stirred until complete mixing of the oil.

Chromatographic conditions: capillary column — RestekRxi®-1 ms 0.25 mm ×30 m× 0.25 µm, sample volume: 1.0 µl, carrier gas — He, carrier gas speed: 1 ml min^{-1}, split ratio 1:25, temperature of column: 40 °C, rise of 2 °C min^{-1} to 280 °C, temperature of evaporator — 280 °C, mass spectrometric detection: temperature — 240 °C, ЕГ$^+$ = 70 eV, the scanning time from 4 to 120 minutes, the scan mode ion 39–500 m/z. The percentages of components are automatically calculated based on the total peak areas of the chromatogram of ions (Fig. 1). Components were identified by mass spectra and the retention times, with use of NIST library.
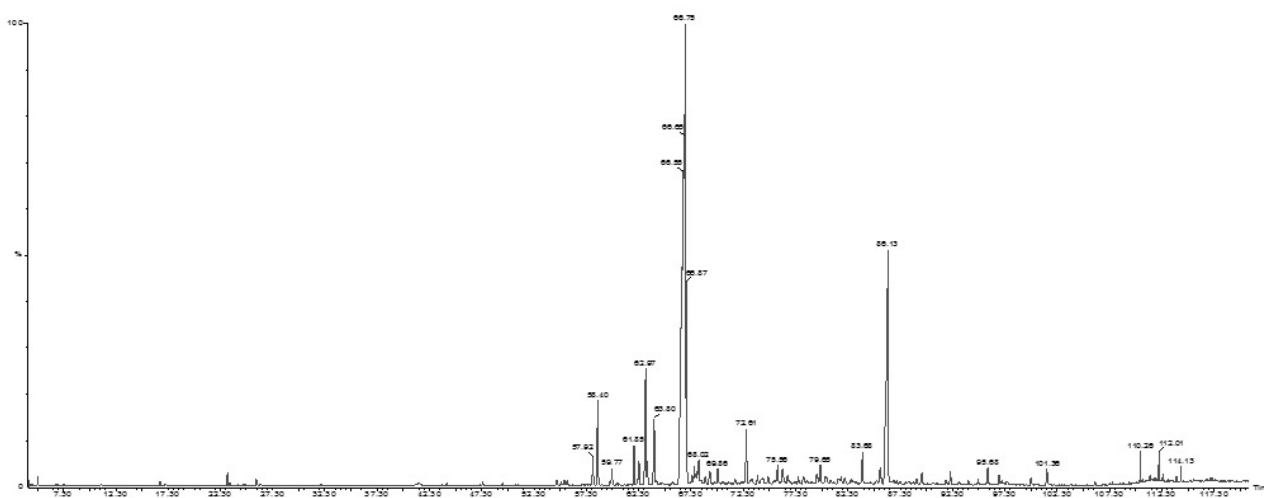
Figure 1. Chromotogram of GC/MS experiment of the essential oil of *P. vulgaris*

Antiradical activity of the essential oil

The antiradical activity of the essential oil was performed in regard to 2,2-diphenyl-1-picrylhydrazyl radical (DPPH). The dependence of the analyte absorbance on the concentration were measured on a spectrophotometer Cary 60 UV-Vis at 520 nm wavelength. Antiradical activity of the essential oil was compared with butylhydroxyanisole (BHA). The values of antiradical activity (ARA) were calculated using the formula shown below:

$$ARA(\%) = \frac{(A_0 - A_t)}{A_0} \times 100 \ \%,$$

where A_0 — is the optical density of control; A_t — is the optical density of the working sample.

DPPH molecule forms a free radical that is stable in different medium and wide range temperature, due to the maximum freedom of the electron delocalization over the entire molecule and spatial shielding atoms bearing the greatest spin density as well as the lack of hydrogen atoms in the positions where may occur the isomerization or disproportionation. In addition, delocalization is causing intense violet color of this radical in the aqueous-alcoholic media, the interaction with the antioxidant, capable of donating a proton; there is a restoration of the radical, resulting in the violet color turns into yellow.

Cytotoxic activity of essential oil

The 55 ml separator funnel was filled with artificial seawater and added 200 mg eggs of *Artemia salina*. Then, it was kept with a soft supply of air for three days, until the crustaceans hatch from eggs. The one side of funnel was covered with aluminum foil, and after 5 minutes, the nauplii, which moved on the bright side of the separator funnel, were removed with a Paster pipette.

20–40 nauplii were placed into each of the 24 micro titer plates with 990 μl of seawater. Dead larvae were counted under a microscope. 10 μl of dimethylsulfoxide solution per 10 mg ml^{-1} sample was added. Actinomycin D or staurosporine was used as a standard comparison reagent, and DMSO was a negative control. After 24 hours of incubation and further maintaining micro titer plates for 24 hours (to ensure immobility) the dead larvae were counted under the microscope.

Mortality P was determined by the following formula:

$$P = \frac{(A - N - B)}{Z} \times 100\%,$$

where A — is the amount of dead nauplii after 24 h; N — is the amount of nauplii died before the test; B — is the average amount of nauplii died in a negative control; Z — is the total amount of larvae [13].

Results of the study the cytotoxic activity of the essential oils are shown in the Table 4.

Results and Discussion

The main components of the studied essential oil are presented in the Table 1. The analytical results revealed the presence of forty nine compounds representing 86.4 %. The essential oil of *P. vulgaris* has as the major compounds: patchoulane (37.4 %), buddledin C (13.9 %), T-cadinol (4.7 %), *trans*-sesquisabinene hydrate (4.1 %), dyhydro-β-agarofuran (2.7 %), (Z)-α-atlantone (1.8 %), dehydronerodiol (1.3 %) and corymbolone (1.2 %). These main compounds put together (65.8 %) of the total chemical composition.

T a b l e 1

Chemical composition of essential oil of *P.vulgaris*

$L_{literature}$	R_{calc}	Compound	Area, %	$R_{literature}$	R_{calc}	Compound	Area, %
1	2	3	4	5	6	7	8
1103±2	1099	Thujone	0.3	1778±N/A	1762	α-Costol	0.6
1480±N/A	1464	Thymylisobutyrate	0.2	1754±10	1769	β-Acoradienol	0.7
1486±3	1503	β-Eudesmene	0.9	1778±4	1777	β-Costol	0.4
1496±0	**1510**	**Dihydro-β-agarofuran**	**2.7**	1777±N/A	1791	Eremophila-1,11-dien-9-one, 8α-hydroxy-	0.3
1549±2	1530	Elemol	0.6	1803±4	1798	2-Naphthalenemethanol, 3,4,6,7,8,8a-hexahydro-5-methyl-8-(1-methylethyl)-, (8R,8aS)-	0.2

1	2	3	4	5	6	7	8
1562±N/A	**1561**	**Dehydronerodiol**	**1.3**	1818±11	1817	Zizanoic acid	0.4
1551±N/A	1568	Diepicedrene-1-oxide	0.9	1832±N/A	1822	*trans*-Valerenylacetate	0.7
1581±2	**1577**	***trans*-Sesquisabinenehydrate**	**4.1**	1813±7	1828	α-Kessylacetate	0.2
1581±2	1580	Caryophylleneoxide	0.7	1845±N/A	1830	Cyperadione	0.3
1610±10	1590	Widdrol	2,0	1861±N/A	1851	(*E*)-Eremophila-1(10),7(11)-dien-12-yl acetate	0.3
1635±N/A	**1633**	**Patchoulane**	**37.4**	**1899±N/A**	**1881**	**Corymbolone**	**1.2**
1640±2	**1635**	**T-Cadinol**	**4.7**	1886±5	1906	Oplopanonylacetate	0.8
1649±2	1642	β-Eudesmol	0.3	**2282±N/A**	**1916**	**Buddledin C ***	**13.9**
1642±2	1646	α-*epi*-Muurolol	0.7	1939±N/A	1956	Verrucarol	0.2
1652±N/A	1649	Cedrane, 8-propoxy-	0.4		1964	*Unknown 1*	0.4
1639±0	1651	Oxacyclotetradeca-4,11-diyne	0.7		2005	*Unknown 2*	0.4
1679±4	1661	Cyclohexanemethanol, 4-ethenyl-α,α,4-trimethyl-3-(1-methyl-ethenyl)-, acetate, [1R-(1α,3α,4β)]-	0.3		2049	*Unknown 3*	0.2
1680±18	1667	Khusimylmethylether	0.5		2065	*Unknown 4*	0.7
1679±N/A	1678	(*E*)-α-Santalal	0.5	2073±N/A	2083	*cis*-10-Heptadecenoic acid	0.4
1693±3	1703	Germacrone	0.2		2134	*Unknown 5*	0.3
1717±4	**1719**	**(*Z*)-α-Atlantone**	**1.8**		2160	*Unknown 6*	0.6
1724±N/A	1726	Thujopsenal	0.3	2497±N/A	2511	Carbonic acid, eicosyl vinyl ester	0.2
1748±N/A	1734	5β,7βH,10α-Eudesm-11-en-1α-ol	0.3	2700	2695	Heptacosane	0.3
1763±3	1749	*cis*-Lanceol	0.2	2900	2892	Nonacosane	0.2
1752±4	1758	α-Sinensal	0.2			**Total**	**86.4**

Note. * — Compared with authentic compound.

The DPPH radical scavenging activity of the essential oil of *P. vulgaris* is shown in the Tables 2, 3. Based on the analysis of the data the essential oil *P. vulgaris* at concentration of 0.75 and 1 mg ml^{-1} has an average antiradical activity compared to BHA.

T a b l e   2

Change in optical density depending on the concentration

No.	Sample	Values of optical density depending on concentration, mg ml^{-1}				
		0.1	0.25	0.5	0.75	1.0
1	BHA	0.1362	0.1333	0.1257	0.1202	0.1145
2	*P. vulgaris* (aerial part)	0.6328	0.5902	0.5380	0.4836	0.4288

T a b l e   3

Antiradical activity of *P. vulgaris* essential oil

No.	Sample	Concentration of essential oil, mg ml^{-1}				
		0.1	0.25	0.5	0.75	1.0
1	BHA	80.82	81.23	82.30	83.08	83.88
2	*P. vulgaris* (aerial part)	16.90	22.50	29.35	36.49	43.69

In the present study the essential oil of *P. vulgaris* with hexane was tested on cytotoxicity against *Artemia salina* nauplii. Based on the experiment (Table 4), it can be concluded that the essential oil *P. vulgaris* in all tested concentrations exhibited cytotoxicity; the mortality of nauplii was 96 %.

T a b l e 4

Cytotoxic activity of essential oil of *P. vulgaris*

Parallel	Amount of nauplii in control		Amount of nauplii in a sample			% surviving nauplii in control	% surviving nauplii in the sample	Mortality, P, %	Presence of neurotoxicity, %
	survivors	died	survivors	died	Parallel				
10.0 mg ml^{-1}									
1	25	1	0	31	0	96	0	96	0
2	26	1	0	30	0				
3	30	0	0	27	0				
Average	25	1	0	29	0				
5.0 mg ml^{-1}									
1	25	1	0	30	0	96	0	96	0
2	26	1	0	24	0				
3	30	0	0	24	0				
Average	25	1	0	26	0				
1.0 mg ml^{-1}									
1	25	1	0	28	0	96	0	96	0
2	26	1	0	28	0				
3	30	0	0	26	0				
Average	27	1	0	27	0				

Conclusions

The results of the GC/MS experiment was showed that the main components of the essential oil of *P. vulagaris* from Akmola region (Kazakhstan) were patchoulane (37.4%), buddledin C (13.9 %), T-cadinol (4.7 %), *trans*-sesquisabinene hydrate (4.1 %) and dyhydro-β-agarofuran (2.7 %). Six components were identified as unknown (Σ 2.6 %). Antiradical activity test were showed that the essential oil has average activity at concentration 0.75 and 1 mg ml^{-1} compared to BHA. It should be noted that in this study we investigated the antiradical activity of the essential oil for the first time. The results of cytotoxic activity assay on *Artemia salina* nauplii exhibited a good activity of the essential oil in all tested concentrations, mortality was 96 %. According to a literature review, the patchoulane is the main component of this essential oil and its derivatives were demonstrated moderate cytotoxic activity in human ovarian cancer cells [15].

It can be concluded that the essential oil of *P. vulgaris* from Kazakhstan is differed significantly by component composition of essential oils from Italy and Iran and it can be a good source of biological active compounds.

References

1 Williams C.A. Variations in lipophilic and vacuolar flavonoids among European Pulicaria species / C.A. Williams, J.B. Harborne, J.R. Greenham, R.J. Grayer, G.C. Kite, J. Eagles // Phytochemistry. — 2003. — Vol. 64. — P. 275–283. DOI: 10.1016/S0031–9422(03)00207–3

2 Chhetri K.B. A Survey of chemical composition and biological activities of Yemeni aromatic medicinal plants / K.B. Chhetri, N.A. Awadh Ali, W.N. Setzer // Medicines. — 2015. — Vol. 2. — P. 67–92. DOI:10.3390/medicines2020067

3 Al-Hajj N.Q.M. Antimicrobial and antioxidant activities of the essential oils of some aromatic medicinal plants (*Pulicaria inuloides — Asteraceae* and *Ocimum forskolei — Lamiaceae* Trop.) / N.Q.M. Al-Hajj, H.X. Wang, C. Ma, Z. Lou, M. Bashari, R. Thabit // Journal Pharmaceutical Research. — 2014. — Vol. 13. — P. 1287–1293. DOI: 10.4314/tjpr.v13i8.13

4 Fawzy G.A. Chemical composition and biological evaluation of essential oils of *Pulicaria jaubertii* / G.A. Fawzy, H.Y. Al Ati, A.A. El Gamal // Pharmacognosy Magazine. — 2013. — Vol. 9. — P. 28–32. DOI:10.4103/0973–1296.108133

5 Ali N.A.A. Chemical composition, antimicrobial, antiradical and anticholinesterase activity of the essential oil of *Pulicaria stephanocarpa* from Soqotra / N.A.A. Ali, R.A. Crouch, M.A. Al-Fatimi, N. Arnold, A. Teichert, W.N. Setzer, L. Wessjohann // Natural Products Communication. — 2012. — Vol. 7. — P. 113–116. DOI: 10.1177/1934578X1200700137

6 Hanbali F.E.L. Chemical composition and antibacterial activity of essential oil of *Pulicaria odora* L. / F.E.L. Hanbali, M. Akssira, A. Ezoubeiri, C.A. Gadhi, F. Mellouki, A. Benherraf, A.M. Blazquez, H. Boira // Journal of Ethnopharmacology. — 2005. — Vol. 99. — P. 399–401. DOI: 10.1016/j.jep.2005.01.012

7 Boumaraf M. Esential oil composition of *Pulicaria undulata* (L.) DC. (*Asteraceae*) growing in Algeria / M. Boumaraf, R. Mekkiou, S. Benyahia, J.C. Chalchat, P. Chalard, F. Benayache, S. Benayache // International Journal of Pharmacognosy and Phytochemical Research. — 2016. — Vol. 8, No. 5. — P. 746–749.

8 Ali N.A. Chemical composition and biological activity of essential oil from *Pulicaria undulata* from Yemen / N.A. Ali, F.S. Sharopov, M. Alhaj, G.M. Hill, A. Porzel, N. Arnold, W.N. Setzer, J. Schmidt, L. Wessjohann // Natural Product Communications. — 2012. — Vol. 7, No. 2. — P. 257–260.

9 Mustafa A.M. Chemical composition and biological activities of the essential oil from *Pulicaria undulata* (L.) C.A. Mey. Growing wild in Egypt / A.M. Mustafa, S.I. Eldahmy, G. Caprioli, M. Bramucci, L. Quassinti, G. Lupidi, D. Beghelli, S. Vittori, F. Maggi // Natural Product Research. — 2018. — P. 1–5. DOI: 10.1080/14786419.2018.1534107

10 Ravandeh M. Screening of chemical composition of essential oil, mineral elements and antioxidant activity *in Pulicaria undulata* (L.) C.A. Mey from Iran / M. Ravandeh, J. Valizadeh, M. Noroozifar, M. Khorasani-Motlagh // Journal of Medicinal Plants Research. — 2011. — Vol. 5, No. 10. — P. 2035–2040.

11 Павлов Н.В. Флора Казахстана / Н.В. Павлов. — Алма-Ата: Наука, 1966. — Т. 9. — С. 318.

12 Casiglia S. Chemical composition of the essential oil from *Pulicaria vulgaris* var. graeca (Sch.-Bip.) Fiori (*Asteraceae*) growing wild in Sicily and its antimicrobial activity / S. Casiglia, L. Riccobono, M. Bruno, F. Senatore, F. Senatore // Natural Product Research. — 2015. DOI: 10.1080/14786419.2015.1055267

13 Sharifi-Rad J. Chemical composition and biological activity of *Pulicaria vulgaris* Essential oil from Iran / J. Sharifi-Rad, A. Miri, S.M. Hoseini-Alfatemi, M. Sharifi-Rad, W.N. Setzer, A. Hadjiakhoondi // Natural Product Communications. — 2014. — Vol. 9, No. 11. — P. 1633–1636. DOI10.1177/1934578x1400901126

14 Sharifi-Rad M. *Pulicaria vulgaris* Gaertn. essential oil: an alternative or complementary treatment for Leishmaniasis / M. Sharifi-Rad, B. Salehi, J. Sharifi-Rad, W.N. Setzer, M. Iriti // Cellular and Molecular Biology. — 2018. — Vol. 64, No. 8. — P. 18–21. DOI: 10.14715/cmb/2018.64.8.3

15 Ahn J.H. 6-Acetoxy Cyperene, a Patchoulane-type Sesquiterpene isolated from *Cyperus rotundus* Rhizomes Induces Caspase-dependent apoptosis in human ovarian cancer cells / J.H. Ahn, T.W. Lee, H. Byun, B. Ryu, K.T. Lee, D.S. Jang, J.H. Choi // Phytotherapy research. — 2015. — Vol. 29. — P. 1330–1338. DOI: 10.1002/ptr.5385

А.Ш. Жанжаксина, Е.М. Сүлеймен, М.Ю. Ишмуратова, Ж.Б. Искакова, Т.М. Сейлханов, Д.А. Бірімжанова, Р.Н. Сүлеймен

Pulicaria vulgaris (*prostrata*) эфир майы және оның биологиялық белсенділігі

Зерттеудің мақсаты — Ақмола облысында (Қазақстан) өсетін *Pulicaria vulgaris (prostrata)* эфир майының химиялық құрамын, радикалға қарсы және цитоуыттылық белсенділігін зерттеу. Эфир майы гидродистилляция тәсілімен алынды және газды хроматография – масс спектрометрия (ГХ/МС) арқылы зерттелді. Нәтижесінде 86.4 % құрайтын 49 компонент анықталды, ал негізгі компоненттері — пачулан (37,4%), буддледин С (13,9 %), Т-кадинол (4,7 %), транс-сесквисабинен гидраты (4,1 %), дигидро-β-агарофуран (2,7 %), (Z)-α-атлантон (1,8 %) және коримболон (1,2 %) болды. Алты компонент белгісіз болып анықталды (2,6 %). Антиоксиданттық белсенділік DPPH еркін радикалдарды қолдану арқылы бағаланды және эфир майы 0,75 және 1 мг/мл концентрацияларда бутилгидроксианизолға (БГА) қарағанда орташа радикалға қарсы белсенділігін көрсетті. Бұл зерттеуде *P. vulgaris* эфир майының радикалға қарсы белсенділігінің нәтижелері алғаш рет жарияланды. *Artemia salina* дернәсілдеріне қарсы цитоуыттылық белсенділік нәтижелеріне сәйкес эфир майы барлық сыналған концентрацияларда өлімге әкелетін уыттылығы бар деген қорытындыға келді. Авторлар бұл нәтижені эфир майының негізгі компонентті — пачуланның аналық бездің қатерлі ісік жасушаларына қарсы белсенділігімен белгілі болуымен түсіндіреді.

Кілт сөздер: *Pulicaria vulgaris*, эфир майы, пачулан, антиоксиданттық, цитоуыттылық белсенділіктер.

А.Ш. Жанжаксина, Е.М. Сулеймен, М.Ю. Ишмуратова, Ж.Б. Искакова, Т.М. Сейлханов, Д.А. Биримжанова, Р.Н. Сулеймен

Эфирное масло *Pulicaria vulgaris* (*prostrata*) и его биологическая активность

Целью данного исследования является изучение химического компонентного состава, антирадикальной и цитотоксической активности эфирного масла *Pulicaria vulgaris (prostrata)*, дико произрастающего в Акмолинской области (Казахстан). Эфирное масло было получено гидродистилляцией и исследовано методом газовой хроматографии – масс-спектрометрии (ГХ/МС). В результате было идентифицировано 49 компонентов, составляющих 86,4 %. Основными компонентами были пачулан (37,4 %), буддледин С (13,9 %), Т-кадинол (4,7 %), транс-сесквисабинен гидрат (4,1 %), дигидро-β-агарофуран (2,7 %), (Z)-α-атлантон (1,8 %) и коримболон (1,2 %). Шесть компонентов были определены как неизвестные (2,6 %). Антирадикальную активность оценивали с использованием свободных радикалов DPPH, и данное эфирное масло показало умеренную антирадикальную активность по срав-

ненno с бутилгидроксианизолом (БГА) при концентрациях 0,75 и 1 мг/мл. В этом исследовании результаты антирадикальной активности эфирного масла *P. vulgaris* публикуются впервые. По результатам цитотоксической активности в отношении личинок *Artemia salina* было сделано заключение, что эфирное масло обладает хорошей летальной токсичностью при всех испытанных концентрациях. Авторы объясняют этот результат наличием основного компонента — пачулана, известного своей активностью в отношении раковых клеток яичников.

Ключевые слова: *Pulicaria vulgaris*, эфирное масло, пачулан, антирадикальная, цитотоксическая активность.

References

1   Williams, C.A., Harborne, J.B., Greenham, J.R., Grayer, R.J., Kite, G.C. & Eagles, J. (2003). Variations in lipophilic and vacuolar flavonoids among European Pulicaria species. *Phytochemistry, 64*, 275–283. DOI: 10.1016/S0031–9422(03)00207–3

2   Chhetri, K.B., Awadh Ali, N.A. & Setzer, W.N. (2015). A Survey of chemical composition and biological activities of Yemeni aromatic medicinal plants. *Medicines, 2,* 67–92. DOI:10.3390/medicines2020067

3   Al-Hajj, N.Q.M., Wang, H.X., Ma, C., Lou, Z., Bashari, M. & Thabit R. (2014). Antimicrobial and antioxidant activities of the essential oils of some aromatic medicinal plants (*Pulicaria inuloides — Asteraceae* and *Ocimum forskolei — Lamiaceae* Trop.). *Journal Pharmaceutical Research, 13,* 1287–1293. DOI: 10.4314/tjpr.v13i8.13

4   Fawzy, G.A., Al Ati, H.Y. & El Gamal, A.A. (2013). Chemical composition and biological evaluation of essential oils of *Pulicaria jaubertii. Pharmacognosy Magazine, 9,* 28–32. DOI:10.4103/0973–1296.108133

5   Ali, N.A.A., Crouch, R.A., Al-Fatimi, M.A., Arnold, N., Teichert, A., Setzer, W.N. & Wessjohann, L. (2012). Chemical composition, antimicrobial, antiradical and anticholinesterase activity of the essential oil of *Pulicaria stephanocarpa* from Soqotra. *Natural Products Communication, 7,* 113–116. DOI: 10.1177/1934578X1200700137

6   Hanbali, F.E.L., Akssira, M., Ezoubeiri, A., Gadhi, C.A., Mellouki, F., Benherraf, A., & Blazquez, A.M. et al. (2005). Chemical composition and antibacterial activity of essential oil of *Pulicaria odora* L. *Journal of Ethnopharmacology, 99*, 399–401. DOI: 10.1016/j.jep.2005.01.012

7   Boumaraf, M., Mekkiou, R., Benyahia, S., Chalchat, J.C., Chalard, P., Benayache, F. & Benayache S. (2016). Essential oil composition of *Pulicaria undulata* (L.) DC. (*Asteraceae*) growing in Algeria. *International Journal of Pharmacognosy and Phytochemical Research, 8(5),* 746–749.

8   Ali, N.A., Sharopov, F.S., Alhaj, M., Hill, G.M., Porzel, A., Arnold, N., & Setzer, W.N., et al. (2012). Chemical composition and biological activity of essential oil from *Pulicaria undulata* from Yemen. *Natural Product Communications, 7(2),* 257–260.

9   Mustafa, A.M., Eldahmy, S.I., Caprioli, G., Bramucci, M., Quassinti, L., Lupidi, G., & Beghelli, D. et al. (2018). Chemical composition and biological activities of the essential oil from *Pulicaria undulata* (L.) C.A. Mey. Growing wild in. *Natural Product Research, 2018,* 1–5. DOI: 10.1080/14786419.2018.1534107

10   Ravandeh, M., Valizadeh, J., Noroozifar, M. & Khorasani-Motlagh, M. (2011). Screening of chemical composition of essential oil, mineral elements and antioxidant activity in *Pulicaria undulata* (L.) C.A. Mey from Iran. *Journal of Medicinal Plants Research, 5 (10)*, 2035–2040.

11   Pavlov, N.V. (1966). *Flora Kazakhstana [Flora of Kazakhstan]*. Alma-Ata: Nauka [in Russian].

12   Casiglia, S., Riccobono, L., Bruno, M., Senatore, F. & Senatore, F. (2015). Chemical composition of the essential oil from *Pulicaria vulgaris* var. graeca (Sch.-Bip.) Fiori (*Asteraceae*) growing wild in Sicily and its antimicrobial activity. *Natural Product Research.* DOI: 10.1080/14786419.2015.1055267

13   Sharifi-Rad, J., Miri, A., Hoseini-Alfatemi, S.M., Sharifi-Rad, M., Setzer, W.N. & Hadjiakhoondi, A. (2014). Chemical composition and biological activity of *Pulicaria vulgaris* Essential oil from Iran. *Natural Product Communications, 9(11)*, 1633–1636. DOI10.1177/1934578x1400901126

14   Sharifi-Rad, M., Salehi, B., Sharifi-Rad, J., Setzer, W.N. & Iriti, M. (2018). *Pulicaria vulgaris* Gaertn. essential oil: an alternative or complementary treatment for Leishmaniasis. *Cellular and Molecular Biology, 64(8)*, 18–21. DOI: 10.14715/cmb/2018.64.8.3

15   Ahn, J.H., Lee, T.W., Byun, H., Ryu, B., Lee, K.T., Jang, D.S. & Choi, J.H. (2015). 6-Acetoxy Cyperene, a Patchoulane-type Sesquiterpene isolated from *Cyperus rotundus* Rhizomes Induces Caspase-dependent apoptosis in human ovarian cancer cells. *Phytotherapy research, 29,* 1330–1338. DOI: 10.1002/ptr.5385

PHYSICAL AND ANALYTICAL CHEMISTRY

R.P. Bhole[1*], S.R. Jagtap[1], C.G. Bonde[2], Y.B. Zambare[1]

*[1]Department of Quality Assurance, Dr. D.Y. Patil Institute of Pharmaceutical Sciences
and Research, Pimpri, Pune, Maharashtra, India;
[2]SVKM's, NMIMS School of Pharmacy, Shirpur, Dist: Dhule, India
(Corresponding author's e-mail: ritesh.bhole@dypvp.edu.in)*

Development and validation of stability indicating HPTLC method for estimation of pirfenidone and characterization of degradation product by using mass spectroscopy

Pirfenidone is used as a novel antifibrotic agent approved for mild-to-moderate idiopathic pulmonary fibrosis. An extensive literature search revealed that, method validation by high-performance thin-layer chromatography (HPTLC) and structural determination by tandem mass spectrometry (MS/MS) method was not reported till date. Precoated silica gels plates were used as a stationary phase. Methanol: ethyl acetate: toluene (1:2:7 v/v) was delivered best separation at 315 nm (Rf 0.49±0.03) by densitometry analysis. Degradation analysis was performed as per ICH guidelines Q2 (R1). Isolation of degradation product was done by the HPTLC method and characterized by using MS/MS method. All the validation parameters were found within the range. Moreover, its possible degradation pathway was also proposed. The Proposed developed and validated HPTLC method was found to be more sensitive, simple, precise, accurate, cost-effective and robust. This method could be applied for the analysis of bulk drug and tablet formulation, degradation study. This degradation pathway of the drug will further help to identify the degradation products of Pirfenidone which may be used for the impurity profiling of the drug.

Keywords: high-performance thin-layer chromatography (HPTLC), pirfenidone, tandem mass spectrometry (MS-MS) studies, degradation mechanism.

Introduction

Pirfenidone is a mini non-peptide molecule of low molecular weight 185.2 g/mol, with a chemical name 5-methyl-1-phenyl-2-(1H) pyridine (Fig. 1). It is an agent that combines anti-inflammatory and anti-fibrotic activity, acting through the control of tumor necrosis factor-α (TNFα) and tumor necrosis factor-β (TNFβ), the pathway, as well as through the modulation of cellular oxidation[1]. Idiopathic pulmonary fibrosis (IPF) is the most common form of incurable and often fatal idiopathic interstitial lung disease [4–6]. The purpose of the ASCEND (A Study of Cardiovascular Events in Diabetes) study was to evaluate and confirm the efficacy and safety of pirfenidone [7].

Figure 1. Structure of Pirfenidone
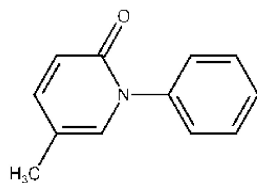
The creation and testing of the analytical method include a sequence of operations that are continuous throughout the life cycle of the product and the substances. It is important to isolate drugs from impurities, degradants, and formulating excipients and analyze them separately for the accurate quantitative determination of drug of interest in a dosage form.

---

* Corresponding author

Considering the quality of the substance and carrying out the content analysis without separating or extracting it became important today, as these extraction or separation processes are found to be time-consuming, repetitive and often costlier [8–9].

A comprehensive literature search revealed that HPTLC system validation and structural determination for Pirfenidone by MS/MS system has not been documented to date. The production and validation of a simple, reliable, accurate and economical, stability-indicating HPTLC method and the identification and characterization of degradation products using MS/MS were therefore considered worthwhile.

Consequently, this research aims to develop simple, precise, cost-effective methods using various analytical tools such as:
− design and validation of the HPTLC method for estimating pirfenidone in a pharmaceutical dosage form;
− MS-MS studies to isolate the potential product for degradation and classify its likely fragmentation pattern.

Experimental

2.1 Chemical and reagents: Pirfenidone was received from Intas Pharmaceutical Ltd, Gujarat as a gift sample. All the chemical used were of analytical grades.

2.2 Preparation of Standard and sample solution: For sample solution 10 mg of pirfenidone was weighed, transferred to a 10 ml volumetric flask, then added 5 ml of methanol and sonicated for 10 minutes. For standard stock solution, twenty tablets of pirfenidone samples were weighed and crushed to obtain a fine powder. The average tablet weight was measured. Through this accurately weighed the tablet powder equivalent to around 10 mg of Pirfenidone was transferred to a 10 ml volumetric flask, added 5 ml of methanol and 10 min ultra sonicated, then made up the methanol amount. 1 ml of this solution was further diluted to 100 µg/ml concentration by using of 10 ml of methanol to form the resulting solution. To remove any particulate matter both the solutions were filtered using Whatman filter paper no. 42.

2.3 Calibration curve preparation: The normal stock solution containing Pirfenidone has been prepared in methanol. Six concentration levels over a range of 200–1200 ng/band in pirfenidone were analyzed for a linear relationship between peaks and concentration.

2.4 Method validations for HPTLC

Proposed process has been validated according to the Criteria for Methodological Validation of the International Conference on Harmonization ICH Q2 (R1).The process was validated using different parameters such as accuracy, precision, specificity and linearity [8–11].

2.5 Accuracy (recovery test): This analysis was performed at three stages, i.e. 80 %, 100 %, and 120 % recovery point, respectively, as shown in Table 2. The solution was done in accordance with the procedure stated in the preparation of the sample solution on and the amount of drug recovered was calculated [12–13].

2.6 Precision: Tablet sample solutions were tested intraday and interday precision at various time intervals on the same day and three different days, respectively. The tablet sample solution was prepared and analyzed like the one defined in the market formulating analysis.

2.7 Linearity: Accurately measured 10 mg of Pirfenidone was transferred to 10 ml volumetric flask, 5ml of methanol was added, and 10 minutes of ultra-sonic pressure was applied, then methanol was removed. Diluted 1 ml of the resulting solution with methanol to 10ml (Pirfenidone concentration 100 µg/ml). The above solution of Pirfenidone was applied to the TLC plates in the range 0.1–0.6 µl using a microsyringe with the help of LINOMAT-V automated sample applicator. The plate was created and scanned under the optimized conditions of chromatography. The peaks achieved for Pirfenidonewere incorporated after scanning. Peak area was recorded for each drug concentration and the calibration curve of Concentration Vs Peak area was constructed for Pirfenidone.

2.8 Robustness: Robustness studies were performed through the shift in mobile step, saturation time of chamber. Most mobile phase and chamber saturation period composition varied within the range of ±0.1 ml and ±2 min, respectively, of the optimized conditions used. Mobile phase volume had varied by ±1 ml. The effect of these changes was investigated on both the Rf values and peak area.

2.9 Detection limit and quantification limit: The limit of detection (LOD) and limit of quantification (LOQ) were calculated separately, based on the standard calibration curve response deviation. To measure the LOD and LOQ the standard deviation of Y-intercept and slope of the calibration curves was used by using formula.

LOD – 3.3 SD/S and LOQ – 10 SD/S,

there SD — is the standard deviation of the response; S — is the slope of the calibration curve.

2.10 Forced degradation study of pirfenidone: In the test of forced degradation, the six samples were prepared by injecting 10 mg of pirfenidone into the product in a 10 ml volumetric flask and adding 3 ml of 0.1 N HCl, 0.1 NaOH, 3 percent H_2O_2 and first 4 flasks of distilled water, respectively. Heat the flask at 80 ºC for acidic and basic conditions for 2 hrs in the water bath and for oxidative condition for 1 hr, and 3 hrs at 80 ºC for distilled water respectively. As per guidelines for force degradation, the photolytic degradation was carried out in UV light (254 nm) for 48 hrs and the drug was kept at 100 ºC for 1 hr for thermal degradation. The remaining two flasks are then moved respectively. All the flasks were removed after the respective time intervals and allowed to cool. The samples were then similarly analyzed as defined under a tablet analysis [14–18].

2.11 Isolation and identification of degradation products by HPTLC-MS/MS: The degradation study was conducted on six conditions of sample stress, but alkaline and acidic these are two conditions of sample stress used in HPTLC-MS/MS studies due to the percentage of degradation rather than other stress. The degraded products are isolated and classified by applying a degraded sample solution to the TLC plate (9 μl-bands) and under optimized chromatographic conditions, the plate was created. It was under the observed 254 nm UV cabinet after drying the plate, and it defined and labeled the degraded band. When the damaged band was found, it was scraped out into the Eppendorf tube and held in methanol overnight. The sample was filtered through Whatman filter paper and subjected to MS/MS on the next day. Two forms of spectra were obtained by the MS/MS studies: Q1 (used for parent compound identification), and Q3 (used fragmentation pattern identification). The MS/MS spectra are shown in Figure 5 and Table 4.

Results and Discussion

3.1 Optimization of Mobile Phase

The mobile phase used for HPTLC analysis was methanol: ethyl acetate: toluene (1:2:7 v/v). They shows good resolution at Rf value of 0.49±0.3. The Pirfenidone HPTLC densitogram shown in Figure 2.
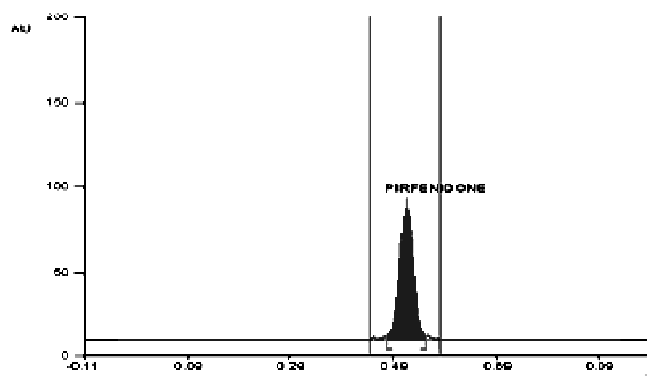
Figure 2.Typical densitogram of Pirfenidone

3.2 Linearity: The pirfenidone linearity equation is $y = 303.11 + 36.612$ with a correlation coefficient (R2) of 0.997; the Peak area for each concentration of drugs was registered, and for Pirfenidone the calibration curve of the Concentration Vs Peak area was constructed. The standard data for the calibration is given in the Table 1. The linearity for Pirfenidone is depicted in Figure 3.

T a b l e   1

Standard calibration data for Pirfenidone

Sr. no	Concentration ng/band	Peak area
1	200	321.79
2	400	653.39
3	600	989.28
4	800	1224.61
5	1000	1518.29
6	1200	1877.52
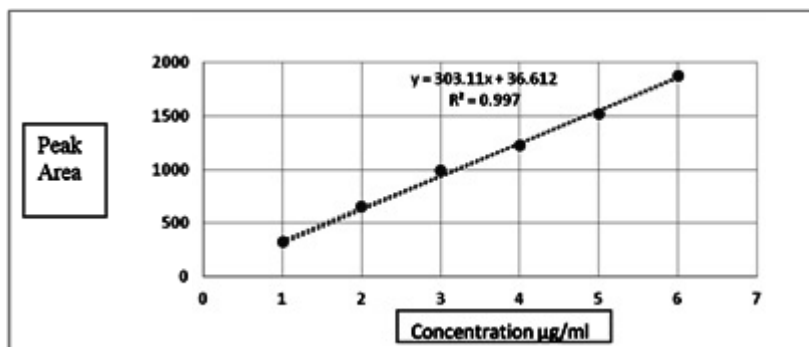
Figure 3. Linearity of the pirfenidone

3.3 Precision and Accuracy: Precision and accuracy tests are shown in Table 2 and Table 3 respectively. It was found to comply with the guidelines of ICH Q2 (R1).

T a b l e 2

Result of precision

Drug	Intraday precision			Inter day precision		
	% label claim	S.D	R.S.D	%label claim	S.D	R.S.D
Pirfenidone	99.46	1.81	1.82	99.70	0.43	0.43

T a b l e 3

Result of accuracy

Level of recovery	Recovery (%)	S.D	% R.S.D
80 %	98.29	0.85	0.86
100 %	100.55	0.20	0.20
120 %	98.62	0.93	0.93

3.4 Robustness: The effect of saturation time, mobile phase shift on both the Rf values and peak area was investigated. Table 4 displays the findings of robustness studies and its statistical validity.

T a b l e 4

Result of robustness studies

Factor	Level	Area	Rf
Saturation time			
5 min	−5	1957.55	0.51
10 min	0	1975.40	0.49
15 min	+5	1986.49	0.47
	S. D ± R. S. D		1.9 ± 0.34
Total mobile phase	**Level**	**Area**	**Rf**
9 ml	−1	1975.44	0.47
10 ml	0	1975.90	0.49
11 ml	+1	1975.23	0.46
	S. D ± R. S. D		1.5 ± 0.26
Time from developing to scanning	**Level**	**Area**	**Rf**
9 ml	5 min	1975.44	0.53
10 ml	30 min	1975.90	0.49
11 ml	60 min	1975.80	0.52
	S. D ± R. S. D		1.1 ± 0.20

3.5 LOD AND LOQ

The sensitivity of the proposed method has been calculated in terms of a detection limit (LOD) and quantification limit (LOQ) 0.034 and 0.104 ng band respectively.

3.6 Forced Degradation Study of Pirfenidone

Forced pirfenidone degradation experiments were performed under various stress conditions such as acidic, alkaline, oxidation, neutral, photolytic, and thermal. Table 5 shows the percent assay of the active material and its Rf values of the degradation products. Acid, alkaline, oxidation, acidic, photolytic, and thermally treated Pirfenidone densitograms are shown in Figure 4, *a–f*, respectively.

T a b l e 5

Results of forced degradation study

Sr. no.	Stress condition	Temperature and time	% assay of active substance	Rf value of degradaned product
1	Acid (0.1 N HCl)	80 ºC for 2 hrs.	80.36 %	0.67, 0.87
2	Alkaline (0.1 N NaOH)	80 ºC for 2hrs.	81.9 %	0.33, 0.47
3	Oxidative (3 % H_2O_2)	80 ºC for 1 hrs.	96.72 %	0.40
4	Neutral	80 ºC for 3 hrs.	91 %	0.12, 0.40, 0.42
5	UV degradation	48 hrs.	97.9 %	0.75
6	Thermal	80 ºC for 1 hr	99.16 %	0.76

a) densitogram of sample treated with (0.1 N HCl)

b) densitogram of sample treated with (0.1 N NaOH)

c) densitogram of sample treated with (3 % H_2O_2)

d) densitogram of sample treated with Neutral

e) densitogram of sample treated with Photo Degradation

f) densitogram of sample treated with Thermal
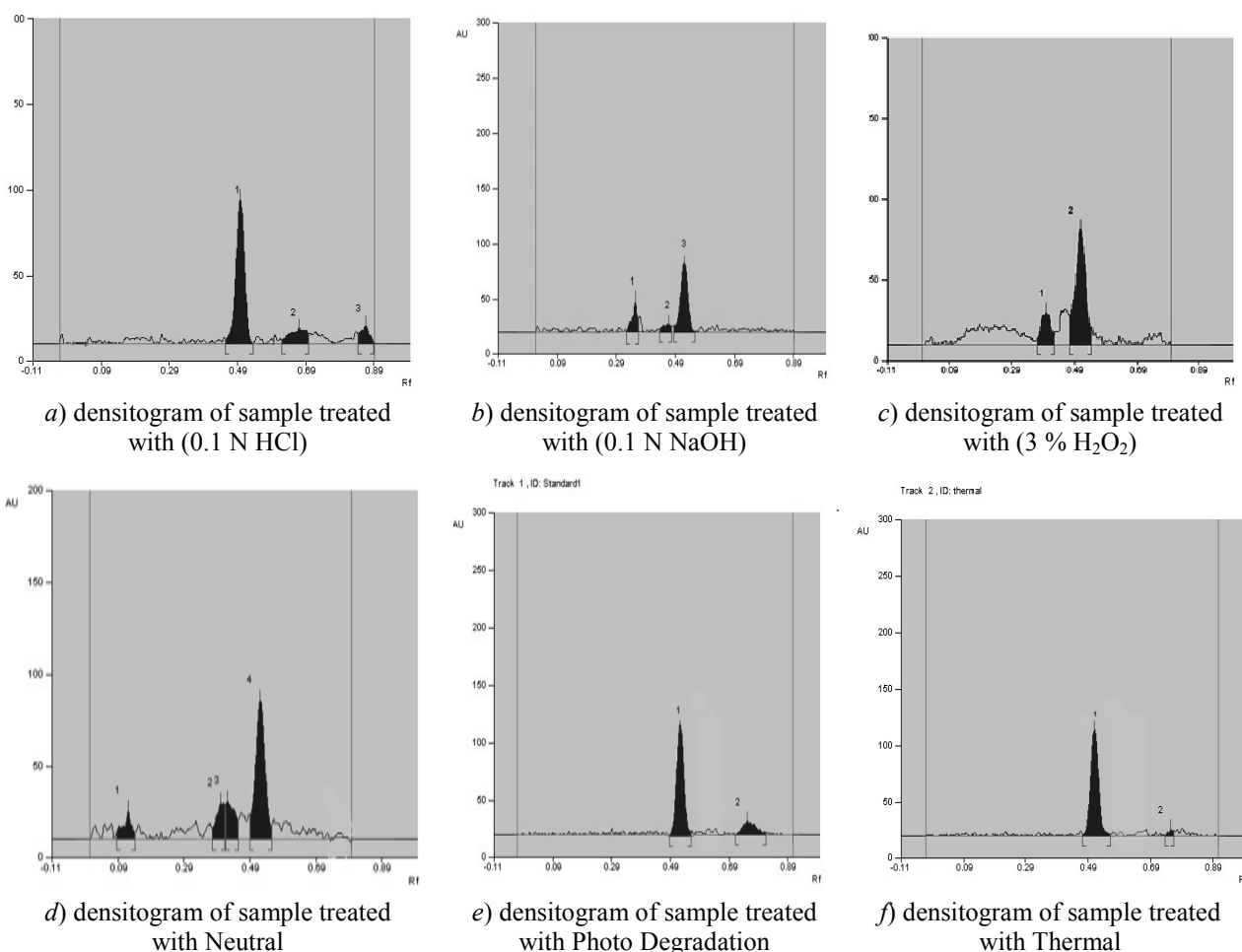
Figure 4. Degradation of Pirfenidone

3.7 Isolation and identification of degrade product by HPTLC — MS/MS (Tandum mass spectroscopy) method

The degradation product has been extracted using the HPTLC method and the degradation product structure was calculated using MS/MS studies. The fragmentation drug pattern was developed by conducting positive electro spray ionization (ESI) mode MS-MS studies in the mass range of 50–1500 g/mol to maximize the mass parameter that specifically informs of the drug's molecular ion peak. Those were further changed to get the medication completely separated.

The MS/MS spectroscopy was primary help to disclose the drug degradation into five degradation products (referred to as DPs I-V, according to the structure in which the peak appeared in the chromatogram from left to right). After degradation five fragmented products was defined based on IR spectra. The five components for the degradation were DP-1, DP-2, DP-3, and DP-4 and DP-5. All result given in the HPTLC-MS/MS range was shown below (Fig. 5).

One oxidation product creates an oxidative stress state. H_2O_2 was oxidized by pirfenidone. The oxidation of ring-A will be postulated. That occurs in the form of DP-1 at nitrogen (m/z = 202.09), as shown in Figure 5, a. In mass spectra, the parent ion of m/z 202.09 was observed. Figure 6 and Table 6 outlined the potential degradation pathway for DP-1 to DP-5. Degradation product-2 and degradation product-3 form acidic stress state. The acid splits the bond between N–C and DP-2 shape. Besides, acidic cleavage occurs on an A-ring to form DP-3. The DP-2 was shown in Figure 5, b (m/z 93.06). As shown in Figure 5, c the parent ion m/z 93.6 is observed in the mass spectrum and DP-3 (m/z 96.06). The parent ion observed for m/z 96.06 is mass spectrum. DP-4 was formed by breaking of C–N bond of ring A cleavage of C=O to DP-4 in alkaline stress condition two degradation product was observed. The DP-4, as shown in Figure 5, d (m/z 78.05). The mass spectrum observes the parent ion into m/z 78.05.

Degradation product (DP-5) was formed by cleavage of C-C bond in ring B of pirfenidone, followed by loss of C=O (Carbonyl group) (m/z 158.1 Fig. 5, e).

a) DP-1

b) DP-2

c) DP-3

d) DP-4

e) DP-5
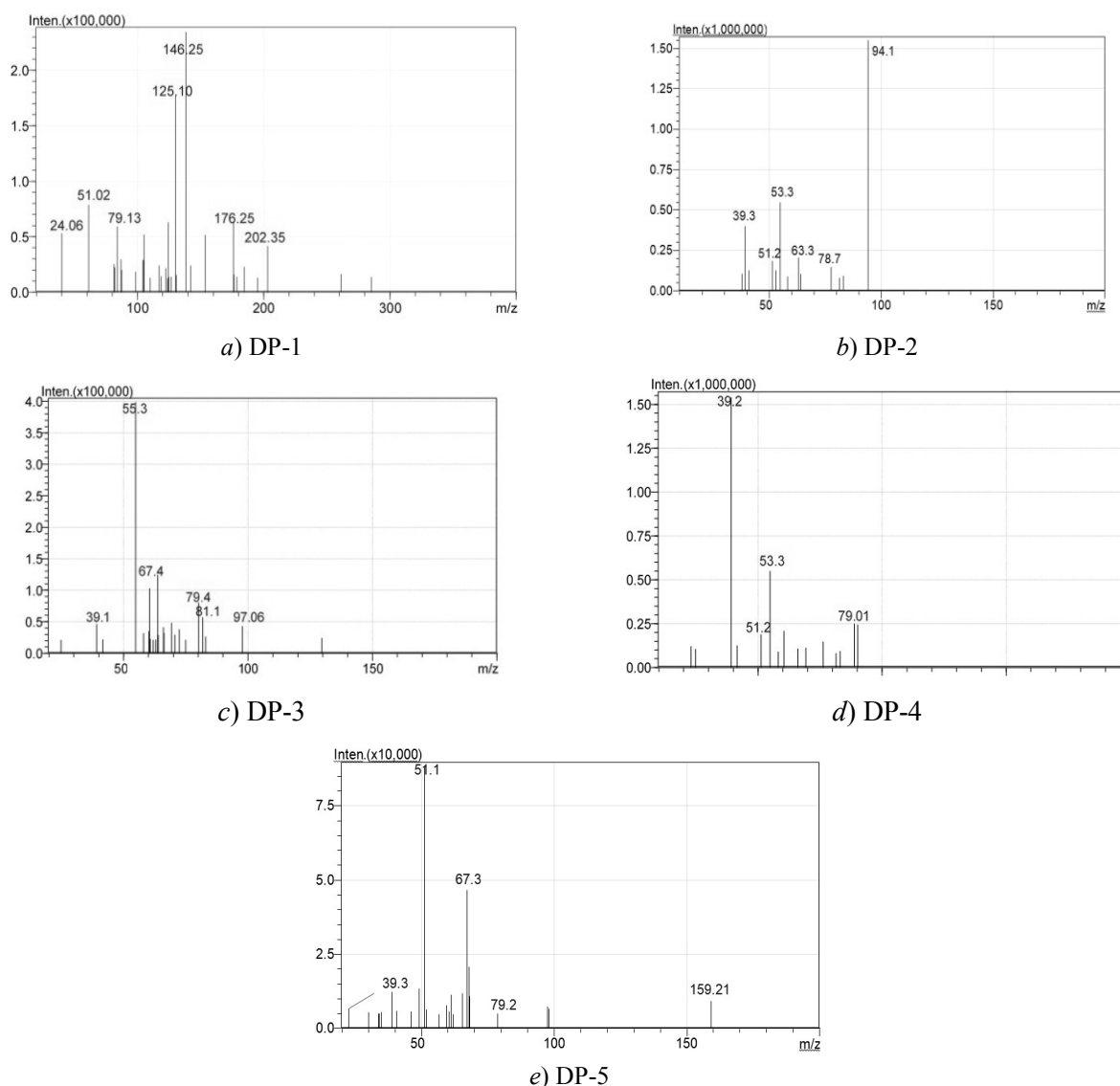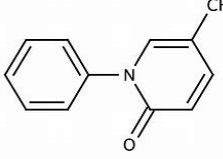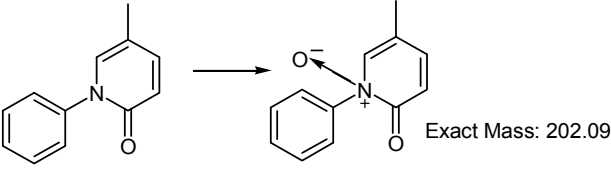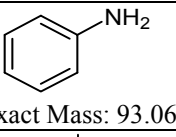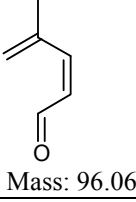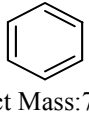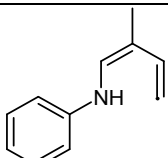
Figure 5. MS/MS spectra of Pirfenidone

T a b l e 6

Summary of degraded product

Parameter	Structure of the degraded product	Possible mechanism
Drug		Pirfenidone
DP-1	Exact Mass: 202.09	H_2O_2 Oxidation at nitrogen
DP-2	NH$_2$ Exact Mass: 93.06	Acidic breakdown of bond
DP-3	O Exact Mass: 96.06	Acidic breakdown of two bond
DP-4	Exact Mass:78.05	Nitrogen carbon bond break in base and benzene ring separate
DP-5	NH	The breakdown of C=O removed in NaOH alkaline condition
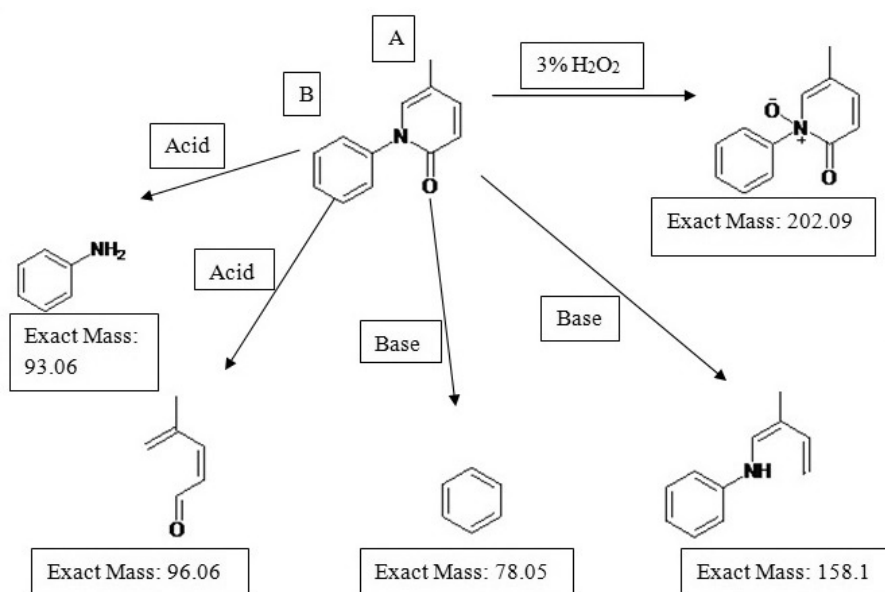
Figure 6. Formation of DP-1, DP-2, DP-3, DP-4, and DP-5 after degradation study

Conclusions

The proposed HPTLC method for estimation of Pirfenidone in pharmaceutical dosage form was found to be accurate, precise, specific and less time consuming. The method was validated as per guidelines of ICH Q2R1. The developed HPTLC method was able to quantitative Pirfenidone in presence of its degradation products. Thus, it can represent good method for analysis of Pirfenidone as there are no reported methods for the same. The fragmentation patterns obtained from HPTLC-MS / MS methods were predicted to show two degradation products in acid and base hydrolysis, while hydrogen peroxide oxidation resulted in one degradation product. Comparison the IR spectrum of pure drugs and finding m /z ratios with various peaks in MS spectra with degradation materials was performed. Thus the present research may be used for routine quality control of pirfenidone-containing pharmaceutical formulations.

References

1   Thorat S.G. Development and validation of simple, rapid and sensitive UV, HPLC and HPTLC methods for the estimation of pirfenidone in tablet dosage form / S.G. Thorat, S.P. Padmane, M.R. Tajne, A.M. Ittadwar // Journal of the Chilean Chemical Society. — 2016. — Vol. 61, No. 2. — P. 2978–2981. DOI: 10.4067/S0717–97072016000200025

2   Oku H. Pirfenidone suppresses tumor necrosis factor alpha, enhances interleukin-10 and protects mice from endotoxic shock / H. Oku, H. Nakazato, H. Horikawa, T. Tsuruta, Y. Suzuki R. // Eur. J. Pharmacol. — 2002. — Vol 446. — P. 167–176. DOI: 10.1016/S0014–2999(02)01757–0

3   Misra H.P. Pirfenidone inhibits NADPH-dependent microsomal lipid peroxidationand scavenges hydroxyl radicals / H.P. Misra, C. Rabideau // Mol. Cell Biochem. — 2000. — Vol. 204. — P. 119–126. doi.org/10.1023/A:1007023532508

4   Rubino C.M. Effect of food and antacids on the pharmacokinetics of pirfenidone in older healthy adults / C.M. Rubino, S.M. Bhavnani, P.G. Ambrose, A. Forrest, J.S.Loutit // Pulmonary Pharmacology & Therapeutics. — 2009. — Vol. 22. — P. 279–282. doi:10.1016/j.pupt.2009.03.003

5   Oku H. Antifibrotic action of pirfenidone and prednisolone: different effects on pulmonary cytokines and growth factors in bleomycin-induced murine pulmonary fibrosis / H. Oku, T. Shimizu, T. Kawabata, M. Nagira, I. Hikita, A. Ueyama, S. Matsushima, M. Torii, A. Arimura // European Journal of Pharmacology. — 2008. — Vol. 590, No. 1–3. — P. 400–408. doi: 10.1016/j.ejphar.2008.06.046

6   Thorat S.G. A validated stability-indicating high-performance thin-layer chromatographic method for the estimation of pirfenidone in tablet formulation / S.G. Thorat, M.R. Tajne, S.P. Padmane, A.M. Ittadwar // JPC-Journal of Planar Chromatography-Modern TLC. — 2015. — Vol. 28, No. 5. — P. 398–401. DOI: 10.1556/1006.2015.28.5.10

7   King, Jr. T.E. A phase 3 trial of pirfenidone in patients with idiopathic pulmonary fibrosis / T.E. King, Jr., W.Z. Bradford, E.A. Fagan, I. Glaspole, M.K. Glassberg, E. Gorina, P.M. Hopkins // New England Journal of Medicine. — 2014. — Vol. 370, No. 22. — P. 2083–2092. doi: 10.1056/NEJMoa1402582

8   ICH, Q1A (R2) Stability Testing of New Drug Substances and Products // Proceedings of the International Conference on Harmonization. — IFPMA, Geneva, 2003.

9   Wankhede S.B. A simple and sensitive HPTLC method for simultaneous analysis of Thiocolchicoside and Ketoprofen in combined dose tablet formulation / S.B. Wankhede, S.S. Chitlange, R.P. Bhole, S.S. Zambare // Analytical Chemistry Letters. — 2012. — Vol. 2, Iss. 5. — P. 301–308. https://doi.org/10.1080/22297928.2012.10648281

10   URL: http://www.intermune.com/Pirfenidone.

11   ICH, Q1B. Stability Testing: Photostability Testing of New Drug Substances and Products // Proceedings of the International Conference on Harmonization. — IFPMA, Geneva, 2003.

12   ICH Q2A. Guidelines, validation procedure; definition and terminology. — 1995. — 60 p.

13   Bhole R.P. A simple and sensitive HPTLC method for simultaneous analysis of phenylephrine hydrochloride and ketorolac tromethamine in combined dose formulation / R.P. Bhole, P.D. Jagdale, S.B. Wankhede, S.S. Chitlange // Analytical Chemistry Letters. — 2015. — Vol. 5, No. 4. — P. 206–215. https://doi.org/10.1080/22297928.2015.1126532

14   Thorat S.G. Determination and pharmacokinetic study of pirfenidone in rat serum by high performance thin-layer chromatography / S.G. Thorat, R.V. Chikhale // Journal of Chromatographic Science. — 2016. — Vol. 54. No. 7. — P. 1115–1119. https://doi.org/10.1093/chromsci/bmw067.

15   Bhole R.P. Development and Validation of Stability Indicating HPTLC-MS Method for Estimation of Empagliflozin in Pharmaceutical Dosage Form / R.P. Bhole, F.R. Tamboli // Analytical Chemistry Letters. — 2018. — Vol. 4, No. 8(2). — P. 244–256. DOI: 10.1080/22297928.2017.1404929

16   Bhole R.P. Development and validation of stability indicating HPTLC method for estimation of dasatinib and characterization of degradation products by using mass spectroscopy / R.P. Bhole, P. Birader, C.G. Bonde // Eur. J. of Analytical Chemistry. — 2018. — Vol. 13, No. 4. — P. 1–11. DOI: https://doi.org/10.29333/ejac/90678

17   Bhole R.P. Identification and characterization of degradation products by using Ms-Ms studies for developed and validated stability indicating HPTLC method for estimation of nintedanib esylate in pharmaceutical dosage form / R.P. Bhole, T. Zombade, C.G. Bonde, Y.B. Zambare // Eur J. of Analytical Chemistry. — 2019. — Vol. 14, No. 2. — P. 60–70. DOI: https://doi.org/10.29333/ejac/90678.

18   Bhole R.P. A Stability Indicating HPTLC Method for apremilast and identification of degradation products using MS/MS / R.P. Bhole, S. Naksakhare, C.G. Bonde, Y.B. Zambare // J. Pharm. Sci. & Res. — 2019. — Vol. 11, No. 5. — P. 1861–1869.

Р.П. Бхоле, С.Р. Ягтап, Ч.Г. Бондэ, Ю.Б. Замбаре

Пирфенидонды анықтаудың ӨЖСХ әдістемесін әзірлеу мен валидациялау және масс-спектроскопия көмегімен алынған ыдырау өнімдерінің сипаттамасы

Пирфенидон өкпенің жеңіл және орташа идиопатикалық фиброзын емдеу үшін мақұлданған жаңа антифиброзды препарат ретінде қолданылады. Әдебиеттерді талдау көрсеткендей, пирфенидонды өнімділігі жоғары сұйық хроматография (ӨЖСХ) көмегімен анықтау әдістемесін валидациялау, сондай-ақ тандемдік масс-спектрометрия (ТМС) әдісінің көмегімен деградация өнімдерін сипаттау осы уақытқа дейін ұсынылмаған. Стационарлық фаза ретінде силикагельмен алдын-ала жабылған пластиналар пайдаланылды. Пирфенидонның ең жақсы бөлінуі (Rf = 0,49±0,03) 315 нм кезінде жылжымалы фаза ретінде метанол:этилацетат:толуол (1:2:7 көлем) қоспасын қолданғанда денситометриялық талдау арқылы анықталды. Деградация талдауы ICH Q2 (R1) әдістемесіне сәйкес жүргізілді. Ыдырау өнімінің бөлінуі ӨЖСХ әдісімен жүргізілді және ТМС әдісі арқылы сипатталды. Барлық валидация параметрлері диапазон шегінде табылды. Сонымен қатар, пирфенидонның ықтимал деградация жолы ұсынылды. Ұсынылып отырған пирфенидонды анықтайтын ӨЖСХ әдісі сезімтал, қарапайым, дәл, экономикалық тиімді және сенімді болып шықты. Бұл әдіс дәрі-дәрмектер мен таблеткалардың массасын талдау, деградацияны зерттеу үшін қолданыла алады. Дәрілік заттың деградацияға ұшырау механизмі дәрілік зат қоспаларының таралу бейінін анықтау үшін пайдаланылуы мүмкін пирфенидонның ыдырау өнімдерін идентификациялауға қосымша көмектеседі.

Кілт сөздер: өнімділігі жоғары сұйық хроматография, пирфенидон, тандемдік масс-спектрометрия әдісімен зерттеулер, деградация механизмі.

Р.П. Бхоле, С.Р. Ягтап, Ч.Г. Бондэ, Ю.Б. Замбаре

Разработка и валидация методики ВЭЖХ определения пирфенидона и характеристика продуктов разложения с помощью масс-спектроскопии

Пирфенидон используется в качестве нового антифиброзного средства, одобренного для лечения легкого и умеренного идиопатического фиброза легких. Анализ литературы показал, что валидация методики определения пирфенидона с помощью высокоэффективной жидкостной хроматографии (ВЭЖХ), а также описание продуктов деградации с помощью метода тандемной масс-спектрометрии (ТМС) до настоящего времени не представлены. В качестве стационарной фазы были использованы пластины с предварительным покрытием силикагелем. Наилучшее разделение пирфенидона (Rf = 0,49±0,03) было отмечено при использовании в качестве подвижной фазы метанол: этилацетат: толуол (1:2:7 об.) смеси при 315 нм с помощью денситометрического анализа. Анализ деградации проводился в соответствии с методологией ICH Q2 (R1). Выделение продукта разложения проводили методом ВЭЖХ и характеризовали с помощью метода ТМС. Все параметры валидации были найдены в пределах диапазона. Также был предложен возможный путь деградации пирфенидона. Предложенный метод ВЭЖХ определения пирфенидона оказался более чувствительным, простым, точным, достоверным, экономически эффективным и надежным. Он может быть применен для анализа массы лекарств и таблеток, исследования деградации. Механизм деградации лекарственного средства дополнительно поможет идентифицировать продукты разложения пирфенидона, которые могут использоваться для определения профиля распределения примесей лекарственного средства.

Ключевые слова: высокоэффективная жидкостная хроматография, пирфенидон, исследования методом тандемной масс-спектрометрии, механизм деградации.

References

1 Thorat, S.G., Padmane, S.P., Tajne, M.R., & Ittadwar, A.M. (2016). Development and validation of simple, rapid and sensitive UV, HPLC and HPTLC methods for the estimation of pirfenidone in tablet dosage form. *Journal of the Chilean Chemical Society, 61(2),* 2978–2981. DOI: 10.4067/S0717–97072016000200025

2 Oku, H., Nakazato, H., Horikawa, H., Tsuruta, T., & Suzuki R., Y. (2002). Pirfenidone suppresses tumor necrosis factor alpha, enhances interleukin-10 and protects mice from endotoxic shock. *Eur. J. Pharmacol, 446,* 167–176. DOI: 10.1016/S0014–2999(02)01757–0

3 Misra, H.P., & Rabideau, C. (2000). Pirfenidone inhibits NADPH-dependent microsomal lipid peroxidationand scavenges hydroxyl radicals. *Mol. Cell Biochem., 204,* 119–126. doi.org/10.1023/A:1007023532508

4 Rubino, C.M., Bhavnani, S.M., Ambrose, P.G., Forrest, A., & Loutit, J.S. (2009). Effect of food and antacids on the pharmacokinetics of pirfenidone in older healthy adults. *Pulmonary Pharmacology & Therapeutics, 22,* 279–282. doi: 10.1016/j.pupt.2009.03.003

5   Oku, H., Shimizu, T., Kawabata, T., Nagira, M., Hikita, I., & Ueyama, A. (2008). Antifibrotic action of pirfenidone and prednisolone: different effects on pulmonary cytokines and growth factors in bleomycin-induced murine pulmonary fibrosis, *European Journal of Pharmacology, 590(1–3)*, 400–408. DOI: 10.1016/j.ejphar.2008.06.046

6   Thorat, S.G., Tajne, M.R., Padmane, S.P., & Ittadwar, A.M. (2015). A validated stability-indicating high-performance thin-layer chromatographic method for the estimation of pirfenidone in tablet formulation. *JPC-Journal of Planar Chromatography-Modern TLC, 28(5)*, 398–401. DOI: 10.1556/1006.2015.28.5.10

7   King, Jr, T.E., Bradford, W.Z., Fagan, E.A., Glaspole, I., Glassberg, M.K., Gorina, E., & Hopkins, P.M. (2014). A phase 3 trial of pirfenidone in patients with idiopathic pulmonary fibrosis. *New England Journal of Medicine, 370(22)*, 2083–2092. doi: 10.1056/NEJMoa1402582

8   ICH, Q1A (R2) (2003). Stability Testing of New Drug Substances and Products, *Proceedings of the International Conference on Harmonization*; IFPMA, Geneva.

9   Wankhede, S.B., Chitlange, S.S., Bhole, R.P., & Zambare, S.S. (2012). A simple and sensitive HPTLC method for simultaneous analysis of Thiocolchicoside and Ketoprofen in combined dose tablet formulation, *Analytical Chemistry Letters, 2(5)*, 301–308. https://doi.org/10.1080/22297928.2012.10648281

10   URL: http://www.intermune.com/Pirfenidone.

11   ICH, Q1B. Stability Testing: Photostability Testing of New Drug Substances and Products, *Proceedings of the International Conference on Harmonization*, IFPMA, Geneva 2003.

12   ICH Q2A. Guidelines, validation procedure; definition and terminology. (1995).

13   Bhole, R.P., Jagdale, P.D., Wankhede, S.B., & Chitlange, S.S. (2015). A simple and sensitive HPTLC method for simultaneous analysis of phenylephrine hydrochloride and ketorolac tromethamine in combined dose formulation, *Analytical Chemistry Letters, 5(4)*, 206–215. https://doi.org/10.1080/22297928.2015.1126532

14   Thorat, S.G., & Chikhale, R.V. (2016). Determination and pharmacokinetic study of pirfenidone in rat serum by high performance thin-layer chromatography, *Journal of Chromatographic Science, 54(7)*, 1115–1119. https://doi.org/10.1093/chromsci/bmw067.

15   Bhole, R.P., & Tamboli, F.R. (2018). Development and validation of stability indicating HPTLC-MS method for estimation of empagliflozin in pharmaceutical dosage form, *Analytical Chemistry Letters, 8(2)*, 244–56. DOI: 10.1080/22297928.2017.1404929

16   Bhole, R.P., Birader, P., &Bonde, C.G. (2018). Development and validation of stability indicating HPTLC method for estimation of dasatinib and characterization of degradation products by using mass spectroscopy, *Eur. J. of Analytical Chemistry, 13(4)*, 1–11, DOI: https://doi.org/10.29333/ejac/90678

17   Bhole, R.P., Zombade, T., Bonde, C.G., & Zambare, Y.B. (2019). Identification and characterization of degradation products by using Ms-Ms studies for developed and validated stability indicating HPTLC method for estimation of nintedanib esylate in pharmaceutical dosage form, *Eur. J. of Analytical Chemistry, 14(2)*, 60–70. DOI: https://doi.org/10.29333/ejac/90678

18   Bhole, R.P., Naksakhare, S., Bonde, C.G., & Zambare, Y.B. (2019). A stability indicating HPTLC method for apremilast and identification of degradation products using MS/MS, *J. Pharm. Sci. & Res., 11(5)*, 1861–1869.

L.S. Egorova, E.A. Leites[*]

Altai State University, Barnaul, Russia
(Corresponding author′s e-mail: leites-elena@yandex.ru)

Extraction-photometric determination of osmium using quaternary water-thiopyrine-trichloroacetic and orthophosphoric acid system

The article is devoted to the extraction-photometric determination of osmium. The aim was to modify the well known extraction-photometric determination of osmium by replacing chloroform, used as an organic solvent in a traditional extraction system, on to water, which is the only liquid component in the layering system. This made it possible to eliminate the toxic organic solvent from the system. The optimal conditions for the osmium extraction were selected, taking with the fact that the consumption of thiopyrine, as an expensive reagent, should be minimal. The results of the developed methodology for determining microgram amounts of osmium with thiopyrine were presented by the example of a model mixture corresponding to the composition of a platinum sponge. The interfering effect of Al (III), B (III), Bi (III), Fe (III), Au (III), Ir (II), Cd (II), Co (II), Ca (II), Si (IV), Mg (II), Mn (II), Cu (II), Mo (VI), As (V), Ni (II), Sn (IV), Pd (II), Rh (II), Pb (II), Ag (I), Sb (III), Te (IV), Cr (III), Zn (II) contained in a platinum sponge was investigated. The interfering effect of copper has been established, which is eliminated by masking with ascorbic acid.

Key words: osmium, thiopyrine, extraction-photometric determination, platinum sponge, complexation, synthesis of drugs, cortisone.

Introduction

Osmium is used to create particularly durable alloys, in the manufacture of hands and axes for measuring equipment, clockworks, and the production of drugs, for example, the cortisone. The high catalytic ability of osmium is used in chemistry and petrochemistry, osmium tetroxide is employed in the synthesis of drugs, and its alloy with platinum is used in the manufacture of cardiac implants, pacemakers and valves.

There are gravimetric, titrimetric, electrochemical methods for the determination of osmium [1–3]. The spectrophotometric methods with organic reagents of various classes are most usually used: thiourea and its derivatives, selenourea, derivatives of mercapto and nitrosoquinolines, aromatic amines, amino alcohols, amino acids, various heterocyclic compounds with various functional and analytical groups (= S, –SH, –OH, –NH$_2$, =NH, ≡N) [4]. Alkali metal and ammonium thiocyanates are used as the inorganic reagents. Osmium is determined by own color of osmium (VI) hexabromide, and by the color of OsO$_4$ in an organic solvent. None of the methods makes it possible to determine osmium in the presence of all the accompanying elements of the platinum group; therefore, it is separated in the form of OsO$_4$ either by selective distillation or by selective extraction. These methods allow to concentrate osmium simultaneously. The most sensitive methods include methods for the determination of osmium using 1,5-diphenylcarbohydrazide, 1-naphthalene-4,6,8-trisulfonic acid and anthranilic acid. Very small amounts of osmium from 0.00l to 0, l μg/ml are determined with the simultaneous use of sulfanilic acid and dimethylamine. Dithiocarbamic acid derivatives are suitable for the osmium determination in the presence of an excess of platinum, palladium, iron, and some other elements [5].

Thiopyrine (TP) and its derivatives form green complexes with Ru (IV) and Os (IV, VIII). The complexes of osmium with thiopyrine and its derivatives well extracted with chloroform in the presence of thiocyanate or trichloroacetate ions [6].

The goal was to modify the well known extraction-photometric determination of osmium by replacing chloroform, used as an organic solvent in a traditional extraction system, on to water, which is the only liquid component in the layering system.

Experimental

Reagents. 6.4 M TCAA and 8.7 M H$_3$PO$_4$, OsO$_4$ solutions, crystalline thiopyrine were used.

---

[*] *Corresponding author*

Equipment. The absorption spectrum of the complex in the extract was taken with respect to the reference solution on a spectrophotometer «Spekol-10» in a quartz cuvette with $l = 1$ cm.

Experimental methodology. The extraction-photometric determination of osmium in a quaternary system without an organic solvent has been studied. It was necessary to choose the optimal conditions for its extraction. The consumption of thiopyrine, as an expensive reagent, should be minimal. The choice of the optimal ratio of acids was carry out by the method of isomolar series.

6.4 M TCAA and 8.7 M H_3PO_4 solutions in various ratios were place in a series of tubes, taking into account that the total volume of the system should not exceed 5 ml. As a result, it was found that sufficient for practical purposes volume of the organic phase is equal to 2 ml. It can be obtained when the volume ratio of acid solutions is 2.5 ml of TCAA and 2.5 ml of H_3PO_4, i.e. 16.0 mmol TCAA and 21.8 mmol H_3PO_4 or at 8:11 molar ratio of acids.

TCAA, 20 µg of Os (VIII) and 30 mg of thiopyrine were placed in a test tube in the above ratio to take the absorption spectrum of the extract. The absorbance of the green-colored extract was measured after phase separation. Containing all the starting components except osmium solution was used as a comparison solution.

Results and Discussion

The maximum light absorption of the complex was observed at $\lambda = 728$ nm. The optical characteristics of the extract are similar to the optical characteristics of the complex of osmium with thiopyrine in aqueous solutions and in chloroform [6].

The reaction of forming a colored compound requires a certain excess of complexing reagent. In some cases, it is sufficient to introduce a small excess (20–30 %) of the reagent compared with the stoichiometrically calculated amount for the complete binding of metal ions to the colored compound. In other cases, a significant excess of reagent is needed when the stability of the colored complex is small. So the optimal amount of reagent has been established. The obtained dependence is shown in Figure 1, from which it can be see that the absorbance of the extract reaches a maximum at 0.12 mmol of thiopyrine. All further studies were performed with an amount of thiopyrine equal to 0.15 mmol.

Verification of compliance with the basic law of light absorption of the extract was carry out under the selected optimal conditions: 21.8 mmol TCAA, 16.0 mmol H_3PO_4, 0.15 mmol thiopyrine, a variable amount of osmium (VIII). The total volume of the system was 5.0 ml, the volume of the organic phase was 2.0 ml. The comparison solutions were prepared in a similar way.
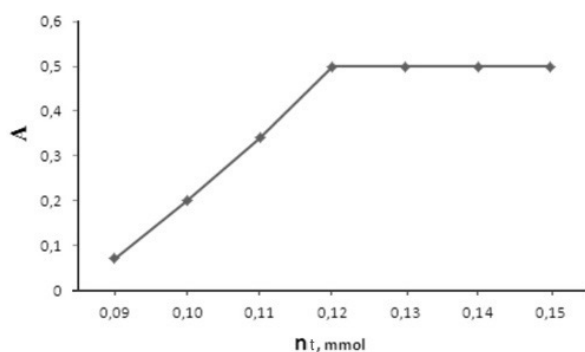
Figure 1. Dependence of the absorbance
of the extract of the Os (VIII)
with thiopyrine complex
on the thiopyrine (t) amount
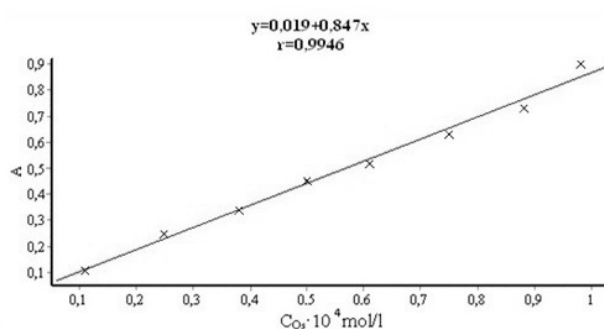
Figure 2. Calibration graph of the extraction-photometric
determination of Os (VIII) with thiopyrine in the water –
thiopyrin – trichloroacetic acid — orthophosphoric acid
tetra-quaternary system

Figure 2 shows the dependence of the absorbance of the extract of the osmium content. A linear relationship was observed when 2 to 40 µg of osmium introduced into the system. This linear relationship is actually a calibration curve line for the extraction-photometric determination of osmium. The calibration graph parameters were calculated using the least squares method. The values for the linear equation parameters $y = ax + b$ (there a and b are coefficients, r is the correlation coefficient, S_a, S_b, S_0 are the standard deviations of the a, b and r parameters) are given in Table 1.

Calculation of the calibration graph equation parameters

a	S_a	b	S_b	r	S_0
$8.8 \cdot 10^3$	$2.3 \cdot 10^{-2}$	$1.2 \cdot 10^{-3}$	$3.6 \cdot 10^2$	0.995	$2.9 \cdot 10^{-2}$

The Os:R molar ratios of 1:4 with TP and 1:2 with dithiopyrilmethane (DTM) were established using the equilibrium shift method. The absorption increases with an increase in the excess of reagent and its maximum value is reached at a thirtyfold excess of thiopyrine. The color of the solutions is stable over time. Law of Beer is observed for 1–20 μg/ml Os. The complexes of osmium with thiopyrine and its derivatives well extracted with chloroform in the presence of thiocyanate or trichloroacetate ions. The light absorption curve line has a maximum at 690 nm in the presence of trichloroacetic acid (TCAA). Law of Beer is valid for 1.5–30 μg/ml osmium, the concentration of TCAA in the solution should be at least 0.05 M. Extraction-photometric determination differs from photometric because it allows to determine the Os in the presence of significant amounts of Ru (even at 1:100 ratio of Os:Ru). Definition of 30 mg/ml of osmium does not interfere with 5-fold amounts of Al (III), Cd (II), Co (II), Cr (III), Fe (III), Mg (II), Mn (II), Ni (II), Pd (II), Ti (IV) and Zn (II), 10-fold amounts of Rh, equal amounts of Pt [6].

The experimental values of the calibration graph points were used to calculate ε_{app}. The obtained value ε_{app} equal to $8.9 \cdot 10^3$ slightly differs from $\varepsilon_{app} = 6.3 \cdot 10^3$ specified in [6] due to a significant change in the composition and properties of the extract.

Well-known Asmus and Bent-French methods were used to determine the Os:TP ratio in the extraction complex [7]. Coincident ratios Os:TP = 1:4 in the complex were obtained, which is consistent with published data.

Osmium is found in such various objects as platinum sponge, copper-nickel-sulfide ores, etc. A model mixture corresponding to the composition of the platinum sponge was chosen to develop the method for determining osmium with thiopyrine. The osmium content in it is $(8–800) \cdot 10^{-4}$ %. Other impurities $(n \cdot 10^{-4})$ are also contained in the platinum sponge: Ag — 200; Al — 100; As — 200; Au — 100; Ir — 20; Ca — 40; Cd — 100; Co — 500; Cr — 40; Cu — 20; Fe — 100; Mg — 100; Mn — 40; Mo — 100; Ni — 40; Os — 800; Pb — 200; Sb — 50; Si — 100; Sn — 50; Tl — 500; Zn — 500.

The influence of foreign ions on the results of the 10 μg osmium determination was studied, since other elements besides osmium are present in the form of impurities in the platinum sponge. The 3–5 % deviation of the extract absorbance from its value, measured when determining osmium without an extraneous ion, was taken as an influence criterion (Table 2).

Influence of interfering ions on the osmium determination

Interfering ion	m_{ion} / m_{Os}	Interfering ion	m_{ion} / m_{Os}
Al (III)	20	Mo (VI)	20
B (III)	10	As (V)	50
Bi (III)	5	Ni (II)	10
Fe (III)	20	Sn (IV)	13
Au (III)	20	Pd (II)	5
Ir (II)	100	Rh (II)	10
Cd (II)	20	Pb (II)	100
Co (II)	100	Ag (I)	50
Ca (II)	10	Sb (III)	50
Si (IV)	200	Te (IV)	10
Mg (II)	20	Cr (III)	100
Mn (II)	5	Zn (II)	10
Cu (II)	3		

It was found that copper and antimony already in 1:1 ratio interfered at the determination of osmium with thiopyrine, all other ions did not interfere at this process. The interfering effect of copper was masked with 0.03 g of ascorbic acid. The determination of osmium in a mixture simulating the composition of a platinum sponge was carried out by the method of additions.

Graphic option. 2.20 μg Os (corresponds to $7.3 \cdot 10^{-2}$ % Os), 5 ml of 8.7 M H_3PO_4, 5 ml of 6.4 M CCl_3COOH, 30 mg of thiopyrine, 0.03 g of ascorbic acid to mask copper, 0.8 ml of a mixture containing 3.0 mg Pt were placed in a 15 ml volumetric tube. The osmium content was gradually increased by addition of 5.0, 15.0; 25.0 and 35.0 μg to the next 4 volumetric tubes, respectively. The comparison solution contained all the starting components except osmium.

The absorbance of the extracts was measured at $\lambda = 728$ nm after complete phase separation. The graph was built in the $A - \omega_{Os}$% coordinates, plotting the absorbance of the extract of the analyzed model solution on the ordinate axis without additional osmium. The absolute value of the segment ω_x, cut off on the ordinate axis, corresponds to $\omega_{Os} = 7.5 \cdot 10^{-2}$ % in the mixture.

Estimated option. The above amounts of phosphoric acid, trichloroacetic acid, thiopirine and mixture, as well as 15.0 μg of osmium (additive) were placed in 2 volumetric tubes with a capacity of 15 ml.

The calculation was carried out according to the formula:

$$\omega_{x=} \frac{A_x}{A_{x+d} - A_x} \cdot \omega_d ,$$

where ω_x is the mass fraction of osmium in the mixture, %; ω_d is the mass fraction of osmium supplement, %; A_x is the absorbance of the extract with a complex of thiopyrine with osmium extracted from a model mixture of a platinum sponge; A_{x+d} is the absorbance of the extract with the addition of osmium.

Determination of osmium in the model mixture of platinum sponge is show in Table 3.

T a b l e 3

Determination of osmium in the model mixture of platinum sponge

Content of Os, ω, %	Found by graphic option, ω, %	Found by estimated option, (ω±δ), %	s_r
$7,3 \cdot 10^{-2}$	$7,5 \cdot 10^{-2}$	$(7,3 \pm 0,2) \cdot 10^{-2}$	0,02

The content of Os obtained by graphical and estimated options of the additive method is consistent with each other.

Conclusions

So the well-known extraction-photometric method for determining osmium was modified by replacing the traditional extraction system with chloroform, as an organic solvent, to a layering system with water as a single liquid component. It allowed to exclude the toxic organic solvent from the system. The optimal conditions for the extraction of osmium were selected: 21.8 mmol TCAA, 16.0 mmol H_3PO_4, 0.15 mmol thiopyrine. A linear relationship was observed when 2 to 40 μg of osmium introduced into the system. The results of the developed methodology for the determination of osmium with thiopyrine were presented by the example of a model mixture corresponding to the composition of a platinum sponge. The interfering effect of Al (III), B (III), Bi (III), Fe (III), Au (III), Ir (II), Cd (II), Co (II), Ca (II), Si (IV), Mg (II), Mn (II), Cu (II), Mo (VI), As (V), Ni (lI), Sn (IV), Pd (II), Rh (II), Pb (II), Ag (I), Sb (IIl), Te (IV), Cr (III), Zn (II) contained in a platinum sponge was investigated. The interfering effect of copper has been established, which is eliminated by masking with ascorbic acid.

References

1 Лосев В.Н. Сорбционно-фотометрическое определение осмия после его выделения из газовой фазы силикагелем, химически модифицированным меркаптогруппами / В.Н. Лосев, И.П. Бахвалова, Ю.В. Кудрина, А.К. Трофимчук // Журн. общ. хим. — 2004. — Т. 74, № 8. — С. 796–799.

2 Barnard C.F.J. Oxidation States of Ruthenium and Osmium / C.F.J. Barnard // Platinum Metals Review. — 2004. — Vol. 48. — P. 157. — DOI:10.1595/147106704X10801

3 Ливингстон С. Химия платиновых металлов / С. Ливингстон. — М.: Мир, 1972. — 366 с.

4 Радушев А.В. Спектрофотометрические методы определения осмия, рутения, золота / А.В. Радушев, Г. Аккерман // Заводск. лаб. — 1978. — Т. 35, № 12. — С. 1431–1433.

5 Воробьева Р.С. Гигиена и токсичность кадмия / Р.С. Воробьева. — М.: Науч. обзор, 1979. — 184 с.

6 Акимов В.К. Тиопирин и его некоторые производные как аналитические реагенты на осмий / В.К. Акимов, А.И. Бусев, Л.Я. Клиот // Журн. аналит. хим. — 1977. — Т. 32, № 5. — С. 1004–1008.

7 Булатов М.И. Практическое руководство по фотоколориметрическим и спектрофотометрическим методам анализа / М.И. Булатов, И.П. Калинкин. — М.: Химия, 1976. — С. 376.

Л.С. Егорова, Е.А. Лейтес

«Су – тиопирин – трихлорацетикалық және ортофосфор қышқылы» төрттік жүйесінің көмегімен осмийді экстракциялық-фотометриялық анықтау

Мақала осмийдің экстракциялық-фотометриялық анықталуына арналған. Мақсаты осмийдің экстракциялық-фотометриялық анықтамасын дәстүрлі экстракция жүйесін хлороформға органикалық еріткіш ретінде қабыршақтайтын жүйе мен бір сұйық компонент — су ауыстыру арқылы өзгерту болды. Бұл жүйе улы органикалық еріткішті жоюға мүмкіндік берді. Осмийді алудың оңтайлы шарттары қымбат реагент ретінде тиопиринді тұтынудың минималды болуын ескере отырып, таңдалды. Тиопиринмен осмийдің микрограмм мөлшерін анықтауға арналған әзірленген әдістеменің нәтижелері платина губкасының құрамына сәйкес модельді қоспаның мысалында келтірілген. Al (III), B (III), Bi (III), Fe (III), Au (III), Ir (II), Cd (II), Co (II), Ca (II), Si (II), Si (кедергі әсері IV), Mg (II), Mn (II), Cu (II), Mo (VI), As (V), Ni (II), Sn (IV), Pd (II), Rh (II), Pb (Платина губкасында орналасқан II), Ag (I), Sb (III), Te (IV), Cr (III), Zn (II). Аскорбин қышқылымен маскирлеу арқылы жойылатын мыстың араласатын әсері анықталды.

Кілт сөздер: осмий, тиопирин, экстракциялық-фотометриялық анықтау, платина губкасы, комплекс түзуші, дәрілік препараттардың синтезі, кортизон.

Л.С. Егорова, Е.А. Лейтес

Экстракционно-фотометрическое определение осмия с помощью четверной системы «вода – тиопирин – трихлоруксусная и ортофосфорная кислоты»

Статья посвящена экстракционно-фотометрическому определению осмия. Цель заключалась в модификации известного экстракционно-фотометрического определения осмия путем замены традиционной экстракционной системы с хлороформом в качестве органического растворителя на расслаивающуюся систему с единственным жидким компонентом — водой. Это позволило исключить из системы токсичный органический растворитель. Выбраны оптимальные условия извлечения осмия с учетом того, что расход тиопирина, как дорогостоящего реагента, должен быть минимальным. Представлены результаты разработанной методики определения микрограммовых количеств осмия с тиопирином на примере модельной смеси, соответствующей составу платиновой губки. Исследовано мешающее влияние Al (III), B (III), Bi (III), Fe (III), Au (III), Ir (II), Cd (II), Co (II), Ca (II), Si (IV), Mg (II), Mn (II), Cu (II), Mo (VI), As (V), Ni (II), Sn (IV), Pd (II), Rh (II), Pb (II), Ag (I), Sb (III), Te (IV), Cr (III), Zn (II), содержащихся в платиновой губке. Установлено мешающее влияние меди, которое устраняют маскированием аскорбиновой кислотой.

Ключевые слова: осмий, тиопирин, экстракционно-фотометрическое определение, платиновая губка, комплексообразование, синтез лекарственных средств, кортизон.

References

1   Losev, V.N., Bakhvalova, I.P., Kudrina, Yu.V., & Trofimchuk, A.K. (2004). Sorbtsionno-fotometricheskoe opredelenie osmiia posle eho vydeleniia iz hazovoi fazy silikahelem, khimicheski modifitsirovannym merkaptohruppami [Sorption-photometric determination of osmium after its separation from the gas phase by silica gel chemically modified with mercapto groups]. *Zhurnal obshchei khimii — Journal of General Chemistry, 74(8)*, 796–799 [in Russian].

2   Barnard, C.F.J. (2004). Oxidation States of Ruthenium and Osmium. *Platinum Metals Review, 48,* 157. doi:10.1595/147106704X10801

3   Livingston, S. (1972). *Khimiia platinovykh metallov [Chemistry of Platinum Metals]*. Moscow: Mir [in Russian].

4   Radushev, A.V., & Akkerman, G. (1978). Spektrofotometricheskie metody opredeleniia osmiia, ruteniia, zolota [Spectrophotometric methods for the determination of osmium, ruthenium, gold]. *Zavodskaia laboratoriia — Factory laboratory, 35(12)*, 1431–1433 [in Russian].

5   Vorobyeva, R.S. (1979). *Hihiena i toksichnost kadmiia [Cadmium Hygiene and Toxicity]*. Moscow: Nauchnyi obzor [in Russian].

6   Akimov, V.K., Busev, A.I, & Kliot, L.Ya. (1977). Tiopirin i eho nekotorye proizvodnye kak analiticheskie reahenty na osmii [Thiopyrin and its some derivatives as analytical reagents for osmium]. *Zhurnal analiticheskoi khimii — Journal of Analytical Chemistry, 32(5)*, 1004–1008 [in Russian].

7   Bulatov, M.I., & Kalinkin, I.P. (1976). *Prakticheskoe rukovodstvo po fotokolorimetricheskim i spektrofotometricheskim metodam analiza [Practical guide to Photocolorimetric and Spectrophotometric Analysis Methods]*. Moscow: Khimiia [in Russian].

L.E. Kalichkina[*], A.A. Bakibaev, V.S. Malkov

National Research Tomsk State University, Russia
(Corresponding author′s e-mail: kalichkina_lyuda@mail.ru)

Spectral study of thione-thiol tautomerization of thiourea in aqueous alcohol solution

In this work we studied the equilibrium of thione–thiol tautomerization by Raman and UV spectroscopies. This type of tautomerization influences on the course and direction of the reaction between thiourea and other organic compounds. The studies were carried out in water and aqueous alcohol medium. Methanol, ethanol, propanol-1 and propanol-2 were used as alcohols. Hydrochloric acid was used to protonate thiourea in water and aqueous alcoholic solutions. UV spectroscopy made it possible to establish the tautomer ratio in water and aqueous alcohol solutions as the ratio of the intensities of absorption bands at 236 and 200 nm. There is an increase in the content of the thiol form and a decrease of the thione form observed in the row water-methanol-ethanol-propanol-isopropyl alcohol. The addition of hydrochloric acid to the thiourea water or aqueous alcohol solutions leads to the increase of the thione form and to the decrease of the thiol form in the composition. The thione form of thiourea can be determine by Raman spectra of –C=S group. The thiol form of thiourea is difficult to detect by Raman spectroscopy due to the overlap of the –S–H bond absorption band with alcohols absorption bands.

Keywords: thiourea, thione–thiol tautomerization, Raman-spectroscopy, UV-spectroscopy, autoprotolysis constant, protonation of thiourea, solvent effects.

Introduction

Thiourea is one of the common reagents to synthesize sulfur-containing heterocyclic compounds. These compounds are used in medicine to produce thiobarbituric acid and sulfathiazolum [1], as a corrosion inhibitor for metals [2], a ligand in chemosensors for transition and rare earth metals [3], etc.

Thiourea has a planar (N_2CS) core; its molecule consists of electron-withdrawing –C=S and electron-donating NH_2 groups; thus, there is an equilibrium between the thione (1) and thiol (2) forms in solution (Fig. 1).
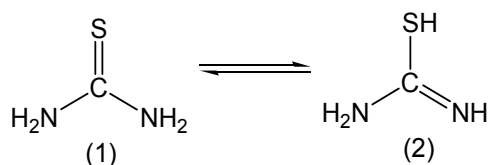
Figure 1. Thiourea thione–thiol tautomerization

The equilibrium of thione–thiol tautomerization depends on many factors, but the pH and type of solvent are the most significant. This type of tautomerization influences on the chemical reaction progress and directions as shown in [4] on the example of the thiourea reaction with glyoxal to obtain 4,5-dihydroxy-imidazolidin-2-thione or tetrahydrothiazolo[5,4-d]thiazole-2,5-diimine. Thus, it is important to identify which thiourea form predominates in solution under different conditions in order to understand the chemistry of the formation of sulfur-containing heterocycles.

The effect of pH on the thione–thiol equilibrium in thiourea aqueous solutions was studied using NMR, HPLC-MS, GC-MS, IR, UV and Raman spectroscopy [4–8]. The influence of methanol, dioxane, and acetonitrile on this equilibrium was studied in Ref. [3]. However, there was no systematic study of thione–thiol tautomerization of thiourea in aqueous alcohol solution.

UV spectroscopy is one of the simplest and most informative methods to investigate the thione–thiol tautomerization. It allows to establish the tautomer ratio in the solutions. A combination of UV and Raman spectroscopy makes it possible to define the isomeric forms of thiourea more precisely.

---

[*] *Corresponding author*

Based on the above, the aim of this work is to investigate the thione–thiol tautomerization of thiourea in aqueous alcohol solution by Raman and UV spectroscopies.

Experimental

Water was purified using a Milli-Q purification system (Merck Millipore, USA). All reagents and chemicals used were of analytical grade. Methanol (99.9 %), Ethanol (99.9 %), Propanol-1, Propanol-2, thiourea (99+ %) were purchased from Acros Organics (USA) and 35 % hydrochloric acid was purchased from Ecos-1 (Russia).

The UV- experiments were carried out using a Shimadzu UV-1800 (Shimadzu, Japan). The spectral data was collected in the range from 200 to 300 nm. Solutions of thiourea in water or water/alcohol 60/40 vol. % with 0.042 mg/ml thiourea concentration were used for UV experiments. Protonation of thiourea were carried out by addition of hydrochloric acid to pH = 2.

Raman spectra were obtained by using iHR SP320 Raman spectrometer from Horiba Scientific. 2 %-Solutions of thiourea in water or water/alcohol 60/40 vol. % were used for Raman experiments.

Results and Discussion

Firstly, the aqueous alcohol solutions of thiourea were investigated by UV spectroscopy. The UV spectra of the thiourea solution in water have two absorption maxima at 200 nm and 236 nm as shown in Figure 2.
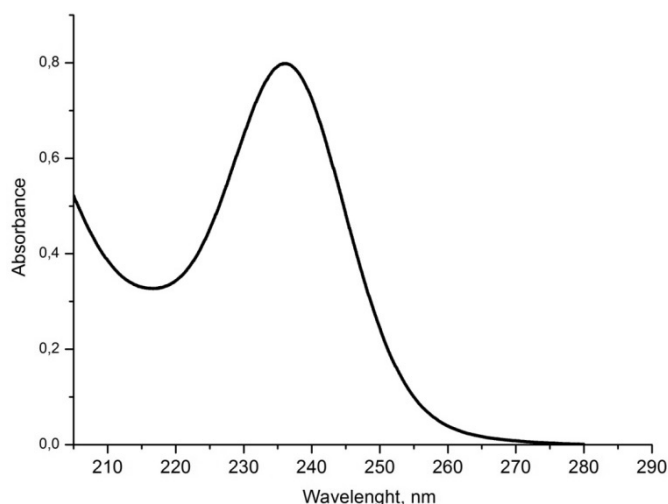
Figure 2. UV spectra of the thiourea solution in water

Absorption at 200 nm is due to the charge transfer between two amino groups, which is characterized by the resonance structure (Fig. 3) and refers to the protonated form of thiourea. Absorption at 236 nm relates to electronic transitions in the –C=S bond [9]. Thus, the first and second maxima are responsible to the presence of thiol form 2 and thione form 1, respectively.
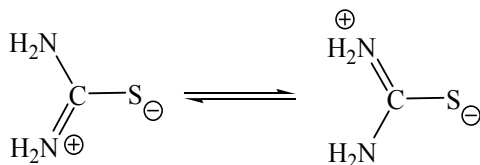
Figure 3. Charge transfer between two amino groups of thiourea

The ratio of the absorbance at 236 and 200 nm (A236/A200) was used to assess the change in the ratio of isomers.

Water is a stronger acid than alcohols; therefore, protonation of thiourea by water is easier. As a result, the use of water as a solvent instead of aqueous alcohol medium leads an increase of the thiol form and a decrease of the thione form in the composition, respectively (Table 1).

Alcohols are weaker acids compared to water due to the presence of an alkyl substituent having a positive inductive effect, which increases the electron density on the oxygen atom and, therefore, reduces the polarity of the O–H bond.

The acidity of alcohols decreases from methanol to propanol, therefore, the amount of the thione form of thiourea increases in the solution.

T a b l e 1

Absorption maxima of thiourea in the water and aqueous alcohol solutions

Solvent	Dielectric constant of solvent, ε	Absorbance at 200 nm (A_1) without hydrochloric acid	Absorbance at 236 nm (A_2) without hydrochloric acid	Absorbance at 200 nm (A_3) with hydrochloric acid	Absorbance at 236 nm (A_4) with hydrochloric acid	A_2/A_1	A_3/A_4
Water	81	0,54	0,75	0,55	0,8	1,55	1,45
Water/methanol 60/40 vol. %	33,1	0,58	0,72	0,57	0,83	1,24	1,42
Water/ethanol 60/40 vol. %	24,3	0,46	0,79	0,57	0,84	1,72	1,40
Water/propanol-1 60/40 vol. %	21,8	0,38	0,92	0,57	0,79	2,42	1,39
Water/propanol-2 60/40 vol. %	18,3	0,38	0,9	1,2	0,63	2,37	0,53

Comparison of the obtained results with reference data on the dielectric constant of solvents (Fig. 4) shows that when the dielectric constant of solvents is increased, the amount of thione form is increased, and the amount of thiol form is decreased. These facts are consistent Ref. [5].
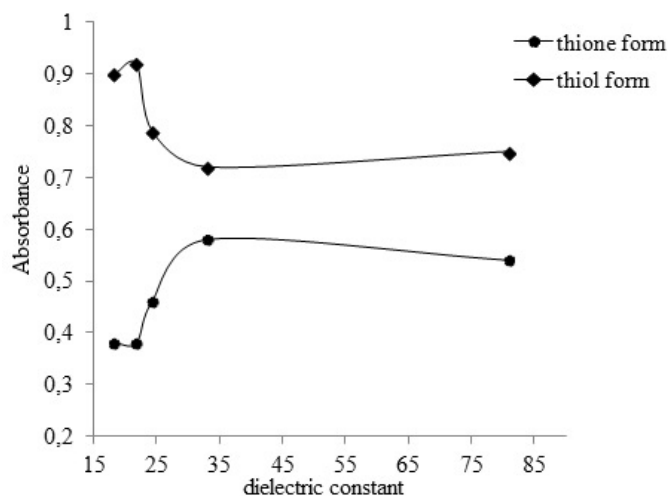
Figure 4. Dependence of thione-thiol forms on dielectric constant of solvents

The addition of hydrochloric acid to the thiourea water or water/alcohols solutions causes an increase of thione form content and a decrease of thiol form content of thiourea. This is due to the decreases of the solvent autoprotolysis constant, and to the easier protonation of thiourea as a stronger base in alcohols.

The equilibrium between the tautomeric forms of thiourea was studied by Raman spectroscopy since the thione group has a characteristic intense band corresponding to stretching vibrations of –C=S in the region of 732 cm^{-1} [10–12]. It is difficult to detect an absorption band with a low intensity in the region of 2800 cm^{-1} for the S–H bond (corresponding to the thiol form of thiourea) due to its overlap with the solvent bands. The absorption band in the region of 481 cm^{-1} (corresponding to the stretching vibrations of the –C–N–C fragment) is overlapped by the absorption bands of propyl and isopropyl alcohols. In view of the above, the effect of the alcohols only on the thione form of thiourea was considered.

The absorption band of the thiourea –C=S group in water/alcohol solutions shifts to a long wave region compared to the same band in water (Table 2). This fact is explained in Ref. [7, 10–12] by the predominance of the thione form of thiourea in solutions.

The maximum shift of the studied band is observed in isopropyl alcohol, which may be due to the steric effects and a more specific interaction of thiourea and isopropyl alcohol.

T a b l e 2

Raman bond thione group in the water and aqueous alcohol solutions

–C=S band in water, cm^{-1}	–C=S band in methanol, cm^{-1}	–C=S band in ethanol, cm^{-1}	–C=S band in propanol-1, cm^{-1}	–C=S band in propanol-2, cm^{-1}
731	738	737	737	743

In addition, the intensity of the Raman band of the thione group is decreased with increasing of the solvent dielectric constant. This also indicates the screening of this group due to the solvation by alcohols [12]. The experimental data obtained by Raman spectroscopy are consistent with the results of UV spectroscopy.

Conclusions

The effect of water/alcohol solutions on the thiourea thione-thiol isomerism was studied by Raman and UV spectroscopies. Using UV spectroscopy, it was shown that the thione form amount is increased in the water-methanol-ethanol-propanol-isopropyl alcohol row. In the same row, the thiol form amount is increased with the addition of hydrochloric acid due to the easier protonation of thiourea in water without acid and in alcohols upon acid addition. It was shown that Raman spectroscopy can be used to determine the thione form of thiourea accounting for –C=S group.

References

1 Shakeel A. Thiourea derivatives in drug design and medicinal chemistry: A short review / A. Shakeel, A. Altaf, A. Qureshi, A. Badshah // Journal of Drug Design and Medicinal Chemistry. — 2016. — Vol. 2, No. 1. — P. 10–20. DOI: 10.11648/j.jddmc.20160201.12

2 Никулина А.Е. 4,5-дигидроксиимидазолидин-2-тион как ингибитор кислотной коррозии стали в соляно-кислых водных средах // А.Е. Никулина, Л.Е. Каличкина, Г.В. Лямина, О.В. Водянкина, В.С. Мальков // Коррозия: материалы и защита. — 2017. — № 7. — Р. 18–22.

3 Vonlanthen M. Thiourea-based fluorescent chemosensors for aqueous metal ion detection and cellular imaging / M. Vonlanthen, C.M. Connelly, A. Linden, N.S. Finney // The Journal of Organic Chemistry — 2014. — Vol. 79, No. 20. — P. 6054–6060. DOI:10.1021/jo500710g

4 Singh M. The Synthetic Challenge of Thioglycolurils / M. Singh., G. Parvari, M. Botoshansky, E. Keinan, O. Reany // Eur. J. Org. Chem. — 2014. — Vol. 5, No. 2. — P. 933–940. DOI: 10.1002/ejoc.201301672

5 Schiessl W. Experimental and theoretical approaches to the protonation of thiourea: a convenient nucleophile in coordination chemistry / W.S chiessl, N. Summa, C. Webera, S. Gubo, C. Dücker-Benfera, R. Puchta, N. Eikema Hommes, R. Eldika // Zeitschrift für anorganische und allgemeine Chemie. — 2005. — Vol. 116, No. 631. — P. 2812–2819 DOI: 10.1002/zaac.200500157

6 Witanowski M. Nitrogen NMR shieldings of thiourea systems as a function of solvent polarity and hydrogen bond effects/ M. Witanowskia, Z. Biedrzyckaa, W. Sicinskaa, G.A. Webb// Journal of Molecular Structure — 2000. — Vol. 516, No. 2–3. — P. 107–112.DOI: 10.1016/S0022–2860(99)00202–1

7 Pang S. Solvent-dependent dynamics of hydrogen bonding structure 5-(methylthio)-1,3,4-thiadiazole-2(3H)-thione as determined by Raman spectroscopy and theoretical calculation / S. Pang, Y. Zhao, X. Liu, J. Xue, X. Zheng // Spectrochimica Acta Part A: Molecular and Biomolecular Spectroscopy. — 2017. — Vol. 171. — P. 470–477. DOI: 10.1016/j.saa.2016.08.023

8 Dimova V. UV spectrophotometric determination of pK's of 1,2,4-triazoline-3-thiones in sodium hydroxide solutions / V. Dimova, I. Jordanov, L. Dimitrov // Journal of the Chilean Chemical Society. — 2016. — Vol. 61, No. 3. — P. 3071–3075. DOI: 10.4067/S0717–97072016000300013

9 Hosoya H. Ultraviolet Absorption Spectra of Aqueous Solutions and Single Crystals of Thioacetamide and Thiourea / H. Hosoya, J. Tanaka, S. Nagakura // Bulletin of the Chemical Society of Japan. — 1959. — Vol. 33, No. 6. — P. 850–860. DOI: 10.1246/bcsj.33.850

10 Ragamathunnisa M. Spectroscopic study on Thiourea and Thiosemicarbazide in Non-aqueous media // M. Ragamathunnisa, E.J. Vasantha Rani, R. Padmavathy, N. Radha // Journal of Applied Physics. — 2013. — Vol. 4, No. 1. — P. 5–8.

11 Brennan N. Structural studies of thallium(I)-thiourea complexes / N. Brennan //Copyright by University of Pretoria. — 2005. P. 88–108.

12 Zhang H. Resonance Raman spectroscopic and theoretical study of geometry distortion of thiourea in 2^{1}A state / H. Zhang, Y. Zhao, X. Zheng // Chin. J. Chem. Phys. — 2012. — Vol. 25, No. 1. — P. 1–10. DOI: 10.1088/1674–0068/25/01/1–10

Л.Е. Каличкина, А.А. Бакибаев, В.С. Мальков

Су-спирт ерітінділерінде тиомочевинаның тион-тиолды таутомериясын спектрлік зерттеу

Мақалада КШ (комбинациялық шашырау) және УК спектроскопия әдістерімен тиомочевинаның тион-тиолды таутомериясының тепе-теңдігі зерттелген. Тион-тиолды изомерия тиомочевина мен басқа да органикалық қосылыстар арасындағы реакцияның барысы мен бағытына әсер етеді. Тион-тиолды изомерияны зерттеу суда және су-спирт ерітінділерінде жүргізілді, спирт ретінде метанол, этанол, пропанол-1, пропанол-2 алынды. Тұз қышқылы суда және су спирт ерітінділерінде тиомочевинаны протондау үшін пайдаланылды. УК-спектроскопия судағы және су-спирт ерітінділеріндегі таутомерлердің қатынасын 236 және 200 нм кезінде сіңіру жолақтарының қарқындылығының қатынасы ретінде орнатуға мүмкіндік берді. Су-метанол-этанол-пропанол-изопропил спирті қатарында тиомочевинаның тиол формасы құрамының артуы және тион формасының азаюы байқалады. Суда немесе су-спирт ерітінділерінде тиомочевинадан тұратын ерітінділерге тұз қышқылын қосу тиомочевинаның тион формасының ұлғаюына және тиол формасының азаюына әкеледі. КШ спектроскопия әдісін –C=S топ бойынша тиомочевинаның тион формасын анықтау үшін пайдаланылады. S–H байланысы сіңіру жолақтарының спирттердің сіңіру жолақтарымен жабылуына байланысты тиомочевинаның тиол формасын комбинациялық шашырау спектроскопиясы арқылы анықтау қиын.

Кілт сөздер: тиомочевина, тион-тиолды таутомерия, КШ-спектроскопия, УК-спектроскопия, автопротолиз тұрақтысы, тиомочевинаны протондау, еріткіш әсері.

Л.Е. Каличкина, А.А. Бакибаев, В.С. Мальков

Спектральное исследование тион-тиольной таутомерии тиомочевины в водно-спиртовых растворах

В статье исследовано равновесие тион-тиольной таутомерии тиомочевины методами КР- и УФ-спектроскопии. Тион-тиольная изомерия влияет на ход и направление реакции между тиомочевиной и другими органическими соединениями. Исследование тион-тиольной изомерии проводили в воде и водно-спиртовых растворах, в качестве спиртов были выбраны: метанол, этанол, пропанол-1, пропанол-2. Соляную кислоту использовали для протонирования тиомочевины в воде и водных спиртовых растворах. УФ-спектроскопия позволила установить соотношение таутомеров в воде и водно-спиртовых растворах как отношение интенсивностей полос поглощения при 236 и 200 нм. В ряду «вода – метанол – этанол – пропанол – изопропиловый спирт» наблюдаются увеличение содержания тиольной формы и уменьшение тионной формы тиомочевины. Добавление соляной кислоты к растворам, состоящим из тиомочевины в воде или в водно-спиртовых растворах, приводит к увеличению содержания тионной формы и уменьшению содержания тиольной формы тиомочевины. Метод КР-спектроскопии по –C=S группе может быть использован для определения тионной формы тиомочевины. Тиольную форму тиомочевины трудно определить с помощью спектроскопии комбинационного рассеяния из-за перекрывания полосы поглощения связи S–H с полосами поглощения спиртов.

Ключевые слова: тиомочевина, тион-тиольная таутомерия, КР-спектроскопия, УФ-спектроскопия, константа автопротолиза, протонизация тиомочевины, эффекты растворителя.

References

1 Shakeel, A., Altaf, A., Qureshi, A., & Badshah, A. (2016). Thiourea derivatives in drug design and medicinal chemistry: A short review. *Journal of Drug Design and Medicinal Chemistry*, *2(1)*, 10–20.

2 Nikulina, A.E., Kalichkina, L.E., Lyamina, G.V., Vodyankina, O.V., Malkov, V.S. (2017). 4,5-Dihidroksiimidazolidin-2-tion kak inhibitor korrozii stali v soliano-kislykh vodnykh sredakh [4,5-dihydroxyimidazolidin-2-thione as an acid corrosion inhibitor for steel in water-hydrochloric acid solutions]. *Korroziia: Materialy i zashchita. — Corrosion: materials and protection.* 7, 18–22 [in Russian].

3 Vonlanthen, M., Connelly, C.M., Linden, A., & Finney, N.S. (2014). Thiourea-based fluorescent chemosensors for aqueous metal ion detection and cellular imaging. *The Journal of Organic Chemistry*, *79(20)*, 6054–6060.

4 Singh, M., Parvari, G., Botoshansky, M., Keinan, E., & Reany, O. (2014). The Synthetic Challenge of Thioglycolurils. *Eur. J. Org. Chem., 5(2)*, 933–940.

5 Schiessl, W., Summa, N., Webera, C., Gubo, S., Dücker-Benfera, C., & Puchta, R., et. al. (2005). Experimental and theoretical approaches to the protonation of thiourea: a convenient nucleophile in coordination chemistry. *Zeitschrift für anorganische und allgemeine Chemie*, *116(631)*, 2812–2819.

6   Witanowskia, M., Biedrzyckaa, Z., Sicinskaa, W, & Webb, G.A. (2000). Nitrogen NMR shieldings of thiourea systems as a function of solvent polarity and hydrogen bond effects. *Journal of Molecular Structure, 516(2),* 107–112.

7   Pang, S., Zhao, Y., Liu, X., Xue, J., & Zheng, X. (2017). Solvent-dependent dynamics of hydrogen bonding structure 5-(methylthio)-1,3,4-thiadiazole-2(3H)-thione as determined by Raman spectroscopy and theoretical calculation. *Spectrochimica Acta Part A: Molecular and Biomolecular Spectroscopy*, *171*, 470–477.

8   Dimova, V., Jordanov, I., Dimitrov, L. UV spectrophotometric determination of pK's of 1,2,4-triazoline-3-thiones in sodium hydroxide solutions (2016). *Journal of the Chilean Chemical Society*, *61(3)*, 3071–3075.

9   Hosoya, H., Tanaka, J., Nagakura, S. (1959). Ultraviolet absorption spectra of aqueous solutions and single crystals of thioacetamide and thiourea. *Bulletin of the Chemical Society of Japan*, *33(6)*, 850–860.

10 Ragamathunnisa, M., Vasantha Rani, E.J., Padmavathy, R., & Radha, N. (2013). Spectroscopic study on thiourea and thiosemicarbazide in non-aqueous media. *Journal of Applied Physics*, *4(1)*, 5–8.

11 Brennan, N.F. (2005). Structural studies of thallium (I) – thiourea complexes. *Magister Scientiae. Pretoria.*

12 Zhang, H., Zhao, Y., Zheng, X. (2012). Resonance Raman spectroscopic and theoretical study of geometry distortion of thiourea in $2^{1}A$ state. *Chin. J. Chem. Phys., 25(1)*, 1–10.

S.A. Zabolotnykh[1*], M.G. Shcherban[2], A.D. Solovyev[2]

[1]Institute of Technical Chemistry, Ural Branch of RAS, Perm, Russia;
[2]Perm State National Research University, Russia
(Corresponding author´s e-mail: zabolotsveta@mail.ru)

Effect of the hydrochloric acid concentration on the surface-active and functional characteristics of linear alkylbenzenesulfonic acid

The surface-active (surface tension, adsorption, molecule cross-sectional area in the adsorption monomolecular layer) and colloidal (viscosity, critical micelle concentration, solubilization) properties in aqueous and hydrochloric acid solutions of anionic surfactant alkylbenzenesulfonic acid (ABSA) were studied. Surface activity of ABSA increases in the presence of hydrochloric acid. Two inflections were established on adsorption isotherms with inorganic acid content of 5 and 10 wt. %, which are indicative of stepwise micelle formation. The ABSA dissociation is suppressed in the presence of hydrochloric acid, and therefore it behaves as a nonionic surfactant, forming micelles at lower concentrations. Mixed micelles, formed by dissociated and non-dissociated surfactant particles, are organized with an increase of ABSA content in mixture. The value of the surfactant limiting adsorption increases significantly at small hydrochloric acid amounts in comparison with an aqueous solution. The formed monomolecular layer is denser in the presence of inorganic acid than in an aqueous solution. The solubilization of Sudan I dye in alkylbenzenesulfonic acid increases with increasing in solution acidity. The extremum points on isotherms of solubilizing ability with 5 and 10 wt. % HCl content are observed at surfactant concentrations corresponding to the beginning and end of the formation of micelles containing alkylbenzenesulfonate ion.

Key words: alkylbenzenesulfonic acid, surface tension, critical micelle concentration, hydrochloric acid, adsorption, monomolecular layer, solubilization, Sudan I.

Introduction

Alkylbenzenesulfonic acid (ABSA) is a raw material for the production of alkylbenzenesulfonates — components of detergents, surfactants for ore flotation [1]. At the same time, ABSA itself is extremely rarely used in both enrichment [2, 3] and ion flotation [4, 5], although it has many advantages: liquidity, mixes well with water, forms a stable foam, forms precipitates with metal ions, and is also a fairly affordable reagent.

To establish the possibility of using ABSA as a flotation reagent in acidic solutions, it is necessary to study the effect of the inorganic acids concentration on the surface-active and micellar properties of ABSA solutions [6].This work is devoted to the study of the colloidal properties of ABSA hydrochloric solutions.

Experimental

Alkylbenzenesulfonic acid is an anionic surfactant with the general formula $C_nH_{2n+1}C_6H_4SO_3H$, $n = 10–14$, the basic substance content is 96 %, and the average molecular weight is 320.9 $g·mol^{-1}$. A stock solution of ABSK was prepared by dissolving an exact portion in distilled water. Solutions with a lower concentration were prepared by appropriate dilution. The hydrochloric acid content of 1, 2, 5 and 10 wt. % was created by introducing the calculated amount of concentrated HCl ($\rho = 1.182$ $g·mL^{-1}$, chemically pure).

All experiments were performed at 23 ºC (296 K). All the data, presented in the work, were obtained by averaging the results of three to four measurements.

The kinematic viscosity of the ABSA solutions was determined by SVM 3000 Stabinger viscometer (Anton Paar).

The surface tension at the «aqueous solution ABSA — air» interface was measured using a DSA 25E KRUSS tensiometer. The surface tension at various ABSA concentrations in model solutions containing 1, 2, 5, and 10 wt. % HCl was measured similarly. The value of the surface tension at the «water–air» boundary at a given temperature was taken from the reference book [7].

The critical micelle concentrations (CMC) of ABSA at different HCl contents were determined from surface tension isotherms: in semilogarithmic coordinates they correspond to the points at which the curved

---

* *Corresponding author*

section passes into a straight line parallel to the X axis [8]. Surface activity (*a*) was calculated from the CMC value (g·L^{-1}) according to the formula:

$$a = \frac{\sigma_0 - \sigma_{CMC}}{CMC},$$

where σ_0 — is the water surface tension; σ_{CMC} — is the solution surface tension during CMC.

The surface tension isotherms also were used to determine the specific adsorption (G_m) of ABSA by the formula:

$$G_m = -\frac{1}{RT}\frac{\Delta\sigma}{\Delta\ln C},$$

where *R* — is the universal gas constant.

The area occupied by the ABSA molecule (S_0) was calculated by the formula:

$$S_0 = \frac{1}{G_m N_A},$$

where N_A — is the Avogadro constant.

The solubilizing ability of ABSA was evaluated in relation to the oleophilic dye Sudan I (1-(phenylazo)-2-naphthol, chemically pure), insoluble in water, but soluble in the hydrophobic part of micelles. The dye content in the solution was determined by measuring the optical density of the solution in 0.5 cm cuvettes by UNICO spectrophotometer at $\lambda = 400$ nm. Then, the amount of solubilized dye (*S*, mg·L^{-1}) in solution was determined using the calibration graph. The optical density of a dye solution (without surfactant) in benzene was measured to construct a calibration graph. For this, an exact weighed portion of the dye was introduced into 25 mL volumetric flask to create its concentration of 10, 20, 30, 40, 50, 60 mg·L^{-1}, a certain benzene amount was added, stirred until the Sudan was dissolved, and the solution was brought to the mark with benzene. The optical densities were in the range 0.07÷0.95. The molar solubilizing ability (S_m) of ABSA solution was calculated as the ratio of the obtained *S* value to the ABSA concentration (*c*, g·L^{-1}) [9]:

$$S_m = \frac{S}{c}.$$

Results and Discussion

As can be seen from the Figure 1 (curve 1), the surface tension decreases sharply in the region of low ABSA concentrations, (to 34 mN·m^{-1}, CMC$_1$ = 0.74 g·L^{-1} ABSA). That represents the gradual filling process of the surface layer with surfactant molecules and reaching the adsorption limit value. After reaching a critical micelle concentration, the decrease in surface tension slows down with increasing ABSA content, that is associated with the micelles formation in the solution volume [10]. A further increase in the ABSA concentration, apparently, causes a transition from spherical micelles formed in solution at low surfactant concentrations to asymmetric, nonspherical micelles, which affects the surface layer state. These changes are also associated with the presence of a slight bend on the surface tension isotherm at ~8.5 g·L^{-1} ABSA and a sharp increase in the solutions viscosity (Fig. 1, curve 2).
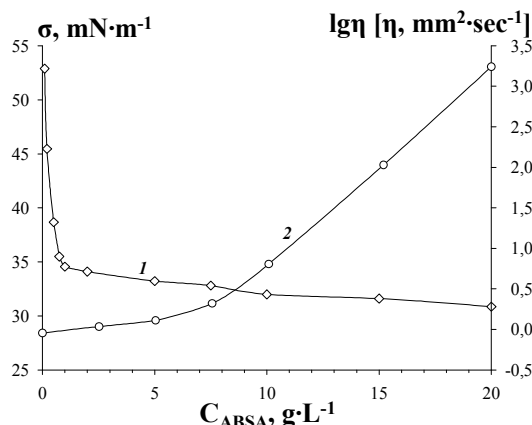
Figure 1. Isotherms of surface tension (*1*) and viscosity (*2*) of ABSA aqueous solutions

The introduction of hydrochloric acid in concentrations of 1 and 2 wt. % leads to an increase in micelle-forming ability, expressed in a decrease of CMC and surface tension during CMC, that is caused by dehydration of the polar groups of the surface-active ions in the electrolyte presence (Fig. 2). Also, with an increase in the inorganic acid concentration, a decrease in the surface tension of the solutions begins with a lower ABSA content.
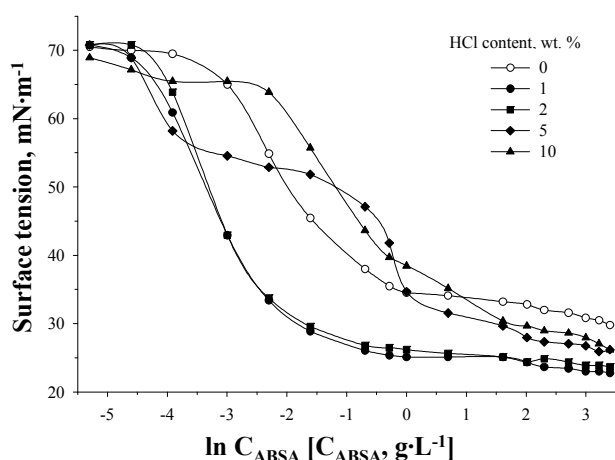
Figure 2. The effect of HCl content on surface tension isotherms of ABSA solutions

On the surface tension curves for 5 and 10 wt. % hydrochloric acid, two bends are observed. Probably, with an increase of the inorganic acid concentration, the ABSA dissociation as a weaker acid ($pK_a = 2,17$ [11]) is suppressed; as a result it behaves similarly to nonionic surfactant and forms premicellar structures in the region of lower concentrations [12]. As the ABSA content increases, the proportion of dissociated ABSA molecules (ABSA-anions) increases, which leads to the formation of mixed micelles, containing both dissociated and non-dissociated surfactant particles. These processes are accompanied by the appearance of another step on the surface tension isotherm. The obtained values of CMC depending on the medium ionic strength are presented in Table 1.

The effect of ionic strength (I) on the surface-active characteristics of ABSA

C, mol·L^{-1} (C, wt. %)	I	lnCMC [CMC, g·L^{-1}]		a, mN·m^2·kg^{-1}
		CMC$_1$	CMC$_2$	
0 (0)	0	−0.3	−	50.30
0.29 (1)	0.29	−1.0	−	121.64
0.58 (2)	0.58	−1.3	−	158.48
1.45 (5)	1.45	−3.5	0.25	554.68
2.92 (10)	2.92	−3.8	−0.28	386.72

An increase of the medium acidity during the transition from water to 10 wt. % HCl, changes the conditions for the monomolecular layer formation, in comparison with an aqueous solution. That is reflected in the change of the height and maximum position on adsorption isotherms calculated from surface tension isotherms (Fig. 3). The initial injection of inorganic acid increases the value of the limiting adsorption sharply in comparison with appropriate aqueous solution. The further increase in the acid content lowers the value of the limiting adsorption, and it is achieved with smaller ABSA amounts.

This also argues in favor of the fact, that the monomolecular layer formation is facilitated with an increase of the HCl concentration. As a result, the molecules transition into volume occurs earlier with an increase in acidity. This process is accompanied by the appearance of desorption branches in solutions containing 5 and 10 wt. % HCl and characteristic extremes on the adsorption isotherms. According to the calculations made on the obtained graphical dependences, the monomolecular layers, formed with the introduction of an inorganic acid, are denser than those formed in an aqueous solution (Table 2). However, the subsequent increase in the medium acidity leads to loosening of the monomolecular layer, what is expressed in the increase of the area occupied by one surfactant molecule in it.
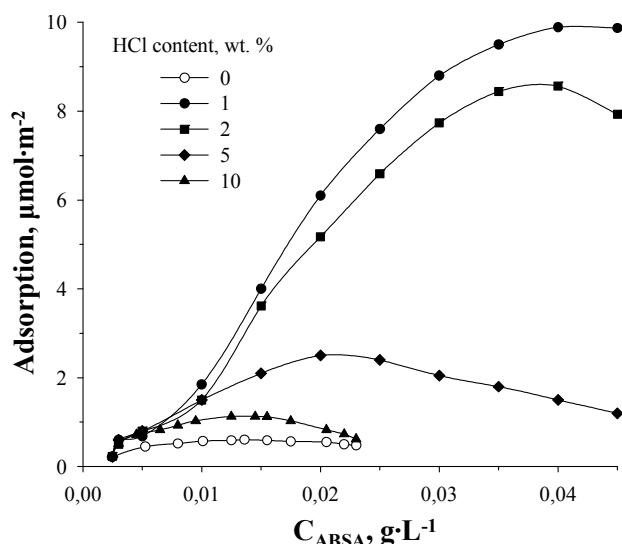
Figure 3. Adsorption isotherms at the «liquid – gas» interface in HCl solutions

Table 2

Influence of ionic strength on the parameters of the ABSA monomolecular layer at the «liquid – gas» interface

C, mol·L^{-1} (C, wt. %)	I	G$_{max}$, μmol·m^{-2}	S$_0$·10^{19}, m^2
0 (0)	0	0.61	27.39
0.29 (1)	0.29	9.89	1.68
0.58 (2)	0.58	8.56	1.94
1.45 (5)	1.45	2.50	6.64
2.92 (10)	2.92	1.13	14.70

The solubilization mechanism is mainly determined by the surfactants nature. Containing polar groups oleophilic dye is introduced into the micelles surface layer in the case of ionogenic surfactants. Its molecules are located between surfactant molecules there, oriented parallel to them and transfer polar groups to the aqueous phase. In this case, the solubilizate can dissolve both in the core and in the hydrophilic shell of the micelles.

The calibration curve was constructed to determine the amount of dye solubilized by ABSA micelles (Fig. 4). It corresponds to the straight line equation obtained by the least squares method [13]:

$$A = 0.0147 \cdot C_{dye} \ (R^2 = 0.9983),$$

where A — is the optical density; C_{dye} — is Sudan I concentration, mg·L^{-1}.
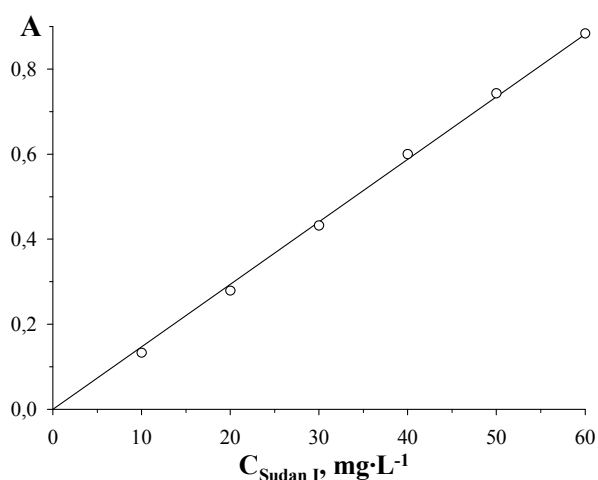
Figure 4. The calibration graph of Sudan I in benzene (UNICO, $\lambda = 400$ nm, $l = 0.5$ cm)

The amount of solubilized dye slowly increases in the initial interval with increasing surfactant concentration. The solubilization isotherms in aqueous solution and in the presence of 1 and 2 wt. % HCl practically match (Fig. 5a). The dye solubilization rise sharply with an increase in the ABSA content in a medium of 5 and 10 wt. % inorganic acid. This is probably due to the transition from one type of micelle to another.

A sharp increase in the solubilizing ability is also observed at high concentrations of hydrochloric acid. Apparently, this is due to protonation of the dye and formation of an ionic associate with the ABSA-anion (Fig. 5b).
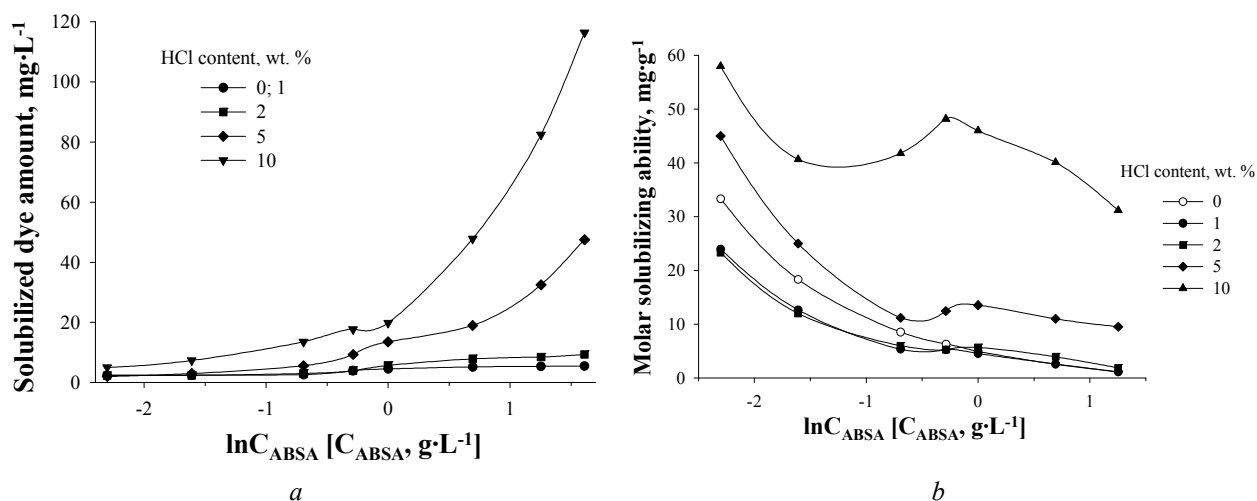
Figure 5. The effect of HCl content on the dye solubilization (*a*) and the solubilizing ability of ABSA solutions (*b*)

Various additives affect colloidal dissolution especially, since they contribute to the micelles enlargement because of their hydrophobization (i.e., lowering the effective degree of dissociation and hydration) [14]. Highs and lows abscissa on isotherms of molar solubilizing ability at acidity of 5 and 10 wt. % HCl coincide with the beginning and end of the formation of micelles containing the ABSA-anion, and the extremes severity increases with increasing concentration of hydrochloric acid (Table 3).

T a b l e 3

Intervals of micelle formation based on ABSA anion and extrema abscissas on solubilizing ability curves

C, mol·L^{-1} (C, wt. %)	ABSA concentration range, g·L^{-1} (ln$C$)	Extreme points, g·L^{-1} (ln$C$)	
		Min	Max
0 (0)	0.05 (−3.00) − 0.74 (−0.30)	−	−
1.45 (5)	0.50 (−0.69) − 1.00 (0)	0.50 (−0.69)	1.00 (0)
2.92 (10)	0.10 (−2.30) − 0.75 (−0.28)	0.20 (−1.60)	0.75 (−0.28)

Conclusions

Some conclusions can be drawn from the research results. The hydrochloric acid introduction changes the structure of the ABSA monomolecular layers and leads to an increase in its surface activity, expressed in a decrease in the critical micelle concentration value. Micelle formation proceeds in several stages in more concentrated hydrochloric acid solutions. In the region of low surfactant concentrations, ABSA dissociation is suppressed in acid medium and micelles, consisting mainly of undissociated molecules, are formed. With an increase in the ABSA content, mixed micelles are formed, containing ABSA-anions and undissociated acid. This correlates with the extrema positions on the solubilizing ability curves. A sharp increase in the solubilizing ability of ABSA in concentrated hydrochloric acid solutions in the studied range of surfactant concentrations can be caused by protonation of the dye and the formation of an ionic associate of the solubilizate with the ABSA anion.

References

1   Абрамзон А.А. Поверхностно-активные вещества: справоч. / А.А. Абрамзон, В.В. Бочаров, Г.М. Гаевой. — Л.: Химия, 1979. — 376 с.

2   Брыляков Ю.Е. Применение алкилбензолсульфокислоты при флотации апатита из руд Хибинского месторождения / Ю.Е. Брыляков, М.Е. Быков, М.А. Кострова, Г.К. Паламарчук // Обогащение руд. — 2003. — № 5. — С. 19–21.

3   Патент № 2318606 РФ. Способ флотации несульфидных руд / А.Ш. Гершенкоп, Г.А. Евдокимова, Ю.Е. Брыляков, Н.В. Воронина, Л.Л. Креймер // Опубл. БИ. 2008. № 2.

4   Абрютин Д.В. Перспективы применения процесса ионной флотации / Д.В. Абрютин, К.А. Стрельцова // Изв. высш. учеб. зав. «Цв. металлургия». — 2013. — № 3. — С. 3–6.

5   Медяник Н.Л. Удаление тяжелых металлов из растворов методом ионной флотации / Н.Л. Медяник, Н.К. Тусупбаев, И.А. Варламова, Х.Я. Гиревая, Н.Л. Калугина // Вестн. Магнитогор. гос. техн. ун-та им. Г.И. Носова. — 2016. — Т. 14, № 1. — С. 18–26. DOI: 10.18503/1995–2732–2016–14–1-18–26

6   Радушев А.В. Физические и химические свойства N-(2-гидроксиэтил)алкиламинов / А.В. Радушев, Д.В. Колташев, Т.Ю. Насртдинова, М.Г. Щербань, Л.Г. Чеканова, М.Д. Плотникова // Журн. прикл. хим. — 2010. — Т. 83, Вып. 8. — С. 1369–1373.

7   Равдель А.А. Краткий справочник физико-химических величин / А.А. Равдель, А.М. Пономарева. — Л.: Химия, 1983. — 232 с.

8   Айвазов Б.В. Практикум по химии поверхностных явлений и адсорбции / Б.В. Айвазов. — М.: Высш. шк., 1973. — 206 с.

9   Лабораторные работы и задачи по коллоидной химии / под ред. Ю.Г. Фролова и А.С. Гродского. — М.: Химия, 1986. — 216 с.

10   Холмберг К. Поверхностно-активные вещества и полимеры в водных растворах; пер. с англ. / К. Холмберг, Б. Йёнссон, Б. Кронберг, Б. Линдман. — М.: БИНОМ, 2007. — 528 с.

11   Заболотных С.А. Использование расслаивающейся системы «вода – антипирин – алкилбензолсульфокислота» для экстракции ионов металлов // С.А. Заболотных, В.О. Желнина, С.А. Денисова, А.М. Елохов, А.Е. Леснов // Журн. Сиб. федерал. ун-та. Сер. Химия. — 2017. — Т. 10, № 4. — С. 536–544. DOI: 10.17516/1998–2836–0047

12   Неудачина Л.К. Применение поверхностно-активных веществ в анализе: учеб. пос. / Л.К. Неудачина, Ю.С. Петрова. — Екатеринбург: Изд-во Урал. ун-та, 2017. — 76 с.

13   Булатов М.И. Практическое руководство по фотометрическим методам анализа / М.И. Булатов, И.П. Калинкин. — Л.: Химия, 1986. — 432 с.

14   Демьянцева Е.Ю. Солюбилизация в растворах поверхностно-активных веществ: учеб.-метод. пос. / Е.Ю. Демьянцева, Р.А. Копнина. — СПб.: СПбГТУРП, 2015. — 31 с.

С.А. Заболотных, М.Г. Щербань, А.Д. Соловьев

Хлорсутек қышқылы концентрациясының сызықтық алкилбензолсульфоқышқылының беттік-белсенді және функционалды сипаттамаларына әсері

Алкилбензолсульфоқышқылының (АБСК) беттік-белсенді (беттік керілу, адсорбция, адсорбциялық мономолекулалық қабаттағы молекуланың көлденең қимасының ауданы) және коллоидтық (тұтқырлық, мицелланың түзілуінің критикалық концентрациясы, солюбилизация) қасиеттері зерттелді. Хлорсутек қышқылының қатысында АБСК беттік-белсенділігі артады. Адсорбция изотермаларында бейорганикалық қышқыл мөлшері 5 және 10 % болған кезде екі иілу сызығы көрінеді, бұл сатылы мицелланың пайда болуын көрсетеді. Хлорсутек қышқылының қатысында алкилбензолсульфоқышқылының диссоциациясы әлсірейді, осыған байланысты ол төмен концентрацияларда мицеллалар түзе отырып, иондық емес беттік-белсенді зат ретінде әрекет етеді. Қоспада алкилбензолсульфоқышқылының мөлшері ұлғайған сайын диссоциацияланған және диссоциацияланбаған беттік-белсенді заттың бөлшектерінен тұратын аралас мицеллалар пайда бола бастайды. Хлорсутек қышқылының аз мөлшерінде сулы ерітіндімен салыстырғанда беттік-белсенді заттың шекті адсорбциясының мәні едәуір артады. Сулы ерітіндіге қарағанда, бейорганикалық қышқыл қатысында пайда болған мономолекулалық қабат тығыз болады. Судан I бояғышының алкилбензолсульфоқышқылымен солюбилизациясы ерітіндінің қышқылдылығы артқан сайын ұлғаяды. Құрамында хлорсутек қышқылы 5 және 10 % болғанда, солюбилизациялау қабілеті изотермаларында құрамында алкилбензолсульфонат — ионы бар мицеллалардың пайда болуының

басталуы мен аяқталуына сәйкес келетін беттік-белсенді зат концентрацияларының экстремумдары байқалды.

Кілт сөздер: алкилбензолсульфоқышқылы, беттік керілу, мицелла түзілуінің критикалық концентрациясы, хлорсутек қышқылы, адсорбция, мономолекулалық қабат, солюбилизация, судан I.

С.А. Заболотных, М.Г. Щербань, А.Д. Соловьев

Влияние концентрации хлороводородной кислоты на поверхностно-активные и функциональные характеристики линейной алкилбензолсульфокислоты

Изучены поверхностно-активные (поверхностное натяжение, адсорбция, площадь поперечного сечения молекулы в адсорбционном мономолекулярном слое) и коллоидные (вязкость, критическая концентрация мицеллообразования, солюбилизация) свойства водных и солянокислых растворов анионного поверхностно-активного вещества (ПАВ) алкилбензолсульфокислоты (АБСК). В присутствии хлороводородной кислоты поверхностная активность АБСК увеличивается. На изотермах адсорбции при содержании неорганической кислоты 5 и 10 мас. % установлено наличие двух перегибов, что свидетельствует о ступенчатом мицеллообразовании. В присутствии хлороводородной кислоты подавляется диссоциация алкилбензолсульфокислоты, в связи с чем она ведет себя как неионное ПАВ, образуя мицеллы при более низких концентрациях. С ростом содержания алкилбензолсульфокислоты в смеси появляются смешанные мицеллы, образованные частицами диссоциированного и недиссоциированного ПАВ. При малых количествах хлороводородной кислоты значительно увеличивается значение предельной адсорбции ПАВ по сравнению с водным раствором. В присутствии неорганической кислоты образующийся мономолекулярный слой является более плотным, чем в водном растворе. Солюбилизация красителя судана I алкилбензолсульфокислотой растет с повышением кислотности раствора. На изотермах солюбилизирующей способности при содержании хлороводородной кислоты 5 и 10 мас. % наблюдаются экстремумы при концентрациях ПАВ, соответствующих началу и окончанию формирования мицелл, содержащих алкилбензолсульфонат-ион.

Ключевые слова: алкилбензолсульфокислота, поверхностное натяжение, критическая концентрация мицеллообразования, хлороводородная кислота, адсорбция, мономолекулярный слой, солюбилизация, судан I.

References

1 Abramzon, A.A., Bocharov, V.V., & Gaevoy, G.M. (1979). *Poverkhnostno-aktivnye veshchestva [Surfactants]*. Leningrad: Khimiia [in Russian].

2 Brylyakov, Yu.Ye., Bykov, M.Ye., Kostrova, M.A., & Palamarchuk, G.K. (2003). Primenenie alkilbenzolsulfokisloty pri flotatsii apatita iz rud Khibinskoho mestorozhdeniia [Application of alkylbenzene sodium sulfo-acid in flotation of the Khibini deposit apatite]. *Obohashchenie rud — Ore dressing, 5,* 19–21 [in Russian].

3 Gershenkop, A.Sh., Evdokimova, G.A., Bryljakov, Yu.Ye., Voronina, N.V., & Kreimer, L.L. (2008). Patent No. 2318606 RF. *Publ. BI, 2* [in Russian].

4 Abryutin, D.V., & Streltsova, K.A. (2013). Perspektivy primeneniia protsessa ionnoi flotatsii [Prospects for the use of the ion flotation process]. *Izvestiia vuzov. Tsvetnaia metallurhiia — Universities' Proceedings. Nonferrous Metallurgy, 3*, 3–6 [in Russian].

5 Medyanik, N.L., Tussupbayev, N.K., Varlamova, I.A., Girevaya, Kh.Ya., & Kalugina, N.L. (2016). Udalenie tiazhelykh metallov iz rastvorov metodom ionnoi flotatsii [Removing of Heavy Metals from Solutions by the Ion Flotation Method]. *Vestnik Mahnitohorskoho hosudarstvennoho tekhnicheskoho universiteta im. H.I. Nosova — Vestnik of Nosov Magnitogorsk State Technical University, 14, 1*, 18–26. DOI: 10.18503/1995–2732–2016–14–1–18–26 [in Russian].

6 Radushev, A.V., Koltashev, D.V., Nasrtdinova, T.Yu., Shcherban, M.G., Chekanova, L.G., & Plotnikova, M.D. (2010). Fizicheskie i khimicheskie svoistva N-(2-hidroksietil)alkilaminov [Physical and chemical properties of N-(2-hydroxyethyl)-alkilamines]. *Zhurnal prikladnoi khimii — Journal of Applied Chemistry, 83, 8*, 1369–1373 [in Russian].

7 Ravdel, A.A., & Ponomareva, A.M. (1983). *Kratkii spravochnik fiziko-khimicheskikh velichin* [A quick reference to physical and chemical quantities]. Leningrad: Khimiia [in Russian].

8 Aivazov, B.V. (1973). *Praktikum po khimii poverkhnostnykh yavlenii i adsorbtsii [Workshop on the chemistry of surface phenomena and adsorption]*. Moscow: Vysshaia shkola [in Russian].

9 Frolov, Yu.G., & Grodskiy, A.S. (Eds.) (1986). *Laboratornye raboty i zadachi po kolloidnoi khimii [Laboratory work and tasks in colloidal chemistry]*. Moscow: Khimiia [in Russian].

10 Holmberg, K., Jonsson, B., Kronberg, B., & Lindman, B. (2007). *Poverkhnostno-aktivnye veshchestva i polimery v vodnykh rastvorakh [Surfactants and polymers in aqueous solutions]*. Moscow: BINOM [in Russian].

11 Zabolotnykh, S.A., Zhelnina, V.O., Denisova, S.A., Elokhov, A.M., & Lesnov, A.E. (2017). Ispolzovanie rasslaivaiushcheisia sistemy «voda – antipirin – alkilbenzolsulfokislota» dlia ekstraktsii ionov metallov [The Water – Antipyrine –

Alkyl Benzene Sulfonic Acid Stratifying System to Extract Metal Ions]. *Zhurnal Sibirskoho federalnoho universiteta. Seriia Khimiia — Journal of the Siberian Federal University. Series Chemistry, 10, 4*, 536–544. DOI: 10.17516/1998–2836–0047 [in Russian].

12 Neudachina, L.K., & Petrova, Yu.S. (2017). *Primenenie poverkhnostno-aktivnykh veshchestv v analize [The use of surface-active substances in the analysis]*. Ekaterinburg: Ural Univ. Publ. [in Russian].

13 Bulatov, M.I., & Kalinkin, I.P. (1986). *Prakticheskoe rukovodstvo po fotometricheskim metodam analiza [Practical guidance to photometric methods analysis]*. Leningrad: Khimiia [in Russian].

14 Demyantseva, E.Yu., & Kopnina, R.A. (2015). *Soliubilizatsiia v rastvorakh poverkhnostno-aktivnykh veshchestv [Solubilization in solutions of surfactants]*. Saint Petersburg: SPbGTURP [in Russian].

INORGANIC CHEMISTRY

L.M. Bogdanova[1], V.A. Lesnichaya[1], N.N. Volkova[1], V.A. Shershnev[1], V.I. Irzhak[1], Yu.S. Bukichev[2], G.I. Dzhardimalieva[1, 2*]

[1]Institute of Problems of Chemical Physics Russian Academy of Sciences, Chernogolovka, Moscow Region, Russia;
[2]Moscow Aviation Insitute (National Research University), Moscow, Russia
(Corresponding author's e-mail: dzhardim@icp.ac.ru)

Epoxy/TiO₂ composite materials and their mechanical properties

The physicomechanical properties and thermal stability of epoxy nanocomposites with TiO_2 (anatase — 75 %, rutile — 25 %) nanoparticles were studied. The TiO_2/epoxy polymer (TiO_2/EP) nanocomposite films were obtained by curing a pre-sonicated mixture of diane-epoxy resin ED-20, 4,4'-diaminodiphenylmethane and TiO_2 nanoparticles using stepwise technique: 90 ºC for 3 hours, then 160 ºC for 3 hours. Tensile tests were carried out according to American Society for Testing and Materials ASTM D882–10. The average size of TiO_2 nanoparticles and microstructure of the obtained nanocomposites were studied by scanning electron microscopy. It was found that addition of the TiO_2 nanoparticles at a concentration above 3 wt.% leads to a decrease in tensile strength at break, apparently due to secondary aggregation processes of nanoparticles. During curing, the average diameter of TiO_2 nanoparticles increases from 40 nm to 60 nm. An increase in the elastic modulus, a slight increase in the glass transition temperature, and a decrease in the elongation at break of epoxy nanocomposites at a concentration of TiO_2 nanoparticles > 1 wt.% indicate an increase in the rigidity of the epoxy matrix. The nanocomposites obtained were shown to be stable at concentrations of TiO_2 nanoparticles up to 5 wt.% and up to 300 ºC in vacuum.

Keywords: epoxy resin, curing, titanium oxide (IV), nanoparticles, tensile strength at break, elastic modulus, elongation at break, thermal stability.

Introduction

The increasing requirements for modern materials lead to intensive search for new composite materials with additional properties (mechanical, magnetic, tribological, radiation protection, etc.). The introduction of inorganic nanoparticles into organic polymers is of considerable interest, because it makes possible to create the hybrid nanocomposite materials with improved properties such as heat resistance, fire resistance, reduced gas permeability, and resistance to chemicals. Titanium oxide (IV) (TiO_2) nanoparticles are often used as inorganic fillers of polymeric materials. Titanium oxide (IV) is one of the most widely used metal oxides for photocatalytic decomposition of organic pollutants in an aqueous or gaseous medium. The photoactivity of TiO_2 is based on the process of a reversible single-electron transition $Ti^{4+} + e^- \rightleftarrows Ti^{3+}$. TiO_2 nanoparticles have a stronger photocatalytic effect than TiO_2 microparticles [1], forming reactive oxygen particles, hydroxyl radicals, H_2O_2, etc. under the influence of UV radiation. Due to exceptional characteristics of TiO_2, i.e. chemical and thermal stability, recycling potential, non-toxicity, and low cost, its applications range is quite wide: self-cleaning materials based on titanium oxide (IV), photocatalysts for the decomposition of organic compounds [2–6], anode materials [7,8], anti-bacterial coatings and packaging [9–12], etc. It is important to note that the induction of bactericidal activity due to photocatalysis is achieved by exposure to soft

---

* Corresponding author

ultraviolet (in the range of 360 nm), in contrast to the hard ultraviolet used in medicine, and is more effective than surface sterilization by ultraviolet [13].

Today one of the most pressing problems is the disposal of accumulated polymer waste, for example, based on thermoplastic materials widely used for the manufacture of packaging films, various containers and utensils for food and household purposes. Approaches based on the incineration of such waste have serious environmental consequences. One of the promising solutions to this problem is the use of polymeric materials, which contain titanium oxide nanoparticles and capable to active photodegradation under visible light. TiO_2-containing nanocomposites based on polystyrene [14], polyvinyl chloride [15], polyethylene [16, 17], polybenzyl methacrylate [18] showed significantly increased degradation rates under UV and sunlight irradiation, as compared to the pure polymers.

Containing TiO_2 nanoparticles thermoset nanocomposites have not been studied so extensively, but existing data show that TiO_2 nanoparticles are more effective than microparticles, for example in regard to mechanical properties. The effect of the size of filler particles on the mechanical properties of epoxy composite materials was studied in [19] using the example of TiO_2. Nano- (nanoparticles with a size of ~50 nm) and microcomposites (particles ~50 μm) were compared.

An increase in mechanical properties was observed at the content of nanoparticles up to 4 vol.%. The subsequent recession in properties is associated with enlargement of particles due to their agglomeration. In the case of microparticles the modulus grows while the strength decreases with filler concentration increasing. As it was shown by us earlier [20, 21], elastic and strength properties of epoxy nanocomposites are affected by both the size of nanoparticles as well as the structure of epoxy matrix and the crosslink density as shown by us earlier.

The purpose of this work was to obtain composites based on TiO_2 nanoparticles and an epoxy polymer (EP) prepared by polycondensation, and to study their mechanical properties.

Experimental

Materials

The schematic structure of the diane-epoxy resin ED-20 used in this work is shown in Figure 1a (epoxide group content is 22.6 %).

4,4'-Diaminodiphenylmethane (DDM) was purchased from Aldrich (Fig. 1, *b*). The scheme of polycondensation between epoxy ED-20 and DDM is shown in Figure 1, *c*.

Nanoparticles of TiO_2 have been prepared in the Institute of Problems of Chemical Physics of Russian Academy of Sciences using microwave irradiation [22], anatase 75 %, rutile 25 %, SSA = 33.0 m²/g, $d_{av.}$ = 46 nm.

Figure 1. Structure of epoxy resin ED-20 (*a*); structure of DDM (*b*); scheme of polycondensation (*c*)

TiO_2/EP nanocomposite films of 80–100 μm thick were synthesized ex situ, i.e. using earlier prepared nanoparticles. The mixture of ED-20, DDM at equimolar ratio, and TiO_2 was heated slightly to dissolve DDM. Then it was degassed under low vacuum, and subjected to ultrasonic treatment using Sonorex Digital 10p instrument at 35 kHz for 40 min to disperse TiO_2 properly. The suspension obtained was poured between the two glass plates, which were put into a specially designed metal form and placed in an oven for further curing. The glass plates were pretreated with a solution of dimethyldichlorosilane in toluene to prevent adhesion. Mixtures were cured at stepwise increase of temperature, the conditions were determined based on calorimetric data in order to achieve a full cure (90 ℃ for 3 hours, 160 ℃ for 3 hours). The opaque, gray-blue

TiO_2/EP films were obtained as a result of curing. The film thickness was measured using a micrometer with a 10 microns accuracy.

The glass transition temperature of TiO_2/EP films was determined by differential scanning calorimetry (DSC) on a Mettler Toledo Star System instrument at a 5 deg/min temperature scan. Mechanical tensile tests were carried out according to ASTM D882–10 on a Zwick / Roell Z 010 universal machine at a 1 mm/min loading speed. Thermogravimetric analysis of the samples was carried out using ATV-14 electronic automatic vacuum thermobalance at a 2.4 deg/min constant heating rate in vacuum (residual pressure 1.2 Pa). Size of nanoparticles was determined using FESEM Zeiss Supra 25 on carbon-coated films.

Results and Discussion

Composition and microstructure of nanocomposites

TiO_2/EP nanocomposites were prepared by ex situ ultrasonic dispersion of TiO_2 nanoparticles in epoxy resin followed by curing in the presence of DDM. According to scanning electron microscopy (SEM) data, TiO_2 nanoparticles are fairly uniformly distributed in the volume of the polymer matrix, nevertheless, nanoparticles aggregation is still observed (Fig. 2). Particle size distribution shows that during curing the average size of nanoparticles increases (from 46 nm to 78 nm at 0.5 wt.% TiO_2).

Physicomechanical properties

As can be seen from the data in Figure 3, T_g weakly depends on the TiO_2 concentration, however, it tends to slightly decrease (173 ºC — 167 ºC) at <1 wt.% concentrations and increase (167 ºC — 173 ºC) at up to 5 wt.% concentrations. The concentration dependence of the elasticity modulus shows similar behavior with 27 % increase in modulus at 3 wt.% concentration

Tensile strength at break decreases sharply at TiO_2 more than 3 wt.% concentrations, which is probably due to secondary agglomeration of TiO_2 (Fig. 4). Therefore, the working concentration should not exceed 3 wt.% TiO_2. The average diameter of TiO_2 increases (from 40 to 60 nm at 0.5 wt.% TiO_2 concentration) during curing. The change in strain at break varies by TiO_2 concentration: less than 1 wt.% concentrations cause its increase, while more than 1 wt.% concentrations cause its decrease. A significant decrease in strain at break by almost 80 % indicates a loss of plasticity and an increase in brittleness. This is consistent with an increase in elastic modulus and glass transition temperature at above 1 wt.% TiO_2 concentrations.
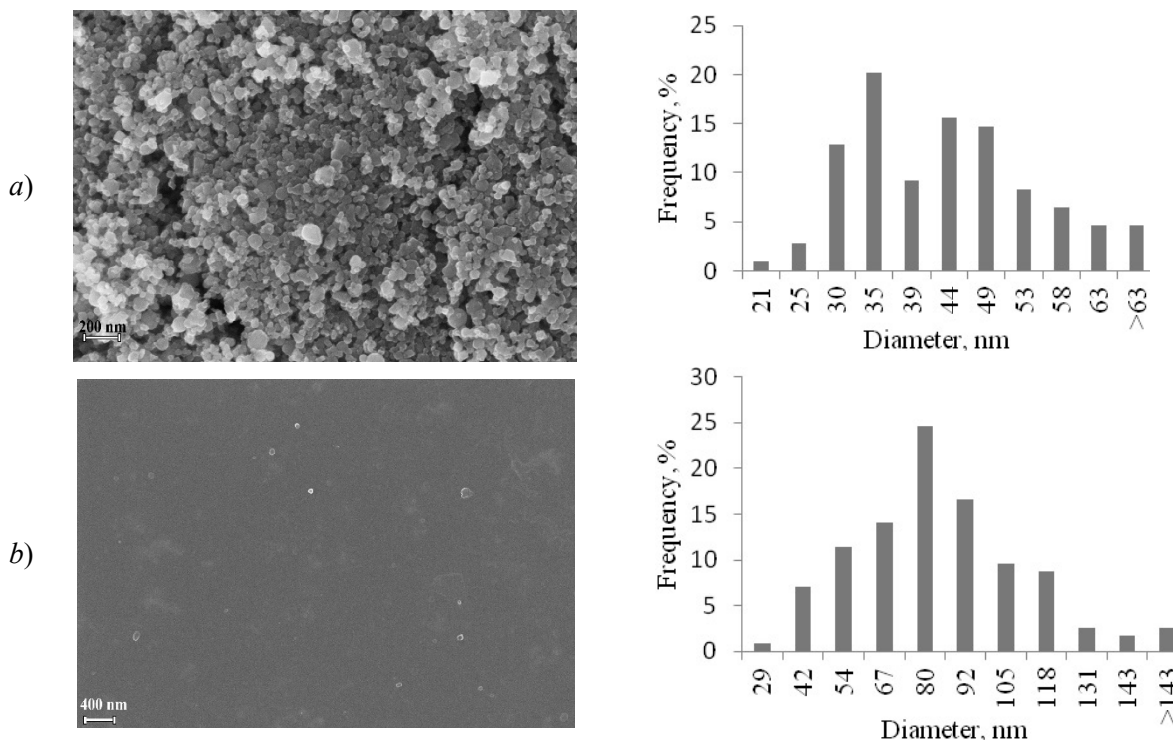
Figure 2. Scanning electron microscope (SEM) image and particle size distribution for TiO_2 nanoparticles (*a*) and TiO_2/EP nanocomposite with 0.5 wt.% of TiO_2 (*b*)
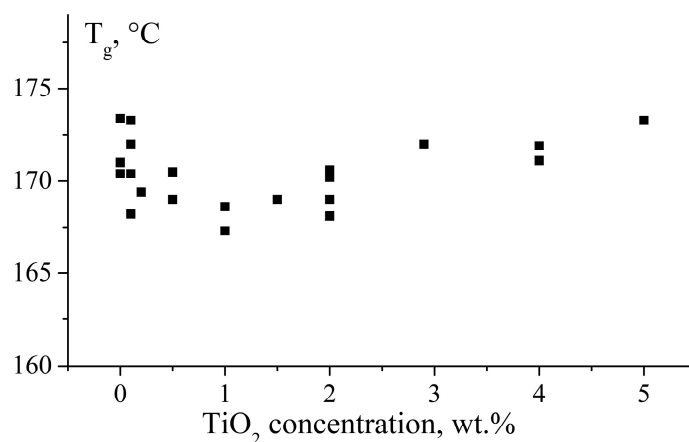
Figure 3. Tg dependence of TiO₂/EP nanocomposites on the concentration of TiO₂ nanoparticles
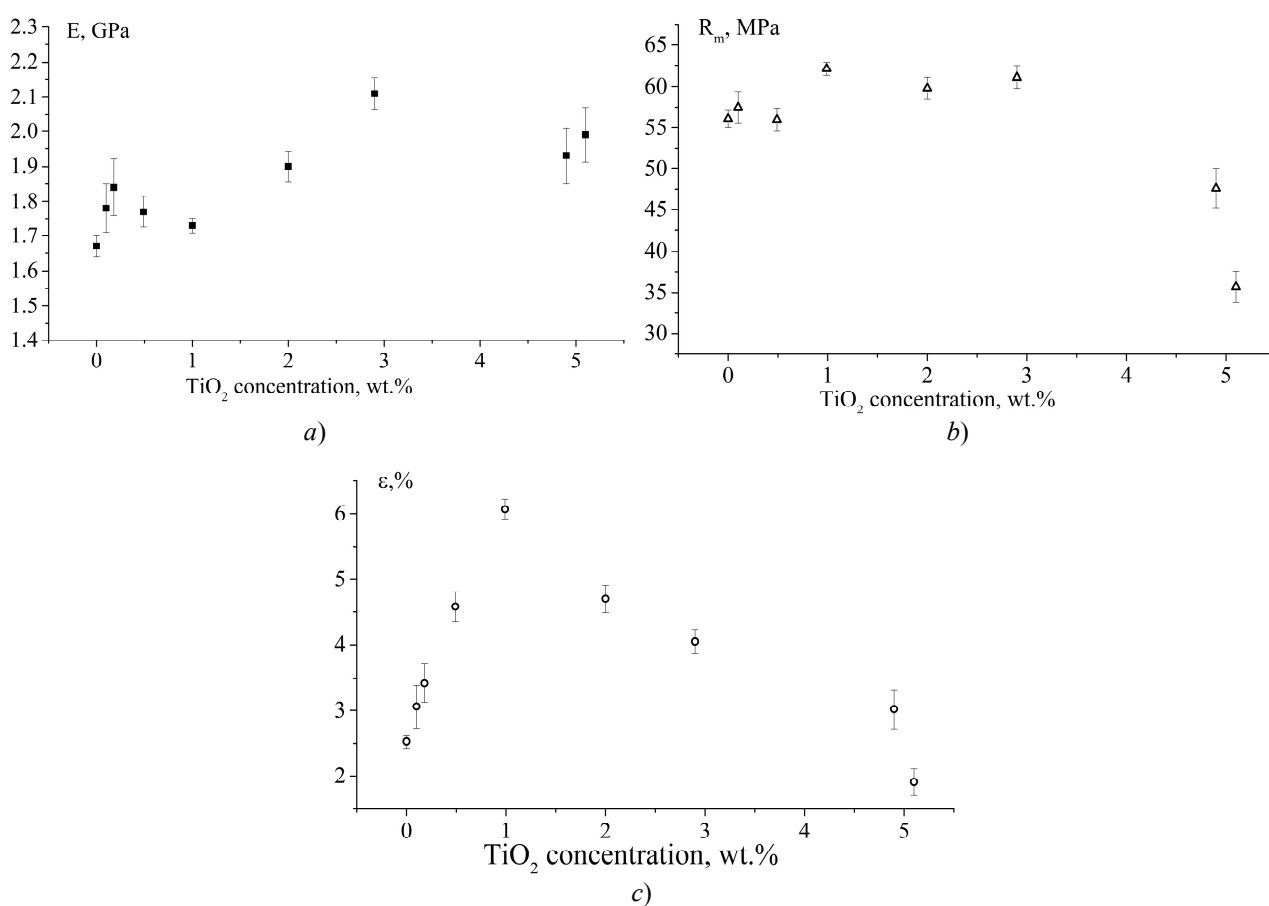
a — elastic modulus, GPa; *b* — tensile strength at break, MPa; *c* — strain at break, %

Figure 4. The dependence of the mechanical properties of TiO₂/EP nanocomposites on the concentration of TiO₂

Thermal stability of nanocomposites

Stability of nanocomposites is essential for its implementation. Therefore, the thermal stability of TiO₂/EP films with different concentrations of TiO₂ was studied. As can be seen from Figure 5, TiO₂/EP are stable at up to 5 wt.% TiO₂ concentrations and up to 300 °C temperatures in vacuum.
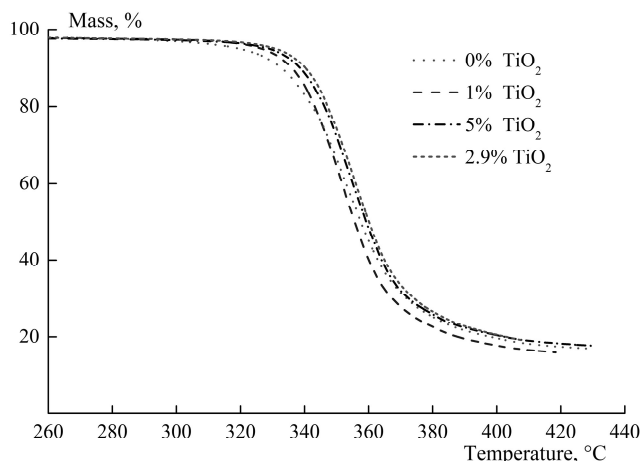
Figure 5. Thermograms of TiO$_2$/EP nanocomposites with 1–5 wt.% filler concentration
(2.4 °C/min heating rate; 1.3 Pa residual pressure)

The results obtained are in good agreement with the literature. It was found that TiO$_2$/polypropylene nanocomposites have the similar thermal stability in the nitrogen atmosphere [23]. The initial and maximum decomposition temperatures increase from 360 °C and 455 °C for the EP to 405 °C and 479 °C for the polymer nanocomposites with 2 wt % TiO$_2$ content.

Conclusions

The TiO$_2$/EP nanocomposites with 0.5–5 wt.% filler content were obtained by ex situ introduction of TiO$_2$ nanoparticles into the epoxy resin ED-20 at the stage of curing in the presence of 4,4′-diamino-diphenylmethane. It was found that the addition of TiO$_2$ nanoparticles at a concentration above 3 wt. % leads to a decrease in tensile strength at break, apparently due to secondary aggregation processes. The average diameter of TiO$_2$ nanoparticles increases from 46 nm to 80 nm during curing. An increase in the elastic modulus, a slight increase in the glass transition temperature and a drop in the elongation at break of the epoxy nanocomposite at concentrations of TiO$_2$ nanoparticles above 1 wt. %, indicate an increase in the rigidity of the nanocomposite matrix. The stability of TiO$_2$/EP in vacuum is shown at temperatures up to 300 °C and filler concentrations up to 5 wt.%.

References

1   Fujishima A. Titanium Dioxide Photocatalysis / A. Fujishima, T.N. Rao, D.A. Tryk // Journal of Photochemistry and Photobiology C: Photochemistry Reviews. — 2000. — No. 1. — P. 1–21.

2   Hamdy M.S. A Novel TiO$_2$ Composite for Photocatalytic Wastewater Treatment / M.S. Hamdy, W.H. Saputera, E.J. Groenen, G. Mul // Journal of Catalysis. — 2014. — Vol. 310. — P. 75–83. DOI: 10.1016/j.jcat.2013.07.017.

3   Song L. Photodegradation of phenol in polymer-modified TiO$_2$ semiconductor particulate system under the irradiation of visible light / L. Song, R. Qiu, Y. Mo, D. Zhang, H. Wei, Y. Xiong // Catalysis Communication. — 2007. — Vol. 8. — P. 429–433.

4   Truppi A. Visible-light-active TiO$_2$-based hybrid nanocatalysts for environmental applicationsю / A. Truppi, F. Petronella, T. Placido, M. Striccoli, A. Agostiano, M.L. Curri, R. Comparelli // Catalysts. — 2017. — Vol. 7, Iss. 4. — P. 100. http://dx.doi.org/10.3390/catal7040100.

5   Khalid N.R. Carbonaceous-TiO$_2$ nanomaterials for photocatalytic degradation of pollutants: A review / N.R. Khalid, A. Majid, M. Bilal Tahir, N.A. Niaz, Sadia Khalid // Ceramics International. — 2017. — Vol. 43. — P. 14552–14571. http://dx.doi.org/10.1016/j.ceramint.2017.08.143.

6   Zhou, T.-T. Flexible TiO$_2$/PVDF/g-C3N4 Nanocomposite with Excellent Light Photocatalytic Performance / T.-T. Zhou, F.-H. Zhao, Y.-Q. Cui, L.-X. Chen, J.-S. Yan, X.-X. Wang, Y.-Z. Long // Polymers. — 2020. — Vol. 12, No. 55. doi:10.3390/polym12010055.

7   Bella F. Combined Structural, Chemometric, and Electrochemical Investigation of Vertically Aligned TiO$_2$ Nanotubes for Na-ion Batteries / F. Bella, A.B. Muñoz-García, F. Colò, G. Meligrana, A. Lamberti, M. Destro, M. Pavone, C. Gerbaldi // ACS Omega. — 2018. — Vol. 3. — P. 8440−8450. DOI: 10.1021/acsomega.8b01117.

8   Liu S. TiO$_2$ nanorods grown on carbon fiber cloth as binder-free electrode for sodium-ion batteries and flexible sodium-ion capacitors / S. Liu, Z. Luo, G. Tian, M. Zhu, Z. Cai, A. Pan, S. Liang // Journal of Power Sources. — 2017. — Vol. 363. — P. 284−290.

9 Murugan K. Synthesis, Characterization and Demonstration of Self-Cleaning TiO₂ Coatings on Glass and Glazed Ceramic Tiles / K. Murugan, R. Subasri, T.N. Rao et al. // Progress in Organic Coatings. — 2013. — Vol. 76, No. 12. — P. 1756–1760. DOI 10.1016/j.porgcoat.2013.05.012.

10 Nandagopal S. Gentamicin Loaded Electrospun Poly(ε-Caprolactone)/TiO₂ Nanocomposite Membranes with Antibacterial Property against Methicillin Resistant Staphylococcus aureus / S. Nandagopal, A. Robin, C.G. Soney, V.P. Jayachandran, K. Nandakumar, T. Sabu // Journal of Polymer-Plastics Technology and Engineering. — 2016. — Vol. 55. — P. 1785–1796. https://doi.org/10.1080/03602559.2016.1171877.

11 Li Q. Enhanced visible light-induced photocatalytic disinfection of E. coli by carbon sensitized nitrogen-doped titanium oxide / Q. Li, R. Xie, Y.W. Li, E.A. Mintz, J.K. Shang // Environmental Science Technology. — 2007. — Vol. 41. — P. 5050–5056.

12 Bodaghi H. Synthesis of clay–TiO₂ nanocomposite thin films with barrier and photocatalytic properties for food packaging application / H. Bodaghi, Y. Mostofi, A. Oromiehie, B. Ghanbarzadeh, Z.G. Hagh // Journal of Applied Polymer Science. — 2015. — Vol. 132. — Article number 41764. DOI: 10.1002/app.41764.

13 Проданчук Н.Г. Наночастицы диоксида титана и их потенциальный риск для здоровья и окружающей среды / Н.Г. Проданчук, Г.М. Балан // Сучасні проблеми токсикології (Современные проблемы токсикологии). — 2011. — № 4. — С. 11–27.

14 Zang L. Solid-phase photocatalytic degradation of polystyrene with modified Nano-TiO₂ catalyst / L. Zang, S. Wang, W. Fa, Y. Hu, L. Tian, K. Deng // Polymer. — 2006. — Vol. 47, No. 24. — P. 8155–8162. doi:10.1016/j.polymer.2006.09.023.

15 Kim S.H. Photocatalytic degradation of flexible PVC / TiO₂ nano hybrid as an eco-friendly alternative to the current waste landfill and dioxin-emitting incineration of post-use PVC / S.H. Kim // Polymer. — 2006. — Vol. 47. — P. 3005–3016.

16 Li Sh. Photocatalytic degradation of polyethylene plastic with polypyrrole/TiO₂ nanocomposite as photocatalyst / Sh. Xu, L. He, F. Xu, Y. Wang, L. Zhang // Polymer-plastics technology and engineering. — 2010. — Vol. 49, No. 4. — P. 400–406.

17 Zhao X. Solid-phase photocatalytic degradation of polyethylene plastic under UV and solar light irradiation / X. Zhao, Z. Li, Y. Chen, Y. Zhu // Journal of molecular catalysis A: Chemical. — 2007. — Vol. 268. — P. 101–106.

18 Данг К.Н. Нанодиоксид титана в полимерных матрицах и фотопревращения с его участием / К.Н. Данг, Н.В. Сидоренко, Е.В. Евстратова, М.А. Ваниев, И.А. Новаков // Изв. вузов. «Технология легкой промышленности». — 2011. — Т. 12, № 2. — С. 97–103.

19 Al-Ajaj I.A. Mechanical Properties of Micro and Nano TiO₂/Epoxy Composites / I.A. Al-Ajaj, M.M. Abd, H.I. Jaffer // International Journal of Mining, Metallurgy & Mechanical Engineering. — 2013. — Vol. 1, No. 2. — P. 93–97.

20 Богданова Л.М. Механические свойства эпоксидных композитов на основе наночастиц серебра, сформированных *in situ* / Л.М. Богданова, Л.И. Кузуб, Э.А. Джавадян, В.И. Торбов, Н.Н. Дрёмова, А.Д. Помогайло // Высокомолекулярные соединения. Сер. А. — 2014. — Т. 56, № 3. — С. 289–295.

21 Богданова Л.М. Эволюция наночастиц серебра, синтезированных *in situ*, в стеклообразной эпоксидной матрице / Л.М. Богданова, В.А. Шершнев, М.Г. Спирин, В.И. Иржак, С.Е. Закиев, Г.И. Джардималиева // Журн. физ. хим. — 2019. — Т. 93, № 7. — С. 1043–1047.

22 Берестенко В.И. Микроволновой хлоридный процесс получения диоксида титана / В.И. Берестенко, В.И. Торбов, В.И. Чукалин, Е.Н. Куркин, И.Л. Балихин, И.А. Домашнев, В.Н. Троицкий, С.В. Гуров // Химия высоких энергий. — 2011. — Т. 45, № 5. — С. 468–472.

23 Esthappan S.K. Effect of titanium dioxide on the thermal ageing of polypropylene / S.K. Esthappan, S.K. Kuttappan, R. Joseph // Polymer Degradation Stability. — 2012. — Vol. 97. — P. 615–620.

Л.М. Богданова, В.А. Лесничая, Н.Н. Волкова,
В.А. Шершнев, В.И. Иржак, Ю.С. Букичев, Г.И. Джардималиева

TiO₂ эпоксидті нанокомпозиттері және олардың механикалық қасиеттері

TiO₂ (анатаз — 75 %, рутил — 25 %) нанобөлшектері бар поликонденсациялық эпоксидті нанокомпозиттердің физика-механикалық қасиеттері және термотұрақтылығы зерттелген. Эпоксидті полимер (TiO₂/ЭП) негізіндегі қалыңдығы 80–100 мкм нанокомпозитті қабықшалар алдын-ала ультрадыбыспен өңделген эпоксидианды шайыр, 4,4'-диаминдифенилметан және TiO₂ нанобөлшектерінің қоспасын сатылы температуралық режим бойынша (90 ºC — 3 сағ) + (160 ºC — 3 сағ) қатайту арқылы алынды. Созылуға механикалық сынақтар ASTM D882–10 стандарты бойынша жүргізілді. TiO₂ нанобөлшектерінің өлшемдері мен алынған нанокомпозиттердің микроқұрылымдары сканерлеуші электрондық микроскопия әдісімен зерттелді. TiO₂ нанобөлшектерін 3 масс. % жоғары қосу нанобөлшектер агрегациясының екіншілік процестері салдарынан беріктіктің төмендеуіне әкеледі. Қатаю процесінде TiO₂ нанобөлшектерінің орташа диаметрі 40 нм-ден 60 нм-ге дейін артады. TiO₂ нанобөлшектерінің концентрациясы >1 масс. % кезінде серпімділік модулінің ұлғаюы, шынылану температурасының жоғарылау тенденциясы және эпоксидті нанокомпозиттердің деформациясының төмендеуі эпоксидті матрицаның қаттылығының артқанын көрсетеді. TiO₂ нанобөлшектерінің концентрациясы 5 масс. % дейін болғанда және вакуумда 300 ºC-қа дейінгі температураларда зерттелген нанокомпозиттердің тұрақтылығы көрсетілген.

Кілт сөздер: эпоксидті шайыр, қатаю, титан диоксиді, нанобөлшектер, механикалық қасиеттер, термиялық тұрақтылық.

Л.М. Богданова, В.А. Лесничая, Н.Н. Волкова,
В.А. Шершнев, В.И. Иржак, Ю.С. Букичев, Г.И. Джардималиева

TiO$_2$ эпоксидные нанокомпозиты и их механические свойства

Исследованы физико-механические свойства и термостабильность поликонденсационных эпоксидных нанокомпозитов с наночастицами TiO$_2$ (анатаз — 75 %, рутил — 25 %). Нанокомпозитные плёнки на основе эпоксидного полимера (TiO$_2$/ЭП) толщиной 80–100 мкм получали отверждением предварительно обработанной ультразвуком смеси эпоксидиановой смолы ЭД-20, 4,4'-диаминодифенилметана и наночастиц TiO$_2$ по ступенчатому температурному режиму (90 ºC — 3 ч) + (160 ºC — 3 ч). Механические испытания на растяжение проводили по стандарту ASTM D882–10. Размеры наночастиц TiO$_2$ и микроструктуру полученных нанокомпозитов изучали методом сканирующей электронной микроскопии. Найдено, что добавление наночастиц TiO$_2$ выше концентрации 3 масс.% приводит к падению прочности, по-видимому, вследствие вторичных процессов агрегации наночастиц. В процессе отверждения средний диаметр наночастиц TiO$_2$ возрастает от 40 до 60 нм. Увеличение модуля упругости, тенденция к повышению температуры стеклования и падение деформации эпоксидных нанокомпозитов при концентрациях наночастиц TiO$_2$ >1 масс.% свидетельствуют о повышении жёсткости эпоксидной матрицы. Показана стабильность изученных нанокомпозитов при концентрациях наночастиц TiO$_2$ до 5 масс.% и температурах до 300 ºC в вакууме.

Ключевые слова: эпоксидная смола, отверждение, диоксид титана, наночастицы, механические свойства, термическая стабильность.

References

1 Fujishima, A.T., Rao, N., & Tryk, D.A. (2000). Titanium Dioxide Photocatalysis. *Journal of Photochemistry and Photobiology C: Photochemistry Reviews. 1*, 1–21.

2 Hamdy, M.S., Saputera, W.H., Groenen, E.J., & Mul G. (2014). A Novel TiO$_2$ Composite for Photocatalytic Wastewater Treatment. *Journal of Catalysis, 310*, 75–83. DOI: 10.1016/j.jcat.2013.07.017

3 Song, L., Qiu, R., Mo, Y., Zhang, D., Wei, H., & Xiong Y. (2007). Photodegradation of phenol in polymer-modified TiO$_2$ semiconductor particulate system under the irradiation of visible light. *Catalysis Communication, 8*, 429–433.

4 Truppi, A., Petronella, F., Placido, T., Striccoli, M., Agostiano, A., Curri, M.L., & Comparelli, R. (2017). Visible-light-active TiO$_2$-based hybrid nanocatalysts for environmental applications. *Catalysts, 7(4),* 100. http://dx.doi.org/10.3390/catal7040100.

5 Khalid, N.R., Majid, A., Tahir, M.B., Niaz, N.A., & Khalid, S. (2017). Carbonaceous-TiO$_2$ nanomaterials for photocatalytic degradation of pollutants: A review. *Ceramics International, 43*, 14552–14571. http://dx.doi.org/10.1016/j.ceramint.2017.08.143.

6 Zhou, T.-T., Zhao, F.-H., Cui, Y.-Q., Chen, L.-X., Yan, J.-S., Wang, X.-X., & Long, Y.-Z. (2020). Flexible TiO$_2$/PVDF/g-C3N4 Nanocomposite with Excellent Light Photocatalytic Performance. *Polymers, 12(55)*. doi:10.3390/polym12010055.

7 Bella, F., Muñoz-García, A.B., Colò, F., Meligrana, G., Lamberti, A., Destro, M., Pavone, M., & Gerbaldi C. (2018). Combined Structural, Chemometric, and Electrochemical Investigation of Vertically Aligned TiO$_2$ Nanotubes for Na-ion Batteries. *ACS Omega, 3*, 8440−8450. DOI: 10.1021/acsomega.8b01117.

8 Liu, S., Luo, Z., Tian, G., Zhu, M., Cai, Z., Pan, A., & Liang, S. (2017). TiO$_2$ nanorods grown on carbon fiber cloth as binder-free electrode for sodium-ion batteries and flexible sodium-ion capacitors. *Journal of Power Sources. 363*, 284−290.

9 Murugan, K., Subasri, R., Rao, T.N., Gandhi, A.S., & Murty, B.S. (2013). Synthesis, characterization and demonstration of self-cleaning TiO$_2$ coatings on glass and glazed ceramic tiles. *Progress in Organic Coatings, 76(12),* 1756–1760. doi:10.1016/j.porgcoat.2013.05.012.

10 Nandagopal, S., Robin, A., Soney, C.G., Jayachandran, V.P., Nandakumar, K., & Sabu, T. (2016). Gentamicin Loaded Electrospun Poly(ε-Caprolactone)/TiO$_2$ Nanocomposite Membranes with Antibacterial Property against Methicillin Resistant Staphylococcus aureus. *Journal of Polymer-Plastics Technology and Engineering, 55*, 1785–1796. https://doi.org/10.1080/03602559.2016.1171877.

11 Li, Q., Xie, R., Li, Y.W., Mintz, E.A., & Shang, J.K. (2007). Enhanced visible light-induced photocatalytic disinfection of E. coli by carbon sensitized nitrogen-doped titanium oxide. *Environmental Science Technology, 41,* 5050–5056.

12 Bodaghi, H., Mostofi, Y., Oromiehie, A., Ghanbarzadeh, B., & Hagh, Z.G. (2015). Synthesis of clay–TiO$_2$ nanocomposite thin films with barrier and photocatalytic properties for food packaging application. *Journal of Applied Polymer Science, 132*, 41764. DOI: 10.1002/app.41764.

13 Prodanchuk, N.G., & Balan, G.M. (2011). Nanochastitsy dioksida titana i ikh potentsialnyi risk dlia zdoroviia i okruzhaiuschei sredy [Titanium dioxide nanoparticles and their potential health and environmental risks]. *Sovremennye problemy toksikolohii — Modern problems of toxicology, 4*, 11–27 [in Russian].

14 Zang, L., Wang, S., Fa, W., Hu, Y., Tian, L., & Deng, K. (2006). Solid-phase photocatalytic degradation of polystyrene with modified Nano-TiO$_2$ catalyst. *Polymer, 47(24)*, 8155–8162. doi:10.1016/j.polymer.2006.09.023.

15 Kim, S.H. (2006). Photocatalytic degradation of flexible PVC / TiO$_2$ nano hybrid as an eco-friendly alternative to the current waste landfill and dioxin-emitting incineration of post-use PVC. *Polymer, 47*, 3005–3016.

16 Xu, Sh., He, L., Xu, F., Wang, Y., & Zhang L. (2010). Photocatalytic degradation of polyethylene plastic with polypyrrole/TiO$_2$ nanocomposite as photocatalyst. *Polymer-plastics technology and engineering, 49(4)*, 400–406.

17 Zhao, X., Li, Z., Chen, Y., & Zhu, Y. (2007). Solid-phase photocatalytic degradation of polyethylene plastic under UV and solar light irradiation. *Journal of molecular catalysis A: Chemical, 268*, 101–106.

18 Dang, K.N., Sidorenko, N.V., Evstratova, E.V., Vaniev, M.A., & Novakov, I.A. (2011). Nanodioksid titana v polymernykh matritsakh i fotoprevrashcheniia s eho uchastiem [Titanium nanodioxide in polymer matrices and phototransformations with its participation]. *Izvestiia vuzov. «Technolohiia lehkoi promyshlennosti» — University Bulletin. Light industry technology, 12(2)*, 97–103 [in Russian].

19 Al-Ajaj, I.A., Abd, M.M., & Jaffer, H.I. (2013). Mechanical Properties of Micro and Nano TiO₂/Epoxy Composites. *International Journal of Mining, Metallurgy & Mechanical Engineering, 1(2)*, 93–97.

20 Bogdanova, L.M., Kuzub, L.M., Dzhavadyan, E.A., Torbov, V.I., Dryemova, N.N., & Pomogailo, A.D. (2014), Mekhanicheskie svoistva epoksidnykh komkpozitov na osnove nanochastits serebra, sformirovannykh *in situ* [Mechanical properties of epoxy composites based on Ag nanoparticles produced *in situ*]. *Vysokomolekuliarnye soedineniia. Seriia A — Polymer science. A, 56(3)*, 289–295 [in Russian].

21 Bogdanova, L.M., Shershnev, V.A., Spirin, M.G., Irzhak, V.I., Zakiev, S.E., & Dzhardimalieva, G.I. (2019). Evolutsiia nanochastits serebra, sintezirovannykh *in situ*, v stekloobraznoi epoksidnoi matritse [Evolution of Ag nanoparticles produced *in situ* in epoxy matrix]. *Zhurnal fizicheskoi khimii — Journal of physical chemistry, 93(7)*, 1043–1047 [in Russian].

22 Berestenko, V.I., Torbov, V.I., Chukalin, V.I., Kurkin, E.N., Balikhin, I.L., Domashnev, I.A., Troitskii, V.N., & Gurov, S.V. (2011). Mikrovolnovoi khloridnyi protsess polucheniia dioksida titana [Microwave chloride process for producing titanium dioxide]. *Khimiia vysokikh enerhii — High energy chemistry, 45(5)*, 468–472 [in Russian].

23 Esthappan, S.K., Kuttappan, S.K., & Joseph, R. (2012). Effect of titanium dioxide on the thermal ageing of polypropylene. *Polymer Degradation Stability, 97,* 615–620.

A.N. Sabitova[1], B.B. Bayakhmetova[2], B.Kh. Mussabayeva[1*],
L.K. Orazhanova[1], K.G. Ganiyeva[1]

[1]Shakarim University of Semey, Kazakhstan;
[2]Semey Medical University, Kazakhstan
(Corresponding author′s e-mail: binur.mussabayeva@mail.ru)

Sorption of heavy metals by humic acids of chestnut soils

The purpose of this article is to study the sorption of heavy metals by humic acids of light and dark chestnut soil. The objects of research are the samples of dark and light chestnut soils, selected from an ecologically clean area of East Kazakhstan. Humic acids (HA) were separated from the soil at different pH values. At the same time the yield of HA was 0.075 % from dark chestnut soil at pH 1.0, and it was 0.017 % from light chestnut at pH = 7.0. Further, the dependence of the sorption degree on the medium acidity was established. It was found that zinc and cadmium are better sorbed in a strongly acidic medium (pH < 1.0; 84.14 %), while lead is preferably sorbed at pH 6.0, and the degree of its sorption is higher (93.54 %). It was established that metals have a mutual effect, suppressing or enhancing the sorption of each other in bi- and polyelement variants. It was shown that cadmium significantly suppresses lead sorption in neutral media. Zinc more often increases the sorption of both cadmium and lead by 3 times. It was concluded that the binding of heavy metal ions by the organic fraction of the soil occurs due to the complexation with humic acids.

Keywords: heavy metals, dark chestnut soils, light chestnut soils (Kastanozems), organic fraction of soil, humic acids, sorption, zinc, lead, cadmium, East Kazakhstan, Borodulikha.

Introduction

Currently, the biosphere receives a huge amount of various pollutants, including heavy metals (HM), as a result of industrial and anthropogenic human activities. One of the most important parts of the biosphere is the soil cover, since in many cases it acts as a buffer, preventing or localizing contamination of other parts of the biosphere. The entry of HM into the biosphere leads to their accumulation in the soil in quantities that repeatedly exceed the background level, which reduces soil productivity and negatively affects the animal and plant world, as well as ultimately the human body [1–3].

Technogenic contribution in to the urban megalopolis soils is mainly manifested in a sharp increase in the specific concentration of mobile forms of Zn, Pb, Cu, and in a lesser extent of Cd, V, Co, Ni [2–4]. Toxic elements in soils are found in the form of light-exchange ions, colloidal particles, complex compounds, isomorphic impurities, complexes with humic acids, adsorbed complexes on iron and manganese hydroxides, on clay dispersed minerals, and carbonates [5–6].

It is known that soils differ in their sorption capacity in relation to heavy metals [7–11]. At the same time, it is believed that the ability to sorption of heavy metals is associated with the presence of specific high-molecular polyfunctional natural ligands in the organic part of the soil-humic acids (HA), fulvic acids and humin. Soils with a large supply of humic acids can bind a large amount of heavy metals. This is facilitated by the presence of a large number of different functional groups in the HA (carboxylic, alcoholic, phenolic, amine, amide, etc.), which provide the formation of strong complexes of these acids with heavy metal ions [12–14]. The interaction between humic acids and metals can occur by forming ionic, covalent, and chelated compounds [15].

The phenomena of ion exchange, surface sorption, coagulation and peptization play an important role in the sorption of HM by the soil fraction. The ratio of the mass fraction of organic matter to metal is important. HM sorption by the organic part of the soil can occur with the participation of carboxyl (–COOH) and phenolic (–OH) groups, this happens by replacing hydrogen with metal ions. Chelate complexes are formed as a result. The metal binds by chelating coordination (homeopolar) bonds and does not behave like a cation. Metal complex: organic matter can also be formed by replacing metal with a hydrogen cation outside the functional groups [16–17].

---

* Corresponding author

Consequently, metals can enter both the cationic and anionic parts of humic acid molecules. It should be noted that the molecules of humus compounds of different soils differ in the number of functional groups and the degree of the «core» condensation. Therefore, sorption is influenced not only by the properties of metals, but also by the structure of humus compounds [18].

Contamination of the soil of East Kazakhstan with heavy metals has been studied by other scientists of Kazakhstan [19–21]. However the sorption degree of heavy metals (Zn, Cd, Pb) by the main components of the organo-mineral matrix of dark and light chestnut soil under conditions of mono- and polyelement pollution will be studied for the first time.

Data on the adsorption capacity of soils can serve as a basis for the development of methods for controlling the transformation of forms of chemical element compounds in areas that have been confirmed by technogenic pollution.

This paper presents the results of studying the processes of zinc, lead, and cadmium sorption in mono- and polyelement variants by humic acids of dark and light chestnut soil from the East Kazakhstan region.

Experimental

The objects of research are the samples of dark and light chestnut soils, selected from an ecologically clean area Borodulikha district of East Kazakhstan.

Borodulikha district is located in the North of the East Kazakhstan region. The total area is 7.2 thousand square meters, bordering the Altay region of the Russian Federation, as well as with Shemonaikha, Beskaragay districts and Semey sity. Soils are saline and chestnut in the West of the district, and black earth (Chernozem) in the East of the district.

There is the Zhezkent mining and processing plant on the territory of the district, which is engaged in the extraction of polymetallic ores, and a number of reprocessing enterprises.

The organic part of dark and light brown was isolated according to the standard method [9], by three-fold extraction with 0.1 M NaOH solution. The soil suspension was filled with an extractant solution and shaken on a rotator for one hour. The resulting suspension was filtered, and the remaining soil in the flask was filled with a new portion of 0.1 M alkali solution. The extraction of organic matter was repeated three times.

Humic acids were separated from the filtrate by adding a 10 % solution of sulfuric acid to pH=1. The resulting precipitate was filtered and washed with water, and then dissolved in 0,1 M sodium hydroxide solution. Separate fractions of humic acids were deposited from the resulting solution by addition of 1 % sulfuric acid solution drop by drop to the resulting solution of humic acids to pH=7. The precipitate was separated by centrifugation after 2 hours of settling. A 1 % solution of sulfuric acid was added to the centrifuge again drop by drop to pH=7. All operations for separation of sediment were repeated similarly according to the above method.

Similar operations were performed by depositing fractions at pH 5.0; 4.0; 3.0; 2.0; 1.0 and at pH<1.0. The resulting fractions were dried on pre-dried paper filters to a constant weight. The mass of fractions was determined by the difference in the mass of «clean» filters and filters with organic matter after drying.

Thus, 7 organic fractions of dark chestnut soil at pH=7.0; 6.0; 4.0; 3.0; 2.0; 1.0 and <1.0, 8 organic fractions of light chestnut soil at pH=7.0; 6.0; 5.0; 4.0; 3.0; 2.0; 1.0 and <1.0 were isolated. The organic fraction at pH=5.0 for the dark chestnut soil was not considered due to the negligible allocation of humic acids into a separate fraction.

The study of sorption processes of heavy metals in mono-, bi- and polyelement variants of organo-mineral matrix of dark chestnut and light chestnut soil was carried out in accordance with [1]. Solutions of $Zn(NO_3)_2$, $Pb(CH_3COO)_2$, and $Cd(CH_3COO)_2$ salts were used for the model test. The salt concentration was 2.5 mmol/ml for mono-and bi-element variants and 1.25 mmol/ml for poly-element variant.

The solution of humic acids isolated at pH=7.0 was divided into 7 equal parts, in which a certain volume of zinc, lead, cadmium salts or their mixtures was added. The following options for applying HM solutions were used:

1. **mono-element** $(Zn(NO_3)_2; Pb(CH_3COO)_2; Cd(CH_3COO)_2)$
2. **bi-element** $(Zn(NO_3)_2 + Pb(CH_3COO)_2)$;
$(Zn(NO_3)_2 + Cd(CH_3COO)_2)$;
$(Pb(CH_3COO)_2 + Cd(CH_3COO)_2)$
3. **poly-element** $(Zn(NO_3)_2 + Pb(CH_3COO)_2 + Cd(CH_3COO)_2)$

A 10 % solution of sulfuric acid was added to the resulting solutions to pH=1.0. Humic acids were precipitated in all studied solutions. Then the solutions were infused for a day and centrifuged. The content of heavy metals (zinc, lead, cadmium, zinc-lead, zinc-cadmium, lead-cadmium, zinc-lead-cadmium) was determined in the centrifugate. The percentage of sorption was determined by the difference in concentration in the initial standard solution and the extract obtained after the sorption process.

Gross content and concentration of water-soluble, acid exchange forms of zinc, cadmium and lead in the analyzed solution was determined by extraction photometric method with ditizone using a photometer.

Results and Discussion

7 well-separated fractions have been formed by the triple extracted organic part of dark chestnut soil and 8 well-separated fractions have been formed by the light chestnut soil. Their isoelectric points correspond to the following pH values of the medium: 7.0; 6.0; 5.0; 4.0; 3.0; 2.0; 1.0 and <1.0.

In all fractions, the content of humic acids and organic fractions from the total content of organic matter was determined by gravimetry (Tables 1, 2).

T a b l e 1

Content of humic acids and organic substances in the dark chestnut soil

Fractions at pH	Humic acids content, %	Organic substances content, %
<1.0	0.075±0.001	29.00±2.15
1.0	0.050±0.002	18.50±1.02
2.0	0.025±0.001	9.15±0.98
3.0	0.013±0.001	3.20±0.24
4.0	0.020±0.001	6.24±0.25
5.0	–	-
6.0	0.034±0.001	11.71±1.13
7.0	0.061±0.002	25.07±1.89

As can be seen in Table 1, the content of humic acids and organic substances prevails in fractions with pH <1.0 (0.075 % and 29.00 %), 1.0 (0.050 % and 18.50 %) and 7.0 (0.061 % and 25.07 %), which indicates that these fractions are enriched with organic substances.

T a b l e 2

Content of humic acids and organic substances in the light chestnut soil

Fractions at pH	Humic acids content, %	Organic substances content, %
<1.0	0.012±0.001	19.00±1.67
1.0	0.013±0.002	14.25±1.19
2.0	0.010±0.001	13.00±1.14
3.0	0.009±0.002	9.55±1.05
4.0	0.009±0.002	12.20±1.17
5.0	0.008±0.001	10.70±1.12
6.0	0.011±0.001	1.85±0.12
7.0	0.017±0.002	20.25±1.53

As can be seen in Table 2, the content of humic acids and organic substances prevails in fractions with pH <1.0 (0.012 % and 19.00 %), and 7.0 (0.017 % and 20.25 %), which indicates that these fractions are enriched with organic substances.

Thus, the highest yield of humic acids and organic substances was obtained at pH 1.0; pH<1.0; pH 7.0 for dark chestnut soil, and at pH<1.0; pH 7.0 for light brown soil.

The isolated fractions of humic acids were studied by IR spectroscopy to determine the identification of functional groups included in the composition.

Figure 1 presents the IR spectrum of humic acids isolated from dark chestnut and light chestnut soils of the Borodulikha region.
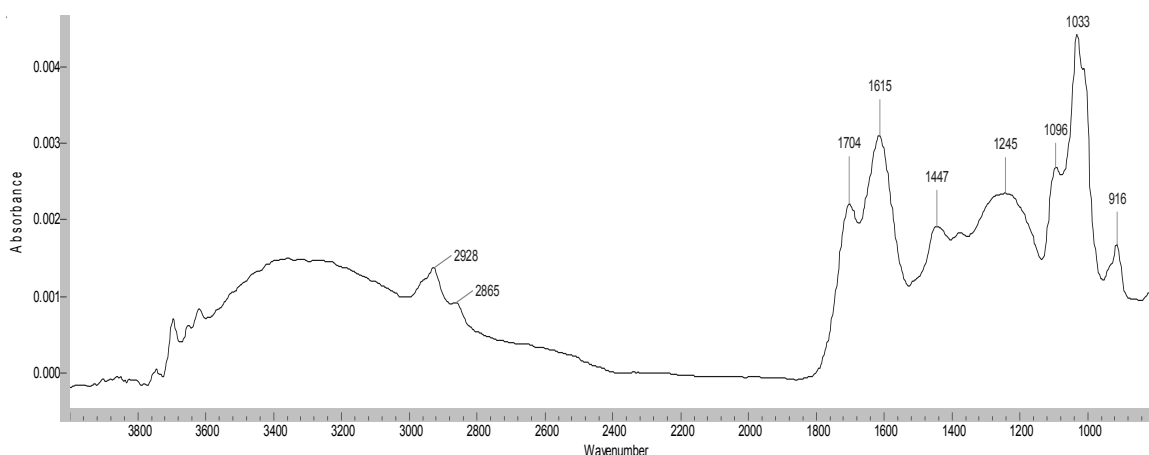
Figure 1. IR spectrum of humic acids

All absorption bands are presented in the IR spectra of the studied humic acids, which is confirmed the presence of the aromatic part (core) and external aliphatic chains in macromolecules. The characteristic absorption bands are in the range of 1000–1800 cm^{-1}. Absorption bands with maxima at 1033 cm^{-1} are caused by fluctuations in the O–H bond of primary alcohol groups. Absorption bands with maxima at 2865 and 2928 cm^{-1} are caused by valence fluctuations of –CH$_3$ and –CH$_2$ groups of the side chain. The narrow band with a maximum at 1704 cm^{-1} belongs to the carboxyl group –COOH. Aromatic and aryl-alkyl esters correspond to the absorption band at 1245 cm^{-1}. The absorption peak at 2865 cm^{-1} indicates the presence of alicyclic compounds. The presence of aromatic rings in humic acid molecules is indicated by the absorption band at 1615 cm^{-1}, which is caused by valence vibrations of the skeletal bonds of the aromatic rings.

The results of zinc, cadmium and lead sorption by organic fractions of dark and light chestnut soil in mono-, bi- and poly-element variants are presented in Tables 3, 4 respectively.

Table 3

Degree of metal sorption by organic fraction of dark chestnut soil in mono-, bi- and poly-element variants

Variant		Degree of sorption, %						
		pH 7.0	pH 6.0	pH 4.0	pH 3.0	pH 2.0	pH 1.0	pH<1.0
Zn		52.06±0.01	55.06±0.03	56.00±0.01	76.59±0.01	72.21±0.01	74.55±0.01	84.14±0.01
Pb		85.71±0.01	93.54±0.02	41.91±0.01	34.57±0.01	37.38±0.01	35.58±0.01	14.14±0.01
Cd		29.02±15.03	56.56±0.01	24.28±0.02	27.29±0.01	22.05±0.01	15.75±0.01	78.06±0.01
Zn/Pb	Zn	76.17±0.01	77.45±0.02	78.17±0.02	54.19±0.01	42.13±0.01	19.97±0,01	68.28±0.01
	Pb	76.97±0.02	77.39±0.02	67.54±0.03	65.11±0.01	71.46±0.01	59.38±0.01	53.43±0.01
Zn/Cd	Zn	76.76±0.03	77.56±0.02	63.15±0.02	66.03±0.01	45.11±0.01	21.78±0.01	63.33±0.01
	Cd	81.09±0.06	81.70±0.06	82.20±0.12	79.42±0.01	54.78±0.02	48.61±0.01	47.14±0.02
Pb/Cd	Pb	13.62±0.02	11.10±0.12	49.77±0.01	47.93±0.01	73.52±0.01	75.19±0.01	54.48±0.01
	Cd	28.77±0.07	39.08±0.04	53.68±5.77	92.48±0.01	93.18±0.01	73.89±0.01	29.21±0.01
Zn/Pb/Cd	Zn	84.25±0.02	84.52±0.01	73.76±0.01	37.18±0.02	62.09±0.01	57.12±0.01	43.19±0.01
	Pb	84.49±5.78	84.35±0.02	80.80±0.01	78.63±0.02	47.88±0.01	11.41±0.01	35.82±0.01
	Cd	90.49±0.02	90.65±0.02	90.04±0.01	88.69±0.02	47.22±0.01	73.48±0.01	57.72±0.01

As can be seen in Table 3, the sorption of zinc was almost identical (sorption degree 52.06 %; 55.06 % and 56.00 %) by organic fractions with pH 7.0; 6.0; 4.0 in mono-element variant. The sorption of zinc was increased with further acidification, for example, it was increased by 1.5 times at pH=3.0 (76.59 %) compared to the value at pH=7.0 (52.06 %).

The degree of zinc sorption increased at pH 7.0; 6.0; 4.0 (76.17 %; 77.45 %; 78.17 %) with equivalent enrichment of each fraction with zinc and lead, except for highly acidic environments.

The cadmium presence also increased the zinc absorption, for example, the sorption degree was increased by 1.5 times at typical for this soil reaction medium pH 7.0–6.0 in comparison with the monoelement experiment. The same results were obtained with the combined presence of lead and cadmium.

The character of lead sorption in various versions of the experiment is similar to that in fractions with isoelectric points at pH 7.0; 6.0; 3.0 and is radically different from fractions with pH 2.0; 1.0; <1.0. The sorption patterns shown at pH 4 are intermediate.

The greatest absorption of lead was observed in pH 7.0; 6.0 fractions; the degree of sorption was decreased with acidification of the medium, for example, it decreased by 2 times at pH 4.0; 1.0 compared to pH 6.0. In the presence of an equivalent amount of zinc, lead sorption was slightly suppressed in fractions with pH 7.0; 6.0; 3.0; 2.0, and Vice versa, it was enhanced by the pH 4.0 and 1.0 medium reaction. Cadmium was even more deactivated processes of lead enrichment:

− by 6.3 times compared to the monoelement experiment in the fraction with pH 7.0;

− by 8.4 times at pH 6.0.

The absorption of lead was not affected by the presence of cadmium in fractions with pH 4.0 and 2.0. The combined presence of zinc and cadmium did not lead to any changes in the lead sorption as compared with mono-element variant reaction by organic fraction of dark chestnut soil (pH 6–7). Consequently, both zinc and cadmium reduce the degree of sorption, but the influence of zinc is more predominant in their combined presence.

Fractions at pH 7.0; 6.0; 4.0, as well as at pH 3.0 and 2.0, showed general regularities in the cadmium sorption in different versions of the experiment. The absorption dynamics is not unequal when the acidity increases.

The presence of zinc has a «catalyzing» effect on the cadmium sorption (approximately 3 times compared to the values of the monoelement variant in fractions with pH 7.0; 6.0; 4.0 and 1.0). The presence of lead does not have significant changes at pH 7.0; 6.0 and slightly increases sorption in more acidic fractions. In poly-element absorption variant, the sorption of cadmium is influenced more by the presence of lead, since sorption is comparable to those regularities that were deduced in the bi-element experiment in the presence of lead alone. Thus, the maximum values of the sorption degree belong to fractions with pH 7.0; 6.0; 4.0 in poly-element absorption variant. The degree of absorption increases almost 3 times compared to the mono-element experiment in these fractions.

Table 4

Degree of metal sorption by organic fraction of light chestnut soil in mono-, bi- and poly-element variants

Variant		Degree of sorption, %							
		pH 7.0	pH 6.0	pH 5.0	pH 4.0	pH 3.0	pH 2.0	pH 1.0	pH<1.0
Zn		23.70±0.01	39.62±0.01	32.08±0.02	33.12±0.01	55.03±0.01	56.11±0.01	53.25±0.02	84.10±0.02
Pb		82.17±0.01	88.21±0.01	27.04±0.01	25.01±0.02	13.13±0.01	18.64±0.2	23.11±0.01	25.70±0.01
Cd		56.23±0.01	40.24±0.02	22.61±0.01	14.51±0.01	13.42±0.01	17.93±0.01	78.04±0.01	83.65±0.02
Zn/Pb	Zn	64.81±0.01	72.40±0.01	10.03±0.03	16.95±0.01	11.46±0.02	37.91±0.01	79.21±0.01	86.32±0.01
	Pb	11.30±0.01	56.72±1.71	65.02±0.01	60.41±0.01	54.36±0.02	51.71±0.01	10.95±0.01	13.47±0.01
Zn/Cd	Zn	72.13±0.02	70.81±0.01	16.94±0.01	6.43±0.01	5.73±0.01	9.34±0.02	18.81±0.01	18.74±0.01
	Cd	63.00±0.02	57.11±0.01	51.82±0.01	62.22±0.01	54.93±0.01	58.81±0.01	51.74±0.01	86.20±0.01
Pb/Cd	Pb	55.64±0.02	54.21±0.02	66.00±0.02	53.36±0.01	53.04±0.02	56.81±0.01	36.07±0.01	26.40±0.02
	Cd	32.11±0.02	73.73±0.01	43.60±0.01	53.23±0.01	59.27±0.02	36.00±0.02	12.40±0.01	16.83±0.02
Zn/Pb/Cd	Zn	79.93±0.01	73.55±0.01	34.21±0.01	36.42±0.01	19.42±0.02	23.83±0.02	49.86±0.01	46.13±0.01
	Pb	67.84±5.77	53.94±0.02	70.12±0.01	73.90±0.01	67.90±0.02	72.82±0.01	69.63±0.01	47.72±0.01
	Cd	83.00±0.02	69.21±0.01	82.84±0.02	76.52±0.01	75.04±0.01	68.43±0.01	59.62±0.01	12.47±0.01

The sorption of zinc by the organic fraction of light chestnut soil was slightly different from dark chestnut soil. Dynamics of pollutant absorption within all factions in mono-variant naturally increased. By the nature of zinc sorption in the presence of lead or cadmium and in the simultaneous presence of lead and cadmium, the fractions can be combined into several microgroups: 1) with pH 7–6; 2) with pH 5; 4; 3; 2; 3) with pH 1; <1. The first group of fractions is active in normal natural conditions, it is increased its sorption in both in bi- and poly-element variants of the experiment. Moreover, the action of lead and cadmium is almost the same.

Lead and cadmium inhibited the sorption of zinc in the second group of humic acids in light chestnut soil. The cadmium had more competitive action there. For example, at pH 2 the sorption of zinc was suppressed by 1.5 times in the presence of lead and it was suppressed by 6 times in the presence of cadmium in

comparison with mono-element variant. Zinc absorption was increased in the presence of lead, and it was suppressed it in the presence of cadmium in the group represented by fractions with pH 1 and <1.

Lead absorption was suppressed with acidification of fractions in the mono-element version of the experiment. Thus, at pH 5, sorption decreased by about 3 times when compared with the fraction with an isoelectric point at pH 7.0.

Data obtained during bi-element and poly-element experiments indicates that, the lead sorption have been suppressed at pH 7.0; 6.0 and have been increased at pH from 5 to <1 by both zinc and cadmium, and their combined presence. The same dynamics of cadmium sorption have been shown by fractions with pH 6.0; 5.0; 4.0; 3.0; 2.0 relative to the presence of both zinc and lead.

Zinc have been demonstrated a greater activating effect. For example, at pH 5.0 the presence of zinc increased the cadmium absorption by 2.3 times compared to the mono-element experiment, and by 1.9 times in the presence of lead alone. The character of cadmium sorption in poly-element enrichment was more influenced by the presence of zinc in all fractions except pH<1.

In general, the cadmium sorption was suppressed when acidified to pH 2.0 (by 3.1 times compared to pH 7.0) in mono-element version; it did not change significantly in poly-element enrichment. Almost all fractions increased the cadmium sorption at 2.7 times level compared to the average value of the mono-element experience of these fractions.

It was shown by the comparison of zinc, lead, and cadmium sorption degree values in a mono-element experiment (Fig. 2), that fraction with pH of 7.0, and 6.0 are indicators for lead (its sorption is more than 1.6 times the sorption of zinc and 3 times more the sorption of cadmium), more acidic fractions are indicators for cadmium (for example, the cadmium sorption is 1.3 times higher sorption of lead and 5.9 times higher sorption of zinc in fraction with pH 3.0).

a) specific sorption (multi-element variant)

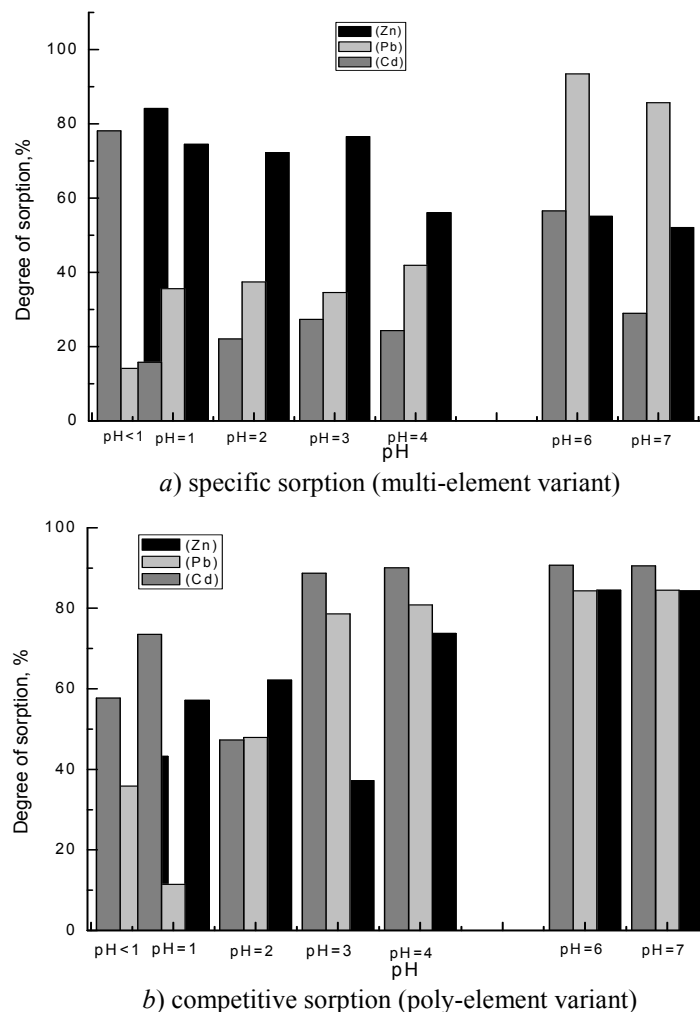*b*) competitive sorption (poly-element variant)

Figure 2. Comparison diagram of heavy metals sorption by the organic matrix of dark chestnut soil

Fractions with the same structure showed similar absorption patterns in the experiment. All the selected fractions can be divided into two groups: 1) pH 7.0; 4.0; 3.0 and 2) pH 1.0. Although the structure of the pH 6.0 fraction differs in spectrum from all others, it is characterized by similarity of the sorption character with the first group of fractions mentioned above. Humic acids with pH 1.0 active medium are in this series separately: the individual spectrum also characterizes the distinctive features in the sorbed capacity. It was shown by the comparison of all three metals sorption values (Fig. 3), that the fraction with a neutral medium showed greater affinity to lead, and the acidificated medium showed greater affinity to zinc in the mono-element version.

a) specific sorption (multi-element variant)

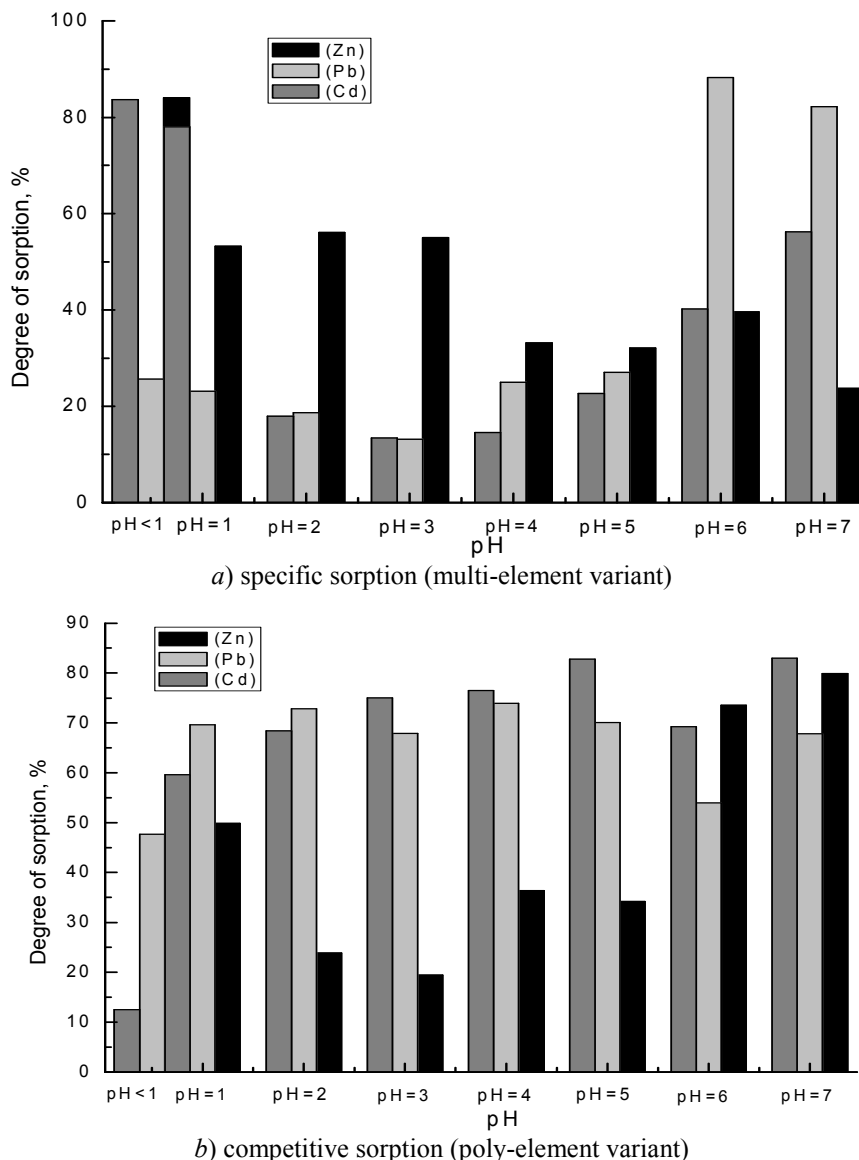*b*) competitive sorption (poly-element variant)

Figure 3. Comparison diagram of heavy metals sorption by the organic matrix of light chestnut soil

As can be seen in Figure 3, the percentage of sorption was highest for zinc and cadmium at pH<1.0. The sorption processes were enhanced for all metals, and lead had a competitive effect on zinc and cadmium with the combined presence of all three ions. Similar dynamics of pollutants absorption were shown by fractions with pH 6.0; 5.0; 4.0; 3.0, which have approximately the same character of spectral curves.

The two studied soils showed different sorption activity. The fractions at pH=7.0 (the active fraction for these soils) and at pH=6 of the two soils absorbed the introduced pollutants differently (Figs. 4–6): dark chestnut soil absorbed more zinc than light chestnut soil under equivalent conditions. This can be explained by the low content of organic matter, and, accordingly, by the small percentage (%) of fractions in light chestnut soil (Tables 3, 4).
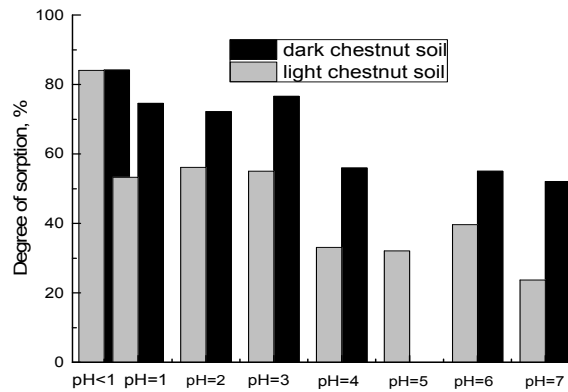
Figure 4. Comparative diagram of zinc sorption in the mono-element experiment
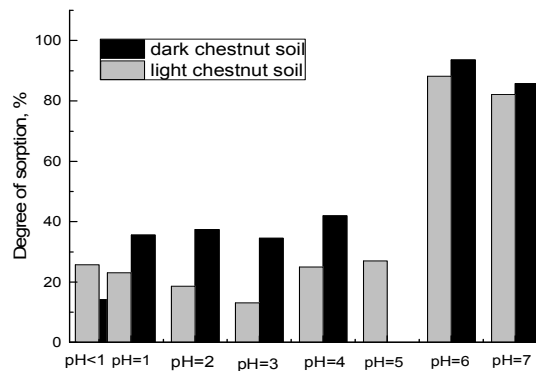

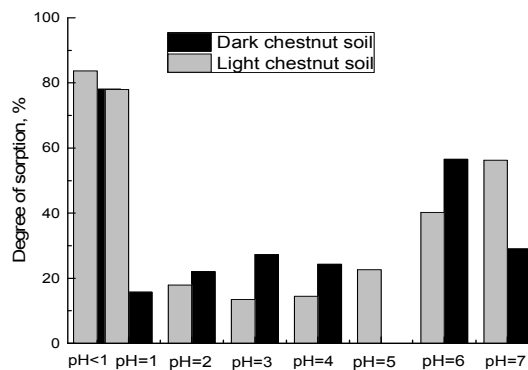Figure 5. Comparative diagram of lead sorption in a single experience

Figure 6. Comparative diagram of cadmium sorption in the mono-element experiment

Thus, since chestnut soils have a slightly alkaline reaction (pH 7.2–7.5) under normal conditions, all three metals have a high affinity for the organic fraction in poly-element contamination conditions. The sorption intensity is suppressed by acidification.

Conclusions

Thus, it was shown by the IR spectroscopy data, that extracted from the dark brown and light brown soils of the Borodulikha region humic acids contain primary and secondary alcohols, aromatic hydrocarbons, carboxylic acids, aromatic and aryl-alkyl esters. The presence of such functional groups as –COOH, –OH in humic acids makes it possible to bind heavy metals to the organic fraction of the soil by forming chelate complexes.

The sorption of heavy metals by the organo-mineral matrix of dark chestnut and light chestnut soil of the ecologically clean Borodulikha region of East Kazakhstan was studied. Soil samples were selected in the Western part of Borodulikha district, where are no industrial enterprises. However, there is deforestation as a

result of forest fires. Today about 15 % of the district's territory is occupied by pine forest, whereas previously the area of the forest was 50 %. Therefore, the study of the degree of soil contamination is relevant.

It was established that the process of zinc, cadmium and lead sorption by organic fractions of dark chestnut and light chestnut soil proceeds differently in mono- and poly-element variants. For mono-element enrichment of the soil, lead is more sorbed by humic acid fractions of the studied soils at pH 7.0 and 6.0, its sorption degree reaches 93.54 %; zinc is more sorbed at acidic pH from 3.0 to < 1 uncharacteristic for these soils; cadmium is more sorbed by pH 1.0 and < 1 fractions, their sorption degree at pH 1.0 is 84.14 %. Sorption of zinc, lead, and cadmium by humic and hymetomelanic acids of organic matter of chestnut soils under conditions of poly-element enrichment is accompanied by the oppression of one heavy metal by another.

Data obtained on the sorption of heavy metals by soils can be used in assessing the impact of anthropogenic emissions on the environment, in developing practical recommendations to reduce the toxic effect of heavy metals. The results of the work can also be practically applied in rationing systems.

References

1 Водяницкий Ю.Н. Загрязнение почв тяжелыми металлами / Ю.Н. Водяницкий, Д.В. Савичев, А.Т. Ладонин. — М.: Изд-во Почвенного ин-та им. В.В. Докучаева РАСХН, 2012. — 306 с.

2 Clarke L.W. Urban legacies and soil management affect the concentration and speciation of trace metals in Los Angeles community garden soils / L.W. Clarke, G.D. Jenerette, D.J. Bain // Environmental Pollution. — 2015. — Vol. 197. — P. 1–12.

3 Sharma R.K. Cadmium minimization in food crops by cadmium resistant plant growth promoting rhizobacteria / R.K. Sharma, G. Archana // Applied Soil Ecology. — 2016. — Vol. 107. — P. 66–78.

4 Piri M. Citric acid decreased and humic acid increased Zn sorption in soils / M. Piri, E. Sepehr, Z. Rengel // Geoderma. — 2019. — Vol. 341. — P. 39–45.

5 Ding H. Characteristics and interactions of heavy metals with humic acid in gold mining area soil at a upstream of a metropolitan drinking water sourse / H. Ding, L. Tang, Y. Nie, H. Ji // Journal of Geochemical Exploration. — 2019. — Vol. 200. — P. 266–275.

6 Фархутдинов Р.М. Связывание свинца, кадмия и меди гуминовыми кислотами озерных донных отложений / Р.М. Фархутдинов, А.А. Каюгин, Л.В. Черкашина // Вестн. Тюмен. гос. ун-та. — 2010. — № 7. — С. 196–202.

7 Малышенко Н.В. Сорбция катионов цинка модифицированными гуминовыми кислотами / Н.В. Малышенко, С.И. Жеребцов, О.В. Смотрина, Л.В. Брюховецкая, З.Р. Исмагилов // Химия в интересах устойчивого развития. — 2015. — № 23. — С. 451–457.

8 Boguta P. Insight into the interaction mechanism of iron ions with soil humic acids. The effect of the pH and chemical properties of humic acids / P. Boguta, V. D'Orazio, N. Senesi, Z. Sokołowska, K. Szewczuk-Karpisz // Journal of Environmental Management. — 2019. — Vol. 245. — P. 367–374.

9 Федоров И.Г. Поведение металлов в присутствии гуминовых веществ в содовых озерах Восточного Забайкалья / И.Г. Федоров, С.В. Борзенко // Вестн. Зайбайкал. гос. ун-та. — 2018. — Т. 2, № 2. — С. 74–80.

10 Wei L. Adsorption behaviors of Cu^{2+}, Zn^{2+} and Cd^{2+} onto proteins, humic acid, and polysaccharides extracted from sludge EPS: Sorption properties and mechanisms / L. Wei, J. Li, M. Xue, Sh. Wang, Q. Zhao // Bioresource Technology. — 2019. — Vol. 291. — P. 121868.

11 Calace N. Adsorbtion isotherms and breakthrough curves to study how humic acids influence heavy metal–soil interactions / N. Calace, D. Deriu, B.M. Petronio // Water Air Soil Pollution. — 2009. — Vol. 204, Iss. 2. — P. 373–380.

12 Boguta P. Study of the Interactions between Zn (II) ions and humic acids / P. Boguta, Z. Sokołowska // Plosone. — 2016. — Vol. 14, No. 4. — P. 1–20.

13 Zherebtsov S.I. Sorption of copper cations from aqueous solutions by brown coals and humic acids / S.I. Zherebtsov, N.V. Malyshenko, L.V. Bryukhovetskaya, Z.R. Ismagilov, S.Y. Lyrshchikov // Solid Fuel Chemistry. — 2015. — Vol. 49, No. 5. — P. 294–303.

14 Карпюк Л.А. Алкоксисилильные производные гуминовых веществ: синтез, строение и сорбционные свойства: дис. … канд. хим. наук: 02.00.03 — «Органическая химия» / Леонид Александрович Карпюк. — М., 2008. — 187 с.

15 Заварзина А.Г. Взаимодействие гуминовых кислот различного происхождения с ионами металлов и минеральными компонентами почв: дис. ... канд. биол. наук: 04.00.03 — «Биогеохимия» / Анна Георгиевна Заварзина. — М., 2000. — 134 с.

16 Будаева А.Д. Сорбция ионов тяжелых металлов гуматами аммония, натрия и калия / А.Д. Будаева, Е.В. Золтоев, Н.В. Бодоев, Т.А. Бальбурова // Фундаментальные исследования. — 2005. — № 9. — С. 112, 113.

17 Добровольский Г.В. Структурно-функциональная роль почв и почвенной биоты в биосфере / Г.В. Добровольский, И.П. Бабьева. — М.: Наука, 2003. — 364 с.

18 Алексеев Ю.В. Тяжелые металлы в почвах и растениях / Ю.В. Алексеев. — Л.: Агропромиздат, 1987. — 142 с.

19 Есенжолова А.Ж. Биоиндикационная способность листьев древесных и кустарниковых насаждений для оценки загрязнения среды тяжелыми металлами в зоне действия металлургического комплекса / А.Ж. Есенжолова, М.С. Панин // Экология и промышленность России. — 2013. — № 7. — С. 49–53.

20 Сибиркина А.Р. Биогеохимические особенности накопления соединений тяжелых металлов различными сообществами сосновых боров Семипалатинского Прииртышья / А.Р. Сибиркина // Современные проблемы науки и образования. — 2014. — № 3. URL: http://www.scienceeducation.ru/117–13005

21 Королев А.Н. Тяжелые металлы в почвах и овощных культурах в зоне влияния цементного завода города Семей / А.Н. Королев, В.А. Боев // Вестн. Омск. гос. аграр. ун-та. — 2017. — № 1. — С. 27–33.

А.Н. Сабитова, Б.Б. Баяхметова, Б.Х. Мұсабаева, Л.К. Оразжанова, К.Г. Ганиева

Күрең топырақтың гумин қышқылдарының ауыр металдарды сорбциялауы

Мақаланың мақсаты ашық және қою-күрең топырағының гумин қышқылдарымен ауыр металдардың сорбциясын зерттеу. Зерттеу объектілері Шығыс Қазақстанның экологиялық таза ауданынан алынған қою және ашық-күрең топырақ үлгілері болып табылады. Гумин қышқылдары (ГҚ) топырақтан әр түрлі рН мәндерінде бөлініп алынды, бұл ретте ГҚ қою-күрең топырақтан ГҚ шығымы рН 1.0 кезінде 0.075 %; рН=7.0 кезінде ашық-күрең топырақтан 0.017 % құрады. Бұдан әрі сорбция деңгейінің орта қышқылдығына тәуелділігі анықталды. Мырыш пен кадмий күшті қышқыл ортада сорбцияланатыны анықталды (рН 1.0–84.14 %), ал қорғасын рН 6.0 — 93.54 % кезінде жақсы сорбцияланады және оның сорбция дәрежесі жоғары. Би- және полиэлементті нұсқаларда металдар бір-бірінің сорбциясын басу немесе күшейту арқылы өзара әсер ететіні анықталды. Кадмий нейтрал ортада қорғасынның сорбциясын едәуір басатыны көрсетілген. Мырыш кадмий мен қорғасын сорбциясын 3 есе арттырады. Ауыр металдар иондарының топырақтың органикалық фракциясымен байланысуы гумин қышқылдарымен комплекс түзілу есебінен болады деген қорытынды жасалды.

Кілт сөздер: ауыр металдар, қою-күрең топырақ, ашық-күрең топырақ, топырақтың органикалық фракциясы, гумин қышқылдары, сорбция, мырыш, қорғасын, кадмий, Шығыс Қазақстан, Бородулиха.

А.Н. Сабитова, Б.Б. Баяхметова, Б.Х. Мусабаева, Л.К. Оразжанова, К.Г. Ганиева

Сорбция тяжелых металлов гуминовыми кислотами каштановых почв

Целью данной статьи является изучение сорбции тяжелых металлов гуминовыми кислотами (ГК) светло- и темно-каштановых почв. Объектами исследования являются образцы темно- и светло-каштановых почв, отобранные из экологически чистого района Восточного Казахстана. Гуминовые кислоты выделены из почвы при различных значениях рН, при этом выход ГК из темно-каштановой почвы при рН<1,0 составил 0,075 %, из светло-каштановой при рН=7,0 — 0,017 %. Далее была установлена зависимость степени сорбции от кислотности среды. Выявлено, что цинк и кадмий сильнее сорбируются в сильно-кислой среде (рН<1,0; 84,14 %), тогда как свинец лучше сорбируется при рН 6,0, причем степень его сорбции выше (93,54 %). В би- и полиэлементных вариантах выявлено, что металлы оказывают взаимное влияние, подавляя или усиливая сорбцию друг друга. Показано, что кадмий значительно подавляет сорбцию свинца в нейтральных средах. Цинк чаще усиливает сорбцию и кадмия и свинца в 3 раза. Сделано заключение, что связывание ионов тяжелых металлов органической фракцией почвы происходит за счет комплексообразования с гуминовыми кислотами.

Ключевые слова: тяжелые металлы, темно-каштановая почва, светло-каштановая почва, органическая фракция почвы, гуминовые кислоты, сорбция, цинк, свинец, кадмий, Восточный Казахстан, Бородулиха.

References

1 Vodyanitsky, Yu. N., Ladonin, D. V., & Savichev, A. T. (2012). *Zahriaznenie pochv tiazhelymi metallami [Contamination of soil with heavy metals]*. Moscow: Publ. house of the V.V. Dokuchaev Soil Institute [in Russian].

2 Clarke, L.W., Jenerette, G.D., & Bain, D.J. (2015). Urban legacies and soil management affect the concentration and speciation of trace metals in Los Angeles community garden soils. *Environmental Pollution, 197,* 1–12.

3 Sharma, R.K., & Archana, G. (2016). Cadmium minimization in food crops by cadmium resistant plant growth promoting rhizobacteria. *Applied Soil Ecology, 107*, 66–78.

4 Piri, M., Sepehr, E., & Rengel, Z. (2019). Citric acid decreased and humic acid increased Zn sorption in soils. *Geoderma, 341*, 39–45.

5 Ding, H., Tang, L., Nie, Y., & Ji, H. (2019). Characteristics and interactions of heavy metals with humic acid in gold mining area soil at a upstream of a metropolitan drinking water sourse. *Journal of Geochemical Exploration, 200,* 266–275.

6 Farhutdinov, R.M., Kayugin, A.A., & Cherkashina, L.V. (2010). Sviazyvanie svintsa, kadmiia i medi huminovymi kislotami ozernykh donnykh otlozhenii [Binding of lead, cadmium and copper by humic acids of lake bottom sediments]. *Vestnik Tiumenskoho hosudarstvennoho universiteta — Bulletin of Tyumen State University, 7,* 196–202 [in Russian].

7 Malyshenko, N.V., Zherebtsov, S.I., Smotrina, O.V., Bryukhovetskaya, L.V., & Ismagilov, Z.R. (2015). Sorbtsiia kationov tsinka modifitsirovannymi huminovymi kislotami [Sorption of zinc cations by modified humic acids]. *Khimiia v interesakh ustoichivoho razvitiia — Chemistry for sustainable development, 23*, 451–457 [in Russian].

8 Boguta, P., D'Orazio, V., Senesi, N., Sokołowska, Z., & Szewczuk-Karpisz, K. (2019). Insight into the interaction mechanism of iron ions with soil humic acids. The effect of the pH and chemical properties of humic acids. *Journal of Environmental Management, 245*, 367–374.

9 Fedorov, I.G., & Borzenko, S.V. (2018). Povedenie metallov v prisutstvii huminovykh veshchestv v sodovykh ozerakh Vostochnoho Zabaikalia [Behaviour of metals in the presence of humic substances in soda lakes of East Transbaikalia]. *Vestnik Zabaikalskoho hosudarstvennoho universiteta — Bulletin of Zabaykalsk State University, 2(2)*, 74–80 [in Russian].

10 Wei, L., Li, J., Xue, M., Wang, Sh., & Zhao, Q. (2019). Adsorption behaviors of Cu^{2+}, Zn^{2+} and Cd^{2+} onto proteins, humic acid, and polysaccharides extracted from sludge EPS: Sorption properties and mechanisms. *Bioresource Technology, 291,* 121868.

11 Calace, N., Deriu, D., & Petronio, B.M. (2009). Adsorbtion isotherms and breakthrough curves to study how humic acids influence heavy metal–soil interactions. *Water Air Soil Pollution, 204(2),* 373–380.

12 Boguta, P., & Sokołowska, Z. (2016). Study of the Interactions between Zn (II) ions and humic acids. *Plosone, 14(4),* 1–20.

13 Zherebtsov, S.I., Malyshenko, N.V., Bryuhovetsaya, L.V., & Lyrshchikov, S.Y. (2015). Sorption of copper cations from aqueous solutions by brown coals and humic acids. *Solid Fuel Chemistry, 49(5),* 294–303.

14 Karpyuk, L.A. (2008). Alkoksisililnye proizvodnye huminovykh veshchestv: sintez, stroenie i sorbtsionnye svoistva [Alkoxysilyl derivatives of humic substances: synthesis, structure and sorption properties]. *Candidate's thesis.* Moscow [in Russian].

15 Zavarzina, A.G. (2000). Vzaimodeistvie huminovykh kislot razlichnoho proiskhozhdeniia s ionami metallov i mineralnymi komponentami pochv [Interaction of humic acids of various origin with metal ions and mineral components of soils]. *Candidate's thesis.* Moscow [in Russian].

16 Budaeva, A.D., Zoltoev, E.V., Bodoev, N.V., & Balburova, T.A. (2005). Sorbtsiia ionov tiazhelykh metallov humatami ammoniia, natriia i kaliia [Sorption of heavy metal ions by ammonium, sodium and potassium humates]. *Fundamentalnye issledovaniia — Fundamental researches, 9*, 112–113 [in Russian].

17 Dobrovolskii, G.V., & Babeva, I.P. (2003). *Strukturno-funktsionalnaia rol pochv i pochvennoi bioty v biosphere [Structural and functional role of soils and soil biota in the biosphere].* Moscow: Nauka [in Russian].

18 Alekseev, Yu.V. (1987). *Tiazhelye metally v pochvakh i rasteniiakh [Heavy metals in soils and plants].* Leningrad: Ahropromizdat [in Russian].

19 Esenzholova, A.Zh., & Panin, M.S. (2013). Bioindikatsionnaia sposobnost listev drevesnykh i kustarnikovykh nasazhdenii dlia otsenki zahriazneniia sredy tiazhelymi metallami v zone deistviia metallurhicheskoho kompleksa [Bioindicative ability of leaves of tree and shrub stands for assessment of heavy metal pollution in the area of operation of the metallurgical complex]. *Ekolohiia i promyshlennost Rossii — Ecology and industry in Russia, 7,* 49–53 [in Russian].

20 Sibirkina, A.R. (2014). Bioheokhimicheskie osobennosti nakopleniia soedinenii tiazhelykh metallov razlichnymi soobshchestvami sosnovykh borov Semipalatinskoho Priirtyshia [The content of heavy metals in the Sands of the pine forest of the Semipalatinsk Irtysh region of the Kazakhstan Republic]. *Sovremennye problemy nauki i obrazovaniia — Modern problems of science and education, 3.* URL: http://www.scienceeducation.ru/117–13005 [in Russian]

21 Korolyov, A.N., & Boev, V.A. (2017). Tiazhelye metally v pochvakh i ovoshchnykh kulturakh v zone vliianiia tsementnoho zavoda horoda Semei [Heavy metals in soils and vegetable crops in the zone of influence of Semey cement plant]. *Vestnik Omskoho hosudarstvennoho ahrarnoho universiteta — Bulletin of Omsk State Agrarian University, 1,* 27–33 [in Russian].

CHEMICAL TECHNOLOGY

A.B. Yeszhanov[1, 2*], S.S. Dosmagambetova[2]

[1]*Institute of Nuclear Physic of the Republic of Kazakhstan, Almaty, Kazakhstan;*
[2]*L.N. Gumilyov Eurasian National University, Nur-Sultan, Kazakhstan*
(Corresponding author′s e-mail: a.yeszhanov@inp.kz)

Phenol solutions treatment by using hydrophobized track-etched membranes

Phenols are one of the most common surface water pollution. The discharge of phenolic waters into water bodies and streams sharply degrade their general sanitary condition, since these compounds have a toxic effect, and phenols can intensively absorb oxygen dissolved in water, which negatively affects the life of organisms in water bodies. Therefore, water treatment of phenols is an important environmental problem. In this study, the hydrophobic polyethylene terephthalate track-etched membranes (PET TeMs) were tested in water treatment from phenol by direct contact membrane distillation (DCMD). Hydrophobic PET TeMs were obtained by UV-graft polymerization of styrene, triethoxyvinylsilane with the addition of vinylimidazole (VIM), as well as by coating with fluorine-containing silanes. Scanning electron microscopy (SEM), Fourier-transform infrared (FTIR) spectroscopy and liquid entry pressure (LEP) analysis were used for membrane characterization. The contact angle after modification of PET TeMs was reached more than 130°. The efficiency of water purification from phenol was evaluated by water-flux measurements and fluorimetric method. The phenols solution was used at a concentration of 0.5, 1 and 2 g/l. The largest permeate flux of hydrophobized membranes was 1.1 kg/ m^2·h.

Keywords: phenol, water treatment, direct contact membrane distillation, UV-induced graft polymerization, styrene, triethoxyvinylsilane, fluorine-containing silanes, track-etched membranes.

Introduction

Nowadays, phenol and its derivatives as by-products of the petrochemical complex, coal and chemical industries, pharmaceuticals are significant pollutants of aquatic ecosystems due to their toxicity, stability, and ability to accumulate in the environment. Sources of phenols in natural water bodies are pharmaceutical effluents, dyes, pesticides, phenol-formaldehyde resins and nonionic surfactants, petrochemical complex enterprises, coal industry, mechanical engineering and chemical industry [1]. The solubility of phenol in water is one of the main causes of wastewater pollution. Moreover, the dangerous effect of phenol on the human body and the environment sets even at very low concentrations [2]. Therefore, water treatment from phenol is an important and urgent problem around the world [3].

Currently various methods for phenol wastewater treatment, such as ozonation [4, 5], wet air oxidation [6], Fenton reaction [7] are known. Also, one of the most effective methods for water treatment from phenol is membrane technology: nano [8] and ultrafiltration [9], as well as reverse osmosis [10]. Recently, DCMD was also used for water treatment from phenols [11, 12].

The essence of MD is based on the separation of the liquid due to the difference in temperature and pressure on both sides. Water evaporates on the hot side, and vapor passes through a hydrophobic membrane and condenses on the cold side. Compared to other membrane processes, MD has high energy efficiency, the process takes place at a relatively low temperature (~50–70 °C on the hot side and ~10 °C on the cold side).

---

* *Corresponding author*

The movement of vapor from the hot to the cold part is due to convection [13]. However, when vapor passes through the membrane, it partially transfers heat to the material, thereby reducing the temperature gradient. Therefore, it is important that the membrane has low thermal conductivity [14–16]. Various types of polymers, for instance, polytetrafluoroethylene (PTFE), polyamide (PA), polypropylene (PP) are used in MD [17–19]. At the same time, the major disadvantages of these polymers are possible fouling, insufficient water flow and high cost [9]. Thus, the task of finding new types of membranes and materials with good hydrophobic properties and high degrees of purification is relevant.

There has been a significant amount of interest for track-etched membrane (TeMs) in MD. A unique feature of TeMs is the control of the number of pores per unit area [20–25], which significantly expands fields of application in sensing [26], catalysis [27–31], lithium-ion batteries [32, 33], template synthesis of nanostructures [34–38]. At the present time various types of polymers are known, intended as a material for TeMs. The most significant are thin films made of poly(ethylene terephthalate) (PET). PET films have high thermal and chemical resistance, transparency, high-tensile strength. However, for the MD process, this type of membrane requires a significant expansion of its hydrophobic characteristics. PET TeMs were hydrophobized and used for purification of saline solutions [13,39] and liquid low-level radioactive wastes treatment [22, 40] by DCMD.

In this paper, UV-induced graft polymerization of triethoxyvinylsilane (TEVS) and styrene as well as covalent binding of perfluorododecyltrichlorosilane (PFDTS) in an *o*-xylene solution were used to increase hydrophobic properties of PET TeMs. Prepared membranes were tested in DCMD for treatment of phenol solutions.

Experimental

Materials

Benzophenone, dimethylformamide, dichloroethane, carbon tetrachloride, TEVS, VIM, PFDTS, *o*-xylene, styrene were purchased from Sigma-Aldrich. Deionized water (18.2 MΩ) was used in all experiments.

Preparation and improvement of hydrophobic properties of the membranes

Fabrication of PET TeMs was done in the following way. Samples 10×15 cm in size, previously irradiated by DC-60 accelerator (Astana branch of Institute of Nuclear Physics) with an energy of 1.75 MeV/nucleon by $^{84}Kr^{15+}$ ions, were treated in sodium hydroxide to obtain membranes with different pore sizes [26].

In order to increase hydrophobic properties of the membranes, three methods of surface modification were considered in comparison. First, modification of PET TeMs was carried out by UV-photoinduced graft polymerization of TEVS. Membranes with pore sizes of d ~ 200 nm were cleaned in order to remove interfering substances on the membrane surface. Then the samples were placed in a solution of the initiator. Further, the samples were immersed in a solution of dichloroethane and TEVS with a concentration range from 5 to 30 % and VIM (0.3–6.6 %) as an additive to graft polymerization. The resulting solution was irradiated under a UV lamp Ultra Vitalux E27 by OSRAM (UVA — 315–400 nm — W = 13.6 W, UVB — 280–315 nm — W = 3.0 W) within 15–180 minutes on both sides.

The second method was carried out by UV-induced graft polymerization of styrene. Styrene is one of the most accessible and widely used hydrophobic monomer. Samples were placed in a solution of styrene in carbon tetrachloride with concentration of 5–40 %. CCl_4 was chosen as solvent since it is transparent in UV-vis region, it can dissolve the monomer and this solvent has low chain transfer constant. Irradiation was carried out under the same conditions as in the first method.

The third method of hydrophobization was achieved by soaking membranes into *o*-xylene solution of PFDTS at different concentration range and time (1–24 h). After that, membranes were washed and dried.

Membrane characterization

The surface morphology of pristine and modified PET TeMs was examined using JSM-7500F scanning electron microscope (SEM) (JEOL, Japan).

To determine the functional groups before and after modification, FTIR spectra were recorded using FTIR spectrometer Agilent Cary 600. Spectra were recorded in the range from 4000 to 400 cm^{-1} with a resolution of 4.0 cm^{-1}. Each sample was measured 32 scans at the room temperature.

The contact wetting angle (CA) of the pristine and modified PET TeMs was measured goniometrically using the static drop method. Measurements were taken from different points of the polymer and the average result was calculated.

Liquid entry pressure (LEP) was measured to determine the minimum pressure necessary for the liquid to pass through the hydrophobic membrane pores. LEP was evaluated using deionized water on on water flow metering equipment as recommended in Ref. [41].

Water transport in membrane distillation process

Direct contact membrane distillation (DCMD) was used to purify water from phenol dissolved in it using modified PET TeMs. The mechanism of the process was described earlier in [13]. Phenol solutions with concentration of 0.5–2.0 g/l was tested. A personal computer connected to the analytical scale was used to record a data.

The flow rate was calculated by the formula:

$$J = \frac{\Delta m}{A \Delta t},$$ (1)

where J — is the flow rate (kg/m^{2}h); Δm — is the water mass in permeate side (kg) per unit time Δt (h); A — is the effective area of membrane (m^2).

Results and Discussion

Modification of PET TeMs and characterization

Hydrophobization of PET TeMs was carried out in three ways: by UV-induced graft polymerization of TEVS with VIM, styrene and covalent bonding of PFDTS with the membrane surface. The first method can be controlled by time of grafting, concentration of monomer, distance to UV-source and concentration of additives. Effect of these parameters on grafting degree and hydrophobic properties was evaluated and results are presented in Figure 1. VIM in concentration range from 0.3 to 3.3 % (v/v) was used as additive to increase grafting degree of TEVS since TEVS has low tendency to graft polymerization. VIM concentration of 3.3 % is optimal to get the most hydrophobic membrane, a further increase in concentration leads to a decrease in hydrophobic properties, caused by the hydrophilic properties of VIM with higher content.
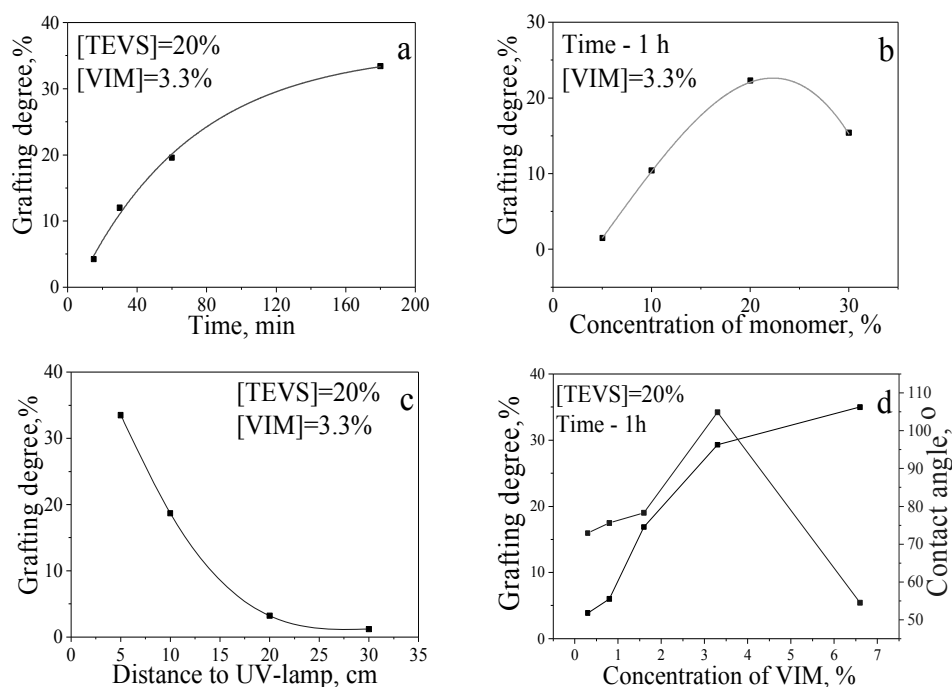

Figure 1. Grafting degree of TEVS onto PET TeMs at variation of time (*a*) and concentration of monomer (*b*), distance to UV-lamp (*c*) and concentration of VIM (*d*)

Figure 1 (*a*) shows a graph of grafting degree versus time of irradiation. With increasing UV-irradiation time, the grafting degree is also gradually grown. An increase in the irradiation time of more than 1h led to the appearance of a gel-like mass, indicating the presence of a homopolymer on the membrane surface. Figure 1 (*b*) represented the dependence of grafting degree on the concentration of the TEVS. The graph clearly demonstrates that the grafting degree reaches maximum value at a concentration of 20 % and a subsequent increase in concentration leads to a decrease of grafting degree. Figure 1 (*c*) shows an effect of the distance

to the UV source on the grafting degree (TEVS concentrations of 20 % and VIM 3.3 % at irradiation time 1 h). It should be noted that increasing the distance from the UV source to the sample leads to a rapid decrease in the grafting degree. At the same time, 5 cm led to formation of a gel and membrane contamination.

Thus, the most suitable parameters for the modification of PET TeMs were found: TEVS concentration of 20 % with a VIM concentration of 3.3 %, distance to UV-source — 10 cm, time of irradiation — 60 min.

The second modification method is based on the UV-graft polymerization of styrene. In Figure 2 (*a*, *b*) shows a linear dependence of grafting degree on time at a constant monomer concentration of 10 % and a distance from UV-source (7 cm).

Grafting degree reaches 12 % after 120 min of grafting. An increase in styrene concentration leads to an increase in the grafting degree up to 43 % at 40 % styrene concentration, as shown in Figure 2 (*c*).
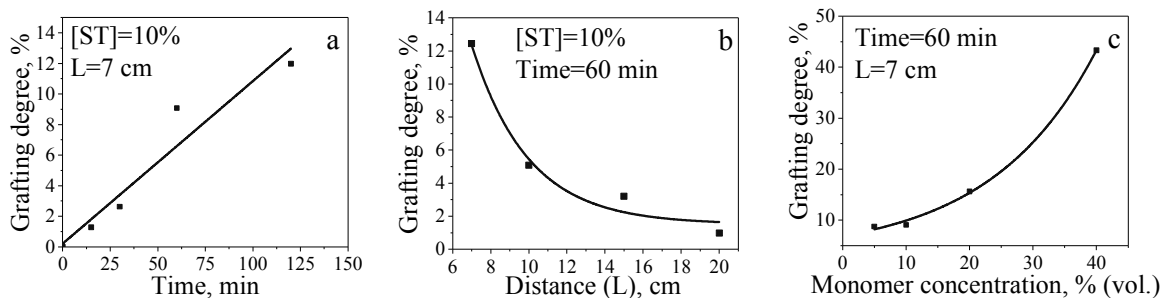

Figure 2. Grafting degree depends on irradiation time (*a*), distance to UV-source (*b*) and monomer concentration (*c*) (pore diameter d ≈200 nm)

The third modification method is based on the soaking of PET TeMs in a solution of *o*-xylene with PFDTS. The principle of the interaction of PFDTS with *o*-xylene is the high hydrolysis ability of the Si–Cl bond, which is able to easily interact with the surface of PET TeMs. Figure 3 (*a*) shows the dependence of the contact angle (CA) on the concentration of PFDTS. As can be seen, the CA reaches a maximum value at an optimal monomer concentration of 20 mM. A further increase in concentration does not lead to a significant change in the CA. The dependence of the CA on the holding time in the reaction was considered. The results are shown in Figure 3 (*b*). The largest CA (134°) was reached after 24 hours. A further increase in time did not significantly affect on the value of the CA.
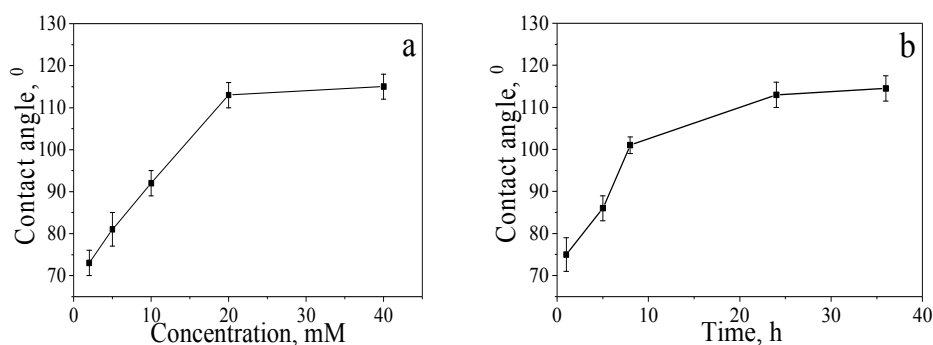

Figure 3. Contact angle (CA) of modified PET TeMs at various concentration of PFDTS (*a*) and reaction time (*b*) (pore diameter of initial PET TeMs is 200 nm)

All hydrophobized PET TeMs were analyzed by methods of contact angle, SEM, FTIR spectroscopy and gas permeability test. Results are presented in Figures 4–6. The measurements of CA were carried out from different places of the sample and the average value was calculated. Images of droplets are shown in Figure 4.

It can be seen, the contact wetting angle of the initial PET TeMs increases significantly from 52 to 83° for PET TeMs-g-TEVS, to 99° for PET TeMs-g-PS and to 134° for PET TeMs–PFDTS.

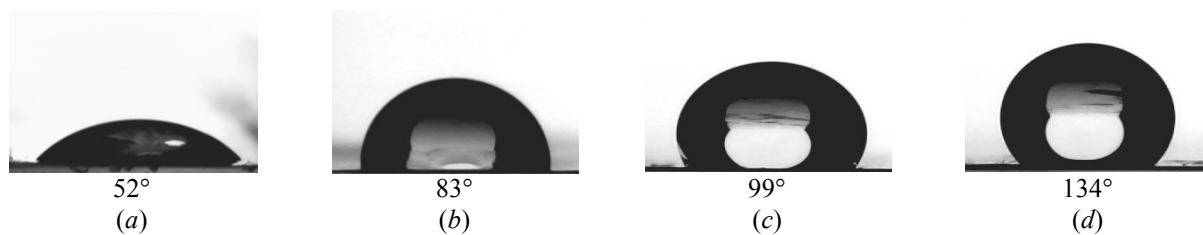|52° | 83° | 99° | 134° |
|(*a*) | (*b*) | (*c*) | (*d*) |

Figure 4. Contact angle (CA) for initial PET TeMs (d ≈ 200 nm) (*a*), PET TeMs-g-TEVS (*b*), PET TeMs-g-PS (*c*), PET TeMs–PFDTS (*d*) (at optimal conditions)
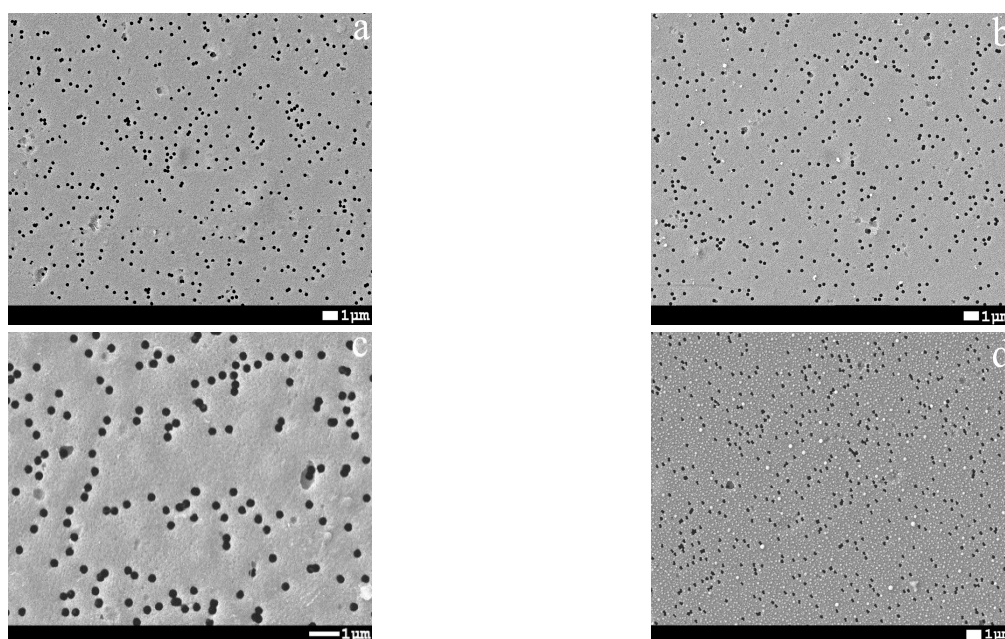

Figure 5. SEM images of initial PET TeMs (*a*), PET TeMs-g-TEVS (*b*), PET TeMs-g-PS (*c*), PET TeMs–PFDTS (*d*)

SEM images of surface initial and modified PET TeMs presented in Figure 5. Modification of PET TeMs has led to a reduction in pore size from 220 ± 15 for initial PET TeMs to 216 ± 4 nm for PET TeMs-g-TEVS, to 215±6 nm for PET TeMs-g-PS and to 174 ± 4 nm for PET TeMs–PFDTS. The decrease in pore size is due to the formation of polymers within the pores.

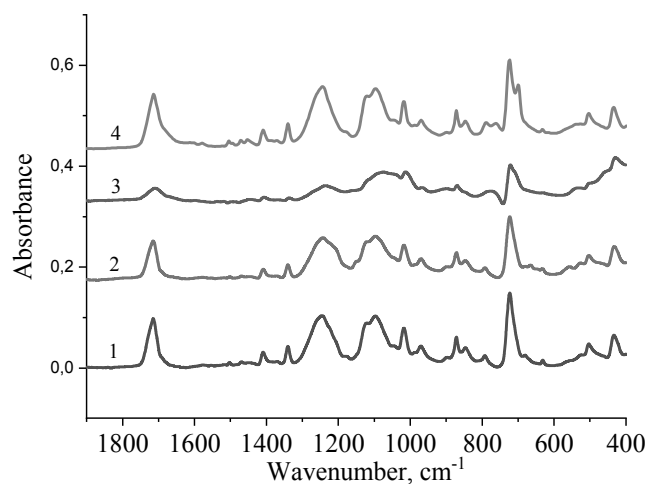Figure 6. FTIR spectra of PET TeMs (*1*), PET TeMs-g-TEVS (*2*), PET TeMs-PFDTS (*3*), PET TeMs-g-PS (*4*)

To identify the characteristic absorption bands of initial and hydrophobized PET TeMs, FTIR analysis was performed. Typical FTIR spectra are shown in Figure 6. Initial PET TeMs characterized by absorption bands at 3400 cm^{-1}, which corresponds to the absorption of the OH groups, 2900–2980 cm^{-1} are aliphatic and benzene CH$_3$ rings. The C=O double bond was observed at an absorption of 1720 cm^{-1}. Pulsation vibrations of the carbon skeleton were found at 1420, 1480, 1612 cm^{-1}. The C(O)–O and O–CH$_2$ bonds were detected at 1220 and 970 cm^{-1}, respectively. Grafting of TEVS led to appearance of new peaks at 1260, 801 cm^{-1} and 1100–1000 cm^{-1} which is related to Si–CH$_3$ and Si–O–Si vibrations respectively. Moreover, absorbance bands with low intensity and shape of shoulders were found at 1649 cm^{-1} (C=C def.), 1497 and 1085 cm^{-1} (C-N def.) related to VIM. Graft polymerization of polystyrene (40 % concentration) led to appearance of new peaks in FTIR spectra characteristic of polystyrene: 1580, 1450 (CH$_2$-deformation), 700 (CH$_2$-rocking mode), 530 cm^{-1} (CH-aromatic), 1480 см$^{-1}$ (C=C aromatic). Covalent bonding of PFDTS led to appearance of new peaks at 1060, 1127 cm^{-1}, as well as peaks of low intensity at 577, 602 and 628 cm^{-1} related to the C-F bond. Characteristics of PET TeMs before and after hydrophobization are presented in Table 1.

T a b l e 1

Characteristics of PET TeMs before and after hydrophobization

Sample	Contact angle, °±4°	Effective pore size, nm	Pore size (from SEM analysis), nm	[Si], % (from EDX analysis)	[F], % (from EDX analysis)	LEP, MPa
Initial PET TeMs	58	198±5	220±8	-	-	0.12
PET TeMs-g-PS	83	215±6	220±15			>0.43
PET TeMs-g-TEVS	89	167±8	216±3	1.5	-	>0.43
PET TeMs–PFDTS	134	148±6	174±4	2.2	11.46	>0.43

Membranes with pore diameters of ≈200nm were hydrophobized at optimal parameters by three methods. LEP analysis (Table 1) showed that hydrophobized membranes with 200 nm can be used in MD in accordance with the recommendations [42]. Hydrophobized PET TeMs have a LEP >0.43 MPa.

Purification of phenol by DCMD

Membrane distillation was carried out using a phenol solution with concentrations of 0.5, 1.0, 2.0 g/l. The process of membrane distillation has already been described earlier in the work. During the experiment, a 50 ml sample was taken every hour to detect traces of phenol.

Figure 7–9 shows water fluxes and electrical conductivity at different concentrations of phenol. PET TeMs-g-TEVS has average water fluxes of 0.71 kg/m^2·h at a phenol concentration of 0.5 g/l, 0.502 kg/m^2·h and 0.546 kg/m^2·h for concentrations of 1.0 g/l and 2.0 g/l respectively. PET TeMs-g-PS has average water fluxes of 0.84 kg/m^2·h at a phenol concentration of 0.5 g/l, 0.770 kg/m^2·h and 0.821 kg/m^2·h for concentrations of 1.0 g/l and 2.0 g/l respectively. PET TeMs — PFDTS has average water fluxes of 1.10 kg/m^2·h at a phenol concentration of 0.5 g/l, 0.92 kg/m^2·h and 1.06 kg/m^2·h for concentrations of 1.0 g/l and 2.0 g/l respectively. Flux changes in concentrations occur with the least differences. It can be associated with temperature instability during DCMD, as well as with more uniform layer of grafted polymer on the surface.

There was a gradual decrease in productivity during the MD process, this is due to the inconsistency of the temperature difference between the cold and hot contours. However, at the same time, the performance of a less concentrated solution is much higher than that of a highly concentrated solution. This is probably due to the fact that there is wetting and contamination of the membrane surface, which reduces productivity.

The efficiency of DCMD was determined by the fluorimetric method and quantitatively performed on a Fluorat-02 analyzer. The selected samples in the process of MD with a volume of 50 ml were diluted to a concentration of 1 mg /dm^3 and measured according to PND F 14.1:2:4.182–02 «The methodology of measuring the mass concentration of phenols in drinking samples, natural and waste water by fluorimetric method on the Fluorat-02 analyzer». The measurement was carried out at least 3 times in the «Measurement» mode and the arithmetic mean was found. As can be seen from Table 2, there is an increase in the concentration in the selected samples with an increase in the concentration of the phenol stock solution.

The increase in concentration in the selected samples is associated with the gradual transfer of phenol from the initial solution to permeate, thereby the permeate becomes more concentrated. Thus, phenols are concentrated in a smaller volume of permeate.
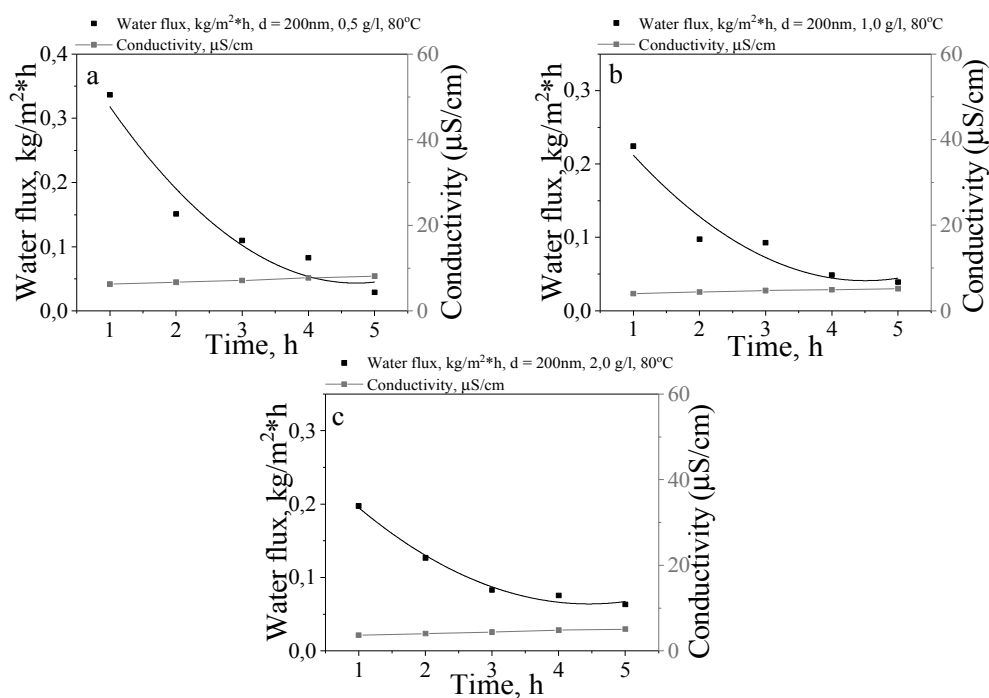
Figure 7. MD water flux and electrical conductivity of PET TeMs-g-TEVS for phenol
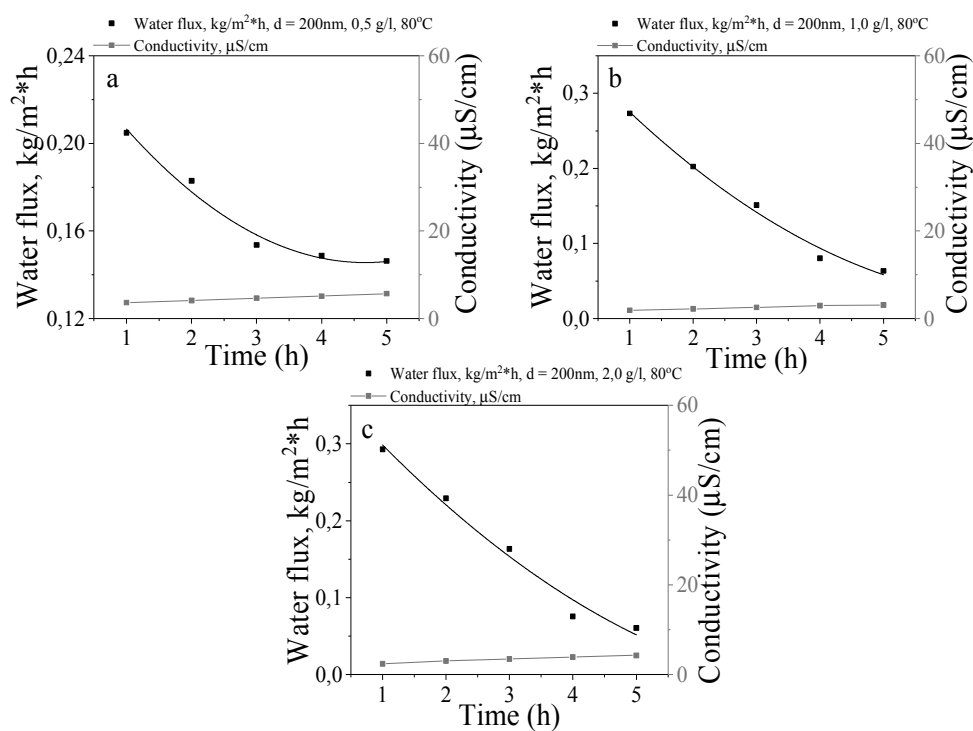with concentrations of 0.5 g/l (*a*); 1.0 g/l (*b*); 2.0 g/l (*c*)

Figure 8. MD water flux and electrical conductivity of PET TeMs-g-PS for phenol
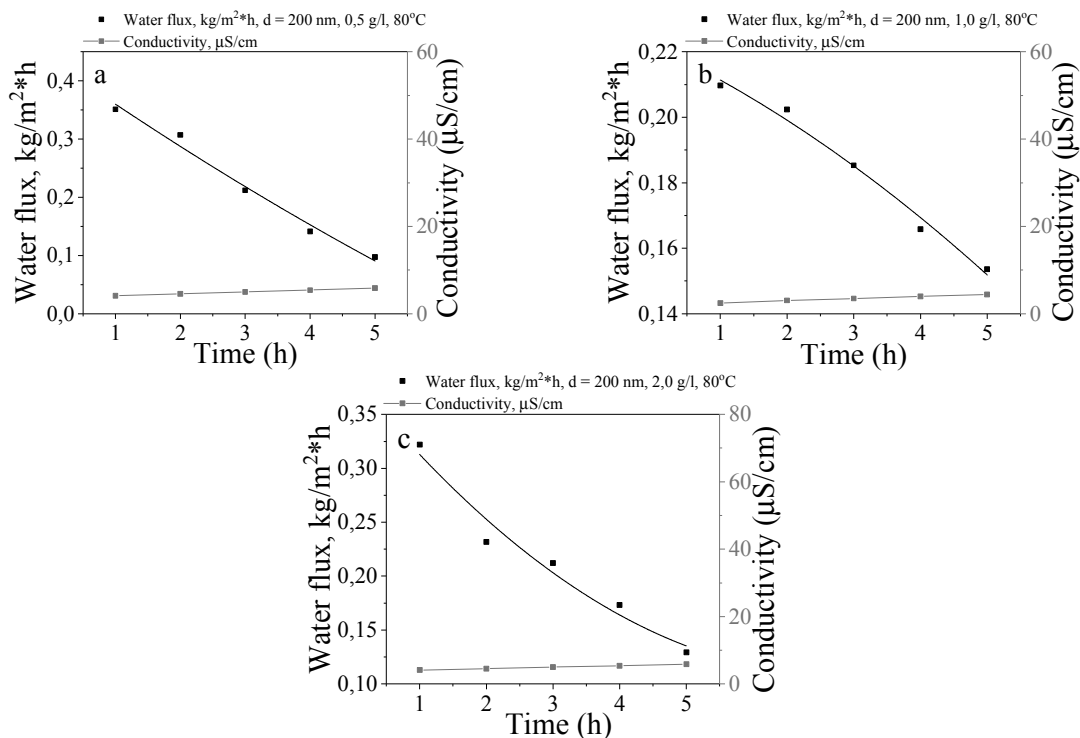with concentrations of 0.5 g/l (*a*); 1.0 g/l (*b*); 2.0 g/l (*c*)

Figure 9. MD water flux and electrical conductivity of PET TeMs–PFDTS for phenol
with concentrations of 0.5 g/l (*a*); 1.0 g/l (*b*); 2.0 g/l (*c*)

T a b l e 2

Phenol concentrations in samples at different sampling times

Phenol concentration, g/l	TEVS			Styrene			PFDTS		
	0.5	1	2	0.5	1	2	0.5	1	2
Initial	3.03±0.01	3.65±0.01	7.15±0.01	0.28±0.02	0.76±0.02	0.46±0.01	0.79±0.03	5.49±0.02	5.59±0.02
After 3h	6.30±0.03	7.85±0.01	16.83±0.04	0.32±0.01	1.01±0.01	19.00±0.02	4.03±0.01	10.17±0.03	12.10±0.03
After 5h	8.51±0.03	8.70±0.04	21.24±0.04	0.85±0.01	2.53±0.03	25.80±0.03	4.81±0.02	11.50±0.01	18.82±0.01

Based on the obtained results, methods of hydrophobization of PET TeMs showed good performance. The most preferred type of modification for membrane distillation is PET TeMs — PFDTS, due to its simplicity, high performance and efficiency.

Conclusions

In this research, the ability of modified PET TeMs in water treatment from phenol was studied. Hydrophobized PET TeMs were obtained by graft polymerization of TEVS and VIM, styrene and covalent binding of PFDTS. Various characteristics of modifying agents on the grafting degree and wetting angle values were studied. Membranes with CA of 134°, 99° and 83° were prepared and further used for DCMD of phenol solutions. Maximum permeate flux 1.1 kg/m^2·h were achieved using PET TeMs–PFDTS. Thus, such methods of membrane hydrophobization can be used in MD process for water purification from phenol.

References

1   Hussain A. Kinetic study for aerobic treatment of phenolic wastewater / A. Hussain, S. Dubey, V. Kumar // Water Resources and Industry. — 2015. — Vol. 11. — P. 81–90. DOI: 10.1016/j.wri.2015.05.002.

2   Mohammadi S. Phenol removal from industrial wastewaters: a short review / S. Mohammadi, A. Kargari, H. Sanaeepur, K. Abbassian, A. Najafi, E. Mofarrah // Desalination and Water Treatment. — 2015. — Vol. 53, No. 8. — P. 2215–2234. DOI: 10.1080/19443994.2014.883327.

3   Zhang M. Ultrasound-assisted electrochemical treatment for phenolic wastewater / M. Zhang, Z. Zhang, S. Liu, Y. Peng, J. Chen, S. Yoo Ki // Ultrasonic Sonochemistry. — 2020. — Vol. 65. — P. 105058. DOI: 10.1016/j.ultsonch.2020.105058.

4   Wang J. Catalytic ozonation for water and wastewater treatment: Recent advances and perspective / J. Wang, H. Chen // Science of Total Environment. — 2020. — Vol. 704. — P. 135249. DOI: 10.1016/j.scitotenv.2019.135249.

5   Huang Y. New phenolic halogenated disinfection byproducts in simulated chlorinated drinking water: Identification, decomposition, and control by ozone-activated carbon treatment / Y. Huang, H. Li, Q. Zhou, A. Li, C. Shuang, Q. Xian, B. Xu, Y. Pan // Water Resources. — 2018. — Vol. 146. — P. 298–306. DOI: 10.1016/j.watres.2018.09.031.

6   Yadav A. Removal of phenol from water by catalytic wet air oxidation using carbon bead-Supported iron nanoparticle-Containing carbon nanofibers in an especially configured reactor / A. Yadav, A. Teja, N. Verma // Journal of Environmental Chemical Engineering. — 2016. — Vol. 48, No. 2. — P. 1504–1513. DOI: 10.1016/j.jece.2016.02.021.

7   Gernjak W. Photo-fenton treatment of water containing natural phenolic pollutants / W. Gernjak, T. Krutzler, A. Glaser, S. Malato, J. Caceres, R. Bauer, A. Fernandez-Alba // Chemosphere. — 2003. — Vol. 50, No. 1. — P. 71–78. DOI: 10.1016/S0045–6535(02)00403–4.

8   Ochando-Pulido J. About two-phase olive oil washing wastewater simultaneous phenols recovery and treatment by nanofiltration / J. Ochando-Pulido, J. Corpas-Martinez, A. Martinez-Ferez // Progress Safety and Environmental Protection. — 2018. — Vol. 114. — P. 159–168. DOI: 10.1016/j.psep.2017.12.005.

9   Victor-Ortega M. Recovery of phenolic compounds from wastewaters through micellar enhanced ultrafiltration / M. Víctor-Ortega, R. Martins, L. Gando-Ferreira, R. Quinta-Ferreira // Colloids and Surfaces A: Physicochemical and Engineering Aspects. — 2017. — Vol. 531. — P. 18–24. DOI: 10.1016/j.colsurfa.2017.07.080.

10   Al-Obaidi M. Removal of phenol from wastewater using spiral-wound reverse osmosis process: Model development based on experiment and simulation / M. Al-Obaidi, C. Kara-Zaïtri, I. Mujtaba // Journal of Water Process Engineering. — 2017. — Vol. 18. — P. 20–28. DOI: 10.1016/j.jwpe.2017.05.005.

11   Hamzah N. Membrane distillation of saline with phenolic compound using superhydrophobic PVDF membrane incorporated with TiO_2 nanoparticles: Separation, fouling and self-cleaning evaluation / N. Hamzah, C. Leo // Desalination. — 2017. — Vol. 418. — P. 79–88. DOI: 10.1016/j.desal.2017.05.029.

12   Hamzah N. Fouling prevention in the membrane distillation of phenolic-rich solution using superhydrophobic PVDF membrane incorporated with TiO_2 nanoparticles / N. Hamzah, C. Leo // Separation and Purification Technology. — 2016. — Vol. 167. — P. 79–87. DOI: 10.1016/j.seppur.2016.05.005.

13   Korolkov I. Preparation of PET track-etched membranes for membrane distillation by photo-induced graft polymerization / I. Korolkov, Y. Gorin, A. Yeshzhanov, A. Kozlovskiy, M. Zdorovets // Materials Chemistry and Physics. — 2018. — Vol. 205. — P. 55–63. DOI: 10.1016/j.matchemphys.2017.11.006.

14   Yao M. A review of membrane wettability for the treatment of saline water deploying membrane distillation / M. Yao, L. Tijing, G. Naidu, S-H Kim, H. Matsuyama, A. Fane, H. Shon // Desalination. — 2020. — Vol. 479. — P. 114312. DOI: 10.1016/j.desal.2020.114312.

15   Hubadillah S. Hydrophobic ceramic membrane for membrane distillation: A mini review on preparation, characterization, and applications / S. Hubadillah, Z. Tai, M. Othman, Z. Harun, M. Jamalludin, M. Rahman, J. Jaafar, A. Ismail // Separation and Purification Technology. — 2019. — Vol. 217. — P. 71–84. DOI: 10.1016/j.seppur.2019.02.014.

16   Siyal M. A review of membrane development in membrane distillation for emulsified industrial or shale gas wastewater treatments with feed containing hybrid impurities // M. Siyal, C-K. Lee, C. Park, A. Khan, J-O. Kim // Journal of Environmental Management. — 2019. — Vol. 243. — P. 45–66. DOI: 10.1016/j.jenvman.2019.04.105.

17   Tang N. Preparation and morphological characterization of narrow pore size distributed polypropylene hydrophobic membranes for vacuum membrane distillation via thermally induced phase separation / N. Tang, Q. Jia, H. Zhang J. Li, S. Cao // Desalination. — 2010. — Vol. 256, No. 1–3. — P. 27–36. DOI: 10.1016/j.desal.2010.02.024.

18   Zhu H. Preparation and properties of PTFE hollow fiber membranes for desalination through vacuum membrane distillation / H. Zhu, H. Wang, F. Wang, Y. Guo, H. Zhang, J. Chen // Journal of Membrane Science. — 2013. — Vol. 446. — P. 145–153. DOI: 10.1016/j.memsci.2013.06.037.

19   Yang X. Performance improvement of PVDF hollow fiber-based membrane distillation process / X. Yang, R. Wang, L. Shi, A. Fane, M. Debowski // Journal of Membrane Science. — 2011. — Vol. 369, No. 1–2. — P. 437–447. DOI: 10.1016/j.memsci.2010.12.020.

20   Korolkov I. Enhancing hydrophilicity and water permeability of PET track-etched membranes by advanced oxidation process / I. Korolkov, A. Mashentseva, O. Guven, M. Zdorovets, A. Taltenov // Nuclear Instruments and Methods in Physics Research Section B: Beam Interactions with Materials and Atoms. — 2015. — Vol. 365. — P. 651–655. DOI: 10.1016/j.nimb.2015.10.031.

21   Korolkov I. The effect of oxidizing agents/systems on the properties of track-etched PET membranes / I. Korolkov, A. Mashentseva, O. Guven, D. Niyazova, M. Barsbay, M. Zdorovets // Polymer Degradation and Stability. — 2014. — Vol. 107. — P. 150–157. DOI: 10.1016/j.polymdegradstab.2014.05.008.

22   Korolkov I. Modification of PET ion track membranes for membrane distillation of low-level liquid radioactive wastes and salt solutions / I. Korolkov, A. Yeshzhanov, M. Zdorovets, Y. Gorin, O. Guven, S. Dosmagambetova // Separation and Purification Technology. — 2019. — Vol. 227. — P. 115694. DOI: 10.1016/j.seppur.2019.115694.

23   Korolkov I. UV-induced graft polymerization of acrylic acid in the sub-micronchannels of oxidized PET track-etched membrane / I. Korolkov, A. Mashentseva, O. Guven, A. Taltenov // Nuclear Instruments and Methods in Physics Research Section B: Beam Interactions with Materials and Atoms. — 2015. — Vol. 365. — P. 419–423. DOI: 10.1016/j.nimb.2015.07.057.

24   Korolkov I. Protein fouling of modified microporous PET track-etched membranes / I. Korolkov, A. Mashentseva, O. Guven, Y. Gorin, M. Zdorovets // Radiation Physics and Chemistry. — 2018. — Vol. 151. — P. 141–148. DOI: 10.1016/j.radphyschem.2018.06.007.

25 Kutuzau M. Optimization of PET ion-track membranes parameters / M. Kutuzau, A. Kozlovskiy, D. Borgekov, I. Kenzhina, M. Zdorovets, A. Chernik, O. Alisienok, A. Shumskaya, E. Kaniukov // Materials today: proceedings. — 2019. — Vol. 7, No. 3. — P. 866–871. DOI: 10.1016/j.matpr.2018.12.086.

26 Zdorovets M. Functionalization of PET track-etched membranes by UV-induced graft (co)polymerization for detection of heavy metal ions in water / M. Zdorovets, I. Korolkov, A. Yeszhanov, Y. Gorin // Polymers (Basel). — 2019. — Vol. 11, No. 11. — P. 1876. DOI: 10.3390/polym11111876.

27 Korolkov I. Electron/gamma radiation-induced synthesis and catalytic activity of gold nanoparticles supported on track-etched poly(ethylene terephthalate) membranes / I. Korolkov, A. Mashentseva, O. Guven, Y. Gorin, A. Kozlovskiy, M. Zdorovets // Materials Chemistry and Physics. — 2018. — Vol. 217. — P. 31–39. DOI: 10.1016/j.matchemphys.2018.06.039.

28 Korolkov I. Radiation induced deposition of copper nanoparticles inside the nanochannels of poly(acrylic acid)-grafted poly(ethylene terephthalate) track-etched membranes / I. Korolkov, O. Guven, A. Mashentseva, A. Bakar Atici, Y. Gorin, M. Zdorovets // Radiation Physics and Chemistry. — 2017. — Vol. 130. — P. 480–487. DOI: 10.1016/j.radphyschem.2016.10.006

29 Korolkov I. The effect of oxidation pretreatment of polymer template on the formation and catalytic activity of Au/PET membrane composites / I. Korolkov, D. Borgekov, A. Mashentseva, O. Guven, A. Bakar Atici, A. Kozlovskiy, M. Zdorovets // Chemical Papers. — 2017. — Vol. 71, No. 12. — P. 2353–2358. DOI: 10.1007/s11696–017–0229–1.

30 Yeszhanov A. Copper nanotube composite membrane as a catalyst in Mannich reaction / A. Yeszhanov, A. Mashentseva, I. Korolkov, Y. Gorin, A. Kozlovskiy, M. Zdorovets // Chemical Papers. — 2018. — Vol. 72. — P. 3189–3194. DOI: 10.1007/s11696–018–0539–y.

31 Mashentseva A. Electron beam induced enhancement of the catalytic properties of ion-track membranes supported copper nanotubes in the reaction of the P-nitrophenol reduction / A. Mashentseva, D. Shlimas, A. Kozlovskiy, M. Zdorovets, A. Russakova, M. Kassymzhanov, A. Borisenko // Catalysts. — 2019. — Vol. 9, No. 9. — P. 737. DOI: 10.3390/catal9090737.

32 Zdorovets M. Investigation of phase transformations and corrosion resistance in $Co/CoCo_2O_4$ nanowires and their potential use as a basis for lithium-ion batteries / M. Zdorovets, A. Kozlovskiy // Scientific Reports. — 2019. — Vol. 9, No. 1. — P. 1–12. DOI: 10.1038/s41598–019–53368–y.

33 Zdorovets M. Study of phase transformations in $Co/CoCo_2O_4$ nanowires / M. Zdorovets, A. Kozlovskiy // Journal of Alloys and Compounds. — 2020. — Vol. 815. — P. 152450. DOI: 10.1016/j.jallcom.2019.152450.

34 Borgekov D. Temperature dependent catalytic activity of Ag/PET ion-track membranes composites / D. Borgekov, A. Mashentseva, S. Kislitsin, A. Kozlovskiy, A. Russakova, M. Zdorovets // Acta Physica Polonica Series A. — 2015. — Vol. 128, No. 5. — P. 871–875. DOI: 10.12693/aphyspola.128.871.

35 Mashentseva A. Impact of testing temperature on the structure and catalytic properties of au nanotubes composites / A. Mashentseva, M. Zdorovets, D. Borgekov // Bulletin of Chemical Reaction Engineering & Catalysis. — 2018. — Vol. 13, No. 3. — P. 405–411. DOI: 10.9767/bcrec.13.3.2127.405–411.

36 Mashentseva A. Catalytic activity of composite track-etched membranes based on copper nanotubes in flow and static modes / A. Mashentseva, M. Zdorovets // Petroleum Chemistry. — 2019. — Vol. 59, No. 5. — P. 552–557. DOI: 10.1134/ S0965544119050074.

37 Mashentseva A. Influence of deposition temperature on the structure and catalytic properties of the copper nanotubes composite membranes / A. Mashentseva, A. Kozlovskiy, M. Zdorovets // Materials Research Express. — 2018. — Vol. 5, No. 6. DOI: 10.1088/2053–1591/aacb5f.

38 Shumskaya A. Evolution of morphology, structure, and magnetic parameters of Ni nanotubes with growth in pores of a PET template / A. Shumskaya, V. Bundyukova, A. Kozlovskiy, M. Zdorovets, K. Kadyrzhanov, G. Kalkabay, E. Kaniukov // Journal of Magnetism and Magnetic Materials. — 2020. — Vol. 497. — P. 165913. DOI: 10.1016/j.jmmm.2019.165913.

39 Korolkov I. Hydrophobization of PET track-etched membranes for direct contact membrane distillation / I. Korolkov, A. Yeszhanov, Y. Gorin, M. Zdorovets, N. Khlebnikov, K. Serkov // Materials Research Express. — 2018. — Vol. 5, No. 6. — P. 065317. DOI: 10.1088/2053–1591/aacc39.

40 Zdorovets M. Liquid low-level radioactive wastes treatment by using hydrophobized track-etched membranes / M. Zdorovets, A. Yeszhanov, I. Korolkov, O. Guven, S. Dosmagambetova, D. Shlimas, Z. Zhatkanbayeva, I. Zhidkov, P. Kharkin, V. Gluchshenko, D. Zheltov, N. Khlebnikov, I. Kuklin // Progress in Nuclear Energy. — 2020. — Vol. 118. — P. 103128. DOI: 10.1016/j.pnucene.2019.103128.

41 Garcia-Payo M. Wetting study of hydrophobic membranes via liquid entry pressure measurements with aqueous alcohol solutions / M. Garcia-Payo, M. Izquierdo-Gil, C. Fernández-Pineda // Journal of Colloid and Interface Science. — 2000. — Vol. 230, No. 2. — P. 420–431. DOI: 10.1006/jcis.2000.7106.

42 Eykens L. Membrane synthesis for membrane distillation: A review / L. Eykens, K. De Sitter, C. Dotremont, L. Pinoy, B. Van der Bruggen // Separation and Purification Technology. — 2017. — Vol. 182. — P.36–51. DOI: 10.1016/ j.seppur.2017.03.035.

А.Б. Есжанов, С.С. Досмағамбетова

Фенол ерітінділерін гидрофобты тректі мембраналармен тазарту

Жер үсті суларының ең көп таралған ластануының бірі құрамында фенол бар заттар болып табылады. Құрамында фенол бар қосылыстар адамның денсаулығы мен қоршаған ортаға кері әсерін тигізеді, өйткені олар суға түскен кезде оттегіні интенсивті сіңіреді. Сондықтан фенолдарды сумен тазарту — басты экологиялық міндет. Суды фенолдардан тазарту полиэтилентерефталат (ПЭТФ ТМ) негізіндегі гидрофобты трек тік мембраналарын қолдану арқылы тікелей жанасатын мембраналық дистилляция әдісімен жүзеге асырылды. Гидрофобты трек тік мембраналар егу полимерлеу және фтор бар

силандармен жабу арқылы алынды. Сканерлеуші электронды микроскопия (СЭМ), Фурье-трансформалы инфрақызыл (ИҚ) спектроскопия және сұйықтықтың ену қысымын талдау гидрофобты ПЭТФ ТМ сипаттау үшін қолданылды. ПЭТФ ТМ модификациялағаннан кейін ылғалдың жанасу бұрышы 130°-дан жоғары болды. Суды фенолдан тазарту тиімділігі су ағынын өлшеу және флуориметриялық әдіспен бағаланды. Фенол ерітіндісі 0,5, 1 және 2 г/л концентрациясында қолданылды. Гидрофобты мембраналардың ең үлкен пермеат ағыны 1,1 кг/м^2 сағ. құрады.

Кілт сөздер: фенол, суды тазарту, тікелей мембраналық сүзу, УК-егу полимерлеу, стирол, триэтоксивинилсилан, құрамында фтор бар силандар, тректі мембраналар.

А.Б. Есжанов, С.С. Досмагамбетова

Очистка растворов фенола гидрофобными трековыми мембранами

Фенолы являются одним из наиболее распространенных загрязнителей поверхностных вод. Сброс фенольных вод в водоемы и водотоки резко ухудшает их общее санитарное состояние, поскольку, во-первых, эти соединения оказывают токсическое действие, а во-вторых, интенсивно поглощают растворенный в воде кислород, что отрицательно сказывается на жизни организмов в водоеме. Поэтому очистка воды от фенолов является важной экологической задачей. В этом исследовании гидрофобные трековые мембраны на основе полиэтилентерефталата (ПЭТФ ТМ) были испытаны при обработке воды от фенола путем прямой контактной мембранной дистилляции. Гидрофобные ПЭТФ ТМ были получены УФ-прививочной полимеризацией стирола, триэтоксивинилсилана с добавкой винилимидазола, а также покрытием фторсодержащих силанов. Полученные гидрофобные ПЭТФ ТМ были охарактеризованы методами сканирующей электронной микроскопии, ИК-Фурье-спектроскопии, анализом давления проскока жидкости. Разработанный метод гидрофобизации ПЭТФ ТМ привел к повышению угла смачивания до 130°. Эффективность очистки воды от фенола оценивали измерением производительности и флуориметрическим методом. Концентрации растворов фенола составляли 0,5, 1 и 2 г/л. Максимальная производительность гидрофобных мембран достигала 1,1 кг/м^2·ч.

Ключевые слова: фенол, очистка воды, прямая контактная мембранная дистилляция, УФ-прививочная полимеризация, стирол, триэтоксивинилсилан, фторсодержащие силаны, трековые мембраны.

N.Zh. Balpanova[1*], A.M. Gyulmaliev[2], Yu.N. Pankin[3], F. Ma[4], K. Su[4], A.I. Khalitova[1],
D.E. Aitbekova[1], A. Tusipkhan[1], M.I. Baikenov[1, 5]

[1]*Karagandy University of the name of academician E.A. Buketov, Kazakhstan;*
[2]*Topchiev Institute of Petrochemical Synthesis, Russian Academy of Sciences, Moscow, Russia;*
[3]*«Kazakhtelekom» , Karaganda, Kazakhstan;*
[4]*Xinjiang University, Urumqi, People's Republic of China;*
[5]*South Ural State University, Chelyabinsk, Russia*
(Corresponding author′s e-mail: nazerke_90@mail.ru)

Simulation of the kinetics of direct coal hydrogenation

The kinetics of coal hydrogenation from the Shenghua deposit (People's Republic of China) has been studied. To calculate the kinetic parameters, experimental data on the hydrogenation of coal from the Shenghua field have been used. The hydrogenation process was carried out at a pressure of 5 MPa, at temperatures from 350 to 440 ºC using a batch reactor. Tetrahydronaphthalene was used as a solvent and donor in the process of coal hydrogenation. The rate constants were calculated using the random search optimization method and the integral Simpson method. It was found that the previously calculated rate constants of the hydrogenation of Shenghua coal (Runge-Kutt method) differ from our data by one order of magnitude. It is supposed that our calculated values of the rate constants are more reliable and adequate than those obtained by the Runge-Kutt method. The limiting rate of coal hydrogenation is observed for the stage of coal conversion into a mixture of gas and oil.

Keywords: kinetics, coal, hydrogenation, Simpson integral method, random search optimization method.

Introduction

Systems of differential equations are used for description of chemical kinetics of the coal and coal tar hydrogenation, heavy oil residues. Earlier [1–6], in the kinetics study of the hydrogenation of heavy and solid hydrocarbon feedstock for the kinetic parameters calculation, rigid types of differential equations systems were used. As is known, the chemical kinetics of complex chemical reactions is characterized by the presence of rapidly and slowly changing variables. Due to the stages of reactions that proceed at different rates, the solution of direct kinetic problems is complicated by the rigidity of the systems of differential equations describing the mechanism of these reactions [7–10]. In recent years, the Runge-Kutt methods, which were previously considered reliable, began to yield their dominant position among the algorithms for solving ordinary differential equations to modified methods capable of solving rigid problems [11, 12]. To solve the problems of chemical kinetics, the random search optimization method [13] and the Simpson's integral method [14] were used for the first time. Earlier these methods were used separately in solving systems of differential equations and did not find application in solving direct kinetic problems when they were combined. In order to determine the kinetic parameters, the experimental data on the Shenhua field coal hydrogenation [15] were used.

The purpose of the article is to use the combination of integral method with optimization of the kinetic model parameters of the Shenhua field coal hydrogenation [15].

Experimental

As shown in [15], the kinetics of the hydrogenation process of coal from the Shenghua field was investigated at a pressure of 5 MPa, at temperatures from 350 to 440 ºC the duration ranges from 0 to 60 minutes in a batch autoclave using tetrahydronaphthalene as a solvent.

The experimental data on the yield of target products and the kinetic model given in the article [15] were processed using the method of optimization of random search and integral calculation according to Simpson's method.

The calculation of the rate constants at the first stage was carried out by minimizing the residual function using the random search method. The selection of values was conducted randomly from a given range,

---

*Corresponding author

with the interval which complied with the calculation accuracy requirement. As a result, such a choice of constants makes it possible to minimize the residual function rather quickly and the minimum is guaranteed to be achieved in an acceptable computation time. At the second stage, the solution of systems of differential equations is performed according to the Simpson's method, which allows to calculate in a short time and with acceptable accuracy. The application of the modified method for solving chemical kinetics problem was previously presented in [1].

Results and Discussion

According to the data [15], the kinematic scheme of the Shenghua field coal hydrogenation is shown in Figure 1.
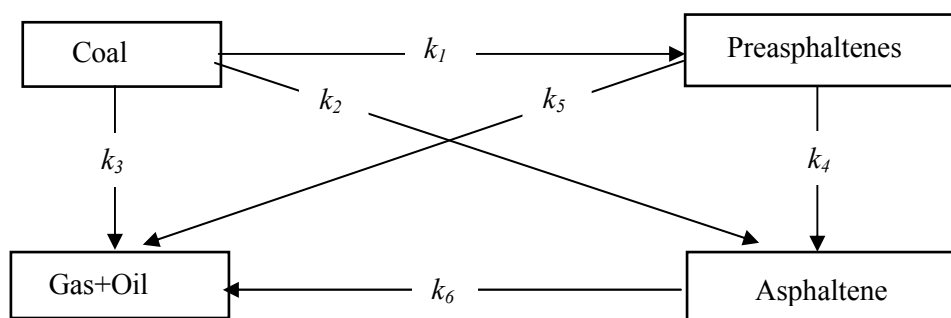

Figure 1. Scheme of the process of the Shenghua field coal hydrogenation

Based on the proposed coal hydrogenation scheme, the following kinetic model was compiled:

$$\frac{dC_1}{d\tau} = -\left(k_1 + k_2 + k_3\right)C_1,$$

$$\frac{dC_2}{d\tau} = k_1C_1 - \left(k_4 + k_5\right)C_2,$$

$$\frac{dC_3}{d\tau} = k_2C_1 + k_4C_2 - k_6C_3,$$ (1)

$$\frac{dC_4}{d\tau} = k_3C_1 + k_5C_2 + k_6C_3.$$

The kinetic curve of the process of the Shenghua field coal hydrogenation is shown, carried out at a temperature range from 360 to 400 ºC with a duration of 0–60 minutes (Fig. 2).

The calculated kinetic parameters of model (1) obtained by the Runge-Kutt method [15] and the Simpson's integral method with random search optimization are presented in Tables 1 and 2 correspondingly.

T a b l e 1

The rate constants of the process of coal hydrogenation in the temperature range 350–440 ºC, calculated by the Runge-Kutt method [15]

t, ºC	Rate constants, min^{-1}					
	k_1	k_2	k_3	k_4	k_5	k_6
350	0.02	0.016	0.012	0.004	0.003	0.002
380	0.028	0.02	0.014	0.006	0.005	0.003
400	0.032	0.023	0.016	0.007	0.006	0.003
420	0.035	0.029	0.021	0.009	0.008	0.004
440	0.042	0.033	0.026	0.013	0.009	0.006
E, kJ/mol	29.11	29.31	31.82	39.97	41.66	46.45

The difference in the rate constants calculated by two independent methods is that the rate constants for k_1-k_3 are an order of magnitude higher, and for k_4-k_6 coincide. It should be noted that the degree of conversion of the coal organic mass into asphaltenes, pre-asphaltenes, gas and oil is 25–29 %. This is a low yield of the conversion of coal organic mass, which does not correspond to high values of the rate constants k_1-k_3. This fact is the reason to believe that the results of calculation by the Simpson's method with random search optimization are more reliable and adequate than the values given in [15].
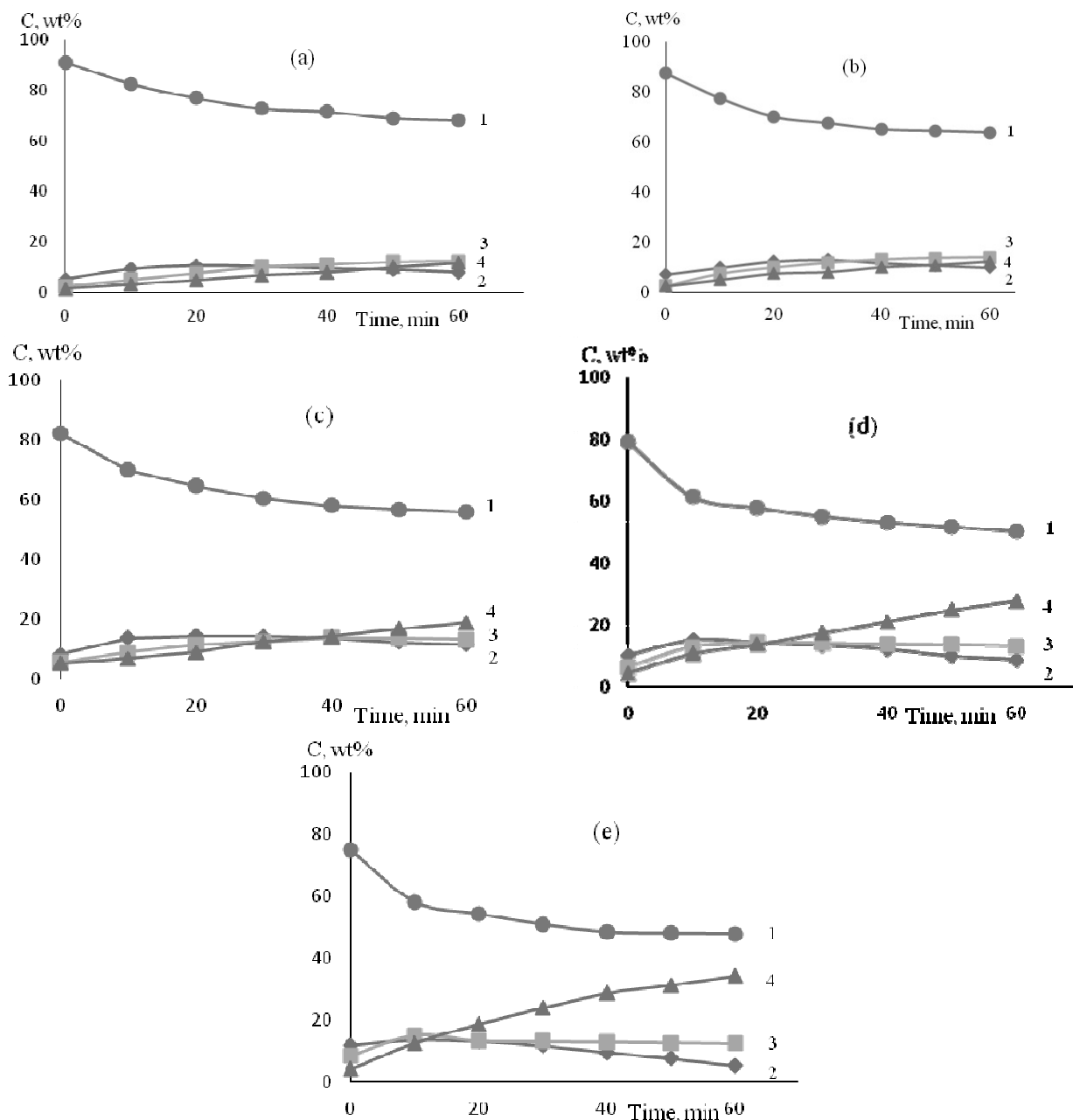
a — 350 ºC; b — 380 ºC; c — 400 ºC; d — 420 ºC; e — 440 ºC.
Reaction products: 1 — ● coal of the Shenhua deposit; 2 — ■ pre-asphaltenes; 3 — ▲ asphaltenes; 4 — ♦ gas and oil

Figure 2. Kinetic curves of products yield of the Shenhua field coal hydrogenation process at a different temperatures

T a b l e   2

The rate constants of the process of coal hydrogenation in the temperature range 350–440 ºC, calculated by the integrated Simpson's method with optimization of random search

t, ºC	Rate constants, min^{-1}					
	k_1	k_2	k_3	k_4	k_5	k_6
350	0.0027	0.0021	0.0011	0.006	0.0048	0.0031
380	0.0038	0.0028	0.0015	0.0097	0.006	0.0081
400	0.004	0.0029	0.0016	0.0108	0.0063	0.0097
420	0.0046	0.0033	0.0019	0.013	0.0069	0.014
440	0.0053	0.0038	0.0021	0.016	0.0075	0.021
E, kJ/mol	28.27	24.97	27.83	39.86	18.73	79.87

From the data shown in Table 2, it can be seen that with increase the temperature, the rate of the hydrogenation reaction of coal from the Shenghua field increases too. The following stages of the process are characterized by low values of the rate constants: the formation of asphaltenes, pre-asphaltenes, gas and oil from coal. With an increase the temperature from 400 ºC to 440 ºC, a sharp growth in the rate constants k_4 and k_6 occurs, which are characteristic of the stages of asphaltene formation from pre-asphaltenes, gas and oil from asphaltenes. Apparently, this is due to the prevalence of the hydrogenolysis reaction over the hydrogenation one. The use of Simpson's method with optimization of random search has shown by the example of calculating chemical kinetics, that the hydrogenation takes place in two stages: at the first stage, from 350 ºC to 400 °C, coal is hydrogenated, at the second stage, from 400 ºC to 440 ºC, hydrogenolysis reactions of the resulting products begin to prevail.

It should be noted that the deviation of the calculation results from the experimental values as a whole was 2.86 %.

Based on the data presented in Table 2, the following series of rate constants for the conversion of the middle fraction into hydrogenation products for different temperatures (ºC) were obtained: 1 — 350; 2 — 380; 3 — 400; 4 — 420; 5 — 440:

$$k_4 > k_5 > k_6 > k_1 > k_2 > k_3 \ (1),$$
$$k_4 > k_6 > k_5 > k_1 > k_2 > k_3 \ (2),$$
$$k_4 > k_6 > k_5 > k_1 > k_2 > k_3 \ (3),$$
$$k_6 > k_4 > k_5 > k_1 > k_2 > k_3 \ (4),$$
$$k_6 > k_4 > k_5 > k_1 > k_2 > k_3 \ (5).$$

According to the results obtained (Table 2), the limiting rate of coal hydrogenation is observed for the stage of coal conversion into a mixture of gas and oil at temperatures from 350 ºC up to 440 ºC.

In Tables 1 and 2 the values of activation energies are given as well. The calculation of the activation energies of the processes proceeding according to the proposed scheme was carried out from the ratio: $tg\alpha = E/R$, where E is the activation energy of the chemical reaction, J/mol; R is a universal gas constant equal to 8.314 Pa m^3/Kmol. Analysis of the data presented in Table 1 shows that the highest value of the activation energy corresponds to the process of gas and oil formation from asphaltenes. The least difficult energetically are the processes of coal destruction with the formation of pre-asphaltenes. As can be seen from the Table 2, the highest activation energy is characteristic for the stage of gas and oil formation from asphaltenes. The most active processes are the reactions of gas and oil formation from pre-asphaltenes.

Conclusions

Thus, to study the process of the Shenhua field coal hydrogenation the random search optimization method and the Simpson's integral method were used for the first time. It was found that our calculations of the kinetic parameters of coal hydrogenation differ from the rate constants obtained using the Runge-Kutt method by one order of magnitude. Moreover, the Simpson's method used with the random search optimization method established the presence of two stages of the coal hydrogenation. The first stage is the hydrogenation process and the second one is hydrogenolysis. It was shown that the limiting rate of coal hydrogenation is observed for the stage of conversion of coal into a mixture of gas and oil. The values of activation energies calculated using the Arrhenius equation are presented. It was also established that the most active processes are the reactions of gas and oil formation from pre-asphaltenes.

References

1 Балпанова Н.Ж. Кинетика гидрогенизации тяжелого и твердого углеводородного сырья / Н.Ж. Балпанова, А.М. Гюльмалиев, Ю.Н. Панкин, Д.Е. Айтбекова, Ф. Ма, К. Су, Д.А. Кайкенов, Г.Г. Байкенова, А.С. Борсынбаев, М.И. Байкенов // Химия твердого топлива. — 2019. — № 5. — С. 68–72. DOI: 10.3103/S0361521919050021.

2 Гюльмалиев А.М. Теоретические основы химии угля / А.М. Гюльмалиев, Г.С. Головин, Т.Г. Гладун. — М.: Изд-во Москов. гос. горн. ун-та, 2003. — 556 с.

3 Dai F. New kinetic model of coal tar hydrogenation process via carbon number component approach / F Dai, M. Gong, C. Li, Z. Li, S. Zhang. // Applied Energy. — 2015. — Vol. 137. — P. 265–272. DOI: 10.1016/j.apenergy.2014.10.009

4 Luo X. Simulation, exergy analysis and optimization of a shale oil hydrogenation process for clean fuels production / X. Luo, Q. Guo, D. Zhang, H. Zhou, Q. Yang // Applied Thermal Engineering. — 2018. — Vol. 140. — P. 102–111. DOI: 10.1016/j.applthermaleng.2018.05.012

5 Dai F. Modeling of fixed bed reactor for coal tar hydrogenation via the kinetic lumping approach / F. Dai, Y. Zhang, E. Xia, Z. Zhang, Z. Zhang, C. Li // Carbon Resources Conversion. — 2018. — Vol. 1, No. 3. — P. 279–283. DOI: 10.1016/j.crcon.2018.11.002

6 Feng X. Kinetic parameter estimation and simulation of trickle-bed reactor for hydrodesulfurization of whole fraction low-temperature coal tar / X. Feng, D. Li, J. Chen, M. Niu, X. Liu, L. L.T. Chan, W. Li // Fuel. — 2018. — Vol. 230. — P. 113–125. DOI: 10.1016/j.fuel.2018.05.023

7 Байназарова Н.М. Оптимизация численных методов решения жестких задач химической кинетики / Н.М. Байназарова, А.А. Юнусов, И.М. Губайдуллин // Научный сервис в сети интернет: поиск новых решений: тр. Междунар. суперкомп. конф. (17–22 сент. 2012 г.). — М.: Изд. дом, 2012. — С. 278–284.

8 Niemeyer K.E. pyJac: Analytical Jacobian generator for chemical kinetics / K.E. Niemeyer, J.C. Nicholas, C.-J. Sung // Computer Physics Communications Curtis. — 2017. — Vol. 215. — P. 188–203. DOI: 10.1016/j.cpc.2017.02.004

9 Sun J. Modeling the hydrotreatment of full range medium temperature coal tar by using a lumping kinetic approach / J. Sun, D. Li, R. Yao, Z. Sun, X. Li, W. Li // Reaction Kinetics, Mechanisms and Catalysis. — 2015. — Vol. 114, No. 2. — P. 451–471. DOI: 10.1007/s11144–014–0791–2

10 Niemeyer K.E. Accelerating moderately stiff chemical kinetics in reactive-flow simulations using GPUs / K.E. Niemeyer, C.-J. Sung // Journal of Computational Physics. — 2014. — Vol. 256. — P. 854–871. DOI: 10.1016/j.jcp.2013.09.025

11 Shi Y. Redesigning combustion modeling algorithms for the Graphics Processing Unit (GPU): Chemical kinetic rate evaluation and ordinary differential equation integration / Y. Shi, W.H. Green, H.-W. Wong, O.O. Oluwole // Combustion and Flame. — 2011. — Vol. 158, No. 5. — P. 836–847. DOI: 10.1016/j.combustflame.2011.01.024

12 Le H.P. GPU-based flow simulation with detailed chemical kinetics / H.P. Le, J.-L. Cambier, L.K. Cole // Computer Physics Communications. — 2013. — Vol. 184, No. 3. — P. 596–606. DOI: 10.1016/j.cpc.2012.10.013

13 Рейзлин В.И. Численные методы оптимизации: учеб. пос. / В.И. Рейзлин. — Томск: Изд-во Томск. политехн. ун-та, 2011. — 105 с.

14 Вержбицкий В.М. Основы численных методов: учеб. пос. / В.М. Вержбицкий. — М.: Высш. шк., 2002. — 840 с.

15 Lin Hua-lin. Kinetics of Shenhua Coal hydroliquefaction / Hua-lin Lin, Yi Xu, Jue Huang, De-xiang Znang, Jin-sheng Gao // Journal of East China University of Science and Technology (Natural Science Edition). — 2009. — Vol. 35, No. 6. — P. 825–828.

Н.Ж. Балпанова, А.М. Гюльмалиев, Ю.Н. Панкин, Ф. Ма, К. Су,
А.И. Халитова, Д.Е. Айтбекова, А. Тусипхан, М.И. Байкенов

Көмір гидрогенизациясының кинетикасын модельдеу

Шенхуа кен орнындағы көмір гидрогенизациясының кинетикасы зерттелген. Кинетикалық параметрлерді анықтау үшін Шенхуа кен орнындағы көмірді гидрогенизациялаудың тәжірибелік деректері пайдаланылды. Гидрогенизация процесі 5 МПа қысымда, 350-ден 440 ºС-ге дейінгі температурада мерзімді реакторды пайдалана отырып жүргізілді. Шенхуа кен орнындағы көмірді гидрогенизациялау процесінде еріткіш және донор ретінде тетрагидронафталин қолданылды. Көмірді гидрогенизациялау процесінің жылдамдық константалары мен активтендіру энергиясының мәндері есептелді. Жылдамдық константаларын есептеу жедел түсіру әдісімен оңтайландыру және Симпсонның интегралды әдісін қолдану арқылы жүргізілді. Шенхуа көмірін гидрогенизациялау процесінің Рунге-Кутта әдісімен есептелген жылдамдық константаларының мәні ұсынылып отырған жедел түсіру әдісімен оңтайландыру арқылы Симпсон әдісін қолданумен есептелген жылдамдық константасының мәндерінен бір бірлікке ерекшеленетіні анықталды. Көмір гидрогенизациясының лимиттеуші жылдамдығы көмірді газ бен май қоспасына айналдыру сатысында байқалатыны анықталды. Аррениус теңдеуін пайдалана отырып, есептелген активтендіру энергиясының мәндері келтірілген.

Кілт сөздер: кинетика, көмір, гидрогенизация, Симпсонның интегралдық әдісі, кездейсоқ іздеуді оңтайландыру әдісі.

Н.Ж. Балпанова, А.М. Гюльмалиев, Ю.Н. Панкин, Ф. Ма, К. Су,
А.И. Халитова, Д.Е. Айтбекова, А. Тусипхан, М.И. Байкенов

Моделирование кинетики прямой гидрогенизации угля

Исследована кинетика гидрогенизации угля месторождения Шенхуа. Для определения кинетических параметров были использованы экспериментальные данные гидрогенизации угля месторождения Шенхуа. Кинетика процесса гидрогенизации проводилась при давлении 5 МПа, при температурах от 350 до 440 ºС с использованием периодического реактора. В качестве растворителя и донора в процессе гидрогенизации угля месторождения Шенхуа использовался тетрагидронафталин. Рассчитаны константы скоростей и энергии активации процесса гидрогенизации угля. Расчет констант скоростей проводился с использованием метода оптимизации случайного поиска и интегрального метода Симп-

сона. Установлено, что ранее рассчитанные константы скоростей методом Рунге-Кутта процесса гидрогенизации угля Шенхуа отличаются от нами рассчитанных констант скоростей с использованием метода Симпсона с оптимизацией случайного поиска на один порядок. Полагаем, что величины констант скоростей, полученные методом Симпсона с оптимизацией случайного поиска, более адекватны, чем величины констант скоростей, рассчитанные методом Рунге-Кутта. Доказано, что лимитирующая скорость гидрогенизации угля наблюдается для стадии превращения угля в смесь газа и масла. Приведены величины энергий активации, полученные посредством уравнения Аррениуса.

Ключевые слова: кинетика, уголь, гидрогенизация, интегральный метод Симпсона, метод оптимизации случайного поиска.

References

1 Balpanova, N.Zh., Giulmaliev, A.M., Pankin, Yu.N., Aitbekova, D.E., Ma, F., & Su, K. et al. (2019). Kinetika hidrohenizatsii tiazheloho i tverdoho uhlevodorodnoho syria [Kinetics of hydrogenation of heavy and solid hydrocarbon raw materials]. *Khimia tverdoho topliva — Solid fuel chemistry, 5*, 68–72. DOI:10.3103/S0361521919050021 [in Russian].

2 Gyulmaliev, A.M., Golovin, G.S., & Gladun, T.G. (2003). Teoreticheskie osnovy khimii uhlia [Theoretical foundations of coal chemistry]. Moscow: Moscow State Mining Univ. Publ. [in Russian].

3 Dai, F., Gong, M., Li, C., Li, Z., & Zhang, S. (2015). New kinetic model of coal tar hydrogenation process via carbon number component approach. *Applied Energy, 137*, 265–272. DOI: 10.1016/j.apenergy.2014.10.009

4 Luo, X., Guo, Q., Zhang, D., Zhou, H., & Yang, Q. (2018). Simulation, exergy analysis and optimization of a shale oil hydrogenation process for clean fuels production. *Applied Thermal Engineering, 140*, 102–111. DOI: 10.1016/j.applthermaleng.2018.05.012

5 Dai, F., Zhang, Y., Xia, E., Zhang, Z., Zhang, Z., & Li, C. (2018). Modeling of fixed bed reactor for coal tar hydrogenation via the kinetic lumping approach. *Carbon Resources Conversion, 1(3)*, 279–283. DOI: 10.1016/j.crcon.2018.11.002

6 Feng, X., Li, D., Chen, J., Niu, M., Liu, X., Chan, L. L. T., & Li, W. (2018). Kinetic parameter estimation and simulation of trickle-bed reactor for hydrodesulfurization of whole fraction low-temperature coal tar. *Fuel, 230*, 113–125. DOI: 10.1016/j.fuel.2018.05.023

7 Bainazarova, N.M., Yunusov, A.A., & Gubaidullin, I.M. (2012). Optimizatsiia chislennykh metodov resheniia zhestkikh zadach khimicheskoi kinetiki [Optimization of numerical methods for solving hard problems of chemical kinetics]. Proceedings from Scientific service on the Internet: the search for new solutions '12: Mezhdunarodnaia superkompiuternaia konferentsiia (17–22 sentiabria 2012 hoda) — International Supercomputer Conference. (pp. 278–284). Moscow: Izdatelskii dom [in Russian].

8 Niemeyer, K. E., Curtis, N. J., & Sung, C.-J. (2017). pyJac : Analytical Jacobian generator for chemical kinetics. *Computer Physics Communications, 215*, 188–203. DOI: 10.1016/j.cpc.2017.02.004

9 Sun, J., Li, D., Yao, R., Sun, Z., Li, X., & Li, W. (2014). Modeling the hydrotreatment of full range medium temperature coal tar by using a lumping kinetic approach. *Reaction Kinetics, Mechanisms and Catalysis, 114(2)*, 451–471. DOI: 10.1007/s11144–014–0791–2

10 Niemeyer, K.E., & Sung, C.-J. (2014). Accelerating moderately stiff chemical kinetics in reactive-flow simulations using GPUs. *Journal of Computational Physics, 256*, 854–871. DOI: 10.1016/j.jcp.2013.09.025

11 Shi, Y., Green, W.H., Wong, H.-W., & Oluwole, O.O. (2011). Redesigning combustion modeling algorithms for the Graphics Processing Unit (GPU): Chemical kinetic rate evaluation and ordinary differential equation integration. *Combustion and Flame, 158(5)*, 836–847. DOI: 10.1016/j.combustflame.2011.01.024

12 Le, H.P., Cambier, J.-L., & Cole, L.K. (2013). GPU-based flow simulation with detailed chemical kinetics. *Computer Physics Communications, 184(3)*, 596–606. DOI: 10.1016/j.cpc.2012.10.013

13 Reizlin, V.I. (2011). *Chislennye metody optimizatsii [Numerical optimization methods]*. Tomsk: Tomsk Polytechn. Univ. Publ. [in Russian].

14 Verzhbitskii, V.M. (2002). *Osnovy chislennykh metodov [Fundamentals of Numerical Methods]*. Moscow: Vysshaia shkola [in Russian].

15 Lin, Hua-lin, Xu, Y., Huang, J., Znang, D-X., & Gao, J-Sh. (2009). Kinetics of Shenhua Coal hydroliquefaction. *Journal of East China University of Science and Technology (Natural Science Edition), 35, 6*, 825–828.

INFORMATION ABOUT AUTHORS

Aitbekova Darzhan Ergalievna — 2nd year PhD student, Karagandy University of the name of academician E.A. Buketov, Universitetskaya street, 28, 100028, Karaganda, Kazakhstan; e-mail: darzhan91@mail.ru;

Arinova Anar Erikovna — PhD Student, Karagandy University of the name of academician E.A. Buketov, Universitetskaya street, 28, 100028, Karaganda, Kazakhstan; e-mail: arinova.777@mail.ru, https://orcid.org/0000-0002-7780-4555;

Baikenov Murzabek Ispolovich — Doctor of chemical sciences, Professor, Karagandy University of the name of academician E.A. Buketov, Universitetskaya street, 28, 100028, Karaganda, Kazakhstan; e-mail: murzabek_b@mail.ru;

Bakibaev Abdigali Abdimanapovich — Doctor of Chemical Sciences, Professor, Leading Researcher of the Laboratory of Organic Synthesis, National Research Tomsk State University, Lenin str., 36, 634050, Tomsk, Russia; e–mail: bakibaev@mail.ru; https://orcid.org/0000-0002-3335-3166;

Balpanova Nazerke Zhumagalievna — 3rd year PhD student, Karagandy University of the name of academician E.A. Buketov, Universitetskaya street, 28, 100028, Karaganda, Kazakhstan; e-mail: nazerke_90@mail.ru;

Bayakhmetova Bulbul Bayakhmetovna — Candidate of chemical sciences, Senior lecturer of Biochemistry and chemical disciplines department, Semey Medical University, Semey, Abay street, 103, Kazakhstan; e-mail: bulbul.bayahmetova@mail.ru; https://orcid.org/0000-0002-5663-5107;

Bhole Ritesh Prakash — PhD, Associate Professor, Dr. D.Y. Patil Institute of Pharmaceutical Sciences and Research, Sant Tukaram Nagar, Pimpri, Pune, 411018, India: e-mail: ritesh.bhole@dypvp.edu.in; orcid ID: 0000-0003-4088-7470;

Birimzhanova Dinara Asylbekovna — PhD, Senior Teacher of chemistry Department, Leading researcher, Institute of Applied Chemistry, L.N. Gumilyov Eurasian National University, Satpaev street, 2, 010000, Nur-Sultan, Kazakhstan; e-mail: dinarko@inbox.ru; https://orcid.org/0000-0002-5572-9339;

Bogdanova Lyudmila Mikhailovna — Candidate of chemical sciences, Senior researcher, Institute of Problems of Chemical Physics Russian Academy of Sciences, ac. Semenov avenue, 1, Chernogolovka, Moscow region, 142432, Russian Federation; e-mail: bogda@icp.ac.ru;

Bolatbay Abylaikhan Nurlanovich — PhD student, Karagandy University of the name of academician E.A. Buketov, Universitetskaya street, 28, 100028, Karaganda, Kazakhstan; e-mail: abylai_bolatbai@mail.ru;

Bonde Chandrakant Ghansham — PhD, Professor, SPTM, NMIMS, School of Pharmacy, Shirpur, Dist: Dhule, India; e-mail: chandrakant.bonde@nmims.edu; https://orcid.org/0000-0001-5712-1119;

Bukichev Yuri Sergeevich — 1st year PhD student, Department of aviation materials and technologies in medicine, Moscow Aviation Institute (National Research University), 125993, Moscow, Volokolamskoe shosse, 4; e-mail: UresBuki4eff@yandex.ru; https://orcid.org/0000-0002-0858-5096;

Burkeev Meyram Zhunusovich — Full Professor, Doctor of Chemical Sciences, Karagandy University of the name of academician E.A. Buketov, Universitetskaya street, 28, 100028, Karaganda, Kazakhstan; e-mail: m_burkeev@mail.ru;

Davrenbekov Santai Zhanabilovich — Assoc. Professor, Karagandy University of the name of academician E.A. Buketov, Universitetskaya street, 28, 100028, Karaganda, Kazakhstan; e-mail: sdavrenbekov@mail.ru;

Dosmagambetova Saule Sarkantaevna — Doctor of chemical sciences, professor, Chemistry Department, L.N. Gumilyov Eurasian National University, Nur-Sultan, Satbaev street, 2, 010000, Kazakhstan, e-mail: dosmagambetova_ss@enu.kz;

Dzhardimalieva Gulzhian Iskakovna — Doctor of chemical sciences, Head of Laboratory of Metallopolymers, Institute of Problems of Chemical Physics Russian Academy of Sciences, ac. Semenov avenue 1, Chernogolovka, Moscow region, 142432 Russian Federation; Professor of Moscow Aviation Institute (National Research University), 125993, Moscow, Volokolamskoe shosse, 4; e-mail: dzhardim@icp.ac.ru; https://orcid.org/0000-0002-4727-8910;

Egorova Ludmila Sergeevna — Candidate of chemical sciences, Leading researcher, Department of Technosphere Safety and Analytical Chemistry Altai State University, Lenin Avenue, 61, Barnaul, Russia; e-mail: egorova@chem.asu.ru;

Fazylov Arman Serikovich — Undergraduate of the Karaganda State Technical University, Nursultan Nazarbayev Ave., 56, 100027, Karaganda, Kazakhstan; e-mail: arman1708@yahoo.com, https://orcid.org /0000-0003-2905-9121;

Fazylov Serik Drakhmetovich — Academician of the National Academy of Sciences of the Republic of Kazakhstan, Doctor of Chemical Sciences, Professor, Chief Researcher, Institute of Organic Synthesis and Coal Chemistry of the Republic of Kazakhstan, Alikhanov street, 1, 100008, Karaganda, Kazakhstan; e-mail: iosu8990@mail.ru, https://orcid.org/0000-0002-4240-6450;

Ganieva Kamila Ganievna — 4th year student, Chemical technologies and ecology department, Shakarim University of Semey, Semey, Tanirbergenov street, 1, Kazakhstan; e-mail: ganieva_kamila@mail.ru; https://orcid.org/0000-0002-7764-7895;

Gazaliev Arystan Maulenovich — Academician of the National Academy of Sciences of the Republic of Kazakhstan, Deputy Director for Research, Institute of Organic Synthesis and Coal Chemistry of the Republic of Kazakhstan, Alikhanov street, 1, 100008, Karaganda, Kazakhstan; https://orcid.org/0000-0003-2161-0329;

Gyulmaliev Agadzhan Mirzoevich — Chief researcher, A.V. Topchiev Institute of Petrochemical Synthesis, RAS, Leninist avenue street, 29, 119991, Moscow, Russia; e-mail: gyulmaliev@ips.ac.ru;

Ibraev Marat Kerimbaevich — Doctor of Chemical Sciences, Professor, Leading researcher, Karaganda State Technical University, Nursultan Nazarbayev Ave., 56, 100027, Karaganda, Kazakhstan; e-mail: mkibr@mail.ru, https://orcid.org/0000-0003-0798-5562;

Irzhak Vadim Isakovich — Doctor of chemical sciences, Principal researcher, Institute of Problems of Chemical Physics Russian Academy of Sciences, ac. Semenov avenue, 1, Chernogolovka, Moscow region, 142432 Russian Federation; e-mail:irzhak@icp.ac.ru;

Ishmuratova Margarita Yulaevna — Candidate of biological sciences, Associated professor, Karagandy University of the name of academician E.A. Buketov, Universitetskaya street, 28, 100028, Karaganda, Kazakhstan; e-mail: margarita.ishmur@mail.ru; https://orcid.org/0000-0002-1735-8290;

Iskakova Zhanar Baktybaevna — Candidate of chemical sciences, L.N. Gumilyov Eurasian National University, Satpaev street, 2, 010000, Nur-Sultan, Kazakhstan; e-mail: zhanariskakova@mail.ru; https://orcid.org/0000-0002-3540-8263;

Jagtap Somnath Ramdas — M. Pharm, Research Scholar, Dr. D.Y. Patil Institute of Pharmaceutical Sciences and Research, Sant Tukaram Nagar, Pimpri, Pune, 411018, India; e-mail: somnath.jagtap@gmail.com;

Kalichkina Liudmila Evgen'evna — Junior Researcher of laboratory «Organic synthesis», National Research Tomsk State University, Tomsk, Arkadiya Ivanova street, 49, 634028, Russia; e-mail: kalichkina_lyuda@mail.ru;

Khalitova Alfiya Ildarovna — Candidate of chemical sciences, Associate professor, Karagandy University of the name of academician E.A. Buketov, Universitetskaya street, 28, 100028, Karaganda, Kazakhstan; e-mail: khalfiya2212@inbox.ru;

Kotelnikov Oleg Alekseevich — Researcher of the Laboratory of Organic Synthesis, Spectroscopist, National Research Tomsk State University, Lenin str., 36, 634050, Tomsk, Russia; e–mail: kot_o_a@mail.ru; https://orcid.org/0000-0002-1241-1312;

Leites Elena Anatolyevna — Candidate of chemical sciences, Senior researcher, Department of Technosphere Safety and Analytical Chemistry Altai State University, Lenin Avenue, 61, Barnaul, Russia; e-mail: leites-elena@yandex.ru;

Lesnichaya Valentina Alekseevna — Candidate of physical-mathematical sciences, Senior researcher, Institute of Problems of Chemical Physics Russian Academy of Sciences, ac. Semenov avenue, 1, Chernogolovka, Moscow region, 142432 Russian Federation; e-mail:lesnich@icp.ac.ru;

Ma Feng Yun — Doctor PhD, Professor, Xinjiang University, 666 Shengli Rd, Tianshan District, Urumqi, XUAR, People's Republic of China; e-mail: ma_fy@126.com;

Malkov Victor Sergeevich — Candidate of Chemical Sciences, Head of the Laboratory of Organic Synthesis, National Research Tomsk State University, Lenin str., 36, 634050, Tomsk, Russia; e–mail: malkov.vics@gmail.com; https://orcid.org/0000-0003-4532-2882;

Muldakhmetov Zeinolla Muldakhmetovich — Academician of NAS RK, Doctor of Chemical Sciences, Professor, Institute Director, Institute of Organic Synthesis and Coal Chemistry of the Republic of Kazakhstan Alikhanov street, 1, 100008, Karaganda, Kazakhstan; e-mail: iosu.rk@mail.ru, https://orcid.org/0000-0001-9497-2545;

Muratbekova Aigul Akezhanovna — Candidate of chemical sciences, Associate professor, Karagandy University of the name of academician E.A. Buketov, Universitetskaya street, 28, 100028, Karaganda, Kazakhstan; e-mail: aigulmuratbekova@mail.ru;

Mussabayeva Binur Khabasovna — Candidate of chemical sciences, Professor of Chemical technologies and Ecology department, Shakarim University of Semey, Tanirbergenov street, 1, Semey, Kazakhstan; e-mail: binur.mussabayeva@mail.ru; https://orcid.org/0000-0003-2209-1209;

Nasikhatuly Ermauyt — Student, Karagandy University of the name of academician E.A. Buketov, Universitetskaya street, 28, 100028, Karaganda, Kazakhstan; e-mail: ermauit@gmail.com;

Nurkenov Oralgazy Aktayevich — Doctor of Chemical Sciences, Professor, Head of laboratory, Institute of Organic Synthesis and Coal Chemistry of the Republic of Kazakhstan, Alikhanov street, 1, 100008, Karaganda, Kazakhstan; e-mail: nurkenov_oral@mail.ru, https://orcid.org/0000-0002-2771-0411;

Orazhanova Lyazzat Kametayevna — Candidate of chemical sciences, Associated professor of Chemical technologies and Ecology department, Shakarim University of Semey, Semey, Tanirbergenov street, 1, Kazakhstan; e-mail: lyazzat.7070@mail.ru; https://orcid.org/0000-0001-7881-0589;

Pankin Yuri Nikolaevich — Leading specialist, Kazakhtelecom JSC, Ermekov street, 31, 100009, Karaganda, Kazakhstan; e-mail: ukinpan@mail.ru;

Panshina Svetlana Yur'evna — Postgraduate of specialty chemistry, Analyst of the Laboratory of Organic Synthesis, National Research Tomsk Polytechnic University, Lenin str., 30, 634050, Tomsk, Russia, National Research Tomsk State University, Lenin str., 36, 634050, Tomsk, Russia; e-mail: janim_svetatusik@mail.ru; https://orcid.org/0000-0001-6824-2645;

Pirniyazov Kudrat Kadambayevich — Junior Researcher, Institute of the Polymer Chemistry and Physics Academy Sciences of Uzbekistan, Tashkent, Uzbekistan; e-mail: qudrat.pirniyazov@mail.ru;

Ponomarenko Oxana Vladimirovna — 3rd year PhD student of specialty chemistry, L.N. Gumilyov Eurasian National University, Satpaev str., 2, 010000, Nur-Sultan, Kazakhstan; e-mail: oksana.ponomarenko.88@mail.ru, https://orcid.org/0000-0002-8172-5139;

Rashidova Sayyora Sharafovna — Doctor of chemical Sciences, Professor, Academician, Director of the Institute of Polymer Chemistry and Physics, Academy of Sciences of the Republic of Uzbekistan, Tashkent Uzbekistan; e-mail: polymer@academy.uz;

Sabitova Alfira Nurzhanovna — PhD, Head of Chemical technologies and Ecology department, Shakarim University of Semey, Semey, Tanirbergenov street, 1, Kazakhstan; e-mail: alfa-1983@mail.ru; https://orcid.org/0000-0002-3360-7998;

Sarsenbekova Akmaral Zhakanovna — Doctor PhD, Senior researcher, Karagandy University of the name of academician E.A. Buketov, Universitetskaya street, 28, 100028, Karaganda, Kazakhstan; e-mail: chem_akmaral@mail.ru;

Seilkhanov Tulegen Muratovich — Candidate of chemical sciences, full professor, Head of the laboratory of Engineering Profile of NMR Spectroscopy, Sh. Ualikhanov Kokshetau university, Kokshetau, Abay street, 76, 020000, Kazakhstan, e-mail: tseilkhanov@mail.ru, https://orcid.org/0000-0003-0079-4755;

Shcherban Marina Grigoryevna — Candidate of chemical sciences, Assistant professor, Physical Chemistry Department, Perm State National Research University, Perm, 614990, Bukireva st., 15, Russia; e-mail: ma-sher74@mail.ru; https://orcid.org/0000-0002-6905-6622;

Shershnev Vitaly Aleksandrovich — Candidate of chemical sciences, Researcher, Institute of Problems of Chemical Physics Russian Academy of Sciences, ac. Semenov avenue, 1, Chernogolovka, Moscow region, 142432 Russian Federation; e-mail: femtos@icp.ac.ru; https://orcid.org/0000-0002-0375-8306;

Solovyev Aleksandr Dmitriyevich — 2nd year student (bachelor), Physical Chemistry Department, Perm State National Research University, Perm, 614990, Bukireva st., 15, Russia; e-mail: solovev_s92@mail.ru; https://orcid.org/0000-0002-7852-3683;

Su Xintai — Doctor PhD, Professor, Xinjiang University, 666 Shengli Rd, Tianshan District, Urumqi, XUAR, People's Republic of China; e-mail: suxintai08@sina.com;

Suleimen Raigul Nurbekkyzy — PhD, Senior teacher, L.N. Gumilyov Eurasian National University, Satpaev street, 2, 010000, Nur-Sultan, Kazakhstan; e-mail: kasim_rai@mail.ru; https://orcid.org/0000-0003-3338-2722;

Suleimen Yerlan Melsuly — Candidate of chemical sciences, PhD, 1) Senior researcher of the laboratory of Engineering Profile of NMR Spectroscopy, Sh. Ualikhanov Kokshetau university, Kokshetau, Abay street, 76, 020000, Kazakhstan; 2) Main Scientific Secretary of Republican collection of microorganisms, Nur-Sultan, Sh. Ualikhanov, 13/1, 010000, Kazakhstan; e-mail: syerlan75@yandex.kz, https://orcid.org/0000-0002-5959-4013;

Tashenov Auezkhan Karipkhanovich — Doctor of Chemical Sciences, Professor, Head of the Department of Chemistry, L.N. Gumilyov Eurasian National University, Satpaev str., 2, 010000, Nur-Sultan, Kazakhstan; e-mail: tashenov_ak@enu.kz; https://orcid.org/0000-0002-6880-2996;

Tazhbaev Yerkebulan Muratovich — Full Professor, Doctor of Chemical Sciences, Karagandy University of the name of academician E.A. Buketov, Universitetskaya street, 28, 100028, Karaganda, Kazakhstan; e-mail: tazhbayev@mail.ru;

Tusipkhan Almas — Doctor PhD, Karagandy University of the name of academician E.A. Buketov, Universitetskaya street, 28, 100028, Karaganda, Kazakhstan; e-mail: almas_kz_22@mail.ru; https://orcid.org/0000-0002-6452-4925;

Vlasova Lenina — Candidate of Chemical Sciences, Professor, head of department, Medical University of Karaganda, Gogol street, 40, 100008, Karaganda, Kazakhstan, e-mail: lenina-vlasova@mail.ru, https://orcid.org /0000-0003-1530-3859;

Volkova Nina Nikolaevna — Candidate of chemical sciences, Senior researcher, Institute of Problems of Chemical Physics Russian Academy of Sciences, ac. Semenov avenue, 1, Chernogolovka, Moscow region, 142432 Russian Federation; e-mail: nnvolkova@rambler.ru; https://orcid.org/0000-0001-6834-3649;

Yeshzhanov Arman Bakhytzhanovich — 3rd year PhD student, chemistry department, L.N. Gumilyov Eurasian National University, Nur-Sultan, Satbaev street, 2, 010000, Kazakhstan; e-mail: a.yeszhanov@inp.kz; https://orcid.org/0000-0002-1328-8678;

Zabolotnykh Svetlana Aleksandrovna — Candidate of chemical sciences, researcher, Laboratory of Organic Complexing Reagents, Institute of Technical Chemistry, Ural Branch of RAS, Perm, 614013, Korolev st., 3, Russia; e-mail: zabolotsveta@mail.ru; https://orcid.org/0000-0001-8307-0386;

Zambare Yogesh Baban — M. Pharm, Dr. D.Y. Patil Institute of Pharmaceutical Sciences and Research, Sant Tukaram Nagar, Pimpri, Pune-411018, India, e-mail: yogesh.zambare@dypvp.edu.in; https://orcid.org/0000-0001-5115-0971;

Zhakupbekova Elmira Zhumantaevna — Candidate of chemical sciences, Assoc. Professor, Karagandy University of the name of academician E.A. Buketov, Universitetskaya street, 28, 100028, Karaganda, Kazakhstan; e-mail: elmira_zhakupbek@mail.ru;

Zhanzhaxina Almira Sheihslamovna — PhD student, L.N. Gumilyov Eurasian National University, Satpaev street, 2, 010000, Nur-Sultan, Kazakhstan; e-mail: almira1986@inbox.ru; https://orcid.org/0000-0001-7388-292X.